AN EFFICIENT METHOD FOR NONLINEAR DYNAMIC ANALYSIS OF 3D SPACE STRUCTURES

HAMIDREZA HASHAMDAR

FACULTY OF ENGINEERING

UNIVERSITY OF MALAYA

KUALA LUMPUR

APRIL 2011

AN EFFICIENT METHOD FOR NONLINEAR DYNAMIC ANALYSIS OF 3D SPACE STRUCTURES

HAMIDREZA HASHAMDAR

THESIS SUBMITTED IN FULFILMENT

OF THE REQUIREMENTS FOR THE DEGREE OF

DOCTOR OF PHILOSOPHY

FACULTY OF ENGINEERING

UNIVERSITY OF MALAYA

KUALA LUMPUR

APRIL 2011

UNIVERSITI MALAYA
ORIGINAL LITERARY WORK DECLARATION

Name of Candidate: Hamidreza Hashamdar

Registration/Matric No: KHA080004

Name of Degree: Doctor of Philosophy

Title of Project Paper/Research Report/Dissertation/Thesis ("this Work"): Development of Theoretical and Numerical Analysis of Laminated Rubber Bearing For Base-Isolated Structures

Field of Study: Civil Engineering

I do solemnly and sincerely declare that:

1) I am the sole author/writer of this Work;
2) This Work is original;
3) Any use of any work in which copyright exists was done by way of fair dealing and for permitted purposes and any excerpt or extract from, or reference to or reproduction of any copyright work has been disclosed expressly and sufficiently and the title of the Work and its authorship have been acknowledged in this Work;
4) I do not have any actual knowledge nor ought I reasonably to know that the making of this work constitutes an infringement of any copyright work;
5) I hereby assign all and every rights in the copyright to this Work to the University of Malaya (UM), who henceforth shall be owner of the copyright in this Work and that any reproduction or use in any form or by any means whatsoever is prohibited without the written consent of UM having been first had and obtained;
6) I am fully aware that if in the course of making this Work I have infringed any copyright whether intentionally or otherwise, I may be subject to legal action or any other action as may be determined by UM.

Candidate's Signature Hamidreza Hashamdar Date: 21 APRIL

Subscribed and solemnly declared before,

Witness's Signature Date: 21 APRIL

Name:

Designation:

ABSTRACT

The aim of this thesis is to develop an efficient method for the nonlinear analysis of space structures with high degree of freedom such as cable structures. Space structures can provide large uninterrupted covered areas such as sport centres, aircraft hangars, tensile cables, etc. The proposed theory for nonlinear analysis of 3D space structure is based on the minimization of the total potential dynamic work. The minimization of the total potential dynamic work is an indirect method which is based on the principle of the convergence of energy in structures. Conventional methods such as superposition methods are direct methods.

The dynamic response analysis of a nonlinear system is based on the evaluation of response for a series of short time intervals using different types of time integration techniques. In dynamic problems, the differential equations arising from the equilibrium of the dynamic forces acting on the mass is solved by implicit or explicit methods. In order to verify the proposed theory, static and dynamic testing of the model is performed. The degree of error by elastic deformation of the frame and degree of symmetry of the model during the static test shows that the boundary condition of the frame is rigid and the frame is symmetric. The results of the dynamic test show that the theoretical and experimental values of the natural frequencies, mode shapes, and modal damping ratios are in good agreement. The dynamic responses calculated due to the exciting structure with various load intensities from different points are also in agreement with the finite element modelling. The influence of the magnitude of the damping ratios in different modes while using an orthogonal damping matrix is negligible. Finally, in comparison to conventional methods, the computational time taken by the proposed method is acceptable.

In general, the reduction in time and cost as well as the highly accurate results obtained justify the use of indirect methods such as the optimization theory. The developed method is found to be a suitable technique for the minimization of the total potential energy function, especially in cases where the number of variables is large and the structure is highly nonlinear. The proposed method decreases computational time and the number of iterations required per time step.

ABSTRAK

Tujuan thesis ini adalah untuk membangunkan satu kaedah baru untuk analisis tak linear bagi struktur ruang yang mempunyai darjah kebebasan yang tinggi seperti struktur kabel. Struktur ruang boleh memberikan kawasan ruang besar tanpa gangguan seperti pusat sukan, hangar pesawat, kabel tegangan, dan sebagainya. Teori yang dicadangkan untuk analisis tak linear struktur ruang 3D adalah berdasarkan pengurangan jumlah potensi kerja dinamik. Pengurangan Mengurangkan jumlah potensi kerja dinamik adalah satu kaedah tak langsung yang berdasarkan prinsip penyatuan tenaga dalam struktur. Kaedah konvensional seperti kaedah tindihan adalah kaedah langsung.

Sistem tak linear tidak mempunyai set tetap bagi vektor eigen dan nilai eigen. Set baru bagi vector eigen dan nilai eigen mesti dikira pada setiap langkah masa dan matriks kekukuhan mesti dinilai semula pada akhir setiap langkah masa. Analisis gerakbalas dinamik bagi sistem tak linear adalah berdasarkan penilaian gerakbalas untuk satu siri jeda masa yang singkat dengan menggunakan pelbagai jenis teknik integrasi masa. Dalam masalah yang dinamik, persamaan pembezaan yang timbul daripada keseimbangan kuasa-kuasa dinamik yang bertindak ke atas jisim diselesaikan dengan kaedah tersirat atau tersurat. Kaedah tersirat atau tersurat menyediakan penyelesaian berangka untuk persamaan gerakan yang dibina untuk satu jeda masa. Mereka mengandaikan bahawa sifat-sifat struktur kekal malar semasa jeda, tetapi ianya dikira semula pada akhir langkah masa. Walau bagaimanapun, ini mungkin tidak mencukupi untuk struktur yang sangat tak linear.

Kaedah tersirat menawarkan kestabilan tanpa syarat pada keupayaan operasi dengan matriks uraian yang agak padat apabila digunakan ke atas struktur linear, tetapi kehilangan kelebihan daripada kestabilan tanpa syarat

apabila digunakan ke atas sistem tak linear. Kaedah-kaedah yang tersurat, sebaliknya, menggunakan kurang ruang untuk penyimpanan didalam komputer, tetapi dihalang oleh ketidakstabilan yang menghadkan saiz langkah-langkah masa. Kaedah tersirat, apabila digunakan ke atas struktur tak linear, memerlukan penyelesaian satu set persamaan tak linear, sedangkan kebanyakan kaedah tersurat memerlukan penyongsangan kepada matriks bukan-pepenjuru. Ini menjadikan penggunaan kaedah konvensional secara meluas memakan masa dan mahal.

Dalam usaha untuk mengesahkan teori yang dicadangkan, ujian statik dan dinamik keatas model telah dilakukan. Darjah kesilapan dengan menggunakan ubah bentuk anjal bagi kerangka dan simetri model semasa ujian statik menunjukkan bahawa keadaan sempadan kerangka adalah tegar dan kerangka adalah simetri. Keputusan ujian dinamik menunjukkan bahawa nilai-nilai teori dan uji kaji bagi frekuensi tabii, bentuk mod, dan mod nisbah redaman adalah menyamai diantara satu sama lain dengan baik. Gerakbalas dinamik yang dikira semasa struktur dikenakan dengan pelbagai keamatan beban dari sudut yang berbeza juga adalah menyamai dengan Permodelan Unsur Terhingga. Pengaruh magnitud nisbah redaman dalam mod yang berbeza semasa menggunakan matriks redaman ortogon boleh diabaikan. Akhir sekali, berbanding dengan kaedah konvensional, masa pengiraan yang diambil oleh kaedah yang dicadangkan adalah memadai untuk diterima.

Secara umum, pengurangan masa dan kos serta keputusan yang sangat tepat memberikan justifikasi kepada penggunaan kaedah tak langsung seperti teori pengoptimuman. Kaedah yang dicadangkan ini didapati menjadi satu teknik yang sesuai untuk meminimumkan jumlah fungsi tenaga keupayaan, terutama dalam kes-kes di mana bilangan pembolehubah yang besar dan keadaan struktur yang sangat tak linear. Kaedah yang dicadangkan mengurangkan masa pengiraan dan bilangan lelaran yang diperlukan setiap langkah masa.

ACKNOWLEDGEMENTS

First of all, I wish to express my heartfelt appreciation to my supervisors Dr Zainah Binti Ibrahim and Dr Mohammed Jameel for their invaluable support and guidance. I would also like to wish my thanks for providing precious advice during my project and sincere comments on my research work which shaped to revision.

Sincere gratitude also goes to many other people who encouraged me along the way and provided me with timely assistance.

Besides that, I would like to dedicate my deeply gratefulness and appreciation to dearest family. In particular, I was inspired by enthusiastic energy of my parents. They truly motivated me to carry on and perform the best by their words of wisdom.

I extend my apologies to anyone I may have failed to mention.

TABLE OF CONTENTS

CHAPTER 1: INTRODUCTION

1.1 Introduction 1

1.2 Problem statement 3

1.3 Proposed solution 5

1.4 Objectives 6

1.5 Scope..6

1.6 Thesis outline...7

2. CHAPTER 2: SCRUTINIZATION OF NONLINEAR OF DYNAMIC RESPONSE METHODS FOR THE ANALYSIS OF STRUCTURAL SYESTEMS

2.1 Introduction 11

2.2 The equation of motion and their solution 12

2.2.1 Hamilton's principle 12

2.2.2 D'Alembert's principle 13

2.2.3 Virtual displacement 13

2.3 The equation of dynamic motion...14

2.4 A formal assessment of nonlinear dynamic response methods 15

2.4.1 The linear acceleration method 15

2.4.2 The Wilson-θ method 19

2.4.3 The Newmark method 24

2.5 The Newmark β =0 method 29

2.5.1 Summary of analysis using the Newmark (β =0) method 30

2.5.2 Stability and accuracy of the Newmark method 30

2.5.3 The central difference method 30

2.5.4 The Fu method of dynamic analysis 32

2.5.5 Summary of the calculation procedure for Fu's method 34

2.5.6 Trujillo's method 35

2.5.7 Additional methods 37

2.6 Conclusions 38

3. CHAPTER 3: SCRUTINIZATION OF TECHNIQUES TO OPTIMIZING FUNCTIONS OF SEVERAL VARIABLES.

3.1 Introduction 40
3.1.1 Lagrange multipliers, and Euclidean space 40

3.2 Scrutinization of problems by advance mathematical...............................41

3.3 The steplength..42

3.4 Choice of descent direction 42

3.5 Gradient methods for the determination of descent directions..................44
3.5.1 The method of steepest descent 44
3.5.2 The method of conjugate gradients 46
3.5.3 The method of Newton-Raphson 47
3.5.4 The method of Fletcher-Reeves 49

3.6 Choice of method...50

3.7 Application of Fletcher-Reeves method for minimizing of strain energy of system and potential energy of loading 51
3.7.1 The expression for the total potential energy 52
3.7.2 Expression for the gradient of the total potential energy 52
3.7.3 The position of minimum total potential energy in the direction of descent 54
3.7.4 Calculation of the steplength 55
3.7.5 Iterative process for the minimization of the total potential energy 56

CHAPTER 4: PROPOSED THEORY

NONLINEAR DYNAMIC RESPONSE ANALYSIS BY MINIMIZATION OF TOTAL POTENTIAL DYNAMIC WORK

4.1 Introduction 58

4.2 Structural property matrices 61
4.2.1 The general mass determinant 61
4.2.2 The stiffness determinant for a pin jointed member 62
4.2.3 The orthogonal damping matrices 62

4.3 Theory of Fletcher-Reeves method 65
4.3.1 The total potential dynamic work (TPDW) by Fletcher-reeves method 65
4.3.2 The gradient of the total potential dynamic work 67

4.4 Minimization of the total potential dynamic work by Fletcher-Reeves method..70

4.5 Determination of the steplength 71

4.6 Calculation procedure of Fletcher-Reeves algorithm................................75

4.7 The optimization of the total potential dynamic work by Newton-Raphson method..76

CHAPTER 5: STATIC TEST

5. NUMERICAL ANALYSIS AND EXPERIMENTAL WORK 78

5.1 Introduction 78

5.2 Design and construction of the model 79

5.3 Instrumentation and Equipment...84

5.3.1 Pressure gauge 84

5.3.2 Data acquisition / logger (Type: TDS – 530 (Touch Screen)) 86

5.3.3 Strain gauge (KFG-5-120–C1-11) 87

5.3.4 LVDT: Linear variable differential transformer 89

5.3.5 Dial Indicator Metric 91

5.3.6 Weights (static loads) 91

5.3.7 Calibration of the recording equipment 92

5.3.8 Software 93

5.4 Theoretical analysis (mathematical modelling)..94

5.5 Linear Static Finite Element Analysis 94

5.6 Static testing of the model 97

5.6.1 The boundary frame 97

5.6.2 The cable net 97

5.7 Discussion and comparison of results 107

5.8 Conclusion..116

6. NUMERICAL ANALYSIS AND EXPERIMENTAL WORK

6.1 Introduction 117

6.2 Numerical analysis and experimental work 118

6.3 Theoretical analysis (mathematical modelling) 118
6.3.1 The lumped mass matrices for a pin-jointed member 118
6.3.2 The stiffness matrix for a pin-jointed member 119
6.3.3 The orthogonal damping matrices 119

6.4 Dynamic finite element analysis using Abaqus 119

6.5 Modal Testing 121
6.5.1 Spectrum, Power spectrum, and Power of a signal 122
6.5.2 Auto-spectrum, Cross-covariance, and Cross-spectrum 123
6.5.3 Coherence spectrum, Time domain, and Time Domain Measurements 123
6.5.4 Frequency response, Frequency spectrum, and Spectrum analysis 124
6.5.5 Design and construction of the model 126
6.5.6 Instrumentation and equipment 126
6.5.7 Test procedure 133
6.5.8 Modal parameter estimation 143
6.5.9 Mode shape 153
6.5.10 Procedure of modal analysis with ME'scope 154
6.5.11 Complexes Exponential 157
6.5.12 Z Polynomial 157

6.6 Parametric study on dynamic response 169
6.6.1 Comparison of the response predicted between the Fletcher-Reeves and the Newton-Raphson methods and linear dynamic response 169
6.6.2 The effect of the magnitude of modal damping on dynamic response 175
6.6.3 The size of the time step, stability and accuracy 179
6.6.4 The comparison of the natural frequencies on case study for cables 180
Figure 6.44: Visual of elements mesh. 181
6.6.5 Linear perturbation on finite element analysis 181

6.7 Conclusions 185

CHAPTER 7: CONCLUSIONS

7. CONCLUSIONS AND RECOMMENDATIONS FOR FUTURE WORK

7.1 General summary and remarks 186

7.2 Conclusion 187

7.3 Recommendations for future work 191
7.3.1 Convergency and scaling 191

7.3.2 Extension of the dynamic theory to include flexible members 192
7.3.3 Damping 193
7.3.4 Inclusion of various types of dynamic loading 194

LIST OF FIGURES

FIGURE 2.1: VISUAL EQUATION OF MOTION IN ACCELERATION METHOD. 16

FIGURE 2.2: ACCELERATION VARIATION OF NEWMARK METHOD. 28

FIGURE 3.1: GEOMETRIC REPRESENTATION OF DECENT THROUGH THE CONTOURS OF A FUNCTION OF TWO VARIABLES. 41

FIGURE 3.2: GEOMETRIC REPRESENTATION OF THE STEEPEST DESCENT METHOD FOR A FUNCTION OF TWO VARIABLES. 44

FIGURE 3.3: GEOMETRIC REPRESENTATION OF RELAXED STEEPEST DESCENT FOR A FUNCTION OF TWO VARIABLES. 45

FIGURE 3.4: GEOMETRIC REPRESENTATION OF THE FLETCHER-REEVES METHOD FOR A FUNCTION OF TWO VARIABLES.

FIGURE 3.5: VISUAL SOLUTION PROCESS FOR SYSTEM BY USING THE TANGENTIAL STIFFNESS METHOD. 47

FIGURE 3.6: VISUAL SOLUTION PROCESS FOR SYSTEM BY USING THE INITIAL STIFFNESS METHOD. 49

FIGURE 3.7: NUMBER OF MEMBER MEETING AT JOINT J. 53

FIGURE 4.1: VISUAL TOTAL POTENTIAL DYNAMIC WORK. 59

FIGURE 4.2: VISUAL OPTIMIZATION OF TOTAL POTENTIAL DYNAMIC WORK ON DESCENT DIRECTION. 59

FIGURE 4.3: CONVERGENCY IN ONE DIRECTION. 60

FIGURE 4.4:.SCHEME OF CONNECTION MEMBERS TO JOINT. 67

FIGURE 4.5: THE FLOW CHART FOR PROGRAMMING THE PROPOSED NONLINEAR DYNAMIC RESPONSE THEORY. 77

FIGURE 5.1: GRID LINES OF THE FLAT NET. 79

FIGURE 5.2: GENERAL VIEW OF THE STEEL FRAME. 80

FIGURE 5.3: STEEL COLUMNS TO SUPPORT THE FRAME. 81

FIGURE 5.4: STEEL BEAMS FITTED WITH HOLLOW CYLINDRICAL STEEL SECTIONS. 81

FIGURE 5.5: CLAMPING CABLES TO THE FRAME BY USING HOLLOW CYLINDRICAL STEEL SECTION AND WEDGE AND BARREL. 82

FIGURE 5.6: CONSTRUCTION OF BEAM STEEL. 84

FIGURE 5.7: VISUAL VIEW OF HANDLE OF PRESSURE GAUGE. 85

FIGURE 5.8: TENSIONING OF THE CABLE WITH THE PRESSURE GAUGE. 85

FIGURE 5.9: THE CHANNELS OF THE TDS-530 DATA LOGGER. 86

FIGURE 5.10: TOP VIEW OF TDS – 530 DATA LOGGER. 87

FIGURE 5.11: STRAIN GAUGE USED ON THE HOLLOW CYLINDRICAL STEEL SECTION. 88

FIGURE 5.12: STRAIN GAUGE USED ON THE WEDGE AND BARREL. 88

FIGURE 5.13: STRAIN GAUGE USED ON STEEL FRAME MADE. 89

FIGURE 5.14: LINEAR VARIABLE DIFFERENTIAL TRANSFORMER USED ON NODES. 90

FIGURE 5.15: LINEAR VARIABLE DIFFERENTIAL TRANSFORMER USED ON STEEL FRAME. 90

FIGURE 5.16: DIAL INDICATOR METRIC USED ON STEEL FRAME. 91

FIGURE 5.17:.GENERAL VIEW OF THE INTENSITIES AND PATTERN OF STATIC LOADS. 92

FIGURE 5.18: VISUAL OF ELEMENTS MESH. 95

FIGURE 5.19: DEFLECTIONS DUE TO CONCENTRATED LOAD ON JOINT 18 . 101

FIGURE 5.20: DISPLACEMENT OF MAJOR, MINOR AXES. 101

FIGURE 5.21: STRAIN OF ELEMENTS (2457, 2246, 1883, 2100, 2921). 102

FIGURE 5.22: DEFLECTIONS DUE TO CONCENTRATED LOAD ON JOINT 11. 105

FIGURE 5.23: DISPLACEMENTS OF MINOR AXIS (4, 11, 18, 25, 32). 105

FIGURE 5.24: STRAIN-TIME GRAPH OF ELEMENTS (1883, 2100, 2246, 2457, 2921). 106

FIGURE 5.25: DEGREE OF SYMMETRIC ABOUT MINOR AXIS WHEN THE LOAD IS PLACED ON NODE 16 AND 20. 107

FIGURE 5.26: DEGREE OF SYMMETRY ABOUT MINOR AXIS WHEN THE LOAD IS PLACED ON NODES 16 AND 20. 108

FIGURE 5.27: DEGREE OF SYMMETRY ABOUT CORNER OF FRAME WHEN THE LOAD IS PLACED ON NODES 16 AND 20. 109

FIGURE 5.28: DEGREE OF SYMMETRIC ABOUT MINOR AXIS WHEN THE LOAD IS PLACED ON NODES 17 AND 19. 110

FIGURE 5.29: DEGREE OF SYMMETRY ABOUT MAJOR AXIS WHEN THE LOAD IS PLACED ON NODES 17 AND 19. 111

FIGURE 5.30: DEGREE OF SYMMETRY ABOUT CORNER OF FRAME WHEN THE LOAD IS PLACED ON NODES 16 AND 20. 111

FIGURE 5.31: DEGREE OF SYMMETRY ABOUT MAJOR AXIS WHEN THE LOAD IS PLACED ON NODES 11 AND 25. 112

FIGURE 5.32:.DEGREE OF SYMMETRIC ABOUT MAJOR AXIS WHEN THE LOAD IS PLACED ON NODE 11 AND 25 113

FIGURE 5.33: DEGREE OF SYMMETRY ABOUT CORNER OF FRAME WHEN THE LOAD IS PLACED ON NODES 11 AND 25. 113

FIGURE 6.1: VISUAL OF FINITE ELEMENT STRUCTURE. 121

FIGURE 6.2: THE VISUAL GRID LINES OF THE FLAT NET. 126

FIGURE 6.3: GENERAL VIEW OF IMPACT HAMMER. 128

FIGURE 6.4: KISTLER 8776A50 CERAMIC SHEAR ACCELEROMETER. 129

FIGURE 6.5: BLOCK SCHEMATIC OF INCREMENTAL ENCODER. 130

FIGURE 6.6: FRONT VIEW OF IMC DEVICE. 131

FIGURE 6.7: BACK VIEW OF IMC DEVICE. 131

FIGURE 6.8: TOP VIEW OF CABLES AND CABLE CONNECTOR. 132

Figure 6.9: Top view of accelerometer-IMC connector device. 133

Figure 6.10: The diagrammatic layout of the experimental setup for modal testing. 134

Figure 6.11: Coherence graph and enlarged image of channel 1 based on reference 3. 136

Figure 6.12: Coherence graph of channel 1 and 2 based on references 3 and 28. 137

Figure 6.13: Excitation graph of channel 1 based on reference 3. 137

Figure 6.14: Transfer function plot for nodes 1 to 3 based on references 3. 138

Figure 6.15: Transfer function graph for node 1 based on references 3 and 28. 138

Figure 6.16: Display of the 3D cursor colour map for nodes 1–8 corresponding to reference 3. 139

Figure 6.17: Time signal graph of channel 3 based on references 3. 140

Figure 6.18: Time signal between nodes 9 and 16 corresponding references 3. 141

Figure 6.19: Harmonic cursor of excitation force for channel 5 based on reference 3. 142

Figure 6.20: The waterfall plot of time signal for nodes 25- 32 based on reference 3. 143

Figure 6.21: The Nyquist plot fundamentals. 146

Figure 6.22: Bode diagram of an FRF for node 1 based on reference 3. 148

Figure 6.23: Bode diagram of an FRF for node 1 based on reference 28. 149

Figure 6.24: CoQuad plot of an FRF for node 1 based on reference 3. 150

Figure 6.25: CoQuad plot of an FRF for node 1 based on reference 28. 151

Figure 6.26: Nyquist Plot of an FRF for node 1 based on reference 3. 151

Figure 6.27: Nyquist diagram of an FRF for node 1 based on reference 28. 152

Figure 6.28: Phase diagram of an FRF for node 3 based on reference 3. 152

Figure 6.29: Phase diagram of an FRF for node 3 based on reference 28. 153

Figure 6.30: The modal frequency and damping plot. 155

Figure 6.31: The general view of the steel construction under study. 158

Figure 6.32: Mode shape 1 of the structure. 159

Figure 6.33: Mode shape 2 of the structure. 160

Figure 6.34: Mode shape 3 of the structure. 161

Figure 6.35: Mode shape 4 of the structure. 162

Figure 6.36: Mode shape 5 of the structure. 163

Figure 6.37: Complexity plot of mode shape 1. 164

Figure 6.38: The logarithmic decrements against amplitudes of vibration. 168

Figure 6.39: The dynamic load plot based on mode shape 1. 170

Figure 6.40: The time history of dynamic load based on mode shape 1. 170

Figure 6.41: The linear and nonlinear dynamic response of joints 11, 25, 32, 39, 46, 53, and 60. 174

Figure 6.42: Build up of the amplitude of joint 32 from t=0 to steady state vibration. 174

Figure 6.43: Visual relationship between degrees of freedom and computing time. 179

LIST OF TABLES

TABLE 5.1: DETAILS AND SPECIFICATIONS OF THE STEEL FRAME. 80

TABLE 5.2: THE SPECIFICATIONS OF FLAT NET AND CABLES. 83

TABLE 5.3: DETAILS OF PROCEDURE OF FINITE ELEMENT ANALYSIS. 96

TABLE 5.4: DEGREE OF SYMMETRY ABOUT THE MAJOR AND MINOR AXES FOR JOINT 18 AND DEFLECTIONS DUE TO CONCENTRATED LOAD ON JOINT 18. 99

TABLE 5.5: DEGREE OF SYMMETRY ABOUT THE MAJOR AND MINOR AXES FOR JOINT 11 AND DEFLECTIONS DUE TO CONCENTRATED LOAD ON JOINT 11. 103

TABLE 5.6: DEGREE OF SYMMETRY ABOUT THE MINOR AXIS WHEN LOADS ARE PLACED ON NODES 4, 11, 16 , 25, AND 32. 114

TABLE 5.7:DEGREE OF SYMMETRY ABOUT THE MAJOR AXIS WHEN LOADS ARE PLACED ON NODES 16, 17, 18, 19, AND 20. 115

TABLE 6.1: THE FEATURES OF FINITE ELEMENT MODELLING. 119

TABLE 6.2: THE CORRELATION DATA BASED ON THE CONVERSION OF THE DB UNIT AND VARIABLES. 125

TABLE 6.3: SPECIFICATION AND FEATURES OF 50 G CERAMIC SHEAR ACCELEROMETER. 129

TABLE 6.4: SETUP PROCEDURE FOR MODAL TESTING WITH IMC DEVICE. 135

TABLE 6.5: THEORETICAL AND EXPERIMENTAL NATURAL FREQUENCIES. 165

TABLE 6.6: THEORETICAL AND FINITE ELEMENT RESULT OF NATURAL FREQUENCIES FOR THE FIRST FIVE MODES 167

TABLE 6.7: THE AMPLITUDE (MM) OF JOINTS 4, 11, 18, 25, 32, 39, 46, 53, 60 AT STEADY STATE VIBRATION AND PRE-TENSION OF 11500 N/LINK 171

TABLE 6.8: THE AMPLITUDE (MM) OF JOINTS 4, 11, 18, 25, 32, 39, 46, 53, 60 AT STEADY STATE VIBRATION AND PRE-TENSION OF 11500, 5500 N/LINK 173

TABLE 6.9: ASSUMED VALUES OF PERCENTAGE OF LOGARITHMIC DECREMENT FOR DAMPING. 175

TABLE 6.10: THE MAXIMUM AMPLITUDE OF JOINT 18, 25, AND 32 FOR COMPOSITE DAMPING CALCULATED BY NEWTON RAPHSON AND FLETCHER- REEVES METHOD. 176

TABLE 6.11: THE MAXIMUM AMPLITUDE (MM) OF THE JOINT SUBJECTED BY THE FLETCHER-REEVES AND NEWTON-RAPHSON ALGORITHMS. 177

TABLE 6.12: THE COMPUTATIONAL TIME (SECONDS) FOR THE MATHEMATICAL MODELS. 178

List of Symbols and Abbreviations

A Cross-sectional area of cable

C (t) Damping matrix

c Variables of damping matrix

C_{sr}, M_{sr} Elements of damping and mass matrices C and M

D_τ Energy dissipated by damping forces up to time τ

D_τ Energy dissipated by damping forces up to time τ

e $_{jn}$ Elastic elongation of member j_n

$e, \Delta e$ Elongation of a member at time τ and during time $\Delta\tau$

E Young Modulus of Elasticity

F Total forces acting on the system's particles

K (t) Stiffness matrix

k Variables of stiffness matrix

L $_{jn}$ Length of member j_n

I_τ ,m,N Inertia energy at time τ , Number of members , and degree of freedom

I The identity matrix

M x a Inertial forces that result from the total forces

M Diagonal mass matrix

P (t) Load vector

$P(\tau)_s$ *and* $P(\tau + \Delta\tau)_s$, F_s = elements of dynamic load vectors P(τ) and $P(\tau + \Delta\tau)$ at time τ and $(\tau + \Delta\tau)$ and Static load vector F

Q Number of member meeting at joint j

S $^{(k)}$ The steplength which defines the position along

S_n Step length along $[V]_n$ to the point where the TPE is minimum

$S_{(k)}$ The steplength to the point along $V_{s(K)}$, where the total potential dynamic work is a latest possible amount.

T_{MIN} Smallest natural period of a system

$T_{\circ jn}$ Initial tension in member j_n

T_{jn} The instantaneous tension in member j_n

T The axial force in the member for any position in displacement space and λ_1, λ_2, and λ3 are the corresponding direction cosines

$T_O, T, \Delta T$ Tension of primary, time τ , and during time step

U_O, U_τ Initial strain energy and strain energy at time τ

V_τ, Q_τ Potential energy of static and dynamic load at time τ

$V_{s(K)}$ The s_{th} element of descent vector, and

V_{ji} The element of the direction vector

$V_{ji(k)}$ Total potential energy

$[V]_n$ The unit descent vector

$X, \dot{X}, \ddot{X}$ Displacement, velocity and acceleration vectors

$x, \dot{x}, \ddot{x}$ Displacement, velocity, acceleration vectors foe elongation vector

ε_n The damping ratio for mode n

ω_n The frequency of mode n

n The mode number,

ϕ_n The nth mode shape vector

FRF Frequency Response Function

IRF Impulse response function

CHAPTER 1: INTRODUCTION

1.1 Introduction

The main aim of this thesis is to provide an efficient method for all aspects of the analysis of space structures. Space structures are structures which resist external actions by distributing their effects among three dimensions. Examples of space structures include multi-layer grids, braced domes, and tensile structures. The conventional analysis methods are usually direct methods which are often employed for the solution of these structures. The conventional methods for structural analysis cannot predict the response of space structures accurately and precisely. Space structures are commonly analysed by indirect methods. Indirect methods are based on the principle of convergence of energy in structures. Space structures can provide large uninterrupted covered areas such as sport centres, aircraft hangars, railway platforms, airport terminals, shopping centres, and warehouses. In mathematics, a nonlinear structure is a structure which does not follow the superposition principle. A nonlinear structural problem is a problem where the variables of the equations cannot be written as linear combinations of independent components. Hence, for the analysis of space structures under nonlinear behaviours, special techniques are required to achieve accurate results.

In the present work, an efficient method is proposed for the nonlinear dynamic analysis of space structures such as a cable-stayed bridge. The cable-stayed bridge belongs is a tension structure (Aschheim et al., 2007). Tensile steel cable is commonly used in tension structures. There are two advantages of using tensile steel in cables. Firstly, the tensile steel in cables increases the load-carrying capacity of the structure elements. Secondly, the tensile steel cables enable the use of large spans for roofs and bridges. These types of structures belong to the category of geometrically nonlinear structures and their nonlinear behaviour must be taken into account in analysis. A number of methods for the nonlinear static analysis of cable structures are investigated by Buchholdt (1982), Guo (2007), and Kaveh (2008). These researchers present theoretical analysis utilizing the continuous membrane approach. Tension structures can be presumed to be discrete systems and thereby unknown nodal variables can be obtained by solving the set of governing equations for all elements of the discrete system. The tension structure consists of a finite number of elements connected at joints or nodes. Nonlinear equations are set up for the condition of joint equilibrium in terms of joint displacements from which the equilibrium displacements can be found using an iterative process. Some researchers such as Kukreti (1989) discuss cable structures as discrete systems, but confine themselves to using variations of the Newton-Raphson method to establish static equilibrium. Other researchers such as Lopez and Yang (López-Mellado, 2002; Yang & Stepanenko, 1994) have used the steepest descent method to determine the static load equilibrium.

It is worth mentioning that the theory of nonlinear dynamic response analysis is still under development. Nevertheless, a number of methods have been developed for the dynamic response analysis of structural systems, but there are only a few methods which can be employed in nonlinear dynamic response analysis (Stefanou, Moossavi, Bishop, & Koliopoulos, 1992). In the present work, a theory for nonlinear dynamic response analysis of 3D space structures is developed based on the minimization of total potential dynamic work.

1.2 Problem statement

In general, various types of cable roof arrangements including beams, nets and grids have been investigated by previous researchers using the conventional linear method. The linear method overestimates the displacement when a structure is stiffening and underestimates the displacement when it is softening. It has been observed that when using conventional methods the number of iterations increased with the increase of degree of freedom and that these methods need large computer storage for solution of the equation of motion. The computational time in conventional methods increase with the increasing degree of freedom in the structures.

Several methods are available for the dynamic response analysis of a linear structure. The mode-superposition method has been used to comparison result in present study. However, nonlinear systems do not have fixed sets of eigenvectors and eigenvalues; instead new sets of eigenvectors and eigenvalues must be revaluated for each time step. This makes the use of the mode-superposition method very time consuming and costly. Apart from the above mentioned, the dynamic response analysis of nonlinear systems in general is based on the evaluation of the response for a series of short time intervals using different types of time integration techniques.

All the currently available methods predict the response of nonlinear assemblies by forward integration in the time domain. The methods are either implicit or explicit. They provide a numerical solution to the equation of motion set up for one interval of time. In the case of nonlinear systems, most of the methods assume that the structural properties remain constant during the interval, but revaluate them at the end and, in some cases, also in the middle of the time step. For highly nonlinear assemblies this may not be sufficient and in such cases it is important to revaluate both the stiffness and the damping during the time step. The implicit methods do usually permit continuous revaluation of stiffness and damping during the iterative process, which is necessary to establish dynamic equilibrium at the end of each time step. However, the revaluation process makes these methods more expensive to use. The difference between the explicit and implicit methods is notable.

The implicit methods offer unconditional stability at the expense of operating with relatively dense decomposed matrices when applied to linear structures, but lose the advantage of unconditional stability when applied to nonlinear systems. The explicit methods, on the other hand, have relatively less computer storage and computation requirements than implicit methods, but they are hampered by instability which limits the size of the time steps. The implicit methods when applied to nonlinear structures require the solution of a set of nonlinear equations, whereas most explicit methods require the inversion of a non-diagonal matrix if consistent mass and non-diagonal damping matrices are used. A considerable amount of information is available concerning the effect of the size of the time intervals on the stability as well as on the accuracy of different methods. However, little attention has been paid to the loss of accuracy caused by updating the stiffness at the end of each time step.

In many cases, the effect of variation of damping has been investigated but has received less attention and the stability criteria have been discussed to the smallest extent possible. For highly nonlinear structures such as cable structures the effect of assuming that stiffness remains constant during each time step can lead to a considerable degree of inaccuracy even when the time steps are small. There may not necessarily be one method for the whole time span of response, since the step-by-step integration permits switching from one method to another. For some type of structures it may be advantageous to apply one method while dynamic load is applied and another method for the continuation of response after the excitation has been ceased.

As mentioned above, one cannot determine which if any of these methods is the best unless the type of structure to be analysed is specified. Hence, it is necessary to find a common method which will be the optimum method based upon the minimization of the total potential dynamic work in order to achieve the dynamic equilibrium at the end of each time step.

1.3 Proposed solution

In the dynamic problem, the task of the analyst is to solve the differential equation arising from the equilibrium of the dynamic forces on the mass. Equilibrium of dynamic forces is established at the beginning and end of each time interval. For this reason, the devising of a proposed method which considers the establishment of each time interval for dynamic analysis under linear and nonlinear structural behaviour is necessary.

Hence, the proposed method should be applicable for the dynamic response analysis of the linear analysis and it should be possible to extend its application to the nonlinear analysis. The new sets of eigenvectors and eigenvalues for each time step for the proposed theory should not be required and stability and accuracy should be achieved. It is anticipated that the proposed theory could be used to evaluate the dynamic response analysis of nonlinear systems based on the response for a series of short time intervals.

The proposed theory should be able to converge more rapidly to the neighbourhood of the solution and achieve good accuracy cause of less iteration to achieve result. It is anticipated that that the proposed theory could be used as a new technique for minimization of total potential energy function, especially in cases where the number of variables is large. The proposed method is based on the step-by-step time integration of the equations of motion. The majority of these methods have been used to minimize the function representing the total potential energy of 3D space structures subjected to static load. The proposed theory converges more rapidly to the neighbourhood of the solution and achieves good accuracy. The present work indicates that this method is the most suitable technique for minimization of total potential energy function, especially in cases where the number of variables is large. The optimization of energy in the proposed theory achieves a decrease in computational time and in the number of iterations per time step.

1.4 Objectives

The main objective of the present work is to develop an efficient nonlinear dynamic method for the nonlinear analysis of 3D space structures with high degree of freedom. The present work develops a nonlinear dynamic response theory for the analysis of high degree of freedom structures subjected to various types of static and dynamic loading.

1.5 Scope

The proposed theory is carried out by numerical testing and experimental work as follows;

1. To carry out static tests to check boundary to be endcaster condition.
2. To assess the degree of error by elastic deformation of the frame by assuming a rigid boundary;
3. To perform static tests to check the degree of symmetry of the model;

4. To conduct static tests with different pattern and intensities of static loading in order to compare the experimental and theoretical values of the static deformation;
5. To find a damping ratio for each mode shape by the calculation of the logarithmic decrement, δ;
6. To evaluate natural frequencies and mode shapes by performing free vibration analysis;
7. To validate theoretical results of natural frequencies through comparison with experimental values;
8. To measure dynamic response due to exciting the structure by using the finite element method with different intensity from different points in order to verify the proposed theory;
9. To compare the predicted nonlinear responses with those obtained by linear modal analysis;
10. To study the influence of the magnitude of damping ratios in different modes while using an orthogonal damping matrix;
11. To compare the computational time and number of iterations of the proposed theory with those of the conventional methods;
12. To study the influence of the time step upon stability and accuracy.

1.6 Thesis outline

The proposed theory is verified with a mathematical model, analytical and in experimental work.

In chapter 2, a number of methods which are usually used for dynamic response analysis are reviewed and uniformly presented. In the review, attention is drawn to some of the problems usually associated with dynamic analysis and the possibility of extending the reviewed methods to cope with nonlinearity due to the significant changes in the geometry of structural systems. The methods reviewed are based on step-by-step time integration of equations of motion.

In chapter 3, the minimization of the total potential dynamic work and the problem of minimization for function of several variables such as the steepest descent, the Newton-Raphson, and Fletcher-Reeves methods are reviewed. The abstract mathematical problems of minimization for function of several variables also are discussed. The optimization technique aims to find a solution to problems by looking for a way to minimize a real function by methodically selecting the integer value of variables from a predefined set. The optimization theory and techniques are used widely in a real-valued objective function.

In chapter 4, a proposed theory for the nonlinear dynamic analysis of space structures is presented. The theory is based on the minimization of the total potential dynamic work. In this chapter a method is presented for predicting the nonlinear dynamic response of a space structure such as a stayed-cable bridge which is assumed to be pin-jointed. Structural property matrices such as mass matrix, stiffness matrix, and orthogonal damping are discussed. The gradient of total potential work and steplength by Fletcher-Reeves method are calculated.

The mathematical model chosen is a flat net and two chapters 5 and 6 are devoted to the verification of the proposed theory through experimental work and finite element analysis. The numerical analysis and experimental work is conducted to verify the proposed nonlinear dynamic theory.

In chapter 5 the proposed theory is verified through experimental work and a mathematical model. The mathematical model chosen is a flat net. A brief description of the type of mass, damping and stiffness matrices used in the numerical analysis are given in this chapter. In this chapter, the proposed theory is investigated through static tests. Static tests are used to check the stiffness of boundary and the degree of symmetry of the model. A static test is used to assess the degree of error by elastic deformation of the frame by assuming it is a rigid boundary. The experimental and theoretical values of the static deformation with different patterns and intensities of static loading are compared.

Chapter 6 is devoted to the verification of the proposed theory through experimental work and finite element analysis. The flat net is excited by simple harmonic loading, resulting in the measurement of natural frequencies and damping ratios in the first five modes of vibration. In this chapter, the damping for each mode shape is found by the calculation of logarithmic decrement, δ. Natural frequencies and mode shapes are evaluated by performing free vibration analysis. The theoretical results of natural frequencies are validated through comparison with the experimental values. Dynamic response due to exciting the structure by the finite element method with different intensity from different points is measured in order to verify the proposed theory. The influence of the magnitude of damping ratios in different modes while using an orthogonal damping matrix is studied. The computational time and number of iterations required by the proposed theory and conventional method are compared. The influence of the time step upon stability and accuracy is investigated.

In chapter 7, conclusions regarding the complete work are discussed along with the recommendations for future work. A solution scheme for nonlinear analysis of 3D space structures subjected to various types of dynamic loading is presented. A general conclusion is then made, namely that the proposed theory can successfully be used for the nonlinear dynamic response analysis of 3D structures with fixed boundaries.

CHAPTER 2: SCRUTINIZATION OF NONLINEAR OF DYNAMIC RESPONSE METHODS FOR THE ANALYSIS OF STRUCTURAL SYESTEMS

2.1 Introduction

The objective of this chapter is to review the methods most commonly used to predict the dynamic response of discrete nonlinear structural systems. Several methods are available for the dynamic response analysis of the linear structure. Of these the mode-superposition method is best known and most commonly used. The method can be extended to the nonlinear analysis. The new sets of eigenvectors and eigenvalues must be calculated at each time step and the stiffness matrix must be revaluated at end of each time step. This makes the use of the mode-superposition method time consuming and costly. However, a version of this method, which does not require the recalculation of the eigenvalue problem, was adopted by Avitabile (2009) and Kirsch and Bogomolni (2007) for the analysis of nonlinear stochastic systems. In general, apart from the above mentioned, the dynamic response analysis of nonlinear system is based on the evaluation of the response for a series of short time intervals using different types of time integration techniques. Basically two classes of algorithms can be identified;

A. Implicit
B. Explicit

The implicit methods are those which predict the response at the end of each time step in terms of the known variables at the beginning of the time step and the unknown variables at the end of the time step. Hence the implicit methods are trial and error producers involving either iterative schemes or the solution of simultaneous equations.

The explicit method predicts the response at the end of time step in terms of the responses at the previous time steps. They do not normally need the solution of a system of equations. In the evaluation of the structural property matrices the mass is assumed to be constant and it can usually be represented as an equivalent system of lumped masses. The damping forces are usually assumed to be viscous and the damping matrix often proportional to the mass and/or the stiffness of the structure. For the structural system with evenly distributed stiffness, a damping matrix evaluated from the knowledge of the damping ratios in the various modes can be used. The stiffness matrix of a nonlinear structure is assumed to consist of elastic and geometric term (Noels, et al., 2004).

2.2 The equation of motion and their solution

The dynamic problems don’t have a single solution like static counterparts. Instead the analyst must establish a succession of solution corresponding to all times of interest in the response period. In the dynamic problems the task of the analyst is to solve the differential equations arising from the equilibrium of the dynamic forces acting on the mass. The differential equation of motion themselves could be derived using Hamilton’s principle, the principle of virtual displacements or direct equilibration of the dynamic forces uses D’Alembert’s principle (Daston, 1979).

2.2.1 Hamilton's principle

Hamilton's principle demonstrates that the dynamics of a physical system is recognized by a variation problem for a functional corresponding a single function. The variation problem is equivalent to permit for the derivation of the various equations of motion of the physical system (Vujanovic, 1978). Hamilton's principle explains that the true evolution of a system described by generalized coordinates between two specified times. The simple example of such a problem is to achieve the curve of small length connecting two points (Synge & Conway, 2000).

2.2.2 D'Alembert's principle

The principle in writing is the total amounts resulting from the forces perform and moment on a system. It is the dynamic analogue to the principle of virtual work for applied forces in a static system (Harrison & Nettleton, 1997; Udwadia & Kalaba, 2002). The total force is written;

$$F_i^{(T)} = m_i a_i , \qquad 2.1$$

where F is the total forces acting on the system's particles

M x a are the inertial forces that result from the total forces

Interchange the inertial forces to the left side shows;

$$F_i^{(T)} - m_i a_i = 0 \qquad 2.2$$

It should be noted that the original vector equation can be recovered by recognizing displacements. This results to the formulation of D'Alembert's principle, which states that, the difference of applied forces and inertial forces for a dynamic system (Chang Jong, 2005).

$$\delta W = \sum_i (F - m_i a_i).\delta r_i = 0, \qquad 2.3$$

2.2.3 Virtual displacement

A virtual displacement (δ) is a supposed extremely small change of system coordinates occurring while time is constant. The total differential of any set of system position vectors that are functions of other variables, $\{q_1, q_2, \ldots, q_m\}$, and time, t might expressed as follows:

$$dr_i = \frac{\partial r_i}{\partial t} dt + \sum_{j=1}^{m} \frac{\partial r_i}{\partial q_j} dq_j \qquad 2.4$$

$$\delta r_i = \sum_{j=1}^{m} \frac{\partial r_i}{\partial q_j} \partial q_j \qquad 2.5$$

The equations are utilized in Lagrangian mechanics to relate generalized coordinates, q_j, to virtual work, δW (Torby & Bruce, 1984).

2.3 The equation of dynamic motion

The equation of dynamic motion for a system can be written as:

$$M\ddot{X} + C(t)\dot{X} + K(t)X = P(t) \qquad 2.6$$

where M= mass determinant

$C(t)$ = Damping matrix $K(t)$ = stiffness matrix

X = Displacement vector $\dot{X}$ = Velocity vector

$\ddot{X}$ = Acceleration vector $P(t)$ = Load vector, t= time

The solution of equation cannot be expressed in the functional form and it is necessary to plot or tabulate to solution curve point by point, beginning at (t_0 , x_0) and then at selected intervals of t, usually equally spaced, until the solution has been extended to cover the required range. Thus the solutions of the nonlinear equations require a step-by-step approach and are normally based on the use of the interpolation or the finite difference equations. The independent variable t is divided into equal intervals Δt, over the range of the desired solution. Thus the variables after n and (n+1) intervals are given by $t_n = n.\Delta t$, and $t_{n+1}=(n+1)\Delta t$ respectively. At time t_n it is assumed that the values of all the parameters as well as the values for same parameters at all previous intervals (n-1), (n-2),…..,2,1 are known. At time t_{n+1} it is assumed that the values of the variable parameters are not known and the purpose of the analysis is to find the value of x_{n+1} and its derivatives which satisfy

$$M \ddot{X}_{n+1} + C_{n+1} \dot{X}_{n+1} + K_{n+1} X_{n+1} = P_{n+1} \quad 2.8$$

In the following sections, the equations of motion for single degree of freedom system and multi degree of freedom system will be discussed.

2.4 A formal assessment of nonlinear dynamic response methods

2.4.1 The linear acceleration method

This method is based on the step-by-step time integration of the equations of motion. A method is linear change of acceleration during each time step is assumed. Equilibrium of the dynamic forces is established at the beginning and at the end of each time interval. The nonlinear nature of a structure is in accordance with the deformed state at the beginning of each time increment.

2.4.1.1 The incremental equation of motion

At time t_n and time $t_{n+1} = t_n + \Delta t$ the condition of dynamic equilibrium is as follows;

$$M \ddot{X}_{n} + C_{n} \dot{X}_{n} + K_{n} X_{n} = P_{n} \quad 2.9$$

$$M \ddot{X}_{n+1} + C_{n+1} \dot{X}_{n+1} + K_{n+1} X_{n+1} = P_{n+1} \quad 2.10$$

Since

$$X_{n+1} = X_n + \Delta X \quad 2.11$$

$$\dot{X}_{n+1} = \dot{X}_n + \Delta \dot{X} \qquad \ddot{X}_{n+1} = \ddot{X}_n + \Delta \ddot{X}$$

$$C_{n+1} = C_n + \Delta C \qquad K_{n+1} = K_n + \Delta K$$

Equation 2.9 may be written as

$$M\Delta\ddot{X}_{n+1} + c_n\Delta\dot{X}_n + k_n\Delta X_n + R_2 = R_1 \qquad 2.12$$

$$R = p_{n+1} - M\ddot{X}_n - c_n\dot{X}_n - k_n X_n \qquad R_2 = \Delta c(\dot{X}_n + \Delta\dot{X}) + \Delta K(X_n + \Delta X)$$

Equation 2.12 is the incremental equation of motion. If it is assumed that the damping and stiffness of a system remain constant during the time step the above equation is simplified as R_2 becomes zero (Stefanou, et al., 1992).

2.4.1.2 Hypothesis of integration of equation of motion

The basic assumption for solving equation 2.10 is the acceleration varies linearly during each time increment. The motion of a mass point as a result of this assumption is indicated in Figure 2.1. In this graph acceleration, velocity and displacement at any time during the time step, when τ =0 at time t n and τ =Δt at time t n+1 are given.

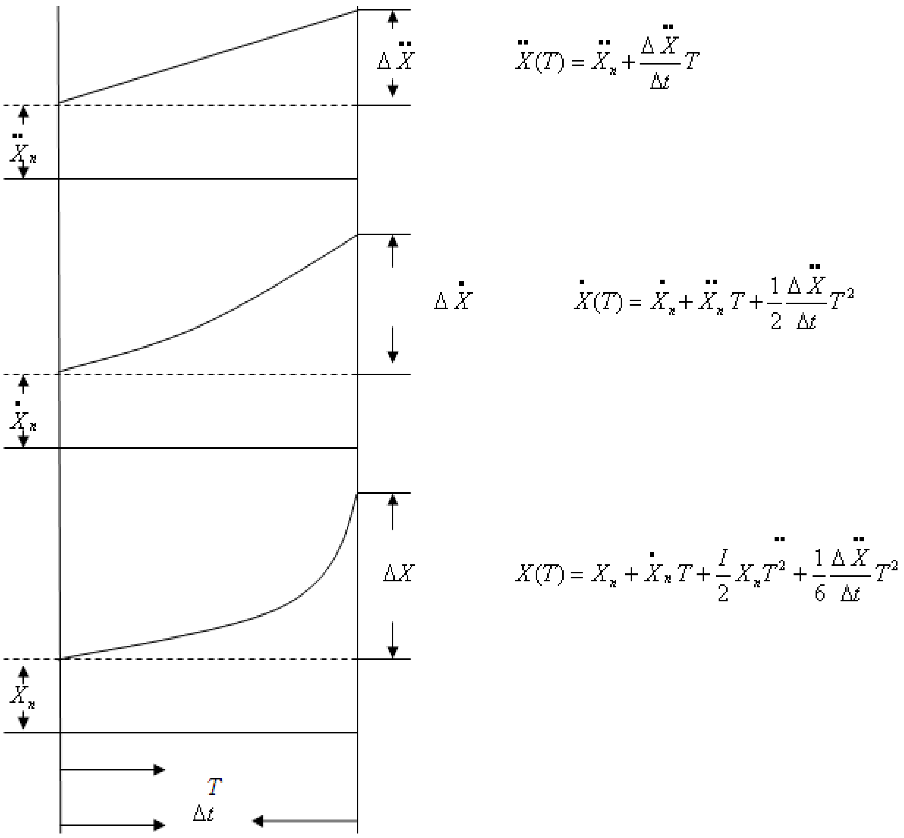

Figure 2.1: Visual equation of motion in acceleration method.

At the end of the time interval when τ=Δt results to the following expressions for the incremental velocity and displacement:

$$\Delta \dot{X} = \ddot{X}_n \Delta t + \frac{1}{2}\Delta \ddot{X} \Delta t \qquad 2.13$$

$$\Delta X = \dot{X}_n \Delta t + \frac{1}{2}\Delta \ddot{X}_n \Delta t^2 + \frac{1}{6}\Delta \ddot{X} \Delta t^2 \qquad 2.14$$

In general it has been found to be convenient to use the incremental displacement as the basic variable and hence the $\Delta\dot{X}$ and $\Delta\ddot{X}$ in terms of ΔX. rearranging equations 2.13 and 2.14 yield;

$$\Delta \ddot{X} = \frac{6}{\Delta t}\Delta X - \frac{6}{\Delta t}\Delta \dot{X}_n - 3\ddot{X}_n \qquad 2.15$$

$$\Delta \dot{X} = \frac{3}{\Delta t}\Delta X - 3\dot{X}_n - \frac{\Delta t}{2}\ddot{X}_n \qquad 2.16$$

Interchange of equation 2.15 into equation 2.16 and suppose K (stiffness) and C (damping) remain constant during the time interval leads to;

$$(m\frac{6}{\Delta t}\Delta X + \frac{3}{\Delta t}\Delta X + k_n)\Delta X = m(\frac{6}{\Delta t}\Delta \dot{X}_n + 3\dot{X}) + C_n(3\dot{X}_n + \frac{\Delta t}{2}\ddot{X}) + R_1 \qquad 2.17$$

2.4.1.3 Scrutinization of calculation procedure of acceleration method

For any given time step beginning at time t_n where the initial values of C_n, K_n, X_n, and $\dot{X}_n$ are known either from the initial conditions or from the calculations of the previous time interval, the analysis consist of the following steps;

Step 1: Calculate the value of $\ddot{x}_n$ from

$$\ddot{X}_n = \frac{1}{m}(p_n - C_n \dot{X}_n - K_n X_n) \qquad 2.18$$

Thus, unbalanced force resulting from the assumption of constant damping and stiffness during the previous step is controlled and the accumulation of the error in the acceleration from this source is avoided.

Step 2: Calculate the next value of $\Delta\dot{X}$, ΔX by solving equations 2.16 and 2.14.

Step 3: Calculate the values of X_{n+1} and $\dot{X}_{n+1}$ using equation 2.11.

The above steps complete the calculation for one time increment and then are repeated for the next interval. The supposition that the stiffness and damping remain constant during a time interval may result in inaccuracies for highly nonlinear system. In such cases an iterative method can be used to update these values during the time step in order to achieve a more correct equilibrium of the dynamic forces. If this is desirable the expression for R2 must be included in equation. 2.18, which will yield

$$\begin{aligned}&(m\frac{6}{\Delta t}+\frac{3}{\Delta t})(c_n+\Delta c)+(k_n+\Delta k)=\\&m(\frac{6}{\Delta t}\dot{X}_n+3\ddot{X}_n)+(c_n+\Delta c)(3\dot{X}_n+3\dot{X}_n+\frac{\Delta t}{2}\ddot{X}_n)-\Delta c\dot{X}_n-\Delta kX_n+R_1\end{aligned} \qquad 2.19$$

The summary of the calculation procedure in this case the values of C_n, k_n, X_n, $\dot{X}_n$ and $\ddot{X}_n$ are given by the initial conditions or from the calculation of the previous time step is as follows:

Step 1: Calculate the first estimate of Δx using equation 2.18.

Step 2: Calculate the value of $\Delta\dot{X}$ and $\Delta\ddot{X}$ using equation 2.17.

Step 3: Calculate the values of X_{n+1}, $\dot{X}_{n+1}$, $\ddot{X}_{n+1}$, C_{n+1}, K_{n+1} using equation 2.11.

Step.4: Calculate the resultant dynamic force F from

$$F=m\ddot{X}_{n+1}+c_{n+1}X_{n+1}+k_{n+1}X_{n+1}-p_{n+1} \qquad 2.20$$

If F is less than a desired value the calculation for the step complete, otherwise

Step 5: Calculate Δx from equation 2.14 and return to step 2 above.

2.4.1.4 Accuracy and stability

According to hypothesis of acceleration method that acceleration varies linearly during any time increment, the accuracy of the method depends on the size of Δt. The time step must be short enough to justify this assumption and also short enough to ensure correct representation of the loading history. The method is only conditionally stable and will diverge if Δt is greater than approximately half the period of vibration. The time step must, however, be considerably smaller than this value to provide accurate result.

2.4.1.5 The linear acceleration method to multi degree of freedom systems

When the above method is employed for the analysis of multi degree of freedom systems the derivation of the incremental equations of motion can be carried out exactly as the one for single degree of freedom systems with equation 2.8. By assuming constant stiffness and damping during the time interval. The final matrix equation by analogy with equation 2.20 will be:

$$(m\frac{6}{\Delta t}\Delta X + \frac{3}{\Delta t}\Delta X + k_n)\Delta x = m(\frac{6}{\Delta t}\Delta \dot{X}_n + 3\dot{X}) + c_n\,(3\dot{X}_n + -\frac{\Delta t}{2}\ddot{X}) + R_1 \qquad 2.21$$

In 1973, Wilson presented a general solution scheme for the dynamic analysis of an arbitrary assemblage of structural elements with both physical and geometrical nonlinearity. The scheme is unconditionally stable and therefore relatively large time steps can be used.

2.4.2 The Wilson-θ method

The Wilson-θ method is a modification of the standard linear acceleration method. The modification is based on the assumption that acceleration varies linearly over an extended computational time step τ, where $\tau = \theta.\Delta t$, this assumption leads to a set of new equations for the dynamic equilibrium at the end of the extended time interval τ. This method is a set of equations relating the accelerations, velocities and the displacement at the end of the actual time step Δt. Time step is also changed by variation of displacement at the end of the extended time step τ. The above requires the introduction of a third subscript t + τ in addition to the subscripts n and n+1 in order to identify the variable parameters at time $(t_n + \tau)$ (Harrison & Nettleton, 1997; Wilson & Callis, 2004).

2.4.2.1 The Wilson-θ method for MDOF system

The condition of dynamic equilibrium at the end of an extended time increment τ, assuming damping and stiffness remain constant during the time increment is expressed as:

$$M\ddot{X}_{t+\tau} + C_n\dot{X}_{t+\tau} + K_n X_{t+\tau} = R \qquad 2.22$$

$$\left[\frac{6}{\Delta t^2}M + \frac{3}{\Delta t}C_n + K_n\right]\Delta X = M\left[\frac{6}{\Delta t}\dot{X}_n + 3\ddot{X}_n\right] + C_n\left[3X_n + \frac{\Delta t}{2}\ddot{X}_n\right] + R_1 \qquad 2.23$$

where

$$R_1 = P_{n+1} - M\ddot{X}_n - C_n\dot{X}_n - K_n X_n \qquad 2.24$$

Calculation of ΔX involves the solution of a set of simultaneous equations as implicit methods. The method is only conditionally stable and as a rule of thumb the size of the time step should be equal to or less than half the smallest natural period of a system to avoid instability. This condition implies the calculation of a large number of steps to cover the required range of analysis. Thus unconditionally stable methods which permit the use of large time steps are likely to be more advantageous when analysing multi degree of freedom system.

2.4.2.2 Unconditionally stable linear acceleration of Wilson θ -method

Several different unconditionally stable step-by-step methods have been developed for dynamic analysis of linear and nonlinear structural system. In linear system solution a recurrence matrix solution is used. Many researchers such as Hughes (1976) investigated about Wilson-θ method by assumption of linear acceleration. For the nonlinear system, however, most of the investigations have been concerned with a particular type of structure and nonlinearity. Where r is a projected load vector given as:

$$R = P_n + \theta * \left(P_{n+1} - P_n\right) \qquad 2.25$$

And

$$\ddot{X}_{t+\tau} = \ddot{X}_n + \Delta \ddot{X}_\tau \quad , \quad \dot{X}_{t+\tau} = \dot{X}_n + \Delta \dot{X}_\tau \quad , \quad X_{t+\tau} = X_n + \Delta X_\tau$$

With above notation the analysis proceed in a similar way to that of the linear change of acceleration method. Substituting equation 2.25 in equation 2.24 will gives the incremental equation of motion for the extended time step τ .

$$M\Delta \ddot{X}_\tau + C_n \Delta \dot{X}_\tau + K_n \Delta X_\tau = R - M \ddot{X}_n - C_n \dot{X}_n - K_n X_n \qquad 2.26$$

The basic relationships arising from the assumption that the acceleration varies linearly during the extended time step are given by analogy with equation 2.26 as;

$$\Delta \dot{X}_\tau = \tau \ddot{X}_n + \frac{\tau}{2} \Delta \ddot{X}_\tau \qquad 2.27$$

$$\Delta X_\tau = \tau \dot{X}_n + \frac{\tau^2}{2} \ddot{X}_n + \frac{\tau^2}{6} \Delta \ddot{X}_\tau \qquad 2.28$$

Which when solved to express $\Delta \ddot{X}_\tau$ and $\Delta \dot{X}_\tau$ in terms of ΔX_τ yields;

$$\Delta \ddot{X}_\tau = \frac{6}{\tau^2} \Delta X_\tau - \frac{6}{\tau} \dot{X}_n - 3 \ddot{X}_n \qquad 2.29$$

$$\Delta \dot{X}_{\tau} = \frac{3}{\tau}\Delta X_{\tau} - 3\dot{X}_{n} - \frac{\tau}{2}\ddot{X}_{n} \qquad 2.30$$

Substituting equations 2.29 and 2.30 in equation 2.26 gives;

$$\left[\frac{6}{\tau^2}M + \frac{3}{\tau}C_n + K_n\right]\Delta X_{\tau} =$$

$$R - K_n X_n + M\left[\frac{6}{\tau}\dot{X}_{n} + 2\ddot{X}_{n}\right] + C_n\left[2\dot{X}_{n} + \frac{\tau}{2}\ddot{X}_{n}\right] \qquad 2.31$$

The determination of ΔX_{τ} requires the solution of a set of simultaneous equations. This is a feature of implicit methods. The setting up of the global stiffness matrix, however, is not usually necessary since the product $K_n X_n$ can be calculated. Finally the acceleration, velocity and displacement vectors at the end of the normal time step Δt are given by:

$$\ddot{X}_{n+1} = \frac{6}{\theta\tau^2}\Delta X_{\tau} - \frac{6}{\theta\tau}\dot{X}_{n} + \left(1 - \frac{3}{\theta}\right)\ddot{X}_{n} \qquad 2.32$$

$$\dot{X}_{n+1} = \dot{X}_{n} + \frac{\Delta t}{2}\left(\ddot{X}_{n+1} + \ddot{X}_{n}\right) \qquad 2.33$$

$$X_{n+1} = X_n + \Delta t\,\dot{X}_{n} + \frac{\Delta t^2}{6}\left(\ddot{X}_{n+1} + 2\ddot{X}_{n}\right) \qquad 2.34$$

These become in turn the initial vectors for the next time step. It should be noted that in the Wilson θ-method the stiffness and damping are assumed to remain constant during the extended time step and are only updated at the end of the real time increment Δt.

2.4.2.3 Scrutinization of calculation procedure of Wilson-θ method

Different calculations procedures are given for the analysis of linear and nonlinear systems together with the following values of θ to ensure unconditionally stable algorithms:

Linear systems $\theta \geq 1.37$

Nonlinear system $\theta \leq 1.37$

For nonlinear system and for any time step (n+1) where the values of C_n, K_n, X_n, $\dot{X}_n$ and $\ddot{X}_n$ are known either from the initial conditions or from the calculation of the previous step. The calculations procedure as follows:

Step 1: From the dynamic stiffness matrix $\left(K_n + \frac{3}{\tau} C_n + \frac{6}{\tau^2} M \right)$

Step 2: From the effective load vector by calculating equation 2.25.

Step 3: Calculate ΔX_τ from equation 2.28.

Step 4: Calculate the acceleration, velocity and displacement vectors $\ddot{X}_{n+1}$, $\dot{X}_{n+1}$ and X_{n+1} respectively at the end of the real time increment Δt using equations 2.32 to 2.34.

Step 5: Update the stiffness and damping matrices.

Step 6: Return to step 1 for the next time step.

2.4.2.4 Discussion of the size of the time step in Wilson-θ method

The two factors which affect the size of the time increment to be used in step-by-step integration methods are stability and accuracy. For unconditionally stable methods such as the Wilson-θ method the size of the time step is chosen only with regard to the accuracy. Hence for a given problem it is necessary to evaluate the frequency components of the dynamic load in order to select a time increment which will enable accurate representation of the loading. In highly nonlinear systems, a smaller time step is required and stability of time step is necessary to ensure sufficient accuracy. The Wilson-θ method appears to be relatively efficient when applied to the analysis of linear and slightly nonlinear systems for which the updating of the stiffness and damping matrices at the end of the time increment only are not likely to lead to large accumulation of errors. For highly nonlinear methods the efficiency of the method may be more questionable as relatively smaller time steps will be needed to ensure sufficient accuracy.

2.4.3 The Newmark method

The methods presented in previous sections were implicit and based upon the assumption of the linear change of acceleration during each time step. Hypothesis in Newmark method will indicate how much of the acceleration at the end of the interval enters into the relationships for velocity and displacement. In 1959 Newmark presented a method which permits different types of variation of acceleration to be taken into account. The main features of this method are given in the following sub-sections. The Newmark-beta method is a method of numerical integration used to solve differential equations (Bradford & Yazdi, 1999). It is used in finite element analysis to model dynamic systems. A differential equation is a mathematical equation for an unknown function of one or several variables that relates the values of the function itself and its derivatives of various orders. The Newmark-β method states that the first time derivative (velocity in the equation of motion) can be solved as,

$$\dot{X}_{n+1} = \dot{X}_n + \Delta t\, \ddot{X}_\gamma \qquad 2.35$$

where

$$\ddot{X}_{\gamma} = (1-\gamma)\,\ddot{X}_{n} + \gamma\,\ddot{X}_{n+1} \qquad 0 \le \gamma \le 1 \tag{2.36}$$

$$\dot{X}_{n+1} = \dot{X}_{n} + (1-\gamma)\Delta t\,\ddot{X}_{n} + \gamma\Delta t X_{n+1} \tag{2.37}$$

Because since the acceleration also varies with time, however, the extended mean value theorem must also be extended to the second time derivative to obtain the correct displacement. Thus,

$$X_{n+1} = X_{n} + \Delta t\,\dot{X}_{n} + \frac{1}{2}\Delta t^{2}\,\ddot{X}_{\beta} \tag{2.38}$$

where $\ddot{X}_{\beta} = (1-2\beta)\,\ddot{X}_{n} + 2\beta X_{n+1} \qquad 0 \le \beta \le 1$ 2.39

Newmark showed that a reasonable value of γ is 0.5, therefore the update rules are,

$$\dot{X}_{n+1} = \dot{X}_{n} + \frac{\Delta t}{2}(\ddot{X}_{n} + \ddot{X}_{n+1}) \tag{2.40}$$

$$X_{n+1} = X_{n} + \Delta t\,\dot{X}_{n} + \frac{1-2\beta}{2}\Delta t^{2}\,\ddot{X}_{n} + \beta\Delta t^{2}\,\ddot{X}_{n+1} \tag{2.41}$$

Setting β to various values between 0 and 1 can give a wide range of results. Typically $\beta = 1/4$, which yields the constant average acceleration in Newmark method. In current Chapter, a framework is presented for solving general problems in solid mechanics. Zienkiewicz (2005), considered several classical models for describing the behaviour of engineering materials. Each model we describe is given in a strain-driven form in which a strain or strain increment obtained from each finite element solution step is used to compute the stress needed to evaluate the internal force as well as a tangent modulus matrix, or its approximation, for use in constructing the tangent stiffness matrix.

2.4.3.1 Newmark's relationships for acceleration, velocity and displacement

Newmark method expressed the velocities and displacements at the end of a time increment in terms of the known parameters at the beginning and the unknown acceleration at the end of the time step as:

$$\dot{X}_{n+1} = \dot{X}_n + (1-\gamma)\ddot{X}_n \, \Delta t + \gamma \, \ddot{X}_{n+1} \, \Delta t \qquad 2.41$$

$$X_{n+1} = X_n + \dot{X}_n \, \Delta t + \left(\frac{1}{2} - \beta\right)\ddot{X}_n \, \Delta t^2 + \beta \, \ddot{X}_{n+1} \, \Delta t^2 \qquad 2.42$$

where γ and β are parameters which can be varied at will. The value of γ is taken to be equal to $\frac{1}{2}$ as other values will produce numerical damping. Equation 2.44 can therefore be written as:

$$\dot{X}_{n+1} = \dot{X}_n + \frac{1}{2}\ddot{X}_n \, \Delta t + \frac{1}{2}\ddot{X}_{n+1} \, \Delta t \qquad 2.43$$

In addition to the expressions for the displacement and velocities the condition of dynamic equilibrium at the end of the time interval is given by;

$$M \, \ddot{X}_{n+1} + C_{n+1} \, \dot{X}_{n+1} + K_{n+1} X_{n+1} = P_{n+1} \qquad 2.44$$

Yield the following expression for the acceleration at the end of the time step.

$$\ddot{X}_{n+1} = M^{-1}\left[P_{n+1} - C_{n+1} \, \dot{X}_{n+1} - K_{n+1} X_{n+1} \right] \qquad 2.45$$

An equation 2.44 is used for the nonlinear analysis of the structural systems by Newmark method. In general unless β is taken as zero the calculation procedure for one time increment can be summarized as in section below.

2.4.3.2 Summary of analysis using the Newmark method

Step 1: Assume value for the acceleration vector $\ddot{X}_{n+1}$ at the end of the time step.

Step 2: Compute the velocity and displacement vectors $\dot{X}_{n+1}$ and X_{n+1} at the end of the time step using equations 2.43 and 2.42.

Step 3: Update the stiffness and damping matrices.

Step 4: Calculate the acceleration vector $\ddot{X}_{n+1}$ using equation 2.45.

Step 5: Compare the computed acceleration vector $\ddot{X}_{n+1}$ with the assumed one. If these are equal or within a permissible difference the calculations for the step have been completed, if not

Step.6: Assume the last calculated value of $\ddot{X}_{n+1}$ to be the initial value in the next iteration of step 2.

The convergence of the process close to the equality of the derived and assumed acceleration (Bernard & Fleury, 2002) . The criterion of the convergence given by Newmark is the equality of the assumed and calculated values of the acceleration at the end of the time step. It is highly unlikely that all the elements in the calculated vector will be equal to the corresponding elements in the assumed vector. A convergence criterion must be included in the process. The criterion may be based upon a comparison of the values of the norm of the vectors and / or upon a comparison of the individual elements given either as a percentage or an absolute difference. The choice of type and magnitude of the permissible difference is a function of the required accuracy and is left to the experience and judgment of the analyst.

2.4.3.3 Interpretation of the parameter β

It is of interest to note how the acceleration during the time interval varies with variations in the values of β. Although it is not possible to define a relationship for all values of β but at least four values, the variation in the acceleration during the time step can be described. Three of these variations are shown in Figure 2.2.

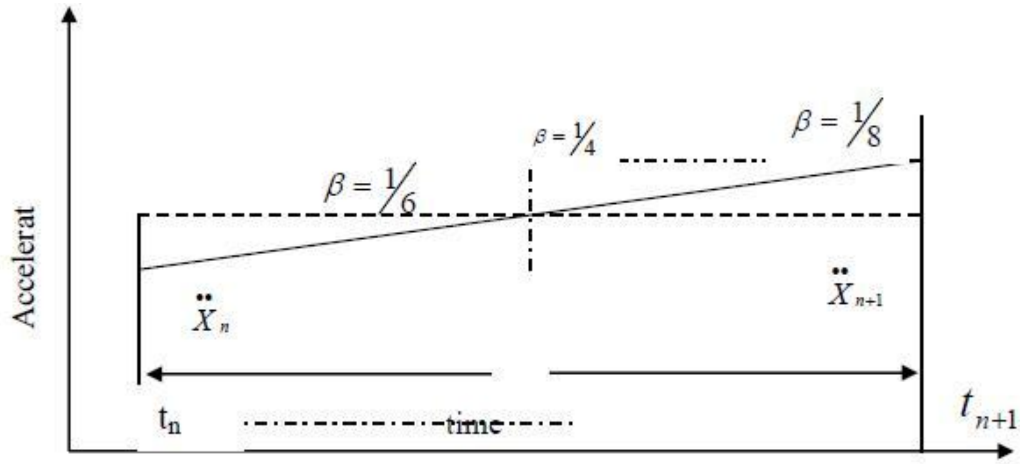

Figure 2.2: Acceleration variation of Newmark Method.

It appears that a choice of $\beta = \frac{1}{2}$ corresponds to assuming a uniform value of the acceleration during the time interval equal to the mean of the initial and final value. A value of $\beta = \frac{1}{2}$ corresponds to assuming a step function with a uniform value to the initial value for the first half of the time increment and a uniform value equal to the final value for the second half. A choice of $\beta = \frac{1}{6}$ corresponds to a linear change of acceleration during the time interval. The latter value of β results in the basic equations as developed in the standard linear acceleration method. The main difference between the two algorithms is that in the Newmark method equilibrium of the total acceleration, velocity and displacement vectors at time t_{n+1} whilst in the other equilibrium is only ensured for the incremental acceleration, velocity and displacement vectors. The latter may result in an accumulation of errors unless the acceleration is recalculated from the equations of motion at the end of the time step. The fourth value of β which can be given a physical interpretation, β =0, will be discussed in the next section (Roy & Dash, 2002).

2.5 The Newmark β =0 method

The value β =0 leads to an explicit algorithm for the Newmark method and is therefore discussed separately. When $\beta = 0$ the expression for the displacement at t_{n+1} is given as;

$$X_{n+1} = X_n + \dot{X}_n \Delta t + \tfrac{1}{2} \ddot{X}_n \Delta t^2 \qquad 2.46$$

Substituting the expression for $\dot{X}_{n+1}$ given by equation 2.51 into equation 2.27 and solving for $\ddot{X}_{n+1}$ yields:

$$\ddot{X}_{n+1} = \left[M + \tfrac{1}{2} C_{n+1} \Delta t\right]^{-1} . \left[P_{n+1} - C_{n+1} \left(\dot{X}_n + \tfrac{1}{2} \ddot{X}_n \Delta t \right) - K_{n+1} X_{n+1} \right] \qquad 2.47$$

The phrase X_{n+1} is known K_{n+1} can be calculated from the product $K_{n+1}\, X_{n+1}$. In some cases this product can be built up as a column vector without formulating the global stiffness matrix. The value of β =0 corresponds to double pulses of acceleration at the beginning and end of the time interval with each double pulse consisting of a part equal to half of the acceleration times. The time interval is occurring just before the end of the preceding interval and the other just after the beginning of the next interval.

2.5.1 Summary of analysis using the Newmark (β =0) method

With the value of K_n, C_n, X_n, $\dot{X}_n$ and $\ddot{X}_n$ given either at the end of the previous time step or from initial conditions the calculation procedure of Newmark (β =0) method for one time interval can be summed as follows:

Step 1: Calculate X_{n+1} from equation 2.46.

Step 2: Set up K_{n+1} and C_{n+1}.

Step 3: Calculate $\ddot{X}_{n+1}$ using equation 2.47.

Step 4: Calculate $\dot{X}_{n+1}$ using equation 2.43.

The above steps complete the calculations for one time interval which may now be repeated for the next step. From the above it can be seen that the calculation of $\ddot{X}_{n+1}$ as a function of Calculate C_{n+1} is only possible for cases where the damping matrix is not a function of the velocity.

2.5.2 Stability and accuracy of the Newmark method

The Newmark method is of the second order accuracy and only conditionally stable. This means that the time interval Δt must be less than a certain value to ensure stability. The size of Δt is a function of the value of β and the smallest period of vibration of a system. Recommendations with respect to the choice of values for β and the size of time intervals are given in Stochastic Newmark scheme (Bernard & Fleury, 2002).

2.5.3 The central difference method

2.5.3.1 The difference equations for acceleration and velocity

The use of difference equations for the solution of ordinary differential equations permits the transformation of the equations of motion into equations which only include the deflection ordinates at the ends of several successive time steps. Probably the most commonly used different in equations for the acceleration and velocity is those given below:

$$\dot{X}_n = \frac{1}{2\Delta t}\left[X_{n+1} - X_{n-1}\right] \qquad 2.48$$

$$\ddot{X}_n = \frac{1}{\Delta t^2}\left[X_{n+1} - 2X_n - X_{n-1}\right] \qquad 2.49$$

It leads to give the derivatives of X at the intermediate of three successive time steps.

2.5.3.2 The explicit central difference algorithm

The condition for equilibrium of the dynamic forces at time t_n is given by:

$$M\ddot{X}_n + C_n\dot{X}_n + K_n X_n - P_n = 0 \qquad 2.50$$

Substituting the expressions for $\dot{X}_n$ and $\ddot{X}_n$ given by equation 2.48 and 2.49 into equation 2.50 and solving for X_{n+1} yields:

$$X_{n+1} = \left[M + \tfrac{1}{2}\Delta t C_n\right]^{-1}\left(\Delta t^2 P_n + \left[2M - \Delta t^2 K_n\right]X_n + \left[\frac{\Delta t}{2}C_n - M\right]X_{n-1}\right) \qquad 2.51$$

Equation 2.56 predicts the displacement vector X_{n+1} at time t_{n+1} explicitly in terms of the variable parameters at time t_n and the displacement vector at time t_{n-1}. Given the displacement vectors X_{n-1} and X_n at time t_{n-1} and t_n respectively the calculation sequence for the central difference method is as follows:

Step 1: Update the damping and stiffness matrices C_{n-1} and K_{n-1} to C_n , and K_n .

Step 2: Calculate the displacement vector X_{n+1} at time t_{n+1} from equation 2.51.

Step 3: Calculate the velocity and acceleration vectors $\dot{X}_n$ and $\ddot{X}_n$ at time t_n .

Step 4: Proceed to the next interval and return to step 1. It should be noted that to start the central difference algorithm from the initial values X_O, $\dot{X}_O$ and $\ddot{X}_O$, the value of X_1 can be determined from

$$X_1 = X_O + \dot{X}_O \Delta t + \tfrac{1}{2} \ddot{X}_O \Delta t^2 \qquad 2.52$$

2.5.3.3 Stability and accuracy of the central difference method

The central difference method is only conditionally stable and requires the time intervals Δt are required to be less than twice the smallest period of a system to ensure stability (Li & Yuan, 2008). The method is of the second order accuracy as far as the step by step integration is concerned. However, the fact that the displacement vector at time t_{n+1} is calculated in terms of the dynamic load vector as well as the stiffness and damping matrices at time t_n are likely to result in a considerable degree of inaccuracy. This will particularly be so if there are any sudden changes in the dynamic forces or if the degree of nonlinearity of the system is high. For such cases, therefore, the size of the time steps may have to be considerably smaller than that dictated by stability (Rio, Soive, & Grolleau, 2005).

2.5.4 The Fu method of dynamic analysis

Fu method is published an explicit algorithm for the solution of ordinary differential equations for two dimensional wave propagation in solids, in which he presented difference equations for a two step calculation within each time interval (Telles & Carrer, 1994). When the method is applied to the structural systems, it first predicts the displacement vector and then calculates the acceleration and velocity vectors at the middle of a time step. It then predicts the displacement vector and from that calculates the acceleration and velocity vectors at the end of the time step.

2.5.4.1 The application of Fu's algorithm to nonlinear structural systems

In the middle of a time step Δt at time $t_{n+1} = \left(n + \frac{1}{2}\right)\Delta t$ Fu gives the following expressions for the displacement and vectors:

$$X_{n+\frac{1}{2}} = X_n + \frac{\Delta t}{2}\dot{X}_n + \frac{\Delta t^2}{24}\left[4\ddot{X}_n - \ddot{X}_{n-\frac{1}{2}}\right] \qquad 2.53$$

$$\dot{X}_{n+\frac{1}{2}} = \dot{X}_n + \frac{\Delta t}{4}\left[\ddot{X}_n + \ddot{X}_{n+\frac{1}{2}}\right] \qquad 2.54$$

Substituting the above expression for $X_{n+\frac{1}{2}}$ and $\dot{X}_{n+\frac{1}{2}}$ into the equation of motion of time $t_{n+\frac{1}{2}}$ and solving for $\ddot{X}_{n+\frac{1}{2}}$ yields:

$$\ddot{X}_{n+\frac{1}{2}} = \left[M + \frac{\Delta t}{4}C_{n+\frac{1}{2}}\right]^{-1}\left(P_{n+\frac{1}{2}} - C_{n+\frac{1}{2}}\left[\dot{X}_n + \frac{\Delta t}{4}\ddot{X}_n\right] - K_{n+\frac{1}{2}}X_{n+\frac{1}{2}}\right) \qquad 2.55$$

Where the damping and stiffness matrices may or may not be update at this stage, depending upon the degree of the nonlinearity of the system. At the end of the time step Δt Fu gives the expressions for the displacement and velocity vectors as:

$$X_{n+1} = X_n + \Delta t\,\dot{X}_n + \frac{\Delta t^2}{6}\left[\ddot{X}_n + 2\ddot{X}_{n+\frac{1}{2}}\right] \qquad 2.56$$

$$\dot{X}_{n+1} = \dot{X}_n + \frac{\Delta t}{6}\left[\ddot{X}_{n+1} + 4\ddot{X}_{n+\frac{1}{2}} + \ddot{X}_n\right] \qquad 2.57$$

Interchange equations 2.56 and 2.57 into equation 2.5, the equation of motion at time t_{n+1}, and solving for $\ddot{X}_{n+1}$ yields:

$$\ddot{X}_{n+\frac{1}{2}} = \left[M + \frac{\Delta t}{6} C_{n+1} \right]^{-1} \cdot \left(P_{n+1} - C_{n+1} \left[\dot{X}_{n} + \frac{\Delta t}{6} \ddot{X}_{n} + \frac{2\Delta t}{6} \ddot{X}_{n+\frac{1}{2}} \right] - K_{n+1} X_{n+1} \right) \qquad 2.58$$

The resulting explicit algorithm can take any nonlinearity into account by updating the damping and stiffness matrices both in the middle and end of a time increment.

2.5.5 Summary of the calculation procedure for Fu's method

Step 1: Calculate the predicted displacement vector at time $t_{n+\frac{1}{2}}$ using equation 2.56.

Step 2: Update the damping and stiffness matrices to time $t_{n+\frac{1}{2}}$.

Step 3: Calculate the acceleration at time $t_{n+\frac{1}{2}}$ using equation 2.58.

Step 4: Update the damping and stiffness matrices to time $t_{n+\frac{1}{2}}$.

Step 5: Calculate the velocity vector at time $t_{n+\frac{1}{2}}$ using equation 2.57.

Step 6: Proceed to the next time step and return to step1.

If X_{O}, $\dot{X}_{O}$ and $\ddot{X}_{O}$ are the initial values the procedure may be started by calculating

the value of $X_{\frac{1}{2}}$ from $$X_{\frac{1}{2}} = X_{O} + \frac{\Delta t}{2} \dot{X}_{O} + \frac{1}{8} \ddot{X}_{O} \Delta t^{2} \qquad 2.59$$

2.5.5.1 Stability and accuracy of Fu's method

The results of a stability investigation of the two variants of Fu's algorithm are presented in (Huang & Chang, 2002). The stability analysis indicates the presence of numerical damping and shows an effective stability limit of $\Delta t/2 < 0.22 T_{MIN}$, where T_{MIN} is the smallest natural period of a system. This is lower than the central difference method. The method is of fourth order accuracy, but again for highly nonlinear systems may require smaller time steps than those required to ensure the stability.

2.5.6 Trujillo's method

Trujillo presented an explicit algorithm for the dynamic response analysis of structural systems in 1977 (Trujillo, 1977) and tested the method for linear problems. For the linear undamped systems the method was shown to be unconditionally stable. An algorithm based upon Trujillo's method has been developed for nonlinear systems by Raman & Kumar but it does not take into account the effect of damping (Raman, Surya Kumar, & Sreedhara Rao, 1988).

2.5.6.1 The Trujillo algorithm

Trujillo splits the stiffness and damping matrices into upper and lower triangular forms as indicated below. The stiffness and damping matrices is given into the subscripts U and L respectively. The following algorithm is divided into a forward and a backward substitution.

Forward substitution:

$$X_{n+1/2} = \left[M + \frac{\Delta t}{2} C_L + \frac{\Delta t^2}{8} K_L \right]^{-1} \cdot \left(\left[M + \frac{\Delta t}{2} C_L - \frac{\Delta t^2}{8} K_U \right] X_n + \left[M + \frac{\Delta t}{4} \left(C_L - C_U \right) \right] \frac{\Delta t}{2} \dot{X}_n + \frac{\Delta t^2}{16} \left[P_{n+1} + P_n \right] \right) \quad 2.60$$

$$\dot{X}_{n+1/2} = \left[X_{n+1/2} - X_n \right] \frac{4}{\Delta t} - \dot{X}_n \quad 2.61$$

Backward substitution:

$$X_{n+1} = \left[M + \frac{\Delta t}{2} C_U + \frac{\Delta t^2}{8} K_U \right]^{-1} \cdot \left(\left[M + \frac{\Delta t}{2} C_U - \frac{\Delta t^2}{8} K_L \right] X_{n+1/2} + \left[M + \frac{\Delta t}{4} (C_U - C_L) \right] \frac{\Delta t}{2} \dot{X}_{n+1/2} + \frac{\Delta t^2}{16} [P_{n+1} + P_n] \right) \quad 2.62$$

$$\dot{X}_{n+1} = \left[X_{n+1} - X_{n+1/2} \right] \frac{4}{\Delta t} - \dot{X}_{n+1/2} \quad 2.63$$

An advantage of this algorithm is that, since it is restricted to the use of diagonal mass matrices only, the coefficient matrices of $X_{n+1/2}$ and X_{n+1} are obtained respectively in the upper and lower triangular forms. Thus the solution of the equations at time $t_{n+1/2}$ is reduced to forward and at time t_{n+1} to backward substitution only. Trujillo suggests two ways of splitting the stiffness and damping matrices. The first one is a symmetric splitting which satisfies the conditions:

$$K_L + K_U = K \quad ; \quad K_L = K_U^T \quad 2.64$$

$$C_l + C_u = C \quad ; \quad C_L = C_U^T \quad 2.65$$

The second way differs from the first only by the manner in which the diagonal elements are distributed. But Kumar, who extended Trujillo's work to apply to nonlinear systems, excludes damping and thus reduces the equilibrium equations at the nth step to

$$M \ddot{X}_n + R_n = P_n \quad 2.66$$

Where R_n the internal force is vector, and presents the following algorithm for the middle and the end of step:

$$\dot{X}_{n+1/2} = \left[M + \frac{\Delta t^2}{8} K_L \right]^{-1} . \left(\left[M - \frac{\Delta t^2}{8} K_L \right] \dot{X}_n - \frac{\Delta t}{2} R_n + \frac{\Delta t}{2} P_n \right) \qquad 2.67$$

$$X_{n+1/2} = X_n + \frac{\Delta t}{4} \left[\dot{X}_n - \ddot{X}_{n+1/2} \right] \qquad 2.68$$

$$\dot{X}_{n+1/2} = \left[M + \frac{\Delta t^2}{4} K_U \right]^{-1} . \left(\left[M - \frac{\Delta t^2}{8} K_U \right] \dot{X}_{n+1/2} - \frac{\Delta t}{2} R_{n+1/2} + \frac{\Delta t}{2} P_{n+1/2} \right) \qquad 2.69$$

$$X_{n+1} = X_{n+1/2} + \frac{\Delta t}{4} \left[\dot{X}_{n+1/2} + \dot{X}_{n+1} \right] \qquad 2.70$$

Nonlinearity is taken into account by updating the stiffness matrix at the end and if necessary in the middle of each time step. For nonlinear problems the algorithm loses its unconditional stability and becomes similar to the Newmark $\left(\beta = 1/4\right)$ method. The size of the time step is, however, mainly governed by the required accuracy.

2.5.7 Additional methods

Apart from those methods which were described in the foregoing sections of this chapter, there are many other methods which are in one way or another interesting and can be applied to different types of structures. The scope of this work does not permit a detailed review of all these methods, but attention is drawn to the papers of the following authors. Argyris (1979) has developed a method for linear systems which permits the use of large time steps by taking into account higher terms in the Hermetian interpolation polynomial. Kilic (2009) has used the method of dynamic relaxation to predict the static and dynamic response of cable networks, and Park (1975) has also contributed to the improvement of direct integration methods.

2.6 Conclusions

All the methods reviewed by the author predict the response of nonlinear assemblies by forward integration in the time domain. In general, the methods are either implicit or explicit provide numerical solutions to the equations of motion set up for one interval of time. They are mainly concerned with the two ends of a given interval and how to get from one end to the other, and for establishing starting values for the next time step. This is satisfactory for the methods developed for the analysis of linear systems.

In the case of nonlinear systems, most of the methods assume the structural properties to remain constant during the interval, but revaluates them at the end and in some cases also in the middle of the time step. For highly nonlinear assemblies this may not be sufficient and in such cases it is important to revaluate both the stiffness and the damping during the time step. The implicit methods do usual permit continuous revaluation of the stiffness and damping during the iterative process to establish dynamic equilibrium at the end of each time step. The revaluation process, however, makes the methods more expensive to use.

The implicit method offer unconditional stability at the expense of operating with relatively dense decomposed matrices when applied to linear structures, but lose the advantage of unconditional stability when applied to nonlinear system. The explicit methods, on the other hand, have relatively less computer storage and computation than the implicit methods, but are hampered by instability which limits the size of the time steps. The implicit methods when applied to nonlinear structures require the solution of a set of nonlinear equations whilst most explicit methods require the inversion of a non-diagonal matrix if consistent mass and non-diagonal damping matrices are used. A considerable amount of information is available concerning the effect of the size of the time intervals on the stability as well as the accuracy of the different methods.

The effect of variation of damping has attracted even less attention. In many cases the stability criteria has been discussed in the absence of damping even though for assemblies with high damping. For highly nonlinear structures such as cable and membrane structures, the stiffness is assumed to be constant during each time step. This assumption can lead to a considerable degree of inaccuracy even when the time steps are small. The degree of inaccuracy will increase as the prediction time increases. One cannot choose any of these methods as the best, unless the type of structure to be analysed is specified.

Once known problem is when the most suitable method is selected for the analysis, this may not necessarily be suitable method for the whole time span of response. Hence, the step by step integration that permits switching from one method to another method is useful to nonlinear analysis. Some types of structures it is advantageous to apply one method while dynamic loads such as sudden shocks or wind gusts are applied and another method for the continuation for response is used after the excitation has ceased.

The present method is based upon the minimization of the total dynamic work in order to achieve in accuracy result in during less time to compare conventional methods. In the following chapter, therefore, a review and a comparison are made of the relevant optimization methods in order to choose the most appropriate minimization algorithm.

CHAPTER 3: SCRUTINIZATION OF TECHNIQUES TO OPTIMIZING FUNCTIONS OF SEVERAL VARIABLES.

3.1 Introduction

In this chapter, the techniques used for minimization of functions of several variables will be discussed. The first optimization technique known is steepest descent. The optimization technique find solution of problems in which it minimizes a real function by integer value of variables from within permission set. The optimization theory and techniques use a real-valued objective function.

3.1.1 Lagrange multipliers, and Euclidean space

The Lagrangian is defined as that which appears under the action integral. In the viewpoint of optimization technique, the method of Lagrange multipliers supplies a strategy for searching the minimum of a function subordinate constraint(Ha, 2005). In mathematics, Euclidean space applies to three-dimensional space of Euclidean geometry. In modern mathematics, it is more common to define Euclidean space using Cartesian coordinates. The result is always a real number (Celebi, et al., 2009; Qi, et al, 2002). Differential geometry of curves is the branch of geometry that deals with smooth curves in the Euclidean space by methods of differentials. The special case of the theory, response to static load is employed to demonstrate the application of the chosen method of minimization. This also enables the presentation of the algorithm for static analysis in line with the forthcoming dynamic theory.

3.2 Scrutinization of problems by advance mathematical

In general the problem of minimization of function of several variables can be stated as:

$$\begin{cases} \text{Minimize} & w = F(X) \equiv f \\ \text{Subject to} & F_i(X) = b_i \quad (i = 1, 2, \ldots, m) \quad m < n \end{cases}$$

Where $X = [X1, X_2 \ldots X_n]$ represents a point in an n-dimensional Euclidean space. The problem is reduced to that of locating an unconstrained minimum of the function f. In such case: $W^* = F(X^*)$ is said to be the global minimum of F(X) at $X = X^*$ if $F(X^*) \leq F(X)$ for all X (Doltsinis & Kang, 2004; Farshi & Alinia-ziazi, 2010). The majority of available methods attempt to locate the unconstrained minimum of a function by generating a set of estimates, each of is intended to nearer to the solution than all previous ones. Figure 3.1 shows geometric representation of decent through the contours of a function of two variables.

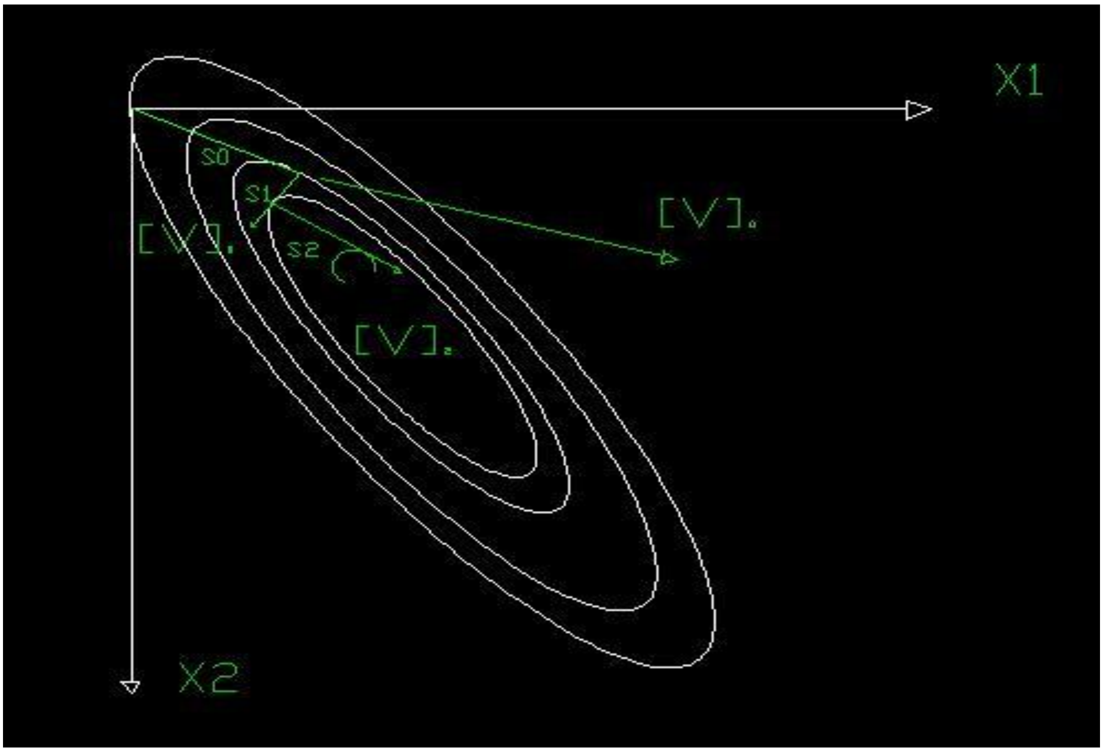

Figure 3.1: Geometric representation of decent through the contours of a function of two variables.

Typically, the position of a new point is found by an iterative process according to the formula:

$$X_{k+1} = X_k + S_k V_k \qquad 3.1$$

where V is a descent direction vector,
S is the steplength, and
K is the iteration number.

3.3 The steplength

The steplength S which defines the position along V, where W is a minimum can usually be determined by:

$$\partial f(X_{k+1}) / \partial X_{k+1} = 0 \qquad 3.2$$

However, the computational effort involved is high and it may sometimes prove more advantageous to calculate S. The steplength is only at selected points or attempt to set bounds on its value rather than to evaluate it exactly. The calculation of the steplength depends on the method of minimization and it is a compromise between the numbers of iterations. The computational efforts involved in each one from iteration and the obtainable accuracy. The term steplength implies that the descent vector V is normalized, although this is not explicitly required in the resulting algorithms.

3.4 Choice of descent direction

The descent method can be classified according to the way in which the descent direction V is found. The descent direction can either be calculated from the values of the function alone, or form values of the function together with values of its partial derivative. The descent direction can also be calculated by the additional information gained from the second partial derivative of the function. In general the methods using the second partial derivatives require less iteration than those relying on the values of the first derivative, but they clearly involve more computation per iteration. Minimization method according to all aspects can further be classified. The information gained in previous iterations is used to calculate the next descent direction. A brief description featuring the outline of the three major classes of methods appear below.

Direct search methods, (C_0- methods) are methods which rely only on evaluation of F(X) at a sequence of point X_1, X_2 … in order to reach the minimum point $X*$. These methods are normally used when the function f is not differentiable. These methods are also subjected to random error or the derivatives are discontinuous.

First order methods (C_1- methods) are methods which make use of the first partial derivatives of the function f for calculation of the descent vector. The existence and continuity of the first partial derivative of f, and g, is essential for this class of methods. Examples of such methods are the method of steepest descent, the method of conjugate gradients and the method of Fletcher-Reeves.

Second order methods (C2- methods) are methods which require the second partial derivatives as well as the first derivative of f. C2- methods are suitable for minimization of functions which can be differentiated twice and in which both derivatives are continuous. Hence, the second partial derivative of a function of several variables is a matrix. These classes of methods require considerable computer storage. The best example of this type of methods is the Newton-Raphson method.

3.5 Gradient methods for the determination of descent directions

The present work represents only these methods which in general are suitable for minimization of potential dynamic work.

3.5.1 The method of steepest descent

This method is characterized by using the negated value of the first partial derivative or gradient of the descent vector. The gradient g can be constructed from:

$$g_i \equiv g(x_i) = \partial f(x)/\partial x_i \qquad i = 1,2,\ldots,n \tag{3.3}$$

And has the Euclidean norm

$$R = (\sum_{i=1}^{n} g_i g_i)^{1/2} \tag{3.4}$$

The direction of steepest descent is given by:

$$V = -g \tag{3.5}$$

The process of minimization is carried out by successive approximation to the location of the minimum value of V in equation 3.1 until R $\leq$ ε, where ε a given tolerance or some other convergency criterion is reached, Figure 3.2.

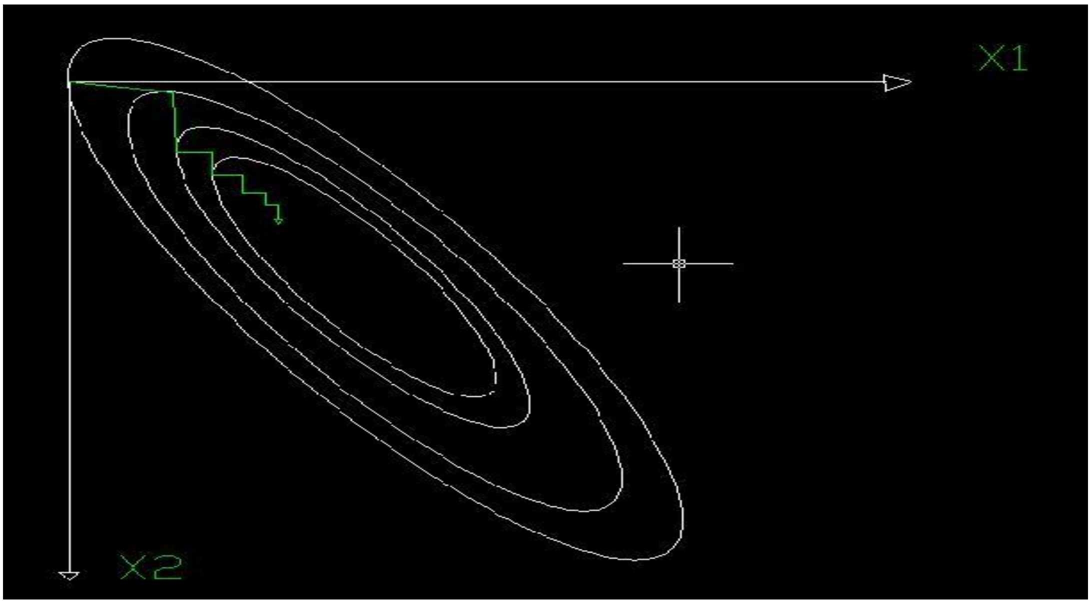

Figure 3.2: Geometric representation of the steepest descent method for a function of two variables.

Figure 3.3 show Geometric representation of relaxed steepest descent for a function of two variables. The resulting oscillatory movement toward the minimum makes the method rather slow.

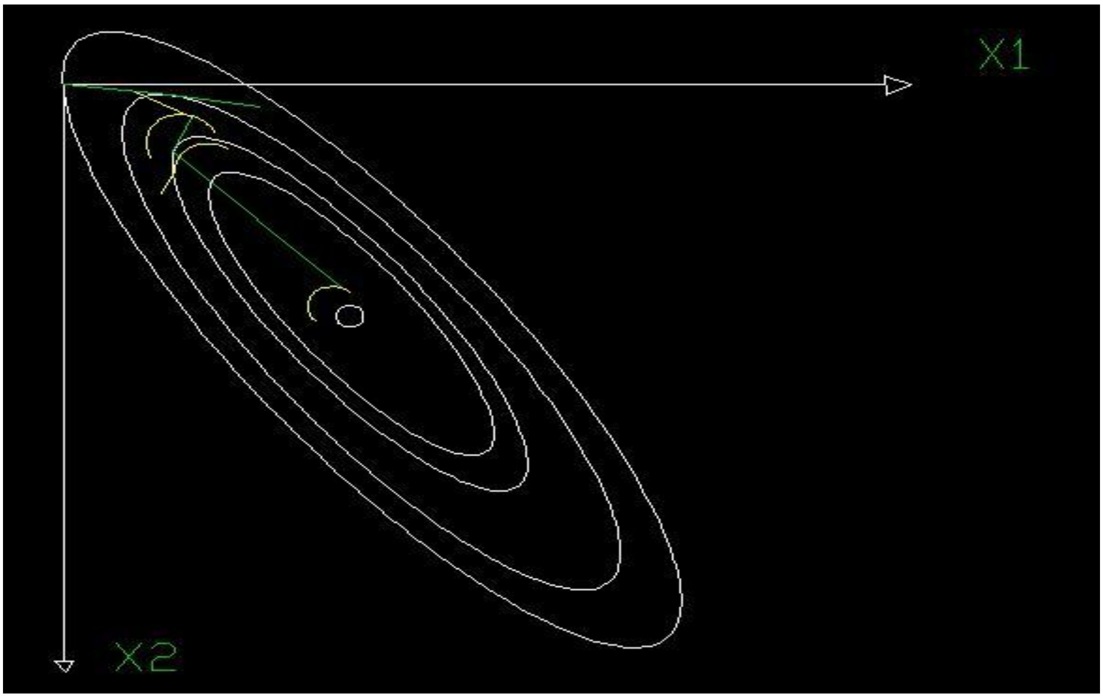

Figure 3.3: Geometric representation of relaxed steepest descent for a function of two variables.

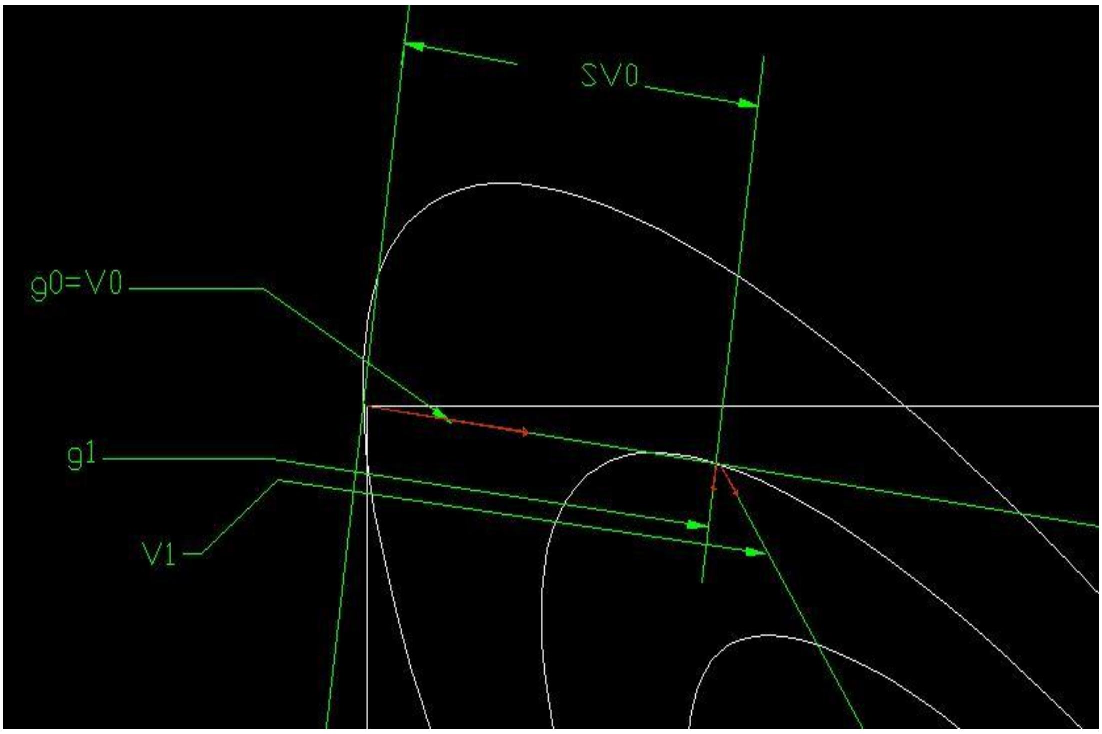

Figure 3.4: Geometric representation of the Fletcher-Reeves method for a function of two variables

The rate of convergency can however be improved by relaxation of the steplength S, in which case the steplength in each iteration is given by h*S instead of S, where 0 < h < 1.0. Geometric representation of relaxed steepest descent for a function of two variables is shown in Figure 3.4 If a relaxation factor is used, equation 3.1 may be written as:

$$X_{k+1} = X_k + h \quad S \quad V_k \qquad 3.6$$

The steplength (S) is either calculated by using the relation given by equation 3.2 or estimated in some other way.

3.5.2 The method of conjugate gradients

The minimization algorithm behaves efficiently in the case of functions of higher order when using conjugate gradient method (Ademoyero, et al., 2004; Yuan, Lu, & Wei, 2009). This serves as a motive for investigating methods developed for the solution of system of linear equations. The conjugate gradients summarize as follow; A set of direction vectors V are said to be conjugate or K-conjugate (k being a positive definite matrix) if:

$$V_i^T = K \quad V_i = 0 \quad i \neq j \ , \ (i, j = 1,2,..., n) \qquad 3.7$$

It can be shown that descent vectors at the k^{th} and $(k+1)^{th}$ iteration, V_k and V_{k+1} satisfy the condition (Babaie-Kafaki, et al., 2001) as follows;

$$V_{k+1}^T \quad K \quad V_k = 0 \qquad 3.8$$

Then $V_k^T (g_k - g_{k+1}) = 0$ And $V_k^T (g_{k+1} - g_k) = 0$

The descent vector V at the (k+1)th iteration is determined by a family of linear combinations of $-g_{k+1}$ and V_k . It is given by:

$$V_{k+1} = -g_{k+1} + \beta_k \quad *V_k \qquad 3.9$$

The most commonly used expression for beta is given by Fletcher and Sorenson (Fletcher, 1972; Sorenson, 1969) and further stated by Fletcher and Reeves as:

$$\beta_k = \frac{g_{k+1}^T \; g_{k+1}}{g_k^T g_k} \tag{3.10}$$

The solution is processed for a single degree of freedom system by using the tangential stiffness method. Visual solution process for system by using the tangential stiffness method is given Figure 3.5.

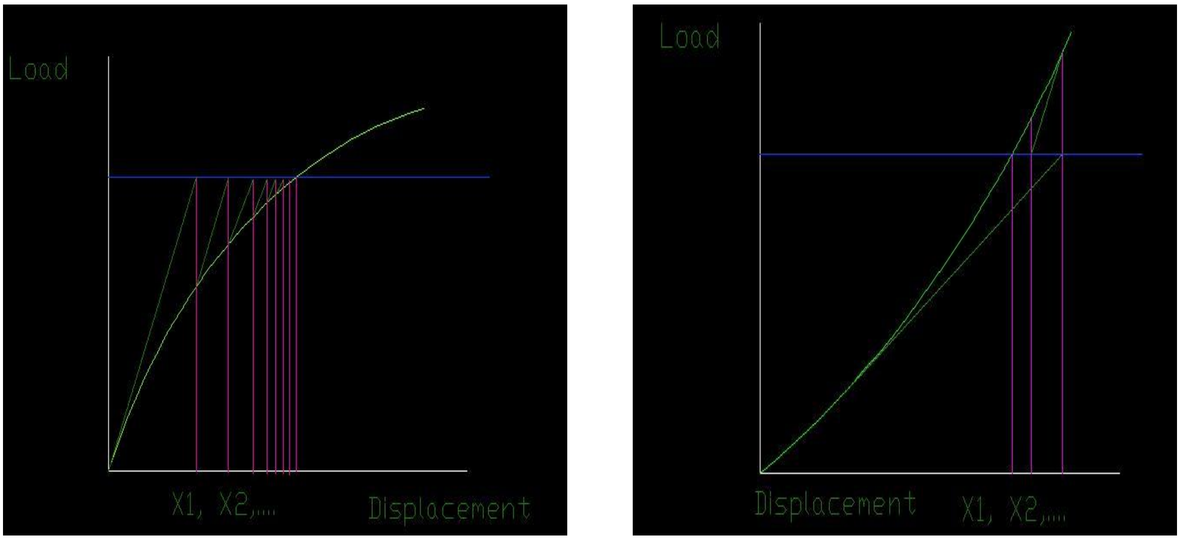

(a) Stiffening System (b) Softening system

Figure 3.5: Visual solution process for system by using the tangential stiffness method.

This solution process is for a single degree of freedom system by using the tangential stiffness method.

3.5.3 The method of Newton-Raphson

The basic idea behind this method is to approximate the given function to a quadratic in each iteration and then use the minimum of this quadratic X_t as the starting point for the next iteration. Equations 3.1 and 3.9 provide the basic algorithm for function minimization by the method of conjugate gradients. Another expression for β to be used for nonlinear functions is given by Yuan (2009) as:

$$\beta_k = \frac{g_{k+1}^T (g_{k+1} - g_k)}{g_k^T g_k} \qquad 3.11$$

At the k_{th} iteration, function f can be approximated to a quadratic in the neighborhood of $X_t = X_k$ as:

$$f_k \equiv f\left(x^t\right) \approx \tfrac{1}{2}\left[x^t - x_k\right]^T k\left[x^t - x_k\right] + \left[x^t - x_k\right]^T g_k \qquad 3.12$$

Where k is the Hessian matrix whose (i, j) th element is found from $\partial^2 f / \left(\partial x_i \partial x_j\right)$.

Now if X_k has a minimum at $X_t = X*$, then for

$$X^* - X_k = \delta X \qquad 3.13$$

Using Taylor's series and ignoring cubic and higher order terms, the gradient at the (k+1) th iteration can be written as:

$$g_{k+1} - g_k = \left[\partial^2 f / \partial X_i \partial X_j\right]_k \cdot \partial X \qquad 3.14$$

The Newton-Raphson method uses $X*$ as the next point, hence $g_{k+1}=0$ and equation 3.14 becomes

$$\delta X = -\left[k_k\right]^{-1} g_k \qquad 3.15$$

The iterative formula for the process of minimization is given as:

$$X_{k+1} = X_K + \delta X \qquad 3.16$$

Substituting the expression for δX given by equation 3.15 into equation 3.16 yields

$$X_{K+1} = X_k - \left[k_k\right]^{-1} g_k \qquad 3.17$$

The criterion of convergency is that $X_k = X_{k+1}$ or that their differences $-\left[k_k\right]^{-1} g_k$ become negligible. The process of minimization by the Newton-Raphson method, described above is normally termed as the tangential stiffness method. For nonlinear problems, it requires the updating and inversion at each iteration (Gopalakrishna & Greimann, 1988; Thai & Kim, 1977). The solution process for a single degree of freedom system is illustrated in Figure 3.6.

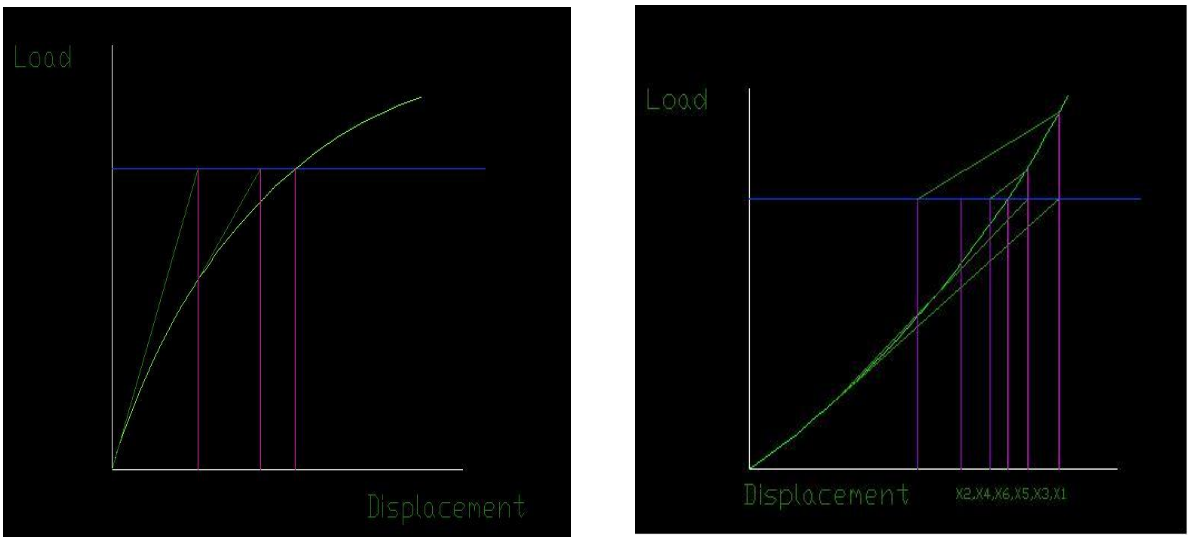

(a) Stiffening System (b) Softening system

Figure 3.6: Visual solution process for system by using the initial stiffness method.

This solution process is for a single degree of freedom system by using the initial stiffness method.

A variation of the above method is the initial stiffness method, in which the tangential stiffness matrix is replaced, at all iterations by the initial stiffness matrix. In this case a complete solution of equation is required for the first iteration. This reduces the computational effort significantly although the number of iterations may be larger than that of the tangential stiffness method. The initial stiffness method can be shown to be convergently more stable than the tangential stiffness method (El-Beltagy & Keane, 1999; Gloeckner, et al., 1976).

3.5.4 The method of Fletcher-Reeves

This method was originally devised by Davidon and later improved by Fletcher and Powell and finally is updated by Reeves. The method avoids explicit construction and inversion of the Hessian matrix k, by using the iterative formula (Wang & Lian, 2006):

$$X_{K+1} = X_k - H_k g_k \tag{3.18}$$

Where

$$H_k = I + \sum_{i}^{k-1} A_i \tag{3.19}$$

And

$$A_i = \frac{V_i V_i^T}{V_i^T x_i} - \frac{H_i \gamma_i \gamma_i^T H_i}{\gamma_i^T H_i \gamma_i} \tag{3.20}$$

And

$$\gamma_i = g_{i+1} - g_i \tag{3.21}$$

In the first iteration H_i = I, the identity matrix. Thus the first step is in the direction of steepest descent. V is descent vector and x is displacement. The slow convergency of the steepest descent method interchanges to overcome by choosing the sequence of H such that as i approach k, H_k becomes approximately equal to k^{-1}. In linear problems, the method converges in n+1 steps in which case H_{n+1} = k^{-1}. In the nonlinear problems, approximately n iterations of equation 3.18 are required to avoid one inversion of the instantaneous stiffness matrix in the Newton-Raphson method.

3.6 Choice of method

The number of methods described in previous section been employed by different researchers to minimize the total potential energy function. The behaviour of each method has been extensively investigated and compared with each other. Buchholdt (1982) in his initial work on cable structures used both the direct and relaxed steepest descent methods and found them to be inefficient in term of computational time. Gopalakrishna (1988) and other have used the Newton-Raphson method with and without modifications, to solve the resulting set of nonlinear equations for cable beams and nets. Thi (1977) also used the Newton-Raphson method to minimize the total potential energy function. He found that method converged rapidly near the solution, but that a slow start made it rather costly to use because of the matrix inversion or complete solution of equations required at each one per iterations. Hence, Newton-Raphson method when applied to function with a larger number of variables requires considerable computer storage to store the Hessian matrix (Buchholdt & Moossavinejad, 1982).

In present work, the Fletcher-Reeves formulation of the conjugate gradient method for minimization of the energy function is presented and comparison with the Newton-Raphson method is done. A more detailed comparative study of minimization techniques will been carried out by this work for finding Fletcher-Reeves method to be one of the most suitable techniques for minimizing the total potential energy function of space structures especially where the number of variables is large. This method pointed out that this new algorithm converges more rapidly to the neighborhood of the solution.

3.7 Application of Fletcher-Reeves method for minimizing of strain energy of system and potential energy of loading

In the following the minimization of the total potential energy function is demonstrated by utilizing of the Fletcher-Reeves method and a new algorithm for dynamic analysis is developed.

3.7.1 The expression for the total potential energy

The total potential energy of a loaded pre-tensioned cable assembly is given by as: W=U+V 3.22

Where

W= the total potential energy

U= the strain energy of the system

V= the potential energy of the loading

Taking the unloaded position of the assembly as datum,

$$W = \sum_{n=1}^{m} U_n + \sum_{j=1}^{j} \sum_{i=1}^{3} F_{ji} X_{ji} \qquad 3.23$$

Where

M= total number of members,

J= total number of cable joints,

Fji= external applied load on joint j in direction i, and

Xji= displacement of joint j in direction i.

The condition for structural equilibrium is that the minimum of total potential energy of the system and it is written as;

$$\partial W / \partial X_{ji} = 0 \quad (j = 1,2,\ldots j) \,\&\, (i = 1,2,3) \qquad 3.24$$

Thus at the solution the gradient vector of the total potential energy function is zero.

3.7.2 Expression for the gradient of the total potential energy

Differentiating equation 3.23 with respect to X_{ji} gives the g_{ji} element of the gradient vector g as;

$$g_{ji} = \partial W / \partial X_{ji} = \sum_{n=1}^{q} \partial U_n / \partial X_{ji} - F_{ji} \qquad 3.25$$

Let

$T_{\circ jn}$ = the initial tension in member jn,

T_{jn} = the instantaneous tension in member jn,

e_{jn} = elastic elongation of member jn,

E = Young Modulus of Elasticity,

A = cross-sectional area of cable,

L_{jn} = length of member jn, and

Q = number of member meeting at joint j as shown in Figure 3.7.

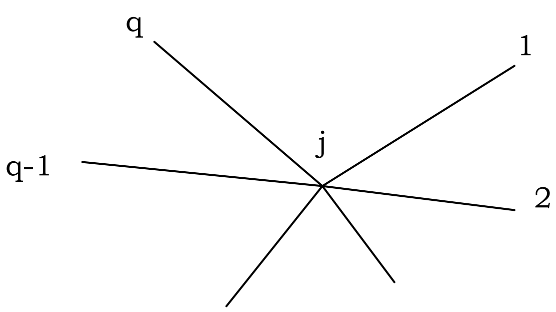

Figure 3.7: Number of member meeting at joint j.

The expression for g_{ji} can then be written as:

$$g_{ji} = \sum_{n=1}^{q} \frac{\partial U_n}{\partial e_{jn}} . \frac{\partial e_{jn}}{\partial X_{ji}} - F_{ji} \quad 3.26$$

The strain energy of member j_n is given as:

$$U_{jn} = T_{\circ jn} e_{jn} + \frac{EA}{2L_{jn}} e_{jn}^2 \quad 3.27$$

Differentiating U_{jn} with respect to e_{jn} yields

$$\partial U_{jn} / \partial e_{jn} = T_{\circ jn} + \frac{EA}{L_{jn}} e_{jn} = T_{jn} \quad 3.28$$

The initial and elongated length of member j_n may be expressed as:

$$L_{jn}^2 = \sum_{i=1}^{3} (X_{ni} - X_{ji})^2 \quad 3.29$$

$$(L_{jn}+e_{jn})^2=\sum_{i=1}^{3}(X_{ni}-X_{ji}+x_{ni}-x_{ji})^2 \qquad 3.30$$

Where X_{ji} is the coordinate of joint j in direction i. Simplifying equation 3.30 and substituting for L_{jn} from equation 3.29 yields the following expression for e_{jn}:

$$e_{jn}=\frac{1}{2L_{jn}+e_{jn}}\sum_{i=1}^{3}\{(X_{ni}-X_{ji})(2X_{ni}-2X_{ji}+X_{ni}-X_{ji})\} \qquad 3.31$$

Differentiating equation 3.30 with respect to X_{ji} yields

$$\partial e_{jn}/\partial X_{ji}=\frac{-1}{L_{jn}+e_{jn}}(X_{ni}-X_{ji}+X_{ni}-X_{ji}) \qquad 3.32$$

Substituting equations 3.28 and 3.32 into equation 3.26 yields the expression for the gradient as:

$$g_{ji}=-\sum_{n=1}^{q}t_{jn}(X_{ni}-X_{ji}+X_{ni}-X_{ji})-F_{ji} \qquad 3.33$$

Where $t_{jn}=T_{jn}/(L_{jn}+e_{jn})$ is the tension coefficient of member j_n.

3.7.3 The position of minimum total potential energy in the direction of descent

The correct value of X for which W is a minimum i.e., g=0 can now be found by the iterative process

$$X_{ji(k+1)}=X_{ji(k)}+S_{(k)}V_{ji(k)} \qquad 3.34$$

Where the suffices (k) and (k+1) denote the (k)th and (k+1)th iteration respectively.

V_{ji} = the element of the direction vector.

$S^{(k)}$ = the steplength which defines the position along $V_{ji(k)}$ where the total potential energy is a minimum.

The expression for V_{ji} when Fletcher-Reeves formulation of the conjugate gradients method is used, given by:

$$V_{ji(k)} = -g_{ji(k)} + \frac{\sum_{j=1}^{J}\sum_{i=1}^{3} g_{ji(k)} g_{ji(k)}}{\sum_{j=1}^{J}\sum_{i=1}^{3} g_{ji(k-1)} g_{ji(k-1)}} V_{ji(k-1)} \qquad 3.35$$

The stationary point in the direction of descent can be found by expressing the total potential energy as a function of the steplength along V_{ji}. Thus the required value of S $^{(k)}$ can be determined by the condition

$$\partial W_{(k)} \big/ \partial S_{(k)} = 0 \qquad 3.36$$

3.7.4 Calculation of the steplength

The required polynomial for steplength is found by substituting the expression for $X_{ji(k+1)}$ given by equation 3.34 into a suitable expression for the total potential energy W. Writing the strain energy term in equation 3.27 as a function of the elongation, equation 3.31, and at the same time substituting for X_{ji} using equation 3.34 lead to first expression for the elongation. It is written as;

$$e_{jn} = \frac{1}{2L_{jn} + e_{jn}} (a_1 + a_2 S + a_3 S^2) \qquad 3.37$$

Where

$$a_1 = \sum_{i=1}^{3} (2(x_{ni} - x_{ji})(x_{ni} - x_{ji}) + (x_{ni} - x_{ji})(x_{ni} - x_{ji}))$$

$$a_2 = \sum_{i=1}^{3} 2((x_{ni} - x_{ji} + x_{ni} - x_{ji})(v_{ni} - v_{ji}))$$

$$a_3 = \sum_{i=1}^{3} (v_{ni} - v_{ji})^2$$

And secondly to the expression for W in terms of the steplength S and its derivative with respect to S as given below:

$$W = C_1 S^4 + C_2 S^3 + C_3 S^2 + C_4 S + C_5 \qquad 3.38$$

$$\partial W / \partial S = 4C_1 S^3 + 3C_2 S^2 + 2C_3 S + C_4 \qquad 3.39$$

Where

$$C_1 = \sum_{n=1}^{m} \left(\frac{EA}{2L(2L+e)^2} a_3^2 \right)_n$$

$$C_2 = \sum_{n=1}^{m} \left(\frac{EA}{L(2L+e)^2} a_2 a_3 \right)_n$$

$$C_3 = \sum_{n=1}^{m} \left(\frac{T_\circ}{2L+e} a_3 + \frac{EA}{2L(2L+e)^2} (a_2^2 + 2a_1 a_3) \right)_n$$

$$C_4 = \sum_{n=1}^{m} \left(\frac{T_\circ}{2L+e} a_2 + \frac{EA}{L(2L+e)^2} a_1 a_2 \right)_n - \sum_{j=1}^{J} \sum_{i=1}^{3} F_{ji} V_{ji}$$

$$C_5 = \sum_{n=1}^{m} \left(\frac{T_\circ}{2L+e} a_1 + \frac{EA}{2L(2L+e)^2} a_1^2 \right)_n - \sum_{j=1}^{J} \sum_{i=1}^{3} F_{ji} X_{ji}$$

3.7.5 Iterative process for the minimization of the total potential energy

The iterative process for the minimization of the total potential energy can be summarizes as follow:

a) Assumptions of a zero value for the displacement vector X.

b) Calculation of the gradient vector g for the assembly from equation 3.33.

c) Calculation of the Euclidean norm of g from $R = \left[g^T g \right]^{1/2}$.

If R is less than a predetermined value, or less than a percentage of the norm of the first gradient, then last calculated value of X is the solution and the iteration process is terminated, otherwise proceed with next step.

d) Calculation of the direction vector (V) from equation 3.35.

e) The direction vector (V) in the first iteration $V = -g$

f) Calculation of the parameters $a_1, a_2 \; a_3$ from equation 3.37.

g) Calculation of the coefficients C_1 to C_5 from equations 3.39.

h) Determination of the value of S by equation 3.36.

i) Calculation of the displacement vector, X from equation 3.34.

j) Calculation of elongation of each member either from equation 3.31

k) Determination of new tension in each member from $T = T_\circ + \frac{EA}{L} e$.

l) Return to step 2 above for the next iteration.

CHAPTER 4: PROPOSED THEORY

NONLINEAR DYNAMIC RESPONSE ANALYSIS BY MINIMIZATION OF TOTAL POTENTIAL DYNAMIC WORK

4.1 Introduction

In this chapter, a method for predicting the nonlinear dynamic response of space structure such as stayed-cable bridge is presented. The cable structures are light and flexible and they undergo appreciable deflections when subjected to external loading. It is also noted that the method of structural analysis should consider the changes of geometry of structures. Hence, the classical linear theories of structural mechanisms cannot be used for the solutions of highly nonlinear structures because high nonlinear structure has maximum changes of geometry and classical theories could not support high nonlinearity behaviour of structure (Wang, Lin, & Tang, 2002; Stefanou & Nejad, 1995).

The numerical example considers is a 7x5 flat net with 105 degrees of freedom. The 7*5 net was also built as an experimental model and tested in order to verify the static and dynamic nonlinear theories. The construction of the experimental model and the results of the tests are given in the next chapters. The cable structures endure significant geometrical displacements particularly for non-symmetrical loading. The proposed method may be used for analysing structures with high degree of freedom and it is able to cope with the inherent nonlinearity of the problem. One of the common methods is Newton-Raphson method and it involves the use of the instantaneous stiffness matrix which has been investigated treating cable structures as discrete system. However, the proposed theory based on Fletcher-Reeves can be achieved in the analysis by minimizing the Total Potential Energy (TPE) of the structural assembly using an iterative procedure. A TPE of a three dimensional structure such as space structure is represented in Figure 4.1 All the points on contour line represent the displacements for which the TPE is constant (Stefanou & Nejad, 1995). The minimum TPE position can be achieved by moving down the energy surface in a given direction until the TPE is a minimum in that direction. The optimization of TPE on descent direction is shown in Figure 4.2. Thus the displacement vector at the (K+1)th iteration is give as;

$$[x]_{n+1} = [x]_n + S_n[\upsilon]_n \qquad 4.1$$

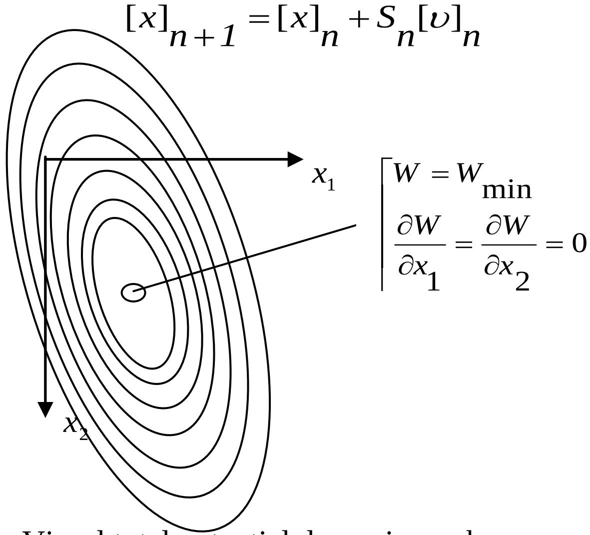

Figure 4.1: Visual total potential dynamic work.

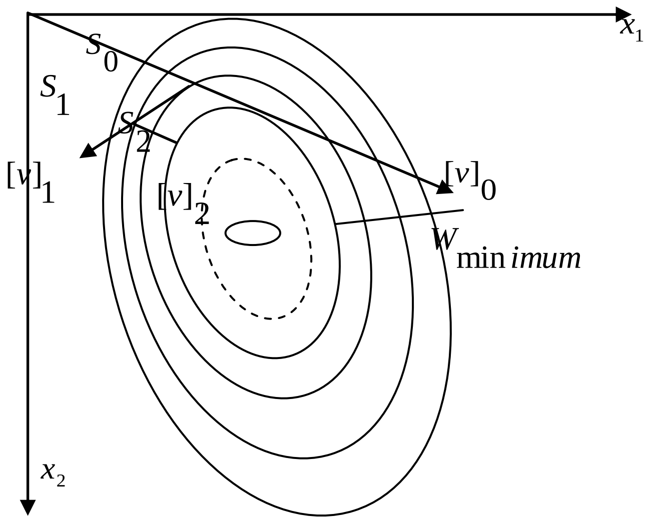

Figure 4.2: Visual optimization of total potential dynamic work on descent direction.

Where $[V]_n$ is the unit descent vector and S_n is the step length along $[V]_n$ to the point where the TPE is minimum. This can be done by replacing the actual displacement vector [x] with a transformed vector [u] where

$$[x] = [H][u] \qquad 4.2$$

And [H] is the scaling matrix. From equation 4.1, and 4.2 [u] at the (n+1) the intersection may be expressed as:

$$[u]_{n+1} = [u]_n + S[V]_n \qquad 4.3$$

It has been shown that when [x] is substituted in the TPE expression [K] is transformed to [K'], where

$$[K] = [\dot{H}]^T [\dot{K}][H]. \qquad 4.4$$

If [H] is chosen such that all the elements on the leading diagonal of $[\dot{K}]$ are unit and $[\dot{K}]$ is symmetric, with its off-diagonal terms tending to zero, then the eigenvalues of $[\dot{K}]$ will be approximately equal. Hence, the rate of convergence of proposed method will be improved. In practice, however, considerable benefit is obtained computationally by choosing [H] as equation 4.5. The convergence in one direction is shown in

$$H_{ii} = [1/K_{ii}]^{1/2}. \qquad 4.5$$

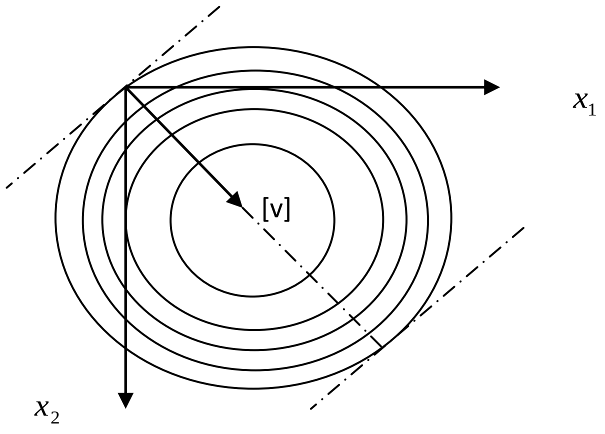

Figure 4.3: Convergency in one direction.

4.2 Structural property matrices

4.2.1 The general mass determinant

The mass matrix can be evaluated as a consistent mass determinant or as a lumped mass determinant depending on the structure to be analysed. The consistent mass determinant for a pin jointed member with three degrees of freedom at each end may be evaluated from

$$\frac{\bar{m}\ L}{6} * \begin{vmatrix} 2 & 0 & 0 & 1 & 0 & 0 \\ 0 & 2 & 0 & 0 & 1 & 0 \\ 0 & 0 & 2 & 0 & 0 & 1 \\ 1 & 0 & 0 & 2 & 0 & 0 \\ 0 & 1 & 0 & 0 & 2 & 0 \\ 0 & 0 & 1 & 0 & 0 & 2 \end{vmatrix} \qquad 4.6$$

where $\bar{m}$ is the mass per unit length and L is the length of member.

The lumped mass determinant for the same member is given as:

$$\frac{\bar{m}\ L}{2} * \begin{vmatrix} 1 & 0 & 0 & 0 & 0 & 0 \\ 0 & 1 & 0 & 0 & 0 & 0 \\ 0 & 0 & 1 & 0 & 0 & 0 \\ 0 & 0 & 0 & 1 & 0 & 0 \\ 0 & 0 & 0 & 0 & 1 & 0 \\ 0 & 0 & 0 & 0 & 0 & 1 \end{vmatrix} \qquad 4.7$$

These matrices represent the self load as well as distributed load along the member. Any concentrated static load applied at a joint must be added to the diagonal element of mass determinant.

From the analysis point of view, experience has shown that as far as cable structures are concerned good accuracy can be achieved by using a lumped mass determinant. The mass matrices for the mathematical model in the present work are considered as lumped mass matrices.

4.2.2 The stiffness determinant for a pin jointed member

For structures subjected to finite displacement the stiffness determinant for structural elements, which may be considered as pin jointed member, must include the change in stiffness caused by geometrical deformations as well as the added stiffness due to the axial force.

The global stiffness determinant for a pin jointed element in such structures is given by:

$$K = \begin{vmatrix} k_{11} & k_{12} \\ k_{21} & k_{22} \end{vmatrix} \tag{4.8}$$

Where $k_{11} = k_{22} = -k_{12} = -k_{21}$

$$= \frac{EA}{L}\begin{vmatrix} \lambda_1^2 & \lambda_1\lambda_2 & \lambda_1\lambda_3 \\ \lambda_2\lambda_1 & \lambda_2^2 & \lambda_2\lambda_3 \\ \lambda_3\lambda_1 & \lambda_3\lambda_2 & \lambda_3^2 \end{vmatrix} + \frac{T}{L}\begin{vmatrix} 1-\lambda_1^2 & -\lambda_1\lambda_2 & -\lambda_1\lambda_3 \\ -\lambda_2\lambda_1 & 1-\lambda_2^2 & -\lambda_2\lambda_3 \\ -\lambda_3\lambda_1 & -\lambda_3\lambda_2 & 1-\lambda_3^2 \end{vmatrix} \tag{4.9}$$

Where T is the axial force in the member for any position in displacement space and λ_1, λ_2, and λ_3 are the corresponding direction cosines.

4.2.3 The orthogonal damping matrices

The damping is energy lost in vibration due to work done by forces resisting the motion. These forces are caused by hysteresis losses in the member, friction in joints and resistance by the surrounding mass of air. In practice the damping matrices are usually constructed from knowledge of the damping ratios in different modes as value for these are more easily obtainable by standard resonance testing. A general orthogonal damping matrix can be set up as a combination of the mass and stiffness matrix and can be shown to be of the from

$$C = M\sum_{b} a_b\left[M^{-1}k\right]^{b} \equiv \sum_{b} C_b \qquad 4.10$$

In which as many terms may be included as desired, and which the values of the constants a_b can be found from the equation

$$\varepsilon_n = \frac{1}{2\omega_n}\sum_{b} a_b\,\omega_n^{2b} \qquad 4.11$$

where $\varepsilon_n =$ the damping ratio for mode n, and $\omega_n =$ the frequency of mode n.

Rayleigh damping which is given by

$$C = a_0 M + a_1 K \qquad 4.12$$

And in which a_0 and a_1 are arbitrary proportionality factors and the use of value Rayleigh damping assumes that the damping ratios in all modes can be expressed by the relationship

$$\varepsilon_n = \frac{1}{2}\left(a_0/\omega_n + a_1\omega_n\right) \qquad 4.13$$

The proposed method of analysis is step by step response calculation in the time domain for a series of small time increments during which equilibrium of dynamic forces at the end of each increment is established by minimization of the total potential dynamic work. In the development of theory it is assumed that the boundary joints are fixed and that the static and dynamic loading is applied at the jointly only. The simplify notation and in order to avoid treble suffices, the following notation have been used. In general elements of the mass and damping matrices M and C are symbolized by double suffices the elements of the displacement, velocity, acceleration and descent vectors by a single. The combination of the two suffices indicates one degree of freedom.

The orthogonal damping matrix is the modal damping matrix which takes advantage of the orthogonality properties of the mode shapes relative to the mass matrix. This damping matrix in which as many modes may be in included as desired is given by:

$$C = M\left(\sum_{n=1}^{N} \frac{2\varepsilon_n \omega_n}{\phi_n^T M \phi_n} \phi_n \phi_n^T\right) M \qquad 4.14$$

Where n =the mode number,

ϕ_n =the nth mode shape vector, and

M=diagonal mass matrix.

The result is non-banded symmetric dynamic matrix irrespective of the number of modes included. To include the damping of all the modes of vibration in equation 4.14 is not a practical proposition, since in most cases only the damping ratios of the first few modes are known with any degree of approximate certainty. In equation 4.14 the contribution to the damping matrix from the damping in a given mode is directly proportional to the magnitude of the modal damping ratio, thus any undamped mode will contribute nothing. In other words, only those modes specifically included in the formulation of the damping matrix will be damped, all another modes will be undamped. The use of equation 4.14 makes it possible to assume values for the damping ratios in higher modes and to study the effect of variations in the damping ratios in the different modes. It should be noted that in this work, since the nonlinear structures in question do not possess fixed mode shapes and frequencies the equivalent linear mode shapes and frequencies are used to obtain the required damping matrix from equation 4.14 The physical interpretation of equation 4.14 is a damping mechanism in which each joint is connected to all the other joints of a structure through viscous dampers. Experience indicates that for structural system with evenly distributed stiffness, such as cable nets, the use of modal damping matrix yields reasonable results. In the numerical experimentation which follows, the modal damping matrix given by equation 4.14 is used to permit variation in the damping ratios in all modes in order to study the effect of these variations on the dynamic response.

4.3 Theory of Fletcher-Reeves method

4.3.1 The total potential dynamic work (TPDW) by Fletcher-reeves method

The total potential dynamic work of a vibrating structure at time τ is given by:

$$W_{\tau} = U_{o} + U_{\tau} - V_{\tau} + D_{\tau} + I_{\tau} - Q_{\tau} \qquad 4.15$$

And at time $\tau + \Delta\tau$, taking the static equilibrium position as datum, by:

$$W_{\tau+\Delta\tau} = U_{O} + U_{\tau} + \sum_{n=1}^{m} \int_{O}^{\Delta e_n} T_n d(\Delta e_n)$$

$$- V_{\tau} - \sum_{s=1}^{N} \int_{O}^{\Delta\tau} F_s \dot{x}_s d(\Delta\tau) \;\; + D_{\varsigma} + \sum_{s=1}^{N} \sum_{r=1}^{N} \int_{O}^{\Delta\tau} C_{sr} \dot{x}_r \dot{x}_s d(\Delta\tau)$$

$$+ I_{\tau} + \sum_{s=1}^{N} \sum_{r=1}^{N} \int_{O}^{\Delta\tau} M_{sr} \ddot{x}_r \dot{x}_s d(\Delta\tau) \; - Q_{\tau} - \sum_{s=1}^{N} \int_{O}^{\Delta\tau} P(r+\Delta\tau)_s \dot{x}_s d(\Delta\tau) \qquad 4.16$$

where

$W_{\tau}, W_{\tau+\Delta\tau}, \; \Delta\tau$ = TPDW at times τ and $(\tau + \Delta\tau)$.

U_O, U_{τ} = initial strain energy and strain energy at time τ .

V_{τ}, Q_{τ} = Potential energy of static and dynamic load at time τ .

D_{τ} = Energy dissipated by damping forces up to time τ .

I_τ ,m,N = Inertia energy at time τ, Number of members , and degree of freedom.

$e, \Delta e$ = Elongation of a member at time τ and during time $\Delta\tau$.

$T_O, T, \Delta T$ = Tension of primary, time τ, and during time step $\Delta\tau$.

$X, \dot{X}, \ddot{X}$ = displacement, velocity and acceleration vectors.

$P(\tau)_s$ *and* $P(\tau+\Delta\tau)_s$, F_s = elements of dynamic load vectors P(τ) and $P(\tau+\Delta\tau)$ at time τ and $(\tau+\Delta\tau)$ and Static load vector F.

C_{sr}, M_{sr} = elements of damping and mass matrices C and M.

Using the relationship

$$\dot{X}_s \, d(\Delta\tau) = d(\Delta X_s) \qquad 4.17$$

And that

$$U_\tau + \sum_{n=1}^{m} \int_O^{\Delta e_n} T_n d(\Delta e_n) = \sum_{n=1}^{m} \int_O^{e_n} (T_n + \Delta T_n) d(e_n) \qquad 4.18$$

Equation 4.14 can be transformed to

$$W_{t+\Delta\tau} = U_O + \sum_{n=1}^{m} \int_O^{e_n} (T_n + \Delta T_n) d(e_n)$$

$$-V_\tau - \sum_{s=1}^{N} \int_O^{\Delta X_s} F_s d(\Delta X_s) \quad + D_\tau + \sum_{s=1}^{N} \sum_{r=1}^{N} \int_O^{\Delta X_s} C_{sr} \dot{X}_r d(\Delta X_s)$$

$$+ I_\tau + \sum_{s=1}^{N} \sum_{r=1}^{N} \int_O^{\Delta X_s} M_{sr} \ddot{X}_r d(\Delta X_s) - Q - \sum_{s=1}^{N} \int_O^{\Delta X_s} P(\tau+\Delta\tau)_s d(\Delta X_s) \qquad 4.19$$

Where ΔX_s is the change in the displacement element X_s during $\Delta\tau$.

4.3.2 The gradient of the total potential dynamic work

The terms for dynamic equilibrium at the end of time increment ΔT is given by:

$$g_s = \partial\left(W_{\tau+\Delta t}\right)/\partial\left(\Delta x_s\right) = 0 \qquad \left(S = 1,2,....,N\right) \tag{4.20}$$

Differentiating equation 4.19 with respect to Δx_s gives the S_{th} element of the gradient vector g as:

$$g_s = \sum_{n=1}^{q}\left(T_{jn} + \Delta t_{jn}\right)d\left(e_{jn}\right)\Big/d\left(\Delta x_s\right) - F_s + \sum_{r=1}^{N} C_{sr}\dot{x}_r + \sum_{r=1}^{N} M_{sr}\ddot{x}_r - p\left(\tau + \Delta\tau\right)_s \tag{4.21}$$

Whereas

$$\frac{\partial\left(V_\tau\right)}{\partial\left(\Delta x_s\right)} = \frac{\partial\left(D_\tau\right)}{\partial\left(\Delta x_s\right)} = \frac{\partial\left(I_\tau\right)}{\partial\left(\Delta x_s\right)} = \frac{\partial\left(Q_\tau\right)}{\partial\left(\Delta x_s\right)} = 0 \tag{4.22}$$

And also

$$d\left(e_{jn}\right) = \frac{d\left(e_{jn}\right)}{d\left(\Delta x_s\right)} d\left(\Delta x_s\right) \tag{4.23}$$

Where the suffix j_n refers to the two ends of member n, and q is the number of members meeting at joint j as shown in Figure 4.4.

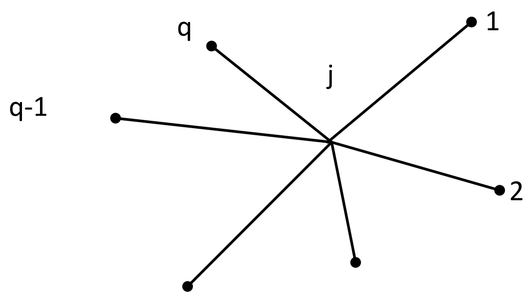

Figure 4.4:.Scheme of connection members to joint.

An expression for g_s above demands the improvement of work for $d\left(e_{jn}\right)/d\left(\Delta x_s\right)$, $\dot{x}_r$ and $\ddot{x}_r$. The strain and rate of change of strain in a pin-jointed part j_n with relate to its displacement is achieved as:

$$L_{jn}^2 = \sum_{i=1}^{3}\left(X_{ni} - X_{ji}\right)^2 \qquad 4.24$$

$$\left(L_{jn} + e_{\ln}\right)^2 = \sum_{i=1}^{3}\left(X_{ni} + x_{ni} + \Delta x_{ni} - X_{ji} - x_{ji} - \Delta x_{ji}\right)^2 \qquad 4.25$$

Where L_{jn} represents the length of member j_n and j_i represents the coordinates of joint j in direction i. The expression for e_{jn} found from equations 4.23 and 4.24 are given by:

$$e_{jn} = \frac{1}{2L_{jn} + e_{jn}} \sum_{i=1}^{3} (2\left(X_{ni} - X_{ji}\right)\left(x_{ni} + \Delta x_{ni} - x_{ji} - \Delta x_{ji}\right)$$

$$+ 2\left(x_{ni} - x_{ji}\right)\left(\Delta x_{ni} - \Delta x_{ji}\right)$$

$$+\left(x_{ni} - x_{ji}\right)^2 + \left(\Delta x_{ni} - \Delta x_{ji}\right)^2) \qquad 4.26$$

Differentiating equation 4.25 with respect to Δx_{ji} yields

$$\frac{\partial(ejn)}{\partial\left(\Delta x_s\right)} = \frac{-1}{\left(L_{jn} + e_{jn}\right)}\left(\left(X_{ni} + x_{ni} + \Delta x_{ni} - X_{ji} - x_{ji} - \Delta x_{ji}\right)\right) \qquad 4.27$$

The expression for the velocity and acceleration vectors $\dot{x}$ and $\ddot{x}$ are found by making the assumption that the acceleration varies linearly during the time step $\Delta\tau$. It is assumed that the change of acceleration remains constant during the time interval. A detail of the motion of a mass point which moves according to the above assumption are and leads to the following expressions for $x, \dot{x}$ and $\ddot{x}$ in condition of the change of movement Δx during the time interval.

$$x_r = x_{or} + \Delta x_r \qquad 4.28$$

$$\dot{x}_r = \dot{x}_{or} + \Delta \dot{x}_r = \frac{3}{\Delta\tau}\Delta x_r - 2\dot{x}_{or} - \frac{\Delta\tau}{2}\ddot{x}_{or} \qquad 4.29$$

$$\ddot{x}_r = \ddot{x}_{or} + \Delta \ddot{x}_r = \frac{6}{\Delta\tau^2}\Delta x_r - \frac{6}{\Delta\tau}\dot{x}_{or} - 2\ddot{x}_{or} \qquad 4.30$$

where

$\Delta \dot{x}, \Delta \ddot{x} =$ The change in the velocity and acceleration vectors during time interval $\Delta\tau$

$x_o, \dot{x}_o, \ddot{x}_o =$ The displacement, velocity, and acceleration vectors at time τ .

Substitution of the expression for $\partial\left(e_{jn}\right)/\left(\Delta x_{ji}\right)$, $\dot{x}$ and $\ddot{x}$ in equation 4.20 yields.

$$g_s = -\sum_{n=1}^{q}\left(t_{jn} + \Delta t_{jn}\right)\left(X_{ni} + x_{ni} + \Delta x_{ni} - X_{ji} - x_{ji} - \Delta x_{ji}\right) - F_s$$

$$+ \sum_{r=1}^{N} C_{sr}\left(\frac{3}{\Delta\tau}\Delta x_r - 2\dot{x}_{or} - \frac{\Delta\tau}{2}\ddot{x}_{or}\right)$$

$$+ \sum_{r=1}^{N} M_{sr}\left(\frac{6}{\Delta\tau^2}\Delta x_r - \frac{6}{\Delta\tau}\dot{x}_{or} - 2\ddot{x}_{or}\right) - \left(P(\tau)_s + \Delta P_s\right) \qquad 4.31$$

Where $\left(t_{jn} + \Delta t_{jn}\right) = \left(T_{jn} + \Delta T_{jn}\right)/\left(L_{jn} + e_{jn}\right)$ is the tension coefficient for member j_n, and $\Delta P_s = P(\tau + \Delta\tau)_s - P(\tau)_s$. Hence, the computational procedure is based upon the achievement of dynamic equilibrium at the end of each time increment. If engage time τ

$$g_s = -\sum_{n=1}^{q} t_{jn}\left(X_{ni} + x_{ni} - X_{ji} - x_{ji}\right) - F_s$$

$$+ \sum_{r=1}^{N} C_{sr}\dot{x}_{or} + \sum_{r=1}^{N} M_{sr}\ddot{x}_{or} - P(\tau)_s = 0 \qquad 4.32$$

And at time $(\tau + \Delta\tau)$

$$g_s = -\sum_{n=1}^{q}\left(\Delta t_{jn}\left(X_{ni} + x_{ni} - X_{ji} - x_{ji}\right) + \left(t_{jn} + \Delta t_{jn}\right)\left(\Delta x_{ni} + \Delta x_{ji}\right)\right)$$

$$+ \sum_{r=1}^{N} C_{sr}\left(\frac{3}{\Delta\tau}\Delta x_r - 3\dot{x}_{or} - \frac{\Delta\tau}{3}\ddot{x}_{or}\right) + \sum_{r=1}^{N} M_{sr}\left(\frac{6}{\Delta\tau^2}\Delta x_r - \frac{6}{\Delta\tau}\dot{x}_{or} - 3\ddot{x}_{or}\right) - \Delta P_s \qquad 4.33$$

which when Δx has assumed the correct value will also be equal to zero.

4.4 Minimization of the total potential dynamic work by Fletcher-Reeves method

The accurate amount of Δx_s at time $(\tau + \Delta\tau)$ for which $g_s = 0$ is achieved by minimization the total potential dynamic work, applying the iterative process

$$\Delta x_{s(k+1)} = \Delta x_{s(k)} + S_{(k)} \quad V_{s(k)} \qquad 4.34$$

At the location which the suffices k and (k+1) denote the k_{th} and $(k+1)_{th}$ iterate respectively, and

$V_{s(K)} =$ The s_{th} element of descent vector, and

$S_{(k)} =$ The steplength to the point along $V_{s(K)}$, where the total potential dynamic work is a latest possible amount.

Using of the Fletcher-Reeves formula for expression for the k_{th} descent vector.

$$V_{s(k)} = -g_{s(k)} + \frac{\sum_{s=1}^{N} g_{s(k)} \; g_{s(k)}}{\sum_{s=1}^{N} g_{s(k-1)} \; g_{s(k-1)}} V_{s(k-1)} \qquad 4.35$$

The starting point in direction of descent can now be achieved by conveying the total potential dynamic work as a function of the steplength and applying the condition that at the stationary point

$$\partial W_{(k)} \big/ \partial S_{(k)} = 0 \qquad 4.36$$

4.5 Determination of the steplength

The required function for steplength polynomial is achieved by substituting the statement for Δx_r given by equation 4.19 into a suitable statement for the total potential dynamic work. Interchange of the statement for acceleration and velocity are provided by equations 4.28 and 4.29 into equation 4.19 and at the equal time writing strain energy terms as a function of the elongation of the members gives first

$$W_{\tau+\Delta\tau} = \sum_{n=1}^{m}\left(U_o + T_o e + \frac{EA}{2L}e^2\right) - V_\tau - \sum_{s=1}^{N}\int_o^{\Delta x_s} F_s\, d(\Delta x_s)$$

$$+ D_\tau + \sum_{s=1}^{N}\sum_{r=1}^{N}\int_o^{\Delta x_s} C_{sr}\left(\frac{3}{\Delta\tau}\Delta x_r - 2\dot{x}_{or} - \frac{\Delta\tau}{2}\ddot{x}_{or}\right) d(\Delta x_s)$$

$$+ I_\tau + \sum_{s=1}^{N}\sum_{r=1}^{N}\int_o^{\Delta x_s} M_{sr}\left(\frac{6}{\Delta\tau^2}\Delta x_r - \frac{6}{\Delta\tau}\dot{x}_{or} - 2\ddot{x}_{or}\right) d(\Delta x_s)$$

$$- Q_\tau - \sum_{s=1}^{N}\int_o^{\Delta x_s} P_{sr}(\tau+\Delta\tau)\, d(\Delta x_s) \qquad 4.37$$

And then after carrying out the integrations

$$W_{\tau+\Delta\tau} = \sum_{n=1}^{m}\left(U_o + T_o e + \frac{EA}{2L}e^2\right) - V_\tau - \sum_{s=1}^{N} F_s \Delta x_s$$

$$+ D_\tau + \sum_{s=1}^{N}\sum_{r=1}^{N} \frac{3}{2\Delta\tau}\Delta x_s C_{sr} \Delta x_r - \sum_{s=1}^{N}\sum_{r=1}^{N} \Delta x_s C_{sr}\left(2\dot{x}_{or} + \frac{\Delta\tau}{2}\ddot{x}_{or}\right)$$

$$I_\tau + \sum_{s=1}^{N}\sum_{r=1}^{N} \frac{3}{\Delta\tau^2}\Delta x_s M_{sr} \Delta x_r - \sum_{s=1}^{N}\sum_{r=1}^{N} \Delta x_s M_{sr}\left(\frac{6}{\Delta\tau}\dot{x}_{or} + 2\ddot{x}_{or}\right)$$

$$-Q_\tau - \sum_{s=1}^{N} P(\tau+\Delta\tau)_s \Delta x_s \qquad 4.38$$

where E_n is the Young's Modulus of Elasticity and A_n is the cross-sectional area of member n. The required statement for e_{jn} as a function of s could be obtained by combining equation 4.28 and 4.31 and is shown by:

$$e_{jn} = \frac{1}{2L_{jn} + e_{jn}}\left(a_1 + a_2 s + a_3 s^2\right) \qquad 4.39$$

Where for a member n,

$$a_1 = \sum_{i=1}^{3}\left(\left(X_{ni} + x_{ni} + \Delta x_{ni} - X_{ji} - x_{ji} - \Delta x_{ji}\right)^2 - \left(X_{ni} - X_{ji}\right)^2\right)$$

$$a_2 = \sum_{i=1}^{3} 2\left(X_{ni} + x_{ni} + \Delta x_{ni} - X_{ji} - x_{ji} - \Delta x_{ji}\right) - \left(v_{ni} - v_{ji}\right)$$

$$a_2 = \sum_{i=1}^{3} 2\left(X_{ni} + x_{ni} + \Delta x_{ni} - X_{ji} - x_{ji} - \Delta x_{ji}\right) - \left(v_{ni} - v_{ji}\right)$$

$$a_3 = \sum_{i=1}^{3}\left(v_{ni} - v_{ji}\right)^2$$

Interchange the statement for e and Δx, as given by equations 4.26 and 4.34 respectively, into equation 4.38 yield the engage in fourth order steplength polynomial for the total potential dynamic work at time $(\tau + \Delta\tau)$:

$$W_{\tau+\Delta\tau} = C_1 S^4 + C_2 S^3 + C_3 S^2 + C_4 S + C_5 \qquad 4.40$$

and its derivative with respect to s as:

$$\partial W_{\tau+\Delta\tau} / \partial S = 4C_1 S^3 + 3C_2 S^2 + 2C_3 S + C_4 \qquad 4.41$$

where for a symmetric matrix A

$$\sum_{s=1}^{N} \sum_{r=1}^{N} X_s A_{sr} Y_r = \sum_{s=1}^{N} \sum_{r=1}^{N} X_r A_{sr} Y_s \qquad 4.42$$

$$C_1 = \sum_{n=1}^{m} \left(\frac{EA}{2L(2L+e)^2} \; a_3^2 \right)_n \qquad C_2 = \sum_{n=1}^{m} \left(\frac{EA}{L(2L+e)^2} \; a_2 a_3 \right)_n$$

$$C_3 = \sum_{n=1}^{m} \left(\frac{T_o}{2L+e} \; a_3 + \frac{EA}{2L(2L+e)^2} \; a_2^2 + \frac{EA}{L(2L+e)^2} \; a_1 a_3 \right)_n$$

$$+ \sum_{s=1}^{N} \sum_{r=1}^{N} \frac{3}{2\Delta\tau} C_{sr} v_s v_r + \sum_{s=1}^{N} \sum_{r=1}^{N} \frac{3}{\Delta\tau^2} M_{sr} v_s v_r$$

$$C_4 = \sum_{n=1}^{m} \left(\frac{T_o}{2L+e} \; a_2 + \frac{EA}{L(2L+e)^2} \; a_1 a_2 \right)_n - \sum_{s=1}^{N} \left(F_s + P(\tau + \Delta\tau)_s \right) v_s$$

$$+ \sum_{s=1}^{N} \sum_{r=1}^{N} \left(\frac{3}{\Delta\tau} \Delta x_r - 2\dot{x}_{or} - \frac{\Delta\tau}{2} \ddot{x}_{or} \right) C_{sr} v_s$$

$$+ \sum_{s=1}^{N} \sum_{r=1}^{N} \left(\frac{6}{\Delta\tau^2} \Delta x_r - \frac{6}{\Delta\tau} \dot{x}_{or} - 2\ddot{x}_{or} \right) M_{sr} v_s$$

$$C_5 = \sum_{n=1}^{m} \left(U_o + \frac{T_o}{2L+e} \; a_1 + \frac{EA}{2L(2L+e)^2} \; a_1^2 \right)_n$$

$$-\sum_{s=1}^{N}\left(F_s + P(\tau+\Delta\tau)_s\right))\Delta x_s + \sum_{s=1}^{N}\sum_{r=1}^{N}\left(\frac{3}{2\Delta\tau}\Delta x_r - 2\dot{x}_{or} - \frac{\Delta\tau}{2}\ddot{x}_{or}\right) C_{sr}\Delta x_s$$

$$+\sum_{s=1}^{N}\sum_{r=1}^{N}\left(\frac{3}{\Delta\tau^2}\Delta x_r - \frac{6}{\Delta\tau}\dot{x}_{or} - 2\ddot{x}_{or}\right) M_{sr}\Delta x_s + \left(D_\tau + I_\tau - V_\tau - Q_\tau\right)$$

The value of C_5 need not be computed whereas only the derivative of W is required S in order to calculate the steplength. The eigenvalue analysis is not directly required by the method. The stability of the method depends on the size of the time increment, which usually should be equal to or less than half the smallest periodic time of the structure. The determination of the size of $\Delta\tau$ therefore requires the determination of the largest eigenvalue of the system. Another way of determining the size of $\Delta\tau$ which avoids the eigensolution is to start with an estimated value for $\Delta\tau$ and then check for stability. If the time step is too large, $\Delta\ddot{x}$ changes sign at every time step before the method becomes unstable. This will usually occur quite early in the integration process. The procedure can therefore be stabilized at an early stage of the calculation by reducing the time step if necessary. Indications of instability due to a too large time step may show up even more clearly if in the formulation of the theory the main variable is taken as the change of acceleration rather than the change of displacement. Not only the stability but also the accuracy of the predicted response depends upon the size of the time increment. If the magnitude of the dynamic loads varies rapidly, $\Delta\tau$ must be small enough to take into account all the frequency components of the dynamic load. Hence, the equilibrium of the dynamic forces at the end of each time step is determined by an iterative process, the accuracy of the predicted response is also a function of degree of convergency imposed.

4.6 Calculation procedure of Fletcher-Reeves algorithm

The flowchart of present algorithm is given in Figure 4.5. The description of all algorithm stages is written as;

Step 1: Determination of the coordinator vector and internal force vector.

Step 2: Assembly of mass matrix and damping matrix.

Step 3: Establishment of the forcing function $P(\tau)$ and size of the time increment $\Delta\tau$.

Step 4: Initiation of the next time interval by calculation of ΔP

Step 5: Calculation of the gradient vector g from equation 4.33. In general it is better to use equation 4.34 which gives the total gradient at time $\tau + \Delta\tau$ and avoids the accumulation of errors.

Step 6: Calculation of the Euclidean norm of g from $R = \left(\sum_{s=1}^{N} g_s g_s \right)^{1/2}$.

Step 7: If R is less than a predetermined value or a percentage of the norm of the first gradient the time step proceed with step 14 otherwise continue with step 9.

Step 8: Calculation of the direction vector in the first iteration $v = -g$

Step 9: Calculation of the parameters a_1, a_2 and a_3 from equation 4.39.

Step 10: Calculation of the coefficients C_1 to C_4 from equation 4.42.

Step 11: calculation of the value of S by equating the dynamic load and of Δx.

Step 12: Determination of new tension in each member from $T = T_o + \frac{EA}{L} e$.

Step 13: Return to step 6 above the next iteration.

Step.14: Calculation of the starting point for the next time increment from equation 4.12. If the required time span of response analysis is covered, the calculation is terminated, if not return to step 5 above.

4.7 The optimization of the total potential dynamic work by Newton-Raphson method

For comparison between Fletcher-Reeves and Newton Raphson method is needed to explain a Newton-Raphson method in more details. Minimization of the total potential dynamic work can be carried out by the Newton-Raphson method described in chapter 3. In Newton-Raphson method Δx is written as;

$$\Delta x_{k+1} = \Delta x_k - \left[K_I + \frac{3}{\Delta\tau} C + \frac{6}{\Delta\tau} M \right]^{-1} \bullet \; g_k \qquad 4.43$$

$$\Delta x_{k+1} = \Delta x_k - \left[K^* \right]^{-1} \bullet \; g_k \qquad 4.44$$

At which point K_I is the instantaneous static stiffness matrix and K^* is the instantaneous dynamic stiffness matrix. The contribution to K_I from a pin jointed member j_n in tension is given as:

$$k_{jn} = \frac{EA - T}{L + e} \bullet \begin{vmatrix} GG^T & -GG^T \\ -GG^T & GG^T \end{vmatrix} + \frac{T}{L} \bullet \begin{vmatrix} I & -I \\ -I & I \end{vmatrix} \qquad 4.45$$

Where T = instantaneous tension in member j_n,

I = the identity matrix, and

$$G^T = \Big[\left(X_{n1} + x_{n1} + \Delta x_{n1}\right) - \left(X_{j1} + x_{j1} + \Delta x_{j1}\right) \;,\; \left(X_{n2} + x_{n2} + \Delta x_{n2}\right) -$$

$$\left(X_{j2} + x_{j2} + \Delta x_{j2}\right) \;,\; \left(X_{n3} + x_{n3} + \Delta x_{n3}\right) - \left(X_{j3} + x_{j3} + \Delta x_{j3}\right) - \Big] \qquad 4.46$$

The convergency criterion can be the reduction of the total out of balance forces. At each on from iteration the incremental displacement is given as:

$$\Delta x = -\left[K^* \right]^{-1} g \qquad\qquad K^* \Delta x = -g \qquad 4.47$$

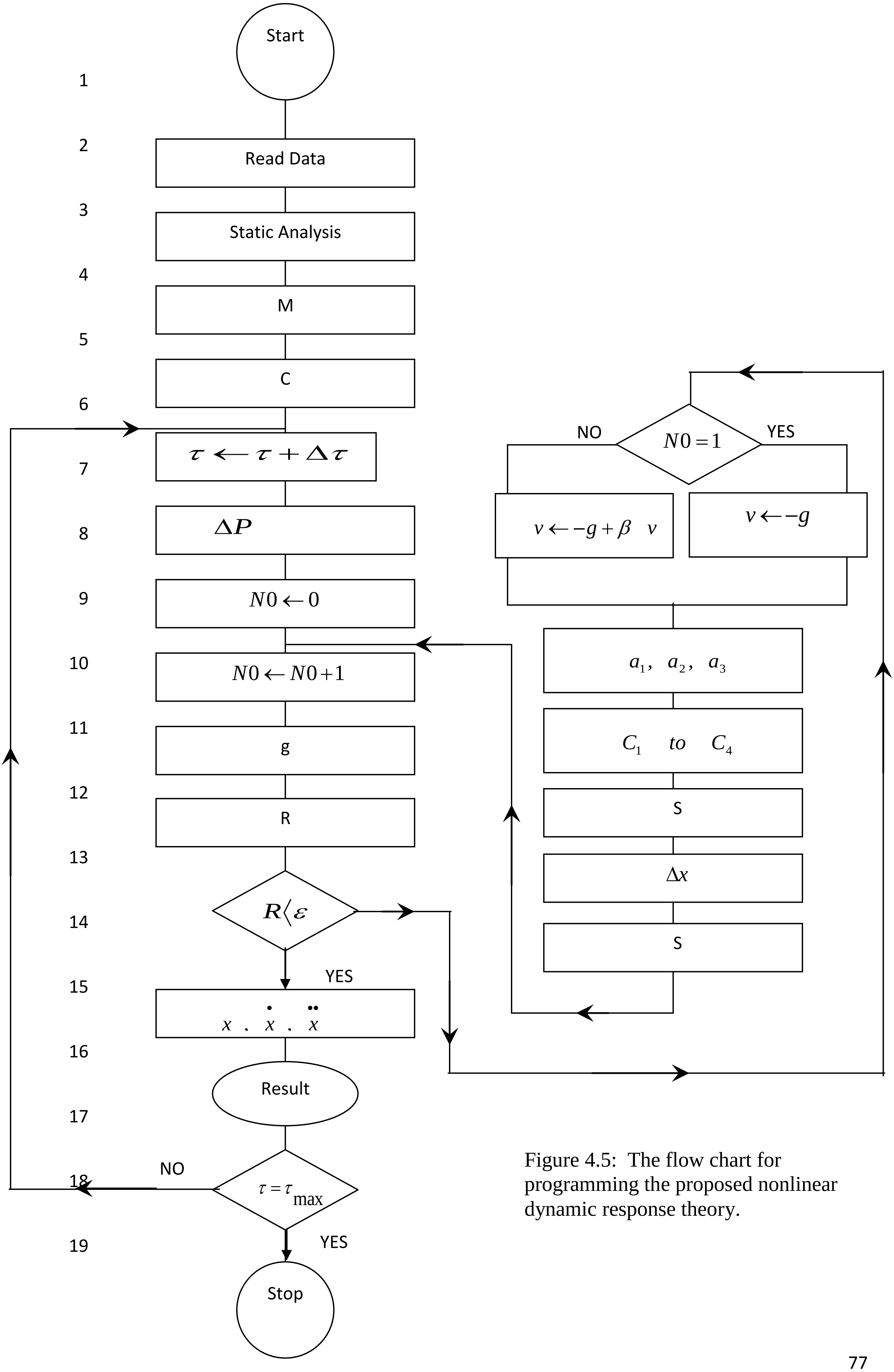

Figure 4.5: The flow chart for programming the proposed nonlinear dynamic response theory.

CHAPTER 5: STATIC TEST

NUMERICAL ANALYSIS AND EXPERIMENTAL WORK

RESULTS AND DISCUSSION

5.1 Introduction

In this chapter the analytical method and mathematical model presented in chapter 4 are used in experimental works. The mathematical model chosen was a 7x5 flat net with 105 degrees of freedom. The 7x5 net was built as an experimental model and tested in order to verify the static and dynamic nonlinear theories given in the previous chapters. The construction of the experimental model and the results of the static tests are given in this chapter.

The objectives of the numerical work described in this chapter are to verify the proposed theory in chapter 4 and to check the programme based upon the static theory given in chapter 3. A rectangular flat net was chosen in order to provide a structure with a high degree of nonlinearity (Nazmy & Abdel-Ghaffar, 1990; Such, et al., 2009). Flat nets are also less difficult to construct accurately than curved nets and thus can be easily represented by a mathematical model.

The main objectives are:

A. To check the stiffness of the boundary and to assess the degree of error introduced by any elastic deformation of the frame when assuming a rigid boundary;

B. To check the degree of symmetry of the model;

C. To compare the experimental and theoretical values of the static deformation by using tests with different pattern and intensities of static loading.

5.2 Design and construction of the model

The grid line of the flat net model together with node numbers is given in Figure 5.1. Figure 5.2 shows a general view of the 7x5 cable net; the cables are at 500 mm intervals and the cable diameter is 15.24 mm. At the points of intersection the cables were clamped together with thin wires. The cable net was contained within a 4 m by 3 m rectangular steel frame. The specification of the steel frame is given in Table 5.1.

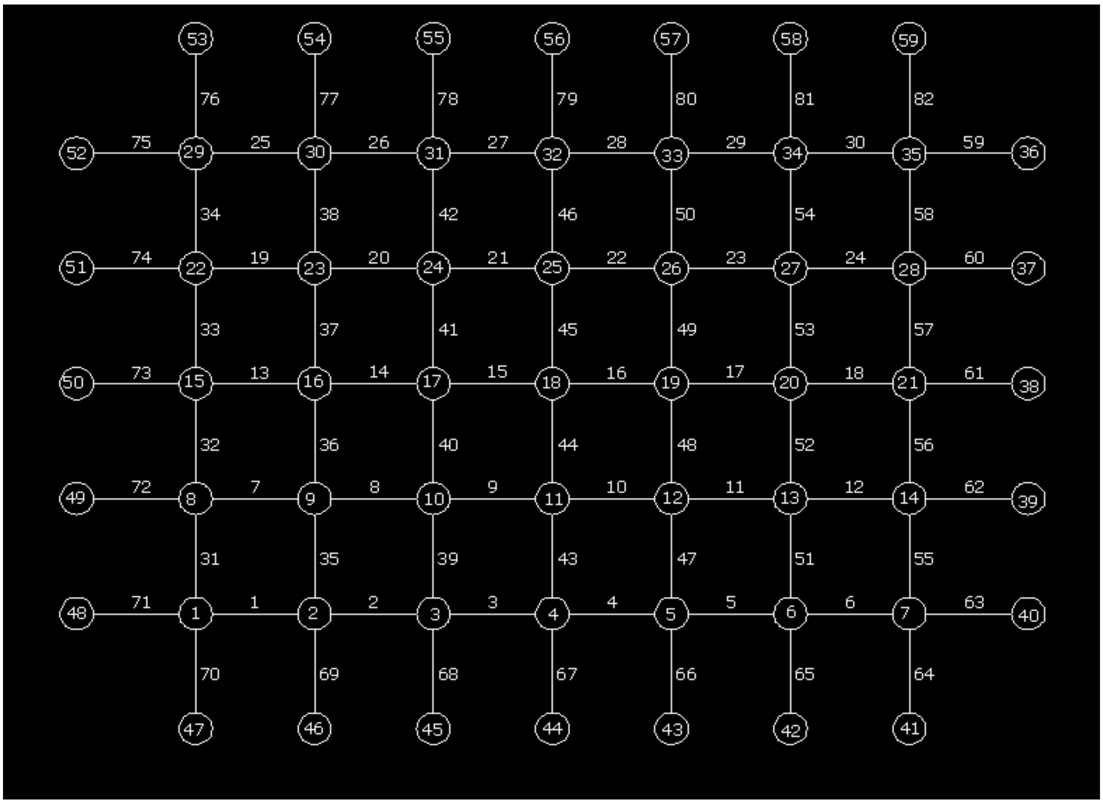

Figure 5.1: Grid lines of the flat net.

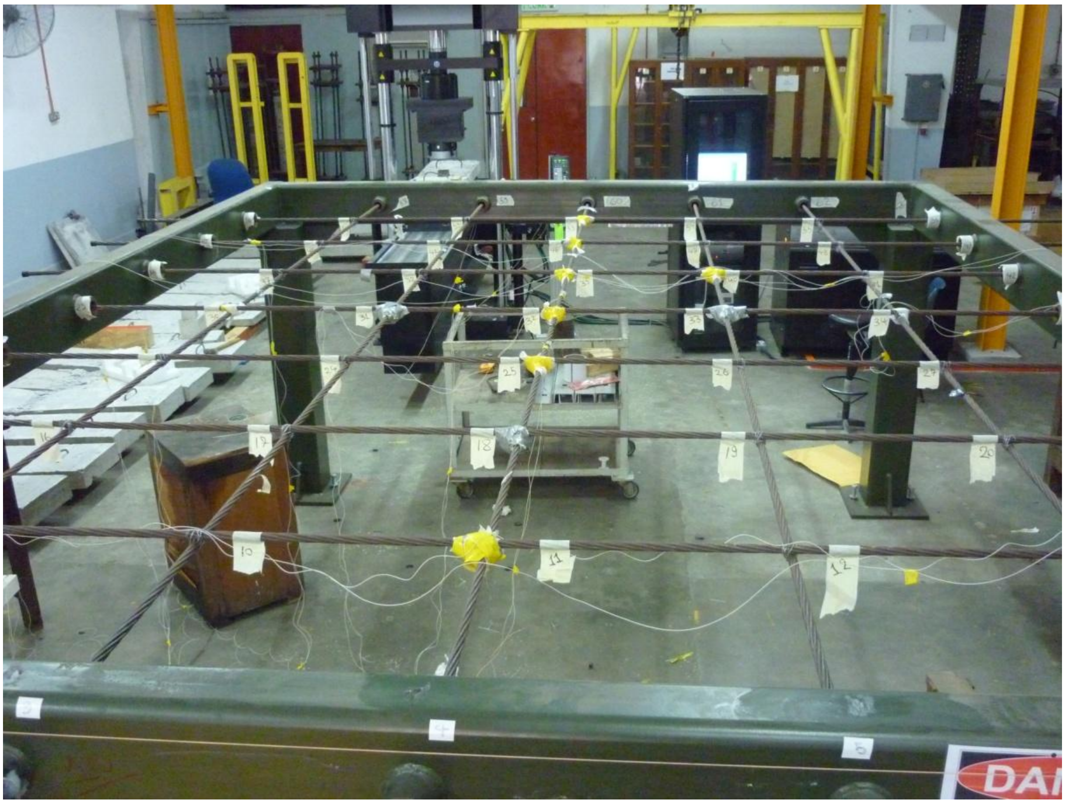

Figure 5.2: General view of the steel frame.

Table 5.1: Details and specifications of the steel frame.

Frame Supported Specification		
Column	1400 mm (box)	Height
Beam	300mm x 400mm (box)	Length by width
Beam Size	100 x 200 x 9 mm (hollow section)	
Column Size	200 x 200 x 9 mm (hollow section)	
Wedge	12 nos	
Barrel	12 nos	
Hollow Cylindrical Steel	12 nos	

General views of construction of column and beam steel frame made are given in Figure 5.3 and Figure 5.4.

Figure 5.3: Steel columns to support the frame.

Figure 5.4: Steel beams fitted with hollow cylindrical steel sections.

In order to make the boundary as rigid as possible the frame was stressed to the floor by means of post tensioning rods passing through the columns. The clamping attachment made for the steel frame is shown in Figure 5.5.

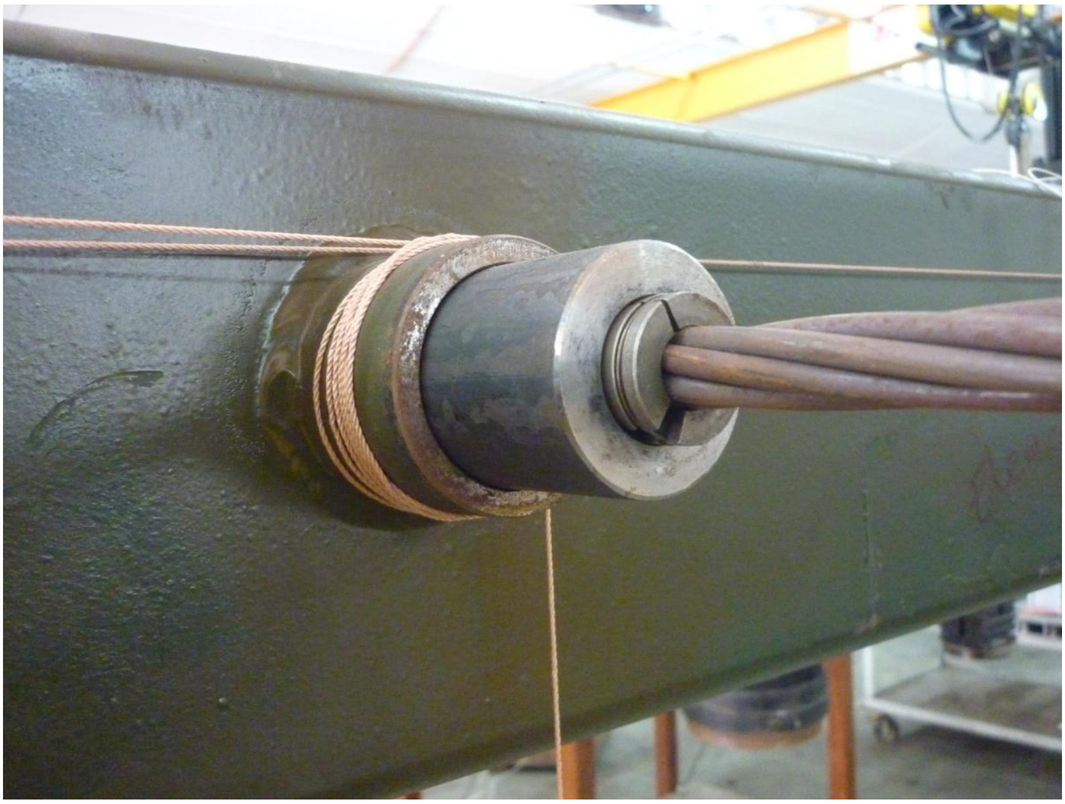

Figure 5.5: Clamping cables to the frame by using hollow cylindrical steel section and wedge and barrel.

Each steel cable was initially tensioned to about 1 KN and then left for two weeks to permit the individual wires in the strands to bed in. Then, the tension on the cables was readjusted to 11.5 KN. This tension was maintained throughout the test programme by checking it at intervals. The wedge and barrel was used on the hollow cylindrical steel section to provide endcaster degree of freedom for the boundary condition of cables. Endcaster joints are used to fix the boundary condition. The specifications of the erected rectangular net and cables are given in Table 5.2.

Table 5.2: The specifications of flat net and cables.

Description	Details
Overall dimensions	3000 x 4000
Spacing of the cables	500 mm
Number of free joints	35
Number of fixed boundary joints	24
Number of links	82
Diameter(mm)	15.34
Section area (mm^2)	142.90
Y/Strength 1% (kN)	244.40
Young’s Modulus	192.60 e11 N/ mm^2
Y/Strength	244.40 KN
Pretension	11500 N/link
Breaking Load (kN)	272.89
Proof Load (kN)	250.17
Total Elongation (%)	6.00
Relax Loss (%)	1.90

The values of tensile strength and Young’s Modulus were obtained from laboratory testing of the steel frame. The values from laboratory make ensure to verify values of tensile strength and Young’s Modulus from its catalogs. The construction of beam steel is shown in Figures 5.6.

Figure 5.6: Construction of beam steel.

5.3 Instrumentation and Equipment

5.3.1 Pressure gauge

The standard instruments used in this calibration are based on the national standards maintained at the National Metrology Laboratory, SIRIM Berhad. The pressure gauges are shown in Figure 5.7 and Figure 5.8. The pressure gauges are used to create tension on the cables of frame.

Measurement uncertainty: 451965 Pascal

Coverage factor: K= 2.31

Average temperature: 24°C

Average Relative Humidity: 56 RH

Figure 5.7: Visual view of handle of pressure gauge.

Figure 5.8: Tensioning of the cable with the pressure gauge.

5.3.2 Data acquisition / logger (Type: TDS – 530 (Touch Screen))

A data logger is used to store the values of strain and deflection on the cables of frame. The TDS-530 is an automatic, multi-channel, scanning data logger used to read strain gauges, thermocouples, Pt RTD temperature sensors, strain gauge based (full bridge) transducers and DC voltage. The data loggers used are shown in Figure 5.9 and Figure 5.10.

Features:

a) Colour LCD monitor with touch panel having excellent contrast
b) Computer interface with RS-232C, USB2.0 or Ethernet LAN
c) Storage of media with onboard data memory and flash memory
d) Simultaneous measurement of strain and temperature

These data loggers have a switch box and can support various sensors. They can also support LAN, USB, and RS-232C ports.

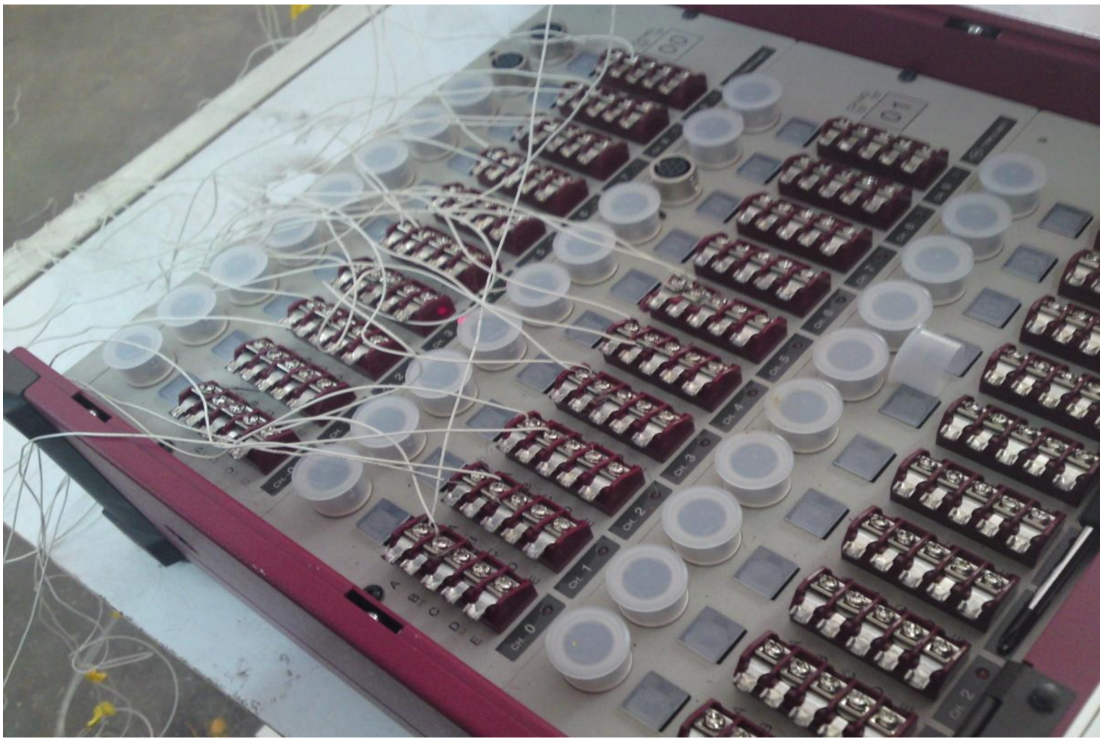

Figure 5.9: The channels of the TDS-530 data logger.

Figure 5.10: Top view of TDS – 530 Data logger.

5.3.3 Strain gauge (KFG-5-120–C1-11)

A strain gauge is a device used to measure the strain of an object. A strain gauge takes advantage of the physical property of electrical conductance and its dependence on not merely the electrical conductivity of a conductor, which is a property of its material, but also the conductor's geometry. The strain gauges used are shown in Figure 5.11 to Figure 5.13. The specifications and features are as follows:

Type: KFG -5- 120 – C1 -11   Gauge Factor: 2.1 (24 C, 50%RH)

Gauge Length: 5 mm

Gauge Resistance: 119.8 Ω (24 C, 50%RH)

Adoptable Thermal Expansion: 11.7 PPM/C

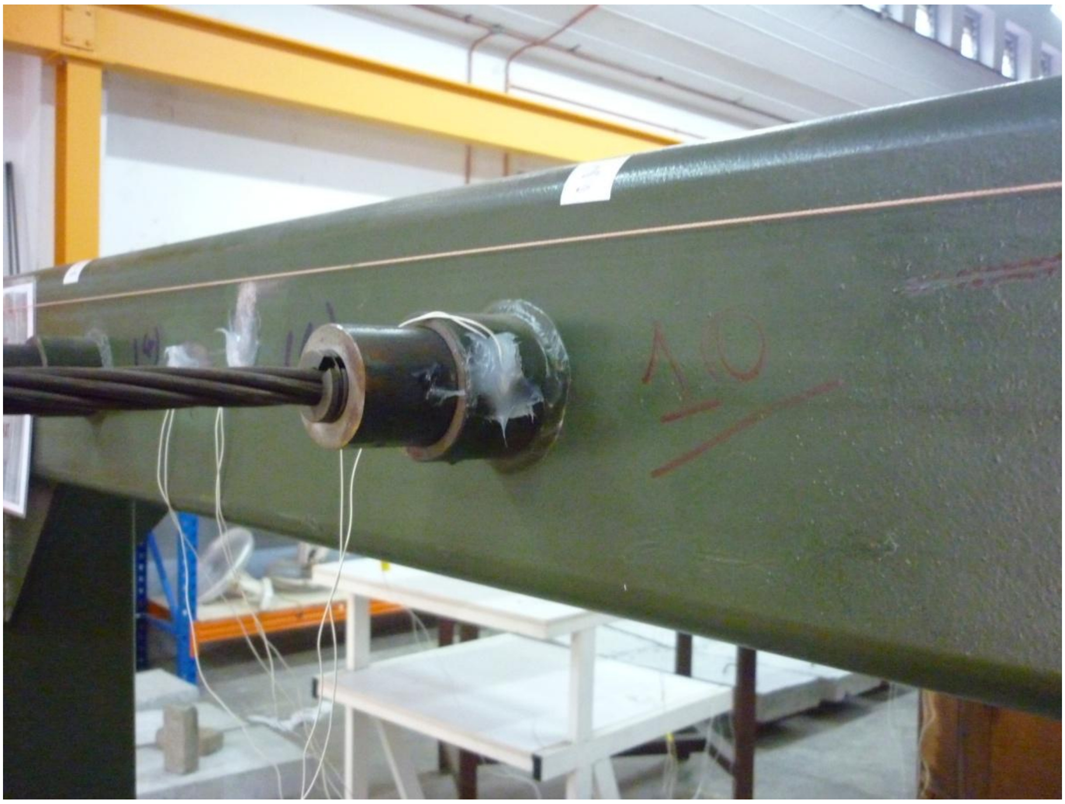

Figure 5.11: Strain gauge used on the hollow cylindrical steel section.

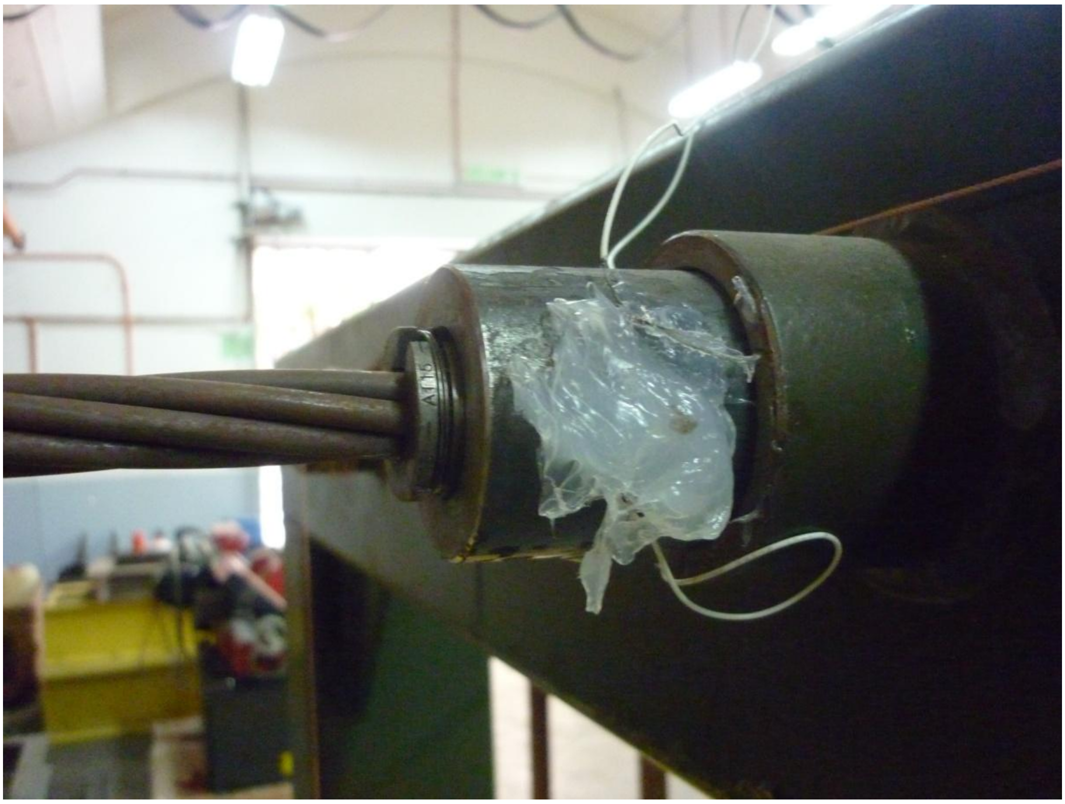

Figure 5.12: Strain gauge used on the wedge and barrel.

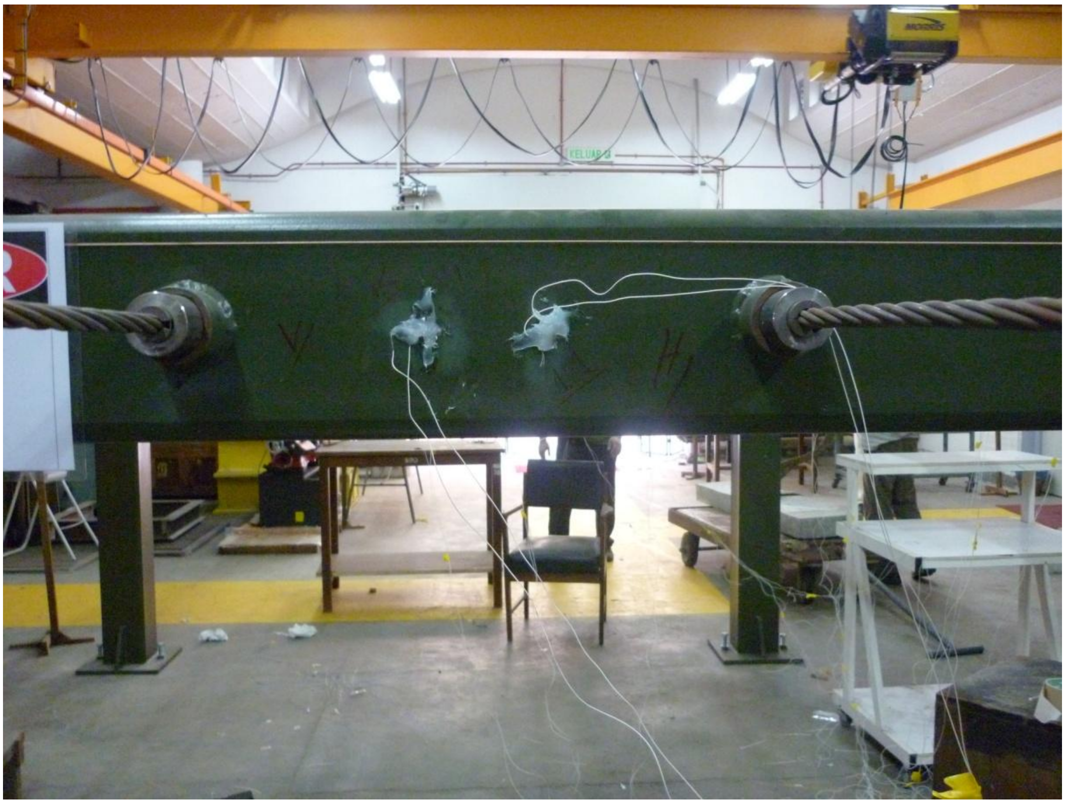

Figure 5.13: Strain gauge used on fabricated steel frame.

5.3.4 LVDT: Linear variable differential transformer

A LVDT is an electrical transformer used to measure linear displacement. The transformer has three solenoidal coils placed end-to-end around a tube. The LVDT is shown in Figure 5.14 and Figure 5.15.

The specifications and features are as follows:

a) Type: PCA – 116 Series
b) Plunger extend: Spring
c) Measuring ranges from ±0.5 mm to ±550 mm
d) Heavy, rugged construction for demanding environments
e) Conditioned outputs available; 4-20 mA, 0-5 V, 0-10 V, ±2.5 V
f) Core + extension, spring loaded and guided core with rod end bearing options

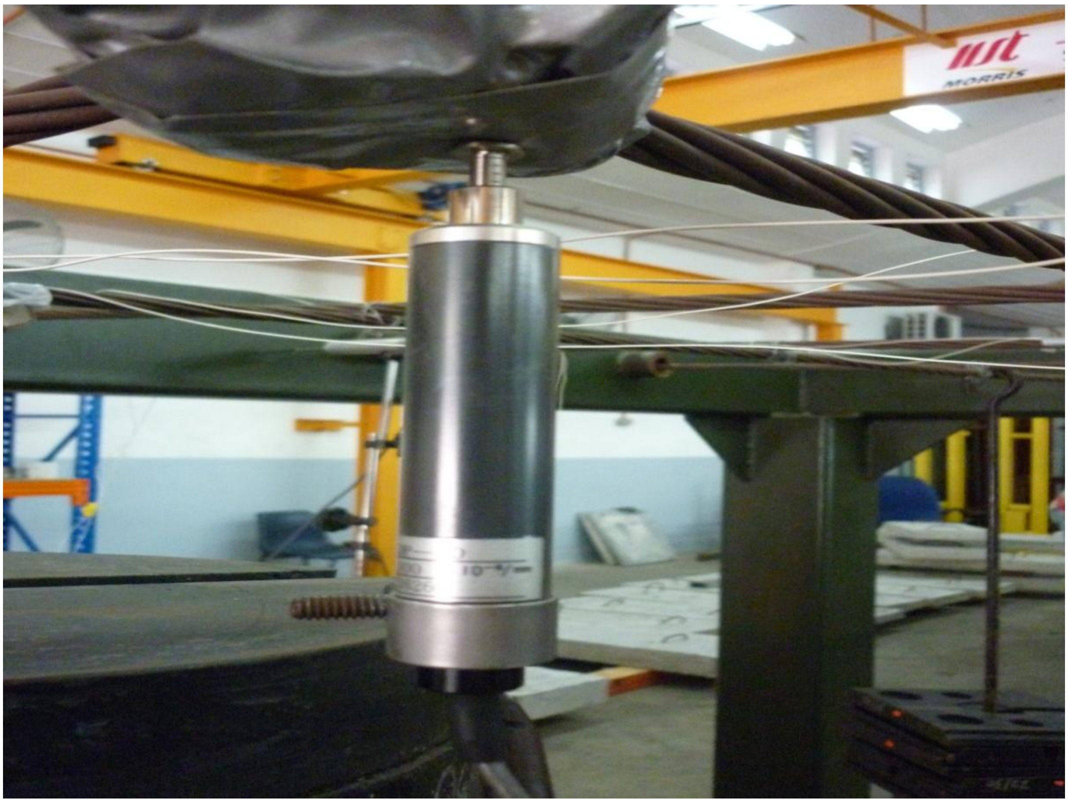

Figure 5.14: Linear variable differential transformer used on nodes.

Figure 5.15: Linear variable differential transformer used on steel frame.

5.3.5 Dial Indicator Metric

A dial indicator metric is used to monitor deflections on both sides of the frame and axis z-deflections on the wedge and barrel. The dial indicator metric is shown in Figure 5.16.

Figure 5.16: Dial indicator metric used on steel frame.

5.3.6 Weights (static loads)

The intensities and the pattern of weight are between 2.5 kg and 20 kg. The static load was applied by means of hangers with the attachments of the transducers. The weights used are shown in Figure 5.17. The position and the amount of the weight for each position depend on the type of test during experimental work.

Figure 5.17:.General view of the intensities and pattern of static loads.

In order to record the static deformation at different points of the net, the core of the eleven linear variable differential transformer (LVDT) were attached to joints 15, 16, 17, 18, 19, 20, 21, 4, 11, 25, and 32.

5.3.7 Calibration of the recording equipment

Calibration is a comparison between the measurements of the known magnitude of one device and another measurement made in a similar way with a second device. Each LVDT was connected to a specific channel and calibrated together with its extension lead by using the dial gauge.

5.3.8 Software

5.3.8.1 Visual Basic language

Visual Basic (VB) is used to develop the programme in the present project because the interface between the input data and the connection to the database is easy to use and flexible. This programme connects to Microsoft Access to use the database. In this programme, the saving of data during iteration of equations is done by Object Linking and Embedding (OLE) and macro in VB. Visual Basic is not only a programming language, but also a complete graphical development environment. This environment allows users with little programming experience to quickly develop useful Microsoft Windows applications which have the ability to use OLE objects, such as an Excel spreadsheet. Visual Basic also has the ability to develop programs that can be used as a front-end application to a database system, serving as the user interface which collects user input and displays formatted output in a more appealing and useful form than many Structured Query Language (SQL) versions are capable of. A macro is a series of commands and functions that are stored in a Microsoft Visual Basic module. In Microsoft Visual Basic, a module is a collection of declarations, statements, and procedures stored together as one named unit.

5.3.8.2 Abaqus software

Abaqus is a suite of software applications for finite element analysis (FEA) and computer-aided engineering (CAE). In this project, Abaqus is used because it is suitable for cable structures and it is also used in automotive, aerospace, and industrial products. The Abaqus software is popular with academic and usually is used to verification result from theoretical methods.

5.4 Theoretical analysis (mathematical modelling)

The theoretical result based on proposed theory in chapter 4 is calculated by structural property matrices for a pin-jointed member with three degrees of freedom at each end.

5.5 Linear Static Finite Element Analysis

The finite element analysis method is a numerical technique used to find approximate solutions of partial differential equations. In finite element, mesh is programmed to contain the material and structural properties which define how the structure will react to certain loading conditions. Nodes are assigned at a certain density throughout the material depending on the anticipated stress levels of a particular area. In this case, the type of line element is B31 and the details are given in Table 5.3. Figure 5.18 shows the mesh of the cable structure.

In the present study, the modelling space is 3D and wire is used for the shape of model. This type of model is deformable and planar. Mass density according laboratory testing is 7860 kg/m^3 and Young's Modulus is 1.926e11 N/m^2. The selected property type is isotropic elastic. The analysis has different steps. The model is considered as symmetric and linear. A general static test is selected to analyse the model. Total number of nodes and line elements are 17319 and 17460, respectively. The mesh is hex mesh with hybrid formulation and kinematic strain.

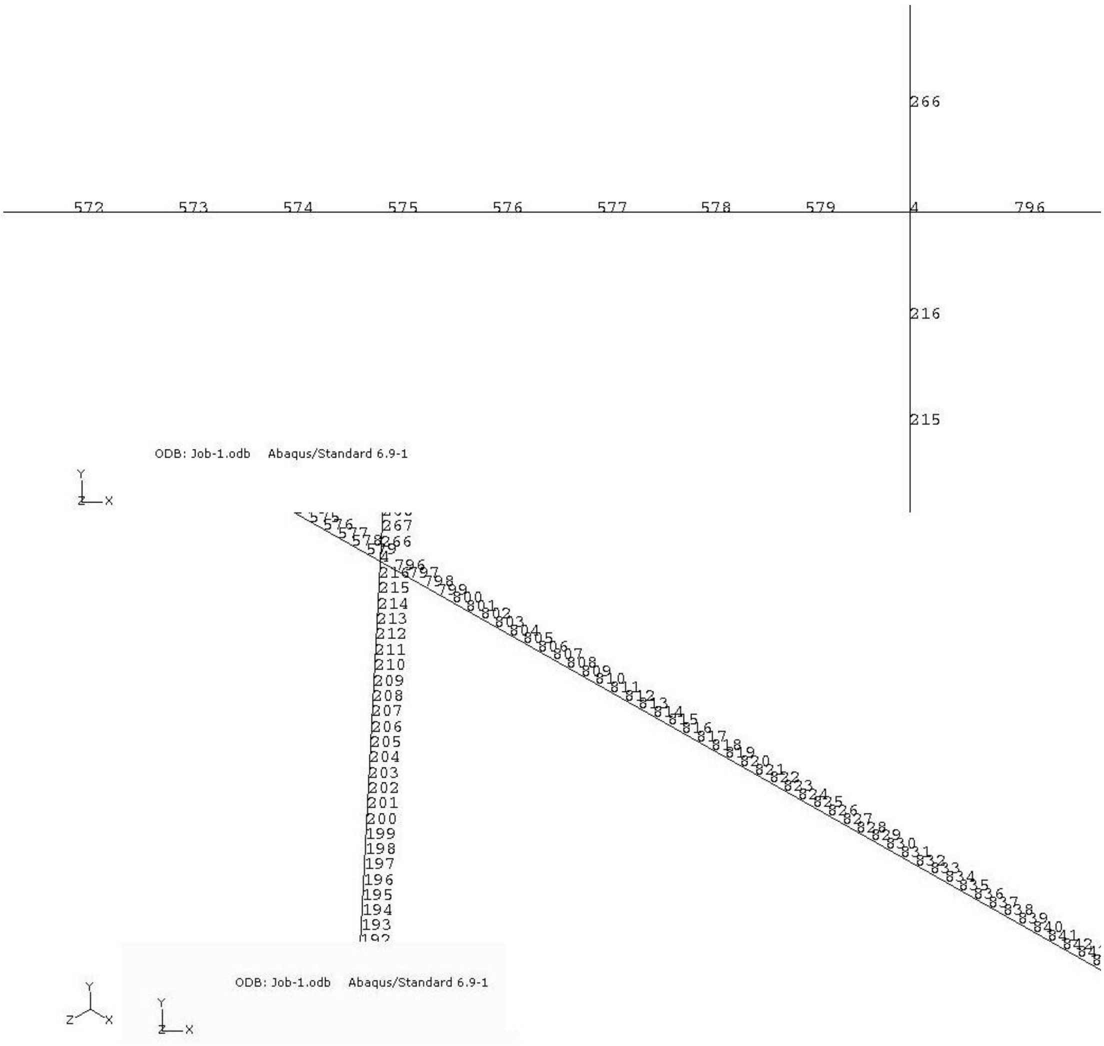

Figure 5.18: Visual of elements mesh.

The cable is modelled as three-dimensional tensioned beam elements. It includes the nonlinearities due to low strain large deformation and pre-tension. A hybrid beam element is used to model the cable. It is hybrid because it employs a mixed formulation involving six displacements and axial tension as nodal degrees of freedom. The hybrid beam element is selected for easy convergence, because linear or nonlinear truss elements can also be considered with associated limitations. The three-dimensional stiffness matrixes in Abaqus are capable of including the geometric stiffness matrix with the elastic stiffness matrix. And hex mesh is used for this modelling.

Table 5.3: Details of procedure of finite element analysis.

PART	
Modelling space	3D
Shape	Wire
Type	Deformable
Type	Planar
PROPERTY	
Mass Density	7860 kg/m^3
Poisson's Ratio	0.3
Type of Elasticity	Isotropic
Young's Modulus	1.926e11 N/m^2
STEP	
Step 1	Initial Static, Linear
Step 2	Perturbation, Method: direct Matrix
Step 3	Symmetric, Static, Linear perturbation
Step 4	Direct Matrix: symmetric, General static
MESH	
Total number of nodes	17319
Total number of linear line elements	17460
Type of linear line elements	B31
Total number of elements	17460

5.6 Static testing of the model

5.6.1 The boundary frame

To check the rigidity of the frame a dial gauge and LVDT is used to measure its movements. The maximum horizontal movement of the boundary due to 2400 N per joint occurred at joints 16 and 20 and measured 0.04 mm at each side. Hence, there is a total change of 0.08 mm in the distance between the two joints. This deflection caused a maximum calculated change of 11.5 kN in tension, i.e., changes of 0.0016% of initial tension in the cable in length of cable, which means that the horizontal deflection is zero. Based on the result, the differences in deflections are considered to be sufficiently small. Hence, it can be assumed that boundary condition for the frame is rigid.

5.6.2 The cable net

Any deficiency in the model could influence the dynamic behaviour and subsequently influence the comparison of experimental and theoretical values difficult. Hence, a static test is carried out to investigate the degree of symmetric behaviour on the frame. The investigation consisted of checking the degree of symmetric behaviour about the major and minor axes. The degree of symmetric behaviour about the minor axis is investigated by first placing an increasing load on joint 11 and then comparing the resultant displacements with those obtained by placing similar loads on joint 25. The degree of symmetric behaviour about the minor axis is similarly studied by first loading joint 16, then joint 20.

Tables 5.4 and 5.5 show the degree of symmetric behaviour about the minor axes of joint 18 and joint 11 respectively. The tables also show the percentage differences between the experimental and theoretical calculated displacements. The average lack in symmetric behaviour about the minor axis over the load range as measured by the percentage difference in the movements of joints 4 and 32 is approximately 0.09%. The lack of symmetry about the minor axis as expressed in terms of the percentage difference in the movements of joints 11 and 25 is approximately 0.07%. The symmetric behaviour charts are given in Figures 5.20 to 5.23.

The final part of the static test consisted of subjecting the net to two different types of concentrated loading. In the first case, the net was loaded with increasing load at joint 18 only. In the second case, the net was subjected to equal and increasing load at joints 1, 7, 29, and 35. In both cases the displacements of major and minor axes were recorded and compared with the theoretically calculated values. The results of the four loading cases, theoretical and experimental, for the major axis and minor axis are shown in Table 5.6. The major axis contains nodes 15, 16, 17, 18, 19, 20, and 21. The minor axis contains nodes 4, 11, 18, 25, and 32. All the static test results, namely the numerical values, visual deflections, and strain graphs are given in Appendix E.

Table 5.4: Degree of symmetry about the major and minor axes for joint 18 and deflections due to concentrated load on joint 18.

LOAD(N) = 2400	THEORETICAL (T)	EXPERIMENTAL (E)	(T – E)/ T*100
Z AXIS DEFLECTIONS (m) NODE 18 (LVDT)	178.6E-03	177.6E-03	0.56
Z AXIS DEFLECTIONS (m) NODE 11 (LVDT)	129.3E-03	127.9E-03	1.08
Y AXIS DEFLECTIONS (mm) BETWEEN NODE 46 – 47 (LVDT)		0.093	
STRAIN GAUGE (µE) BETWEEN 42-43 (HORIZONTAL) ON FRAME		45.63E-6	
STRAIN GAUGE (µE) BETWEEN 39-40 (HORIZONTAL) ON FRAME		38.76E-6	
STRAIN GAUGE (µE) BETWEEN 42-43 (VERTICAL) ON FRAME		67.98E-6	
STRAIN GAUGE (µE) BETWEEN 39-40 (VERTICAL) ON FRAME		46.783E-6	
STRAIN GAUGE (µE) BETWEEN 56-57 (VERTICAL) ON FRAME		67.51E-6	
STRAIN GAUGE (µE) BETWEEN 56-57 (HORIZONTAL) ON FRAME		42.95E-6	
STRAIN GAUGE (µE) NODE 58 (VERTICAL) ON WEDGE&BARREL		13.15E-6	
STRAIN GAUGE (µE) NODE 38 (VERTICAL) ON HOLLOW CYLINDRICAL STEEL		73.27E-8	
STRAIN GAUGE (µE) BETWEEN 49-50 (HORIZONTAL) ON FRAME		17.56E-6	
STRAIN GAUGE (µE) BETWEEN 49-50 (VERTICAL) ON FRAME		28.257E-6	
STRAIN GAUGE (µE) ELEMENT 69 (VERTICAL) ON CABLE	179.6E-06	175.3E-06	2.39
STRAIN GAUGE (µE) ELEMENT 16 (VERTICAL) ON CABLE	6.416E-06	6.255E-06	2.51

LOAD(N) = 2400	THEORETICAL (T)	EXPERIMENTAL (E)	(T – E)/ T*100
STRAIN GAUGE (µE) ELEMENT 44 (VERTICAL) ON CABLE	21.12E-06	20.65E-06	2.23
STRAIN GAUGE (µE) ELEMENT 15 (VERTICAL) ON CABLE	6.43E-06	6.12E-06	4.82
STRAIN GAUGE (µE) ELEMENT 45 (VERTICAL) ON CABLE	21.15E-06	20.44E-06	3.36
DEFLECTIONS (mm) BETWEEN NODE 43–44 (DIAL INDICATOR METRIC)		0	
AXIS Z – DEFLECTIONS (mm) NODE 37 ON WEDGE&BARREL (DIAL INDICATOR METRIC)		0.78	
Z AXIS DEFLECTIONS (m) NODE 4 (LVDT)	50.75E-03	50.11E-03	1.26
Z AXIS DEFLECTIONS (m) NODE 25 (LVDT)	127.9E-03	127.15E-03	0.59
Z AXIS DEFLECTIONS (m) NODE 32 (LVDT)	50.75E-03	50.15E-03	1.18
Z AXIS DEFLECTIONS (m) NODE 15 (LVDT)	25.83E-03	24.33E-03	5.81
Z AXIS DEFLECTIONS (m) NODE 16 (LVDT)	74.46E-03	72.56E-03	2.55
Z AXIS DEFLECTIONS (m) NODE 17 (LVDT)	135.7E-03	133.25E-03	1.81
Z AXIS DEFLECTIONS(m) NODE 19 (LVDT)	135.7E-03	134.99E-03	0.52
Z AXIS DEFLECTIONS (m) NODE 20 (LVDT)	74.46E-03	73.25E-03	1.63
Z AXIS DEFLECTIONS (m) NODE 21 (LVDT)	25.83E-03	25.45E-03	1.47
Z AXIS DEFLECTIONS (m) NODE 1 (LVDT)	8.298E-03	8.112E-03	2.24
Z AXIS DEFLECTIONS (m) NODE 7 (LVDT)	8.298E-03	8.211E-03	1.05
Z AXIS DEFLECTIONS (m) NODE 29 (LVDT)	8.298E-03	8.256E-03	0.51
Z AXIS DEFLECTIONS (m) NODE 35 (LVDT)	8.298E-03	8.0253E-03	3.29

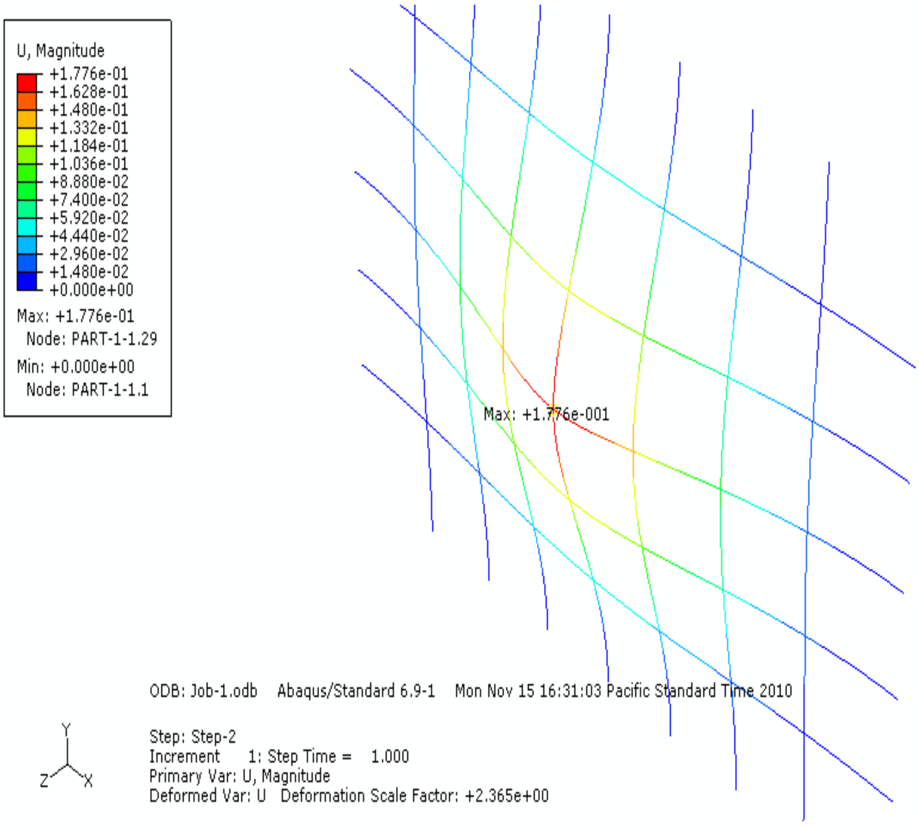

Figure 5.19: Deflections due to concentrated load on joint 18.

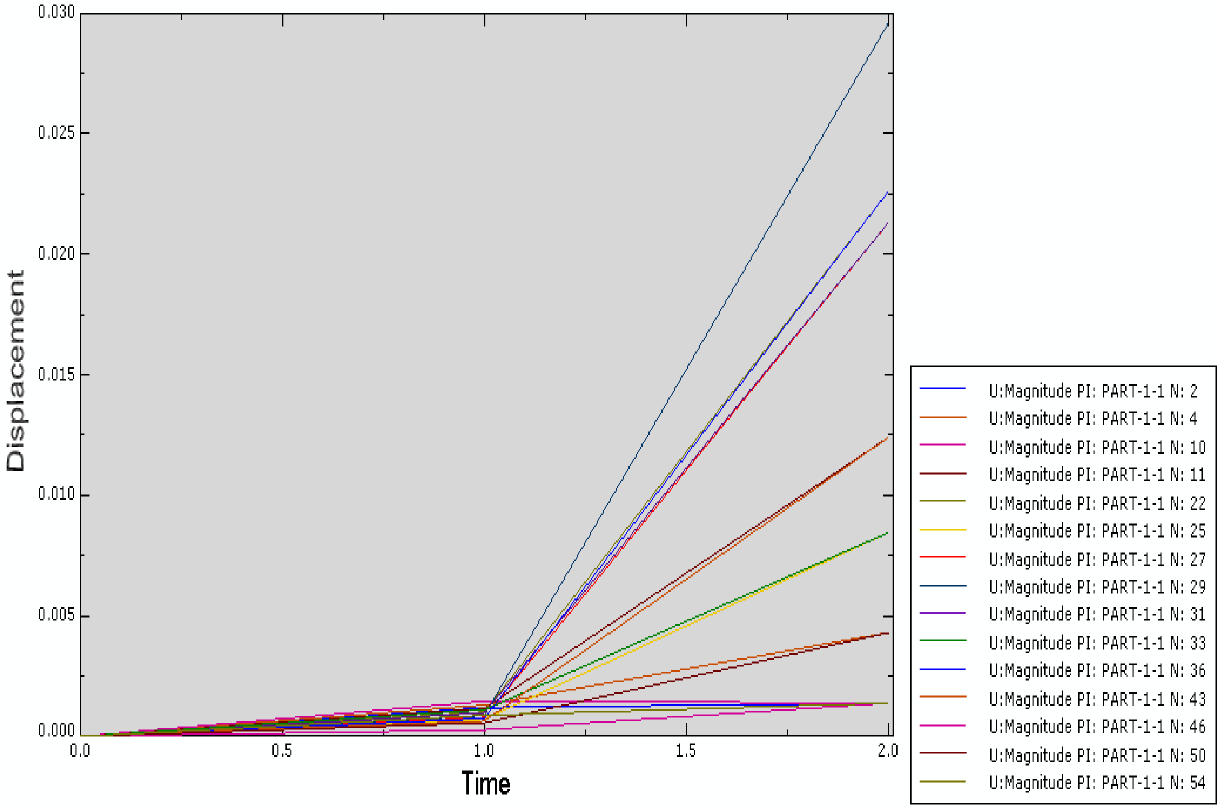

Figure 5.20: Displacement of major, minor axes.

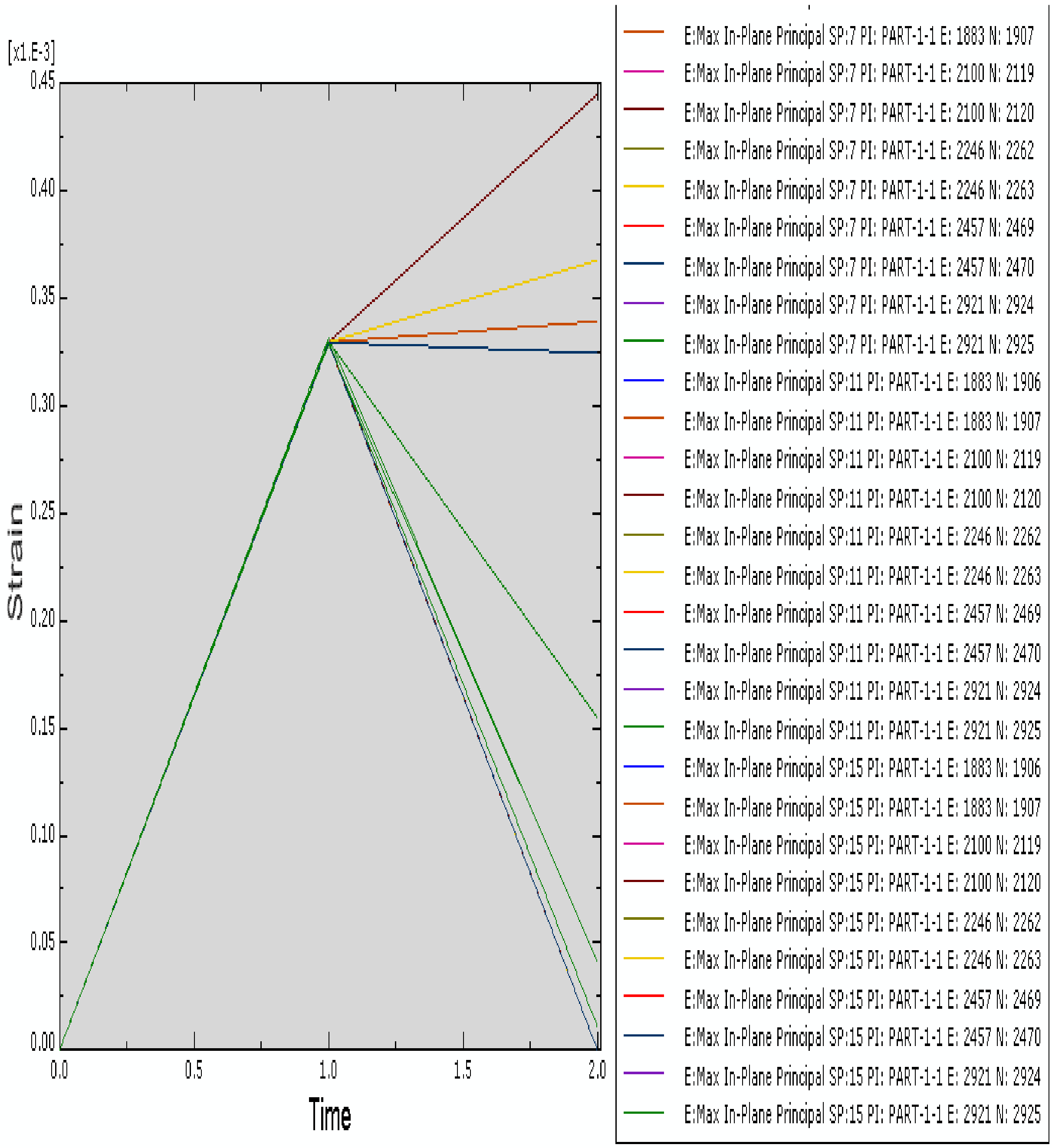

Figure 5.21: Strain of elements (2457, 2246, 1883, 2100, and 2921).

Table 5.5: Degree of symmetry about the major and minor axes for joint 11 and deflections due to concentrated load on joint 11.

LOAD(N) = 2400	THEORETICAL (T)	EXPERIMENTA L (E)	(T – E)/ T*100
Z AXIS DEFLECTIONS (m) NODE 18 (LVDT)	127.9E-03	125.2E-03	2.11
Z AXIS DEFLECTIONS (m) NODE 11 (LVDT)	142.3E-03	141.5E-03	0.56
Y AXIS DEFLECTIONS (mm) BETWEEN NODE 46 – 47 (LVDT)		0.097	
STRAIN GAUGE (µE) BETWEEN 42-43 (HORIZONTAL) ON FRAME		45.63E-6	
STRAIN GAUGE (µE) BETWEEN 39-40 (HORIZONTAL) ON FRAME		38.76E-6	
STRAIN GAUGE (µE) BETWEEN 42-43 (VERTICAL) ON FRAME		67.98E-6	
STRAIN GAUGE (µE) BETWEEN 39-40 (VERTICAL) ON FRAME		46.783E-6	
STRAIN GAUGE (µE) BETWEEN 56-57 (VERTICAL) ON FRAME		67.51E-6	
STRAIN GAUGE (µE) BETWEEN 56-57 (HORIZONTAL) ON FRAME		42.95E-6	
STRAIN GAUGE (µE) NODE 58 (VERTICAL) ON WEDGE&BARREL		13.15E-6	
STRAIN GAUGE (µE) NODE 38 (VERTICAL) ON HOLLOW CYLINDRICAL STEEL		73.27E-8	
STRAIN GAUGE (µE) BETWEEN 49-50 (HORIZONTAL) ON FRAME		17.56E-6	
STRAIN GAUGE (µE) BETWEEN 49-50 (VERTICAL) ON FRAME		28.257E-6	
STRAIN GAUGE (µE) ELEMENT 69 (VERTICAL) ON CABLE	297.5E-06	295.6E-06	0.64
STRAIN GAUGE (µE) ELEMENT 16 (VERTICAL) ON CABLE	236.7E-06	234.3E-06	1.01

LOAD(N) = 2400	THEORETICAL (T)	EXPERIMENTAL (E)	(T – E)/ T*100
STRAIN GAUGE (µE) ELEMENT 44 (VERTICAL) ON CABLE	31.94E-06	31.00E-06	2.94
STRAIN GAUGE (µE) ELEMENT 15 (VERTICAL) ON CABLE	236.7E-06	236.2E-06	0.21
STRAIN GAUGE (µE) ELEMENT 45 (VERTICAL) ON CABLE	8.79E-06	8.22E-06	6.48
DEFLECTIONS (mm) BETWEEN NODE 43–44 (DIAL INDICATOR METRIC)		0	
AXIS Z – DEFLECTIONS (mm) NODE 37 ON WEDGE&BARREL (DIAL INDICATOR METRIC)		0.78	
Z AXIS DEFLECTIONS (m) NODE 4 (LVDT)	67.78E-03	65.28E-03	3.69
Z AXIS DEFLECTIONS (m) NODE 25 (LVDT)	78.68E-03	77.28E-03	1.78
Z AXIS DEFLECTIONS (m) NODE 32 (LVDT)	29.54E-0	29.24E-0	1.02
Z AXIS DEFLECTIONS (m) NODE 15 (LVDT)	20.70E-03	20.32E-03	1.84
Z AXIS DEFLECTIONS (m) NODE 16 (LVDT)	54.46E-03	53.23E-03	2.26
Z AXIS DEFLECTIONS (m) NODE 17 (LVDT)	104.2E-03	101.5E-03	2.59
Z AXIS DEFLECTIONS (m) NODE 19 (LVDT)	104.2E-03	102.1E-03	2.02
Z AXIS DEFLECTIONS (m) NODE 20 (LVDT)	59.30E-03	57.22E-03	3.51
Z AXIS DEFLECTIONS(m) NODE 21 (LVDT)	20.70E-03	20.52E-03	0.87
Z AXIS DEFLECTIONS (m) NODE 1 (LVDT)	7.726E-03	7.700E-03	0.34
Z AXIS DEFLECTIONS (m) NODE 7 (LVDT)	7.726E-03	7.700E-03	0.34
Z AXIS DEFLECTIONS (m) NODE 29 (LVDT)	5.590E-03	5.40E-03	3.4
Z AXIS DEFLECTIONS (m) NODE 35 (LVDT)	5.590E-03	5.40E-03	3.4

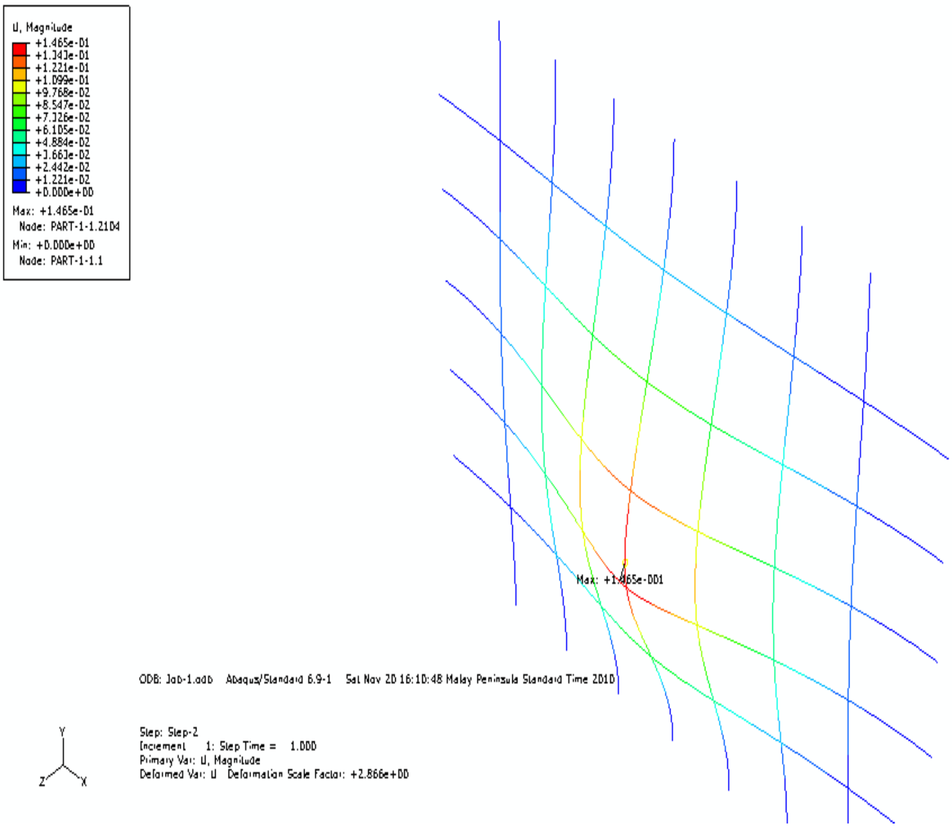

Figure 5.22: Deflections due to concentrated load on joint 11.

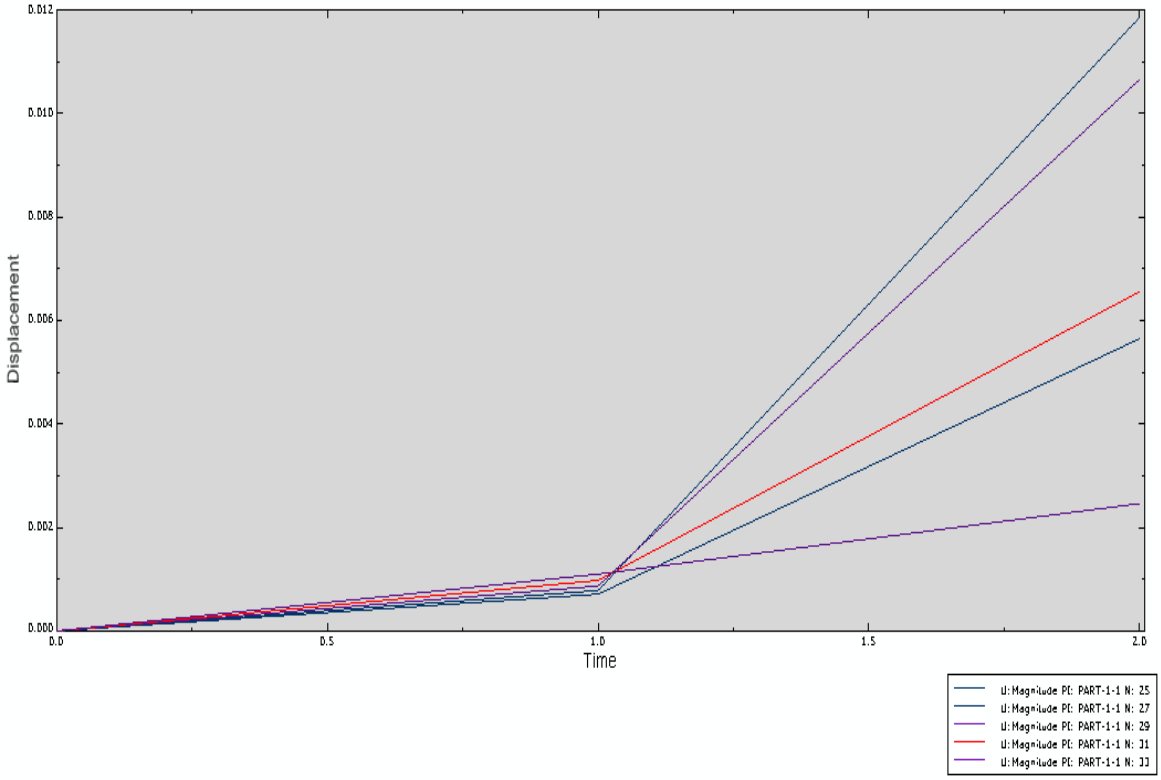

Figure 5.23: Displacements of minor axis (4, 11, 18, 25, 32).

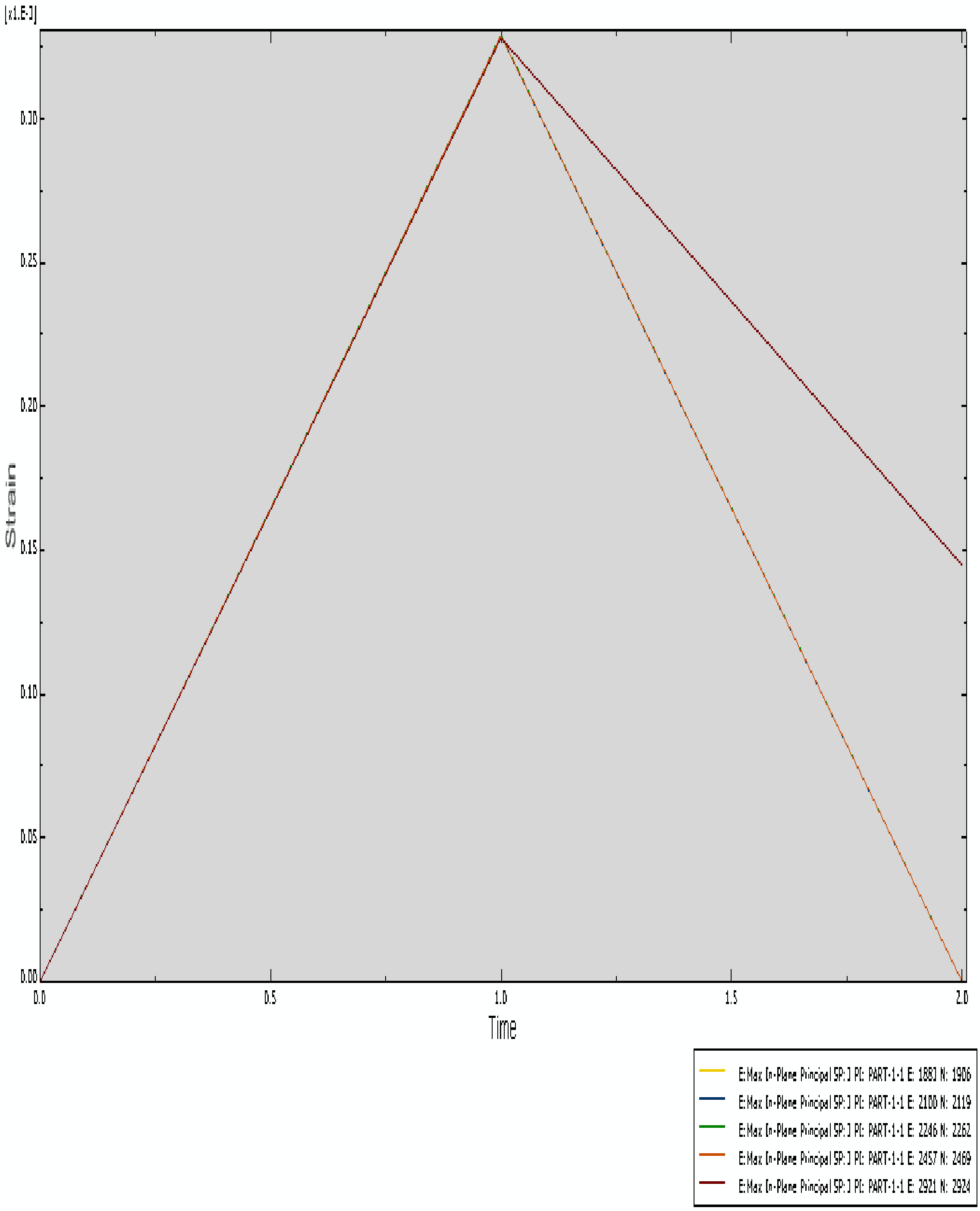

Figure 5.24: Strain-time graph of elements (1883, 2100, 2246, 2457, 2921).

5.7 Discussion and comparison of results

In this section, the theoretical and experimental results are compared. The results indicate that the percentage difference between the theoretical and experimental displacements decreases with increasing loading. For the maximum loading at joint 18, the percentage differences of measured displacement between the theoretical and experimental ranged from 2.1% to 5.3%. Hence, the percentage differences between theoretical and experimental result are acceptable. Figure 5.25 shows the relationship between loads and deflection in the minor axis when concentrated load is placed on node 16 and node 20. The deflection in the graph is measured in units, each of which is equivalent to one metre. The deflection steadily climbs from 2.55 cm in node 4 and is projected to reach 7.45 cm on node 18. From this point onwards, it is projected to decline dramatically until it reaches 2.55 cm on node 32.

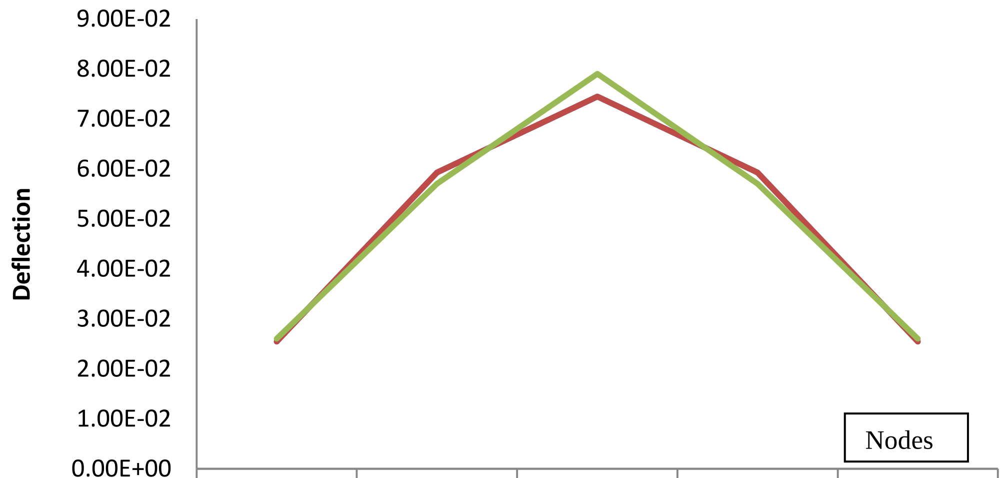

	4	11	18	25	32
ELN 16	2.55E-02	5.93E-02	7.45E-02	5.93E-02	2.55E-02
ELN 20	2.55E-02	5.93E-02	7.45E-02	5.93E-02	2.55E-02
TLN 16,20	2.60E-02	5.70E-02	7.90E-02	5.70E-02	2.60E-02

Figure 5.25: Degree of symmetry about minor axis when the load is placed on nodes 16 and 20.

ELN 16: Experimental result of load on node 16 ELN 20: Experimental result of load on node 20

TLN 16: Theoretical result of load on node 16 TLN 20: Theoretical result of load on node 20

The graphs of the experimental result and the theoretical result confirm that the difference between them is negligible. Figure 5.26 shows the relationship between loads and deflection in the major axis. When the concentrated load is placed on node 20, the deflection gradually increases from 0.535 cm on node 15. It reaches a peak of 12.7 cm on node 20. From this point onwards, it is projected to drop sharply until it reaches 0.607 cm on node 15. When concentrated load is placed on node 16, the deflection from about 0.607 cm on node 15 rapidly rises to reach a peak of 12.7 cm on node 16. From this point onwards, it is projected to fall slightly until it reaches 0.535 cm units on node 21. The difference between the theoretical and experimental values is negligible. The degree of symmetry about the corner of frame when the load is placed on nodes 16 and 20 is almost zero, as shown in Figure 5.26.

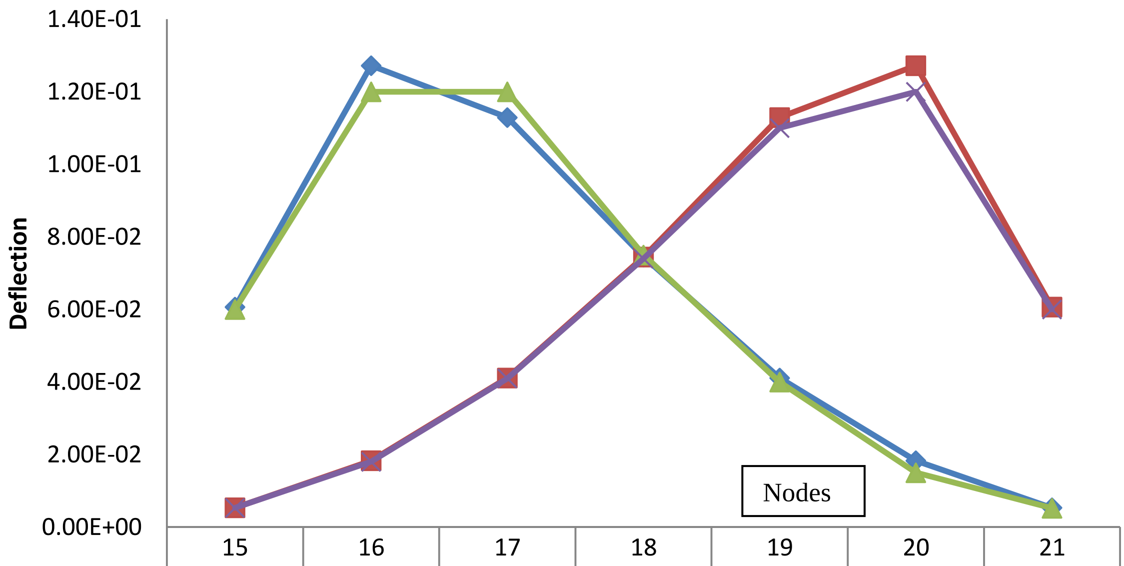

	15	16	17	18	19	20	21
ELN 16	6.07E-02	1.27E-01	1.13E-01	7.45E-02	4.11E-02	1.83E-02	5.35E-03
ELN 20	5.35E-03	1.83E-02	4.11E-02	7.45E-02	1.13E-01	1.27E-01	6.07E-02
TLN 16	6.00E-02	1.20E-01	1.20E-01	7.50E-02	4.00E-02	1.50E-02	5.20E-03
TLN 20	5.30E-03	1.80E-02	4.10E-02	7.40E-02	1.10E-01	1.20E-01	6.00E-02

Figure 5.26: Degree of symmetry about minor axis when the load is placed on nodes 16 and 20.

ELN 16: Experimental result of load on node 16   ELN 20: Experimental result of load on node 20

TLN 16: Theoretical result of load on node 16   TLN 20: Theoretical result of load on node 20

The degree of symmetry about the corner of frame when the load is placed on nodes 16 and 20 is shown in Figure 5.27. When the concentrated load is placed on node 16, the deflection rapidly increases from node 1 until node 7 and from this node onward, deflection drops slightly and is projected to reach minimum deflection on node 35. The experimental and theoretical results are in good agreement.

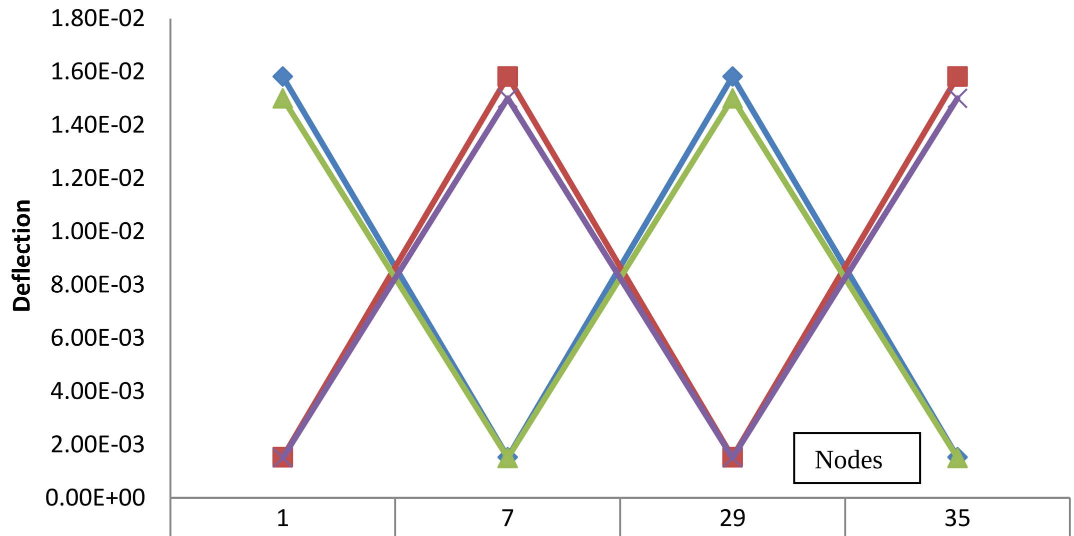

	1	7	29	35
ELN 1	1.58E-02	1.53E-03	1.58E-02	1.53E-03
ELN 7	1.53E-03	1.58E-02	1.53E-03	1.58E-02
ELN 29	1.50E-02	1.50E-03	1.50E-02	1.50E-03
ELN 35	1.50E-03	1.50E-02	1.50E-03	1.50E-02

Figure 5.27: Degree of symmetry about corner of frame when the load is placed on nodes 16 and 20.

ELN 1: Experimental result of load on node 1 ELN 7: Experimental result of load on node 7

ELN 29: Experimental result of load on node 29 ELN 35: Experimental result of load on node 35

Figure 5.28 shows the relationship between loads and deflection in minor axis. When concentrated load is placed on node 18, the deflection climbs slowly between nodes 4 and 18 from 5.08 cm until 17.9 cm of deflection and dropped slowly to node 32.

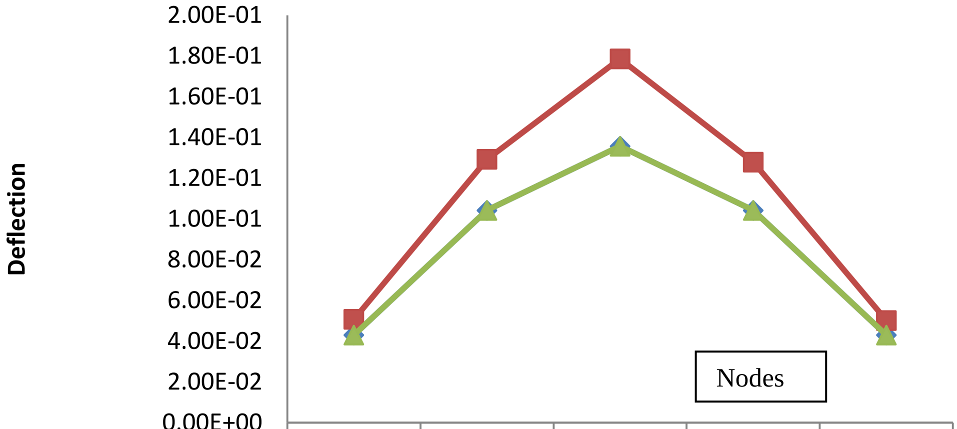

	4	11	18	25	32
Load on Node 17	4.30E-02	1.04E-01	1.36E-01	1.04E-01	4.30E-02
Load on Node 18	5.08E-02	1.29E-01	1.79E-01	1.28E-01	5.02E-02
Load on Node 19	4.30E-02	1.04E-01	1.36E-01	1.04E-01	4.30E-02

Figure 5.28: Degree of symmetric about minor axis when the load is placed on nodes 17, 18, and 19.

Figure 5.29 shows what occurs when concentrated load is placed on node 17, 18, and node 19. The deflection of node 18 soars between nodes 15 and 17 from 4.31 cm until 16.7 cm. From this point onwards, it is projected to decline slightly to reach 1.31 mm on node 21. The differences of deflection in the minor and major axes are negligible.

Figure 5.30 shows the degree of symmetry about the minor axis when the load is placed on nodes 17, 18, and 20. The comparative deflection, when the load is placed on nodes 17 and 19 separately, suggests that the degree of symmetry is probably zero. Therefore the boundary condition of the frame is rigidity.

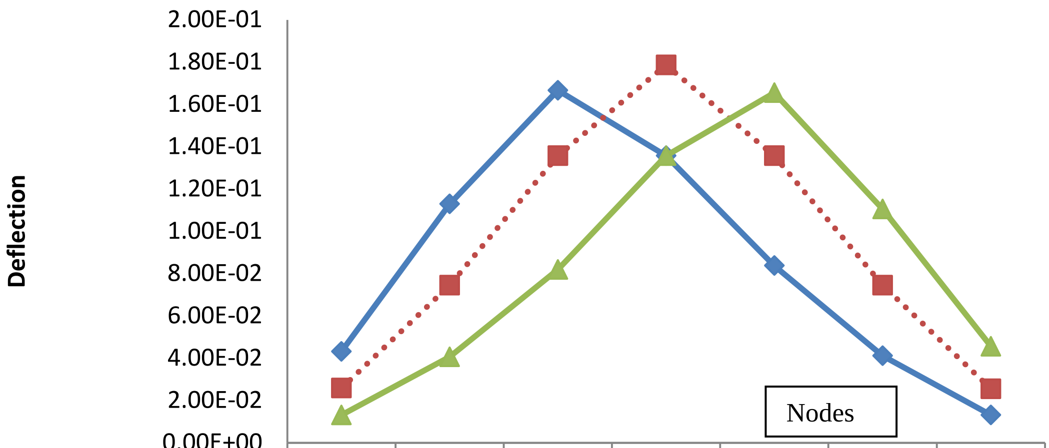

	15	16	17	18	19	20	21
Load on Node 17	4.31E-02	1.13E-01	1.67E-01	1.36E-01	8.37E-02	4.11E-02	1.31E-02
Load on Node 18	2.58E-02	7.45E-02	1.36E-01	1.79E-01	1.36E-01	7.45E-02	2.55E-02
Load on Node 19	1.31E-02	4.06E-02	8.19E-02	1.36E-01	1.66E-01	1.11E-01	4.56E-02

Figure 5.29: Degree of symmetry about major axis when the load is placed on nodes 17, 18, and 19.

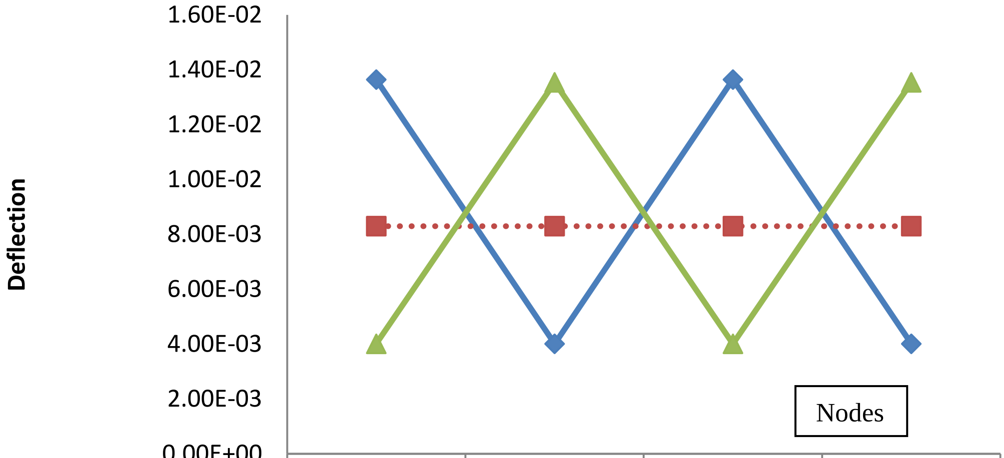

	1	7	29	35
Load on Node 17	1.36E-02	4.01E-03	1.36E-02	4.01E-03
Load on Node 18	8.30E-03	8.30E-03	8.30E-03	8.30E-03
Load on Node 19	4.01E-03	1.35E-02	4.01E-03	1.35E-02

Figure 5.30: Degree of symmetry about corner of frame when the load is placed on nodes 17, 18, and 19.

Figure 5.31 shows the relationship between loads and deflection in the major axis when the load is placed on nodes 11 and 25. The deflection between node 15, 16, 17 and 19, 20, and 21 is subsequently compared. The behaviour and value of the deflection are in good agreement.

Figure 5.32 shows that when the load is placed on node 1, 7, 29, and 35, the deflection of node 18 soars to 2.58 cm until it reaches 17.9 cm. From this point onward, the deflection declined to 2.58 cm on node 21. The theoretical and experimental values are in good agreement.

Figure 5.33 shows that the deflection appears to level off and remained constant at about 0.77 cm of deflection. From this point onwards, the deflection drops slowly from nodes 7 to 29 and remains constant from about 0.559 cm on nodes 29 to 35. Hence, the boundary condition is rigidity. The values of deflection when loads are placed on the minor and major axes at the same time are given in Table 5.5 and Table 5.6 and Appendix C.

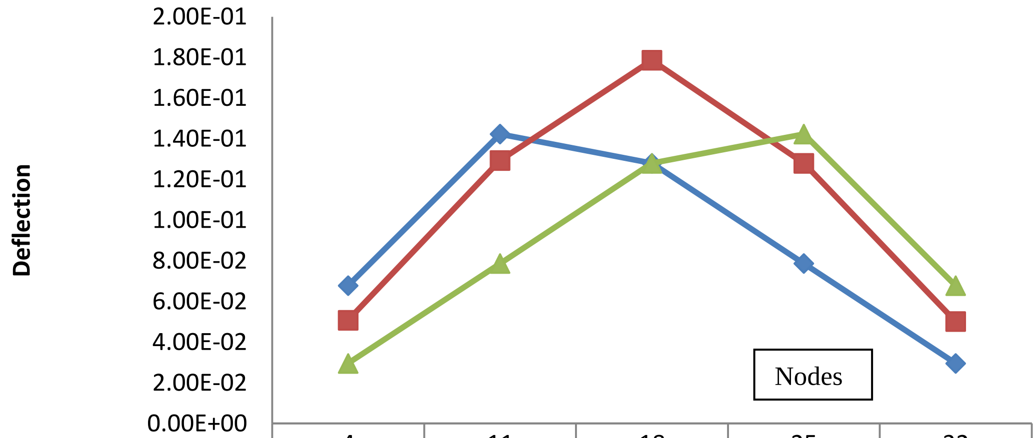

	4	11	18	25	32
Load on Node 11	6.78E-02	1.42E-01	1.28E-01	7.87E-02	2.95E-02
Load on Node 18	5.08E-02	1.29E-01	1.79E-01	1.28E-01	5.02E-02
Load on Node 25	2.95E-02	7.87E-02	1.28E-01	1.42E-01	6.78E-02

Figure 5.31: Degree of symmetry about major axis when the load is placed on nodes 11 18, and 25.

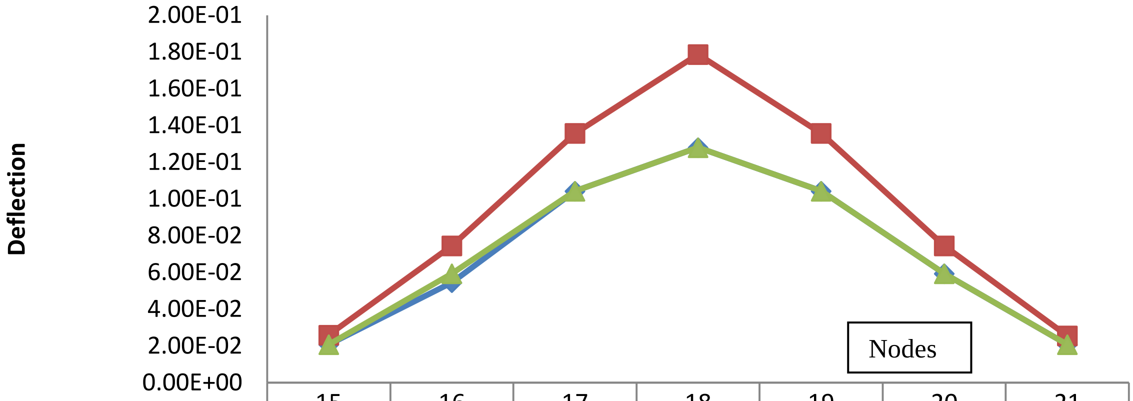

	15	16	17	18	19	20	21
Load on Node 11	2.07E-02	5.45E-02	1.04E-01	1.28E-01	1.04E-01	5.93E-02	2.07E-02
Load on Node 18	2.58E-02	7.45E-02	1.36E-01	1.79E-01	1.36E-01	7.45E-02	2.55E-02
Load on Node 25	2.07E-02	5.93E-02	1.04E-01	1.28E-01	1.04E-01	5.93E-02	2.07E-02

Figure 5.32:.Degree of symmetric about major axis when the load is placed on node 11, 18, and 25

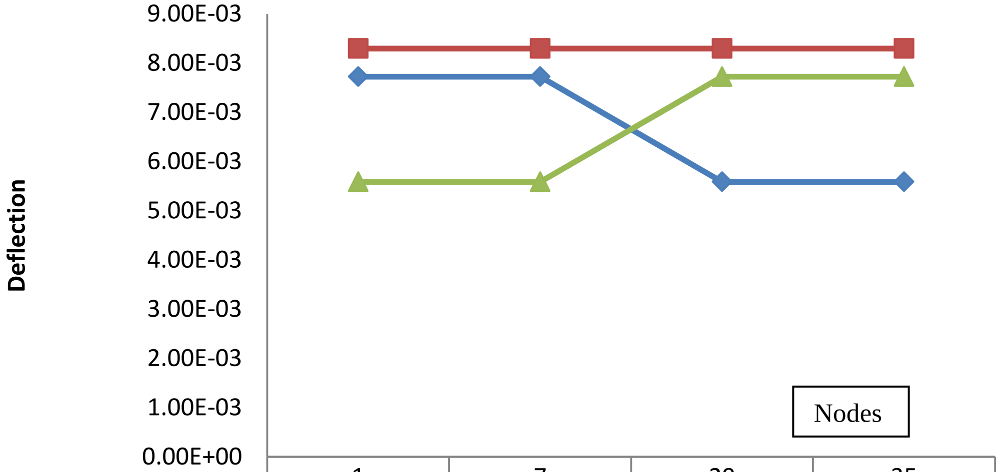

	1	7	29	35
Load on Node 11	7.73E-03	7.73E-03	5.59E-03	5.59E-03
Load on Node 18	8.30E-03	8.30E-03	8.30E-03	8.30E-03
Load on node 25	5.59E-03	5.59E-03	7.73E-03	7.73E-03

Figure 5.33: Degree of symmetry about corner of frame when the load is placed on nodes 11, 18, and 25.

Table 5.6: Degree of symmetry about the minor axis when loads are placed on nodes 4, 11, 16 , 25, and 32.

Load on Node	4	11	18	25	32
Def.Node	**Minor Axis**				
4		67.78E-03	50.75E-03	29.54E-03	
11		142.3E-03	129.3E-03	78.68E-03	
18		127.9E-03	178.6E-03	127.9E-03	
25		78.68E-03	127.9E-03	142.3E-03	
32		29.54E-3	50.15E-03	67.78E-03	
15		20.70E-03	25.83E-03	20.70E-03	
16		54.46E-03	74.46E-03	59.30E-03	
17		104.2E-03	135.7E-03	104.2E-03	
18		127.9E-03	178.6E-03	127.9E-03	
19		104.2E-03	135.7E-03	104.2E-03	
20		59.30E-03	74.46E-03	59.30E-03	
21		20.70E-03	25.45E-03	20.70E-03	
1		7.726E-03	8.298E-03	5.590E-03	
7		7.726E-03	8.298E-03	5.590E-03	
29		5.590E-03	8.298E-03	7.726E-03	
35		5.590E-03	8.298E-03	7.726E-03	

Table 5.7:Degree of symmetry about the major axis when loads are placed on nodes 16, 17, 18, 19, and 20.

Load on Node	16	17	18	19	20
Def.Node	Major Axis				
4	25.46E-03	43.02E-03	50.75E-03	43.02E-03	25.46E-03
11	59.30E-03	104.2E-03	129.3E-03	104.2E-03	59.30E-03
18	74.46E-03	135.7E-03	178.6E-03	135.7E-03	74.46E-03
25	59.30E-03	104.2E-03	127.9E-03	104.2E-03	59.30E-03
32	25.46E-03	43.02E-03	50.15E-03	43.02E-03	25.46E-03
15	60.67E-03	43.12E-03	25.83E-03	13.09E-03	5.348E-03
16	127.2E-03	112.9E-03	74.46E-03	40.58E-03	18.32E-03
17	112.9E-03	166.6E-03	135.7E-03	81.88E-03	41.11E-03
18	74.46E-03	135.7E-03	178.6E-03	135.7E-03	74.46E-03
19	41.11E-03	83.74E-03	135.7E-03	165.5E-03	112.9E-03
20	18.32E-03	41.11E-03	74.46E-03	110.5E-03	127.2E-03
21	5.348E-03	13.09E-03	25.45E-03	45.55E-03	60.67E-03
1	15.82E-03	13.64E-03	8.298E-03	4.008E-03	1.527E-03
7	1.527E-03	4.008E-03	8.298E-03	13.54E-03	15.82E-03
29	15.82E-03	13.64E-03	8.298E-03	4.008E-03	1.527E-03
35	1.527E-03	4.008E-03	8.298E-03	13.54E-03	15.82E-03

5.8 Conclusion

The values between the calculated and experimental static deflections are in agreement with each other. The small differences are due to experimental devices and environment condition. The static test checked the stiffness of the boundary and shows that the degree of error for any elastic deformation of the frame is almost negligible. Hence, the result verifies that the frame is symmetric and rigid. Tests conducted with different patterns and intensities of static loading in order to compare the experimental and theoretical values of the static deformation showed that the deflection calculated by the proposed nonlinear method gives reasonably accurate results.

CHAPTER 6: DYNAMIC TEST

NUMERICAL ANALYSIS AND EXPERIMENTAL WORK

RESULTS AND DISCUSSION

6.1 Introduction

The objectives of the experimental work described in this chapter are to validate the dynamic theory proposed in chapter 4 and to check the software programme based upon the static theory given in chapter 3. This chapter presents the dynamic part of the numerical analysis (theoretical modelling and Finite Element Analysis) and dynamic testing of the experimental model. In dynamic theory, it is assumed that the cable attachments at the boundary do not move. Thus, a net with as rigid a boundary as possible had to be constructed. The objectives of the numerical analysis and the dynamic experimental work in this chapter can be summarized as the follows:

A. To carry out modal testing in order to compare the theoretical and experimental values of natural frequencies, mode shapes, and modal damping ratios;

B. To perform a parametric study of the dynamic response due to exciting the structure with different intensities from different points in order to verify the proposed theory;

C. To compare the predicted nonlinear responses with those obtained by linear modal analysis;

D. To study the influence of the magnitude of the damping ratios in the different modes when using an orthogonal damping matrix;

E. To compare the computational time by using the Fletcher-Reeves and Newton-Raphson algorithms;

F. To study the influence of the time step upon stability and accuracy.

6.2 Numerical analysis and experimental work

In this chapter, the details are presented of the mathematical modelling, Finite Element Analysis, modal testing, and parametric study conducted on the dynamic response of the experimental model.

6.3 Theoretical analysis (mathematical modelling)

The theoretical result based on the proposed theory in chapter 4 is calculated based on the structural property matrices presented in chapter 5 for a pin-jointed member with three degrees of freedom at each end.

6.3.1 The lumped mass matrices for a pin-jointed member

$$\frac{\bar{m} L}{3} * \begin{vmatrix} 1 & 0 & 0 & 0 & 0 & 0 \\ 0 & 1 & 0 & 0 & 0 & 0 \\ 0 & 0 & 1 & 0 & 0 & 0 \\ 0 & 0 & 0 & 1 & 0 & 0 \\ 0 & 0 & 0 & 0 & 1 & 0 \\ 0 & 0 & 0 & 0 & 0 & 1 \end{vmatrix} \qquad 6.1$$

Equation 6.1 represents the lumped mass matrices for a pin-jointed member where $\bar{m}$ is the mass over length (L) and L is the length of member.

6.3.2 The stiffness matrix for a pin-jointed member

$$= \frac{EA}{L}\begin{vmatrix} \lambda_1^2 & \lambda_1\lambda_2 & \lambda_1\lambda_3 \\ \lambda_2\lambda_1 & \lambda_2^2 & \lambda_2\lambda_3 \\ \lambda_3\lambda_1 & \lambda_3\lambda_2 & \lambda_3^2 \end{vmatrix} + \frac{T}{L}\begin{vmatrix} 1-\lambda_1^2 & -\lambda_1\lambda_2 & -\lambda_1\lambda_3 \\ -\lambda_2\lambda_1 & 1-\lambda_2^2 & -\lambda_2\lambda_3 \\ -\lambda_3\lambda_1 & -\lambda_3\lambda_2 & 1-\lambda_3^2 \end{vmatrix} \qquad 6.2$$

where T is the axial force in the axial force and λ_1, λ_2 and λ_3 are the corresponding direction cosines.

6.3.3 The orthogonal damping matrices

This damping matrix is one in which many modes can be given by:

$$C = M\left(\sum_{n=1}^{N}\frac{2\varepsilon_n\omega_n}{\phi_n^T M\phi_n}\phi_n\phi_n^T\right)M \qquad 6.3$$

where n = the mode number.

ϕ_n = the nth mode shape vector.

M = diagonal mass matrix.

6.4 Dynamic finite element analysis using Abaqus

As mentioned in chapter 5, the type of line element is B31 and the modelling space is 3D. Wire is used for the shape of the model. The model type is deformable and planar. According to laboratory testing, mass density is 7860 kg/m^3 and Young's Modulus is 1.926e11 N/m^2. The selected property is isotropic elastic. During dynamic testing, the type of analysis is changed according to the kind of structural analysis being undertaken. In this case, the Lanczos frequency solver and dynamic modal analysis of normalized eigenvalues by mass is considered. The parameters of the model according to finite element modelling are given in Table 6.1. Figure 6.1 shows the visual mesh of the finite element structure. Table 6.1: The features of finite element modelling.

Part	
Modelling space	3D
Shape	Wire
Type	Deformable, planar
Property	
Mass density	7860 kg/m^3
Poisson's Ratio	0 .3
Type of elasticity	Isotropic
Young's Modulus	1.926e11 N/m^2
Step	
Step 1	Initial Static, Linear
Step 2	Perturbation, Method: direct Matrix, Method: direct Matrix storage: symmetric.
Step 3	Symmetric, Static, Linear perturbation, Static, Linear perturbation Method: direct Matrix storage: symmetric.
Step 4	Frequency , Eigensolver: Lanczos Normalize eigenvectors by mass.
Step 5	Modal dynamic, Load variation with time is instantaneous.
Mesh	
Total number of nodes	19755
Total number of linear line elements	19879
Linear line elements type	B31

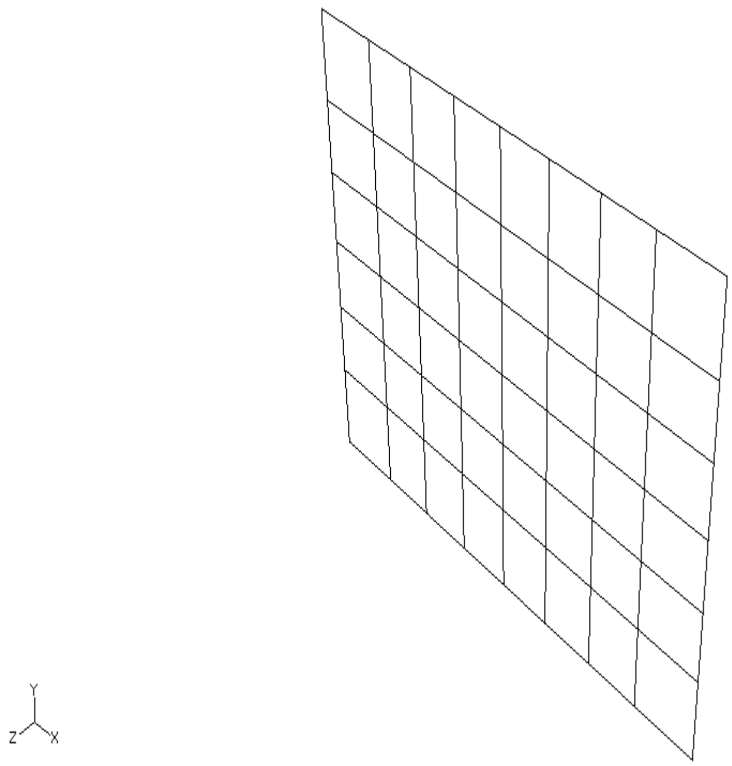

Figure 6.1: Visual of finite element structure.

6.5 Modal Testing

Modal analysis is defined as the process of characterizing the dynamics of a structure in terms of its modes of vibration. The eigenvalues of the equations of motion correspond to the frequencies at which the structure tends to vibrate with a predominant, well-defined deformation. The amplitude of this wave motion on the structure is specified by the corresponding eigenvector. Each mode of vibration, then, is defined by an eigenvalue (resonant frequency) and a corresponding eigenvector (mode shape). Preliminary modal testing showed that the net possessed very low damping. This finding, together with the fact that the only one point is excited, made it difficult to achieve standing mode shapes. Ideally, to obtain pure modes of vibration the number of exciters should equal the number of degrees of freedom. In the end, stand waves were obtaining after different testing methods such as the Nyquist, Bode, and CoQuad were applied. The advantages of the transfer function method are:

a) Impact testing is quick and inexpensive;
b) Prior knowledge of modes is not required;
c) Digital accuracy and repeatability;
d) Essentially unlimited frequency resolution;
e) Easier to make measurements and statistical estimation of modal parameters;
f) Reduced effects of noise and nonlinear distortion.

In modal testing, it is assumed that structural motion can be described by linear second order equations and that only one mode exists at each pole location. The scrutinizing process used to characterize the dynamics of a structure in modal testing needs to be given the signal processing parameters. The signal processing parameters are provided in the following subsections 6.5.1 to 6.5.4.

6.5.1 Spectrum, Power spectrum, and Power of a signal

The spectrum is the Fourier transform of the signal. The result is an array of coefficients with units that are the same as the signal per Hz. The power spectrum is the square of the Fourier transform of the signal. The result is an array of coefficients with units of power per Hz. The power of a signal is equal to the square-root of the average of the squares of the magnitude of each time point of the signal.

6.5.1.1 Energy spectrum, Convolution, and Auto-Covariance

The energy spectrum is the square of the Fourier transform of the signal. The result is an array of coefficients with the units of power per Hz per second or in other words energy per Hz. Convolution is an operation in which the time points of two signals are mapped to each other. The result is a single value. The auto-covariance function is a function of lag or the shift in time of a function or time series. The result is a single value for each lag.

6.5.2 Auto-spectrum, Cross-covariance, and Cross-spectrum

An auto-spectrum is the Fourier transforms of an auto-covariance function of a signal or time series. The result is an array of coefficients. The coefficients are squared to convert the result into an auto-power spectrum. The cross-covariance function is a function of the lag or the shift in time between two signals or time series. The result is a single value for each lag. A cross-spectrum is the Fourier transform of a cross-covariance function between two signals or time series. The result is an array of coefficients. The units are the same as the input signals. The coefficients are squared to convert the result into a cross-power spectrum.

6.5.3 Coherence spectrum, Time domain, and Time Domain Measurements

The coherence spectrum normalizes the cross-spectrum. Normalization is achieved by dividing each coefficient of the cross-spectrum by the square root of the product of the spectrum for each individual signal. The values are between 0 and 1. The coefficients are squared to convert the result into a coherence spectrum. The time domain is a term used to describe the analysis of mathematical functions, or physical signals, with respect to time. In the time domain, the signal or function's value is known for all real numbers. In order to display operating deflection shapes (ODSs) or mode shapes from a set of time domain measurements, they must be acquired so that each measurement represents a shape component of the structure at the same moment in time. This procedure is typically too expensive. Instead, the data is usually acquired a few channels at a time in separate measurement sets (Trench, 1961).

6.5.4 Frequency response, Frequency spectrum, and Spectrum analysis

Frequency response is the measure of any system's output spectrum in response to an input signal. The frequency spectrum of a time-domain signal is a representation of that signal in the frequency domain. The frequency spectrum can be generated via a Fourier transform of the signal, and the resulting values are usually presented as amplitude and phase, both plotted versus frequency. Spectrum analysis is the technical process of decomposing a complex signal into simpler parts. Spectrum analysis can be performed on the entire signal. A signal can be broken into short segments and spectrum analysis may be applied to these individual segments (Carayannis et al., 1986). The Fourier transform of a function produces a frequency spectrum which contains all of the information about the original signal. These two pieces of information can be represented as a two-dimensional vector, as a complex number, or as magnitude (amplitude) and phase in polar coordinates (Twigg & Hasler, 2009).

6.5.4.1 Impulse response function (IRF), Transfer function, and coherence

In signal processing, the impulse response function (IRF) of a dynamic system is its output when presented with a brief input signal, or impulse. A transfer function is a mathematical representation of the relation between the input and output of a linear time-invariant system. The Fast Fourier Transform (FFT) and the power spectrum are powerful tools that can be used to analyse and measure signals from plug-in data acquisition devices (Twigg & Hasler, 2009). The spectral coherence is a statistic that can be used to examine the relation between two signals or data sets. It is commonly used to estimate the power transfer between the input and the output of a linear system. The spectrum coherence programme is given in Appendix A. The decibel unit is used to signal processing from modal testing. The decibel (dB) is a logarithmic unit that describes a ratio of two measurements. The use of dB units allows ratios of various sizes to be described using numbers with which it is easy to work. The equation used to describe the difference in intensity between two measurements is as follows:

$$\text{Delta X (dB)} = 10\ \text{Log}_{10}(X_2/X_1) \qquad 6.4$$

where delta X is the difference in some quantity expressed in decibels, X_1 and X_2 are two different measured values of X, and the log is to base 10. The ratios of two different values are given in Table 6.2.

Table 6.2: The correlation data based on the conversion of the dB unit and variables.

Ratio between Measurement 1 and 2	Equation	dB
1	dB = 10 log (1)	0 dB
2	dB = 10 log (2)	3 dB
10	dB = 10 log (10)	10 dB
100	dB = 10 log (100)	20 dB

6.5.5 Design and construction of the model

The design and construction of the model is explained in chapter 5. The visual grid line of the model is given in Figure 6.2, which shows the numbers of nodes and elements that are applied for the purposes of set up of model.

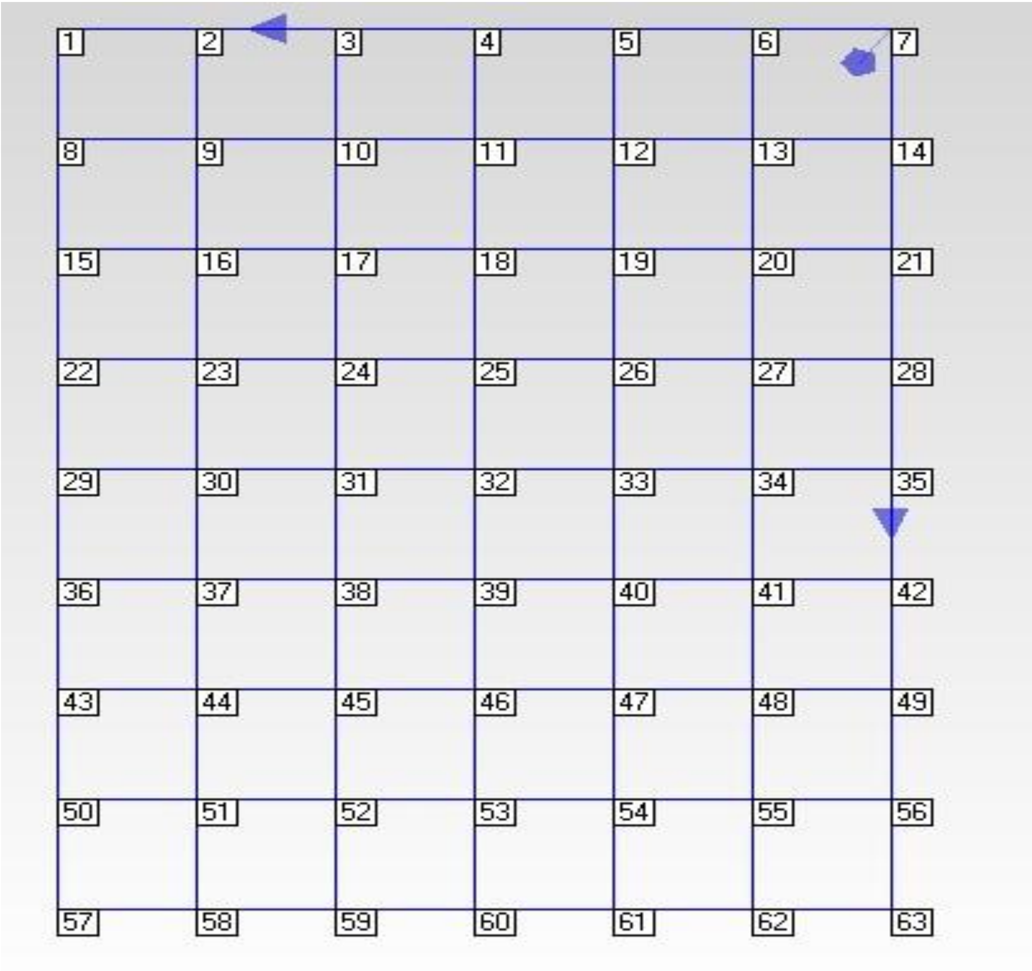

Figure 6.2: The visual grid lines of the flat net.

6.5.6 Instrumentation and equipment

In addition to the equipment used in static testing described in chapter 5, further equipment was used in dynamic testing to excite the structure and record the vibrations. This equipment is described in the following subsections 6.5.6 1 to 6.5.6.6.

6.5.6.1 IMC WAVE IMC WAVE acoustic workstation software

The IMC WAVE acoustic workstation software is designed for use in noise and vibration testing. When IMC WAVE is used in conjunction with CRONOS-PL hardware it provides a reliable, standards based testing system that is easy to configure and operate. The hardware setup and software configuration can be further simplified by using TEDS sensor recognition combined with ISO standard tests. The system can be expanded with analogue and field bus channels, enabling the number of applications to be extended far beyond that of conventional vibration analysers.

6.5.6.2 ME'scopeVES software

ME'scope VES (Visual Engineering Series) software is a family of software packages and options that make it easier to observe, analyse, and document noise and vibration problems in machinery and structures. The ME'scope VES software is used to display and analyse experimental multi-channel time and frequency domain data that is acquired during the operation of a machine or through the forced vibration of a structure.

6.5.6.3 Impact hammer

Impact hammers are used in modal analysis to determine component or system response to impacts of different amplitude and duration. Impact hammers are used in the modal and structural behaviour analysis of all types of components and systems. The pulse duration, a measurement of the time the hammer is imparting a force on the object being tested, is a very short span of time that is often measured in milliseconds. In general, harder tips will deform less during impact and will have shorter pulse duration than softer tips. The impact hammer used in this research is shown in Figure 6.3. Typically the hardest tips are used to measure response at the highest frequencies.

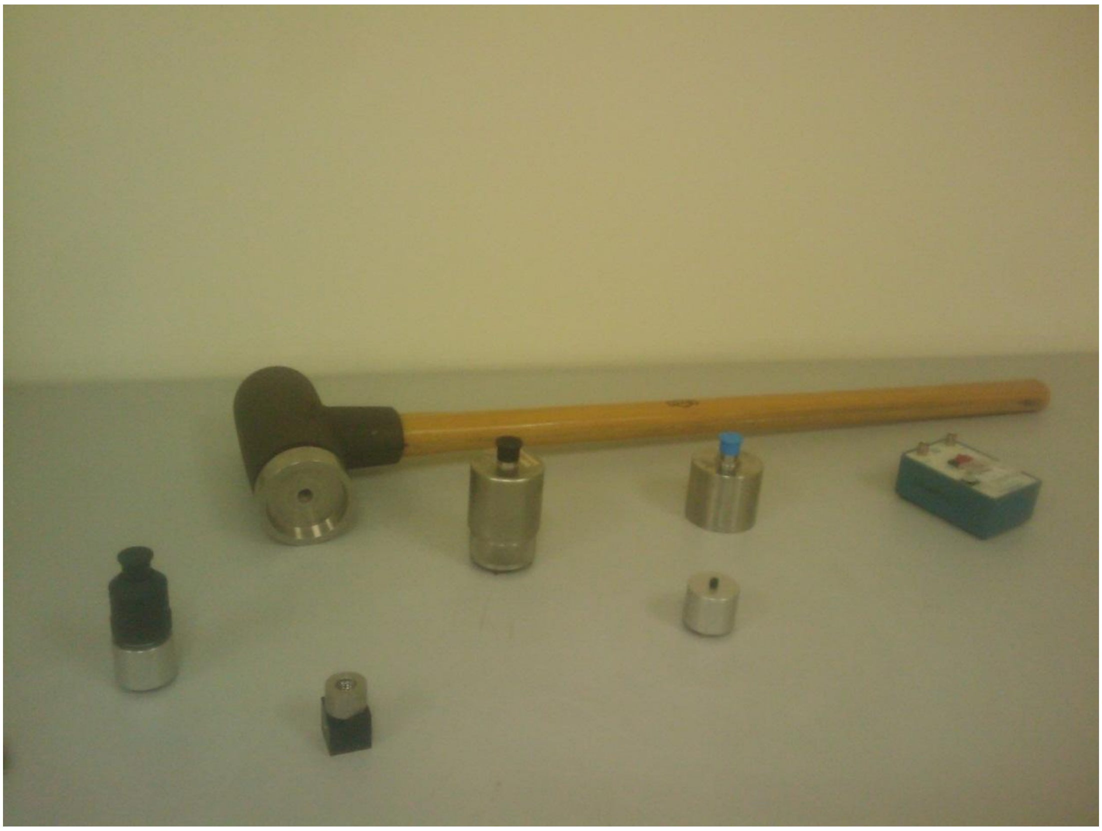

Figure 6.3: General view of impact hammer.

6.5.6.4 Ceramic shear accelerometer (50 g lightweight, voltage mode)

The 50 g ceramic shear accelerometer is suitable for use in the present work in terms of its measurement range and also because it has a small envelope size and is light weight. Miniature models, such as this one, are designed for minimal mass loading are still capable of generating a significant signal. The ceramic sensing element components are carefully designed to provide the level of performance most often required for general-purpose vibration measurements. The specification and features of the 50 g ceramic shear accelerometer are shown in Table 6.3. The actual accelerometer (Kistler 8776A50) used in this study is shown in Figure 6.4.

Table 6.3: Specification and features of 50 g ceramic shear accelerometer.

Specification	Type 8776A50	
Model (Single axis or triaxial)		Single axis linear
Range	g	±50
Sensitivity	mV/g	100
Frequency Range	Hz	1...7000
Mass	g	4
Diameter	mm	10.16
Housing/Base		Titanium

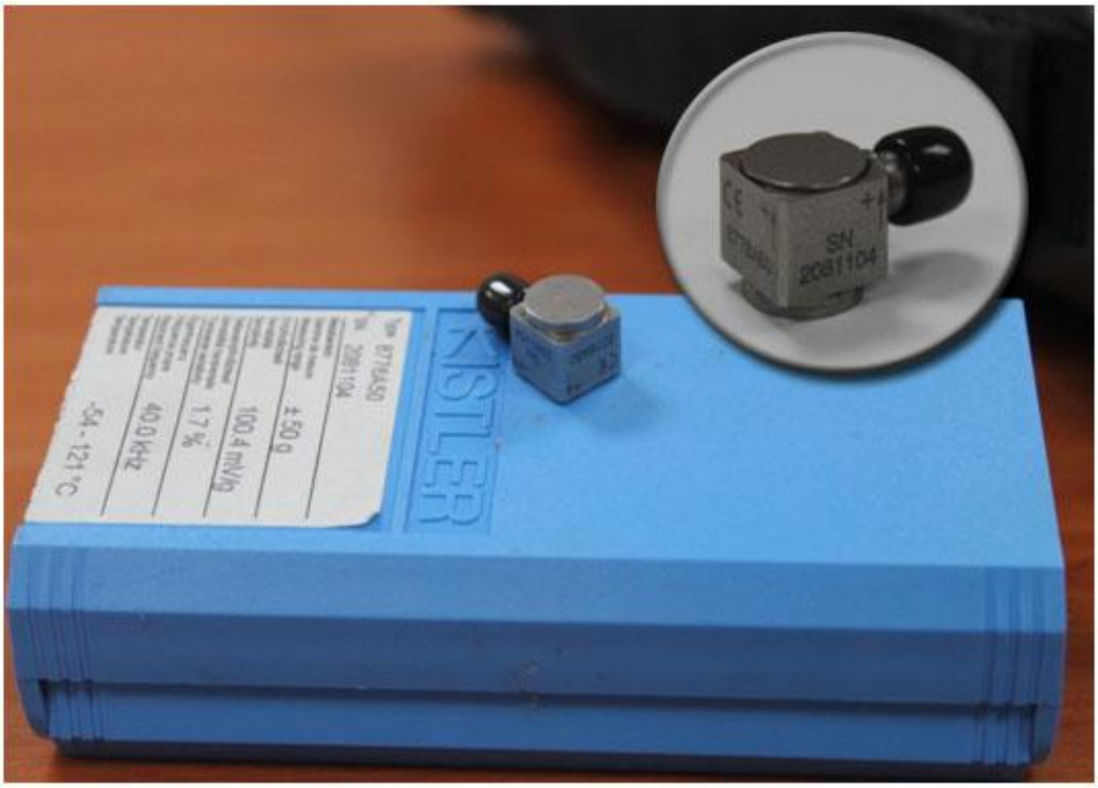

Figure 6.4: Kistler 8776A50 ceramic shear accelerometer.

6.5.6.5 Data acquisition device (IMC CL 7016-1)

This device is equipped for vibration analysis. The IMC CL 7016-1 is used to receive and process data from structures. The IMC CL 7016-1 consists of a smart network-cable. The IMC WAVE software is a platform of this device. IMC WAVE's individual software modules make order tracking as well as spectral and sound power analyses possible with the click of a button. The channel construction of this incremental encoder device is shown in Figure 6.5. The actual IMC device used in this work is shown in Figure 6.6 and Figure 6.7. The IMC CL-7016-1 comes as an 8- or 16-channel universal measurement device with sampling rates of up to 100 kHz per channel. The device is especially well suited to frequently changing measurement tasks. The input channels are differential and equipped with per-channel signal conditioning including filters. The specification and features of this device are:

a) Connection via TCP/IP at data rates of up to 100Mbit.
b) Auto-start capability independent of PC and computational and control functions via online FAMOS data analysis software.
c) Removable hard drive for data storage and up to 512 channels can be recorded.

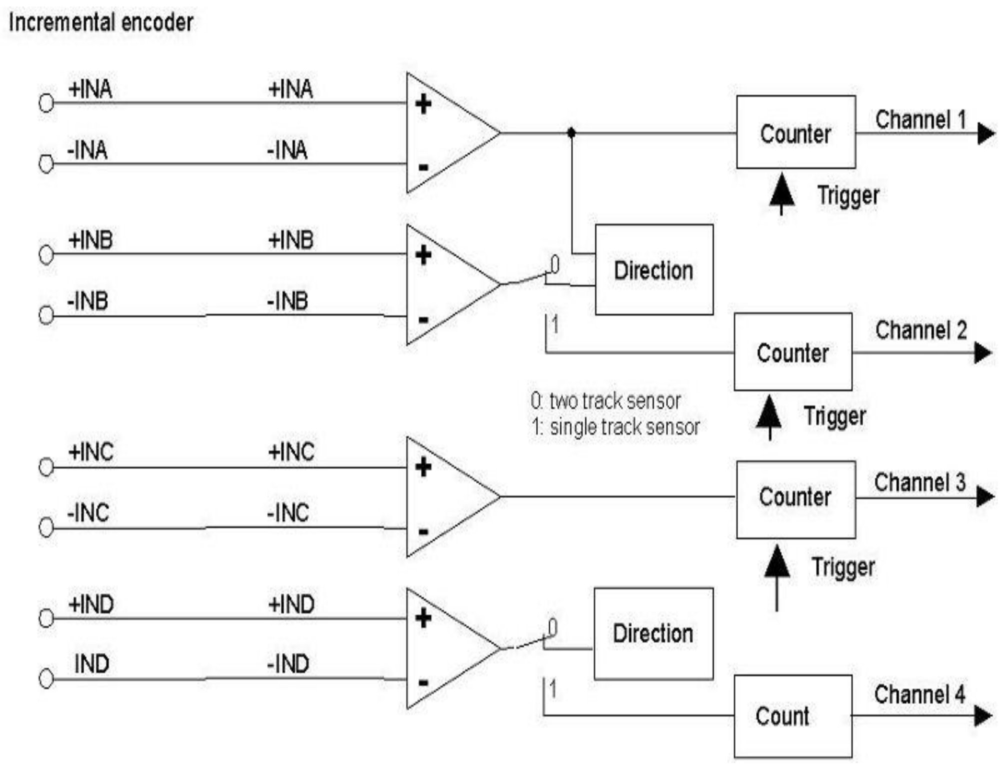

Figure 6.5: Block Schematic of incremental encoder.

Figure 6.6: Front view of IMC device.

Figure 6.7: Back view of IMC device.

6.5.6.6 Connectors

Electronic cables are used to connect the sensors in parallel. These cables are utilized together with cable plugs and sockets. Protective covers are used to protect the connectors from contamination. The cables used in this study are shown in Figure 6.8 and Figure 6.9.

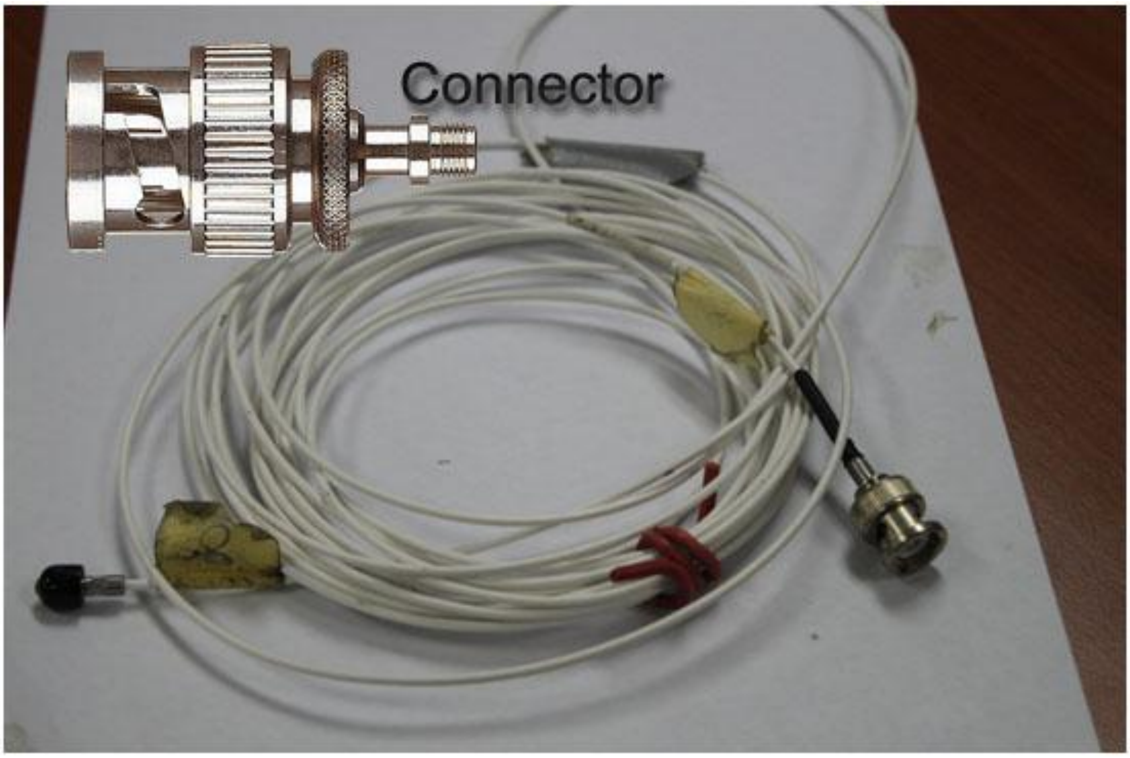

Figure 6.8: Top view of cables and cable connector.

All the cables used in this study are designed to provide optimum signal transmission. In the present experimental work, Kistler's premium cables and connectors are used. Kistler connectors are high-quality stainless steel. Noise and intermittent operation are eliminated because there is no plating to wear off. Stainless steel also reduces the weight by 50% compared to conventional cables. These cables can be used with both low and high impedance sensors.

Figure 6.9: Top view of accelerometer-IMC connector device.

6.5.7 Test procedure

6.5.7.1 The flat net

As mentioned in chapter 5, the final part of the static testing consisted of subjecting the net to two different types of concentrated loading. In the first case, the net was loaded with increasing load at central joint 32 only. In the second case, the net was subjected to equal and increasing load at all joints. The results proved the hypothesis that the frame net has a rigid boundary.

6.5.7.2 Equipment setup

A diagram showing the layout of the equipment is given in Figure 6.10. In order to record the static and dynamic deformation at different points of the net, the cores of eight transducers were attached to joints 1, 2, 3, 4, 5, 6, 7, and 8 in order to obtain the signal from the accelerometer and the core of one transducer was attached to reference node 3 or 28 in order to excite the structure. The position of the accelerometer is changed consecutively to reach node 63 until the procedure has been completed for all joints.

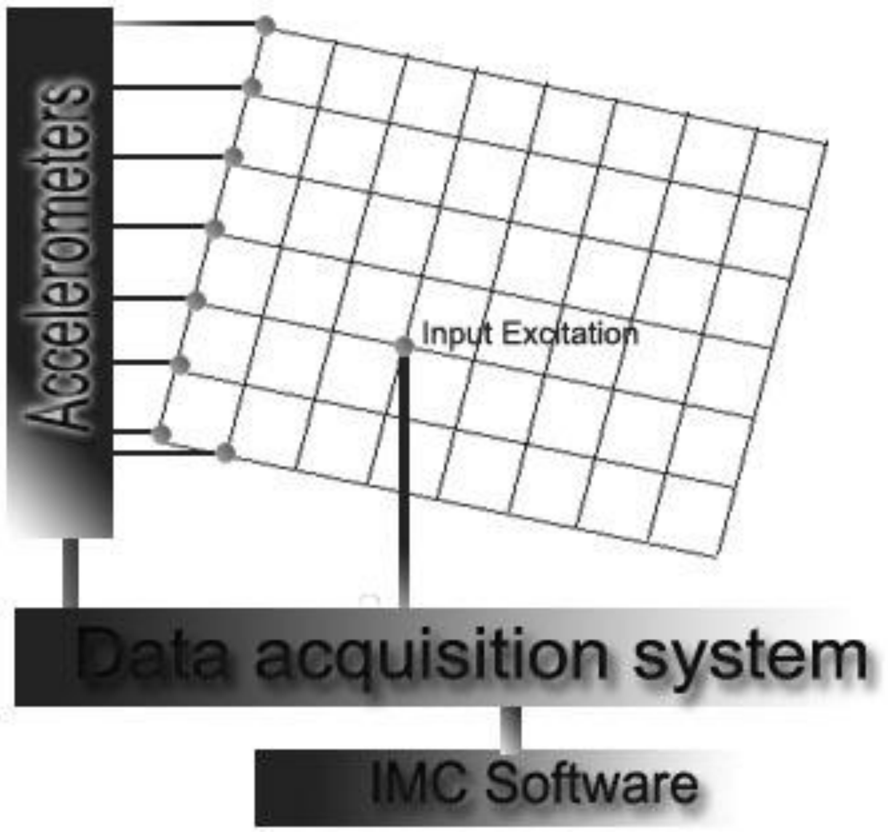

Figure 6.10: The diagrammatic layout of the experimental setup for modal testing.

The construction setup for the accelerometer sensor to join to nodes and the acquisition file from IMC device in the different references is shown in Table 6.4. The acquisition frequencies are according to transfer function plot.

Table 6.4: Setup procedure for modal testing with IMC device.

Setup/Channel	Nodes	Position of hammer	File name
1	1-8	Node 3	15:20:43 (1)
2	1-8	Node 28	15:28:19 (9)
3	9-16	Node 3	15:50:26 (1)
4	9-16	Node 28	15:51:45 (2)
5	17-24	Node 3	16:05:32 (3)
6	17-24	Node 28	16:07:22 (6)
7	25-32	Node 3	16:21:31 (9)
8	25-32	Node 28	16:22:29 (10)
9	33-40	Node 3	16:33:58 (12)
10	33-40	Node 28	16:37:44 (1)
11	41-48	Node 3	16:50:09 (2)
12	41-48	Node 28	16:50:55 (3)
13	49-56	Node 3	17:03:44 (5)
14	49-56	Node 28	17:04:27 (6)
15	57-63	Node 3	17:13:29 (7)
16	57-63	Node 28	17:14:24 (8)

Data from all measurements are shown in Figures 6.11– 6.21 and Appendix E. Briefly, Figure 6.11 shows a typical coherence graph for nodes 1–8 based on reference node 3. Figure 6.11 also is an enlarged view that shows the coherence graph for the range of 0–600 Hz. The coherence signal dropped sharply between 0 and 35 Hz from 1 to 0.557 ratio units. From this point onwards the coherence shot up to reach 0.774 units. The ratio of 0.378 is highest percentage in the graph in Figure 6.11. Figure 6.12 shows the visual comparison of thee coherence graph based on references 3 and 28. The signals output from reference 3 are suitable because ratios of the amounts based on reference 3 are higher than the ratio amounts of reference 28 and are close to 1. This means that the received signals have linear behaviour and are sufficient to analyse modal. The excitation graph for nodes 1 to 8 based on reference 3 is shown Figure 6.13. The transfer function plots for nodes 1-8 are given in Figures 6.14 (based on reference 3) and Figure 6.15 (based on references 3 and 28). Figures 6.13 and 6.14 show that the primary value for node 1 is more than node 2 and node 3, respectively. In Figure 6.14 it is demonstrated that amplitude starts from 14 mg/N when using reference node 3 and amplitude starts from 9 mg/N when using reference node 28. It should be mentioned that the vibration of the structure at reference 3 is closer in distance to node 1 compared to the vibration at reference node 28.

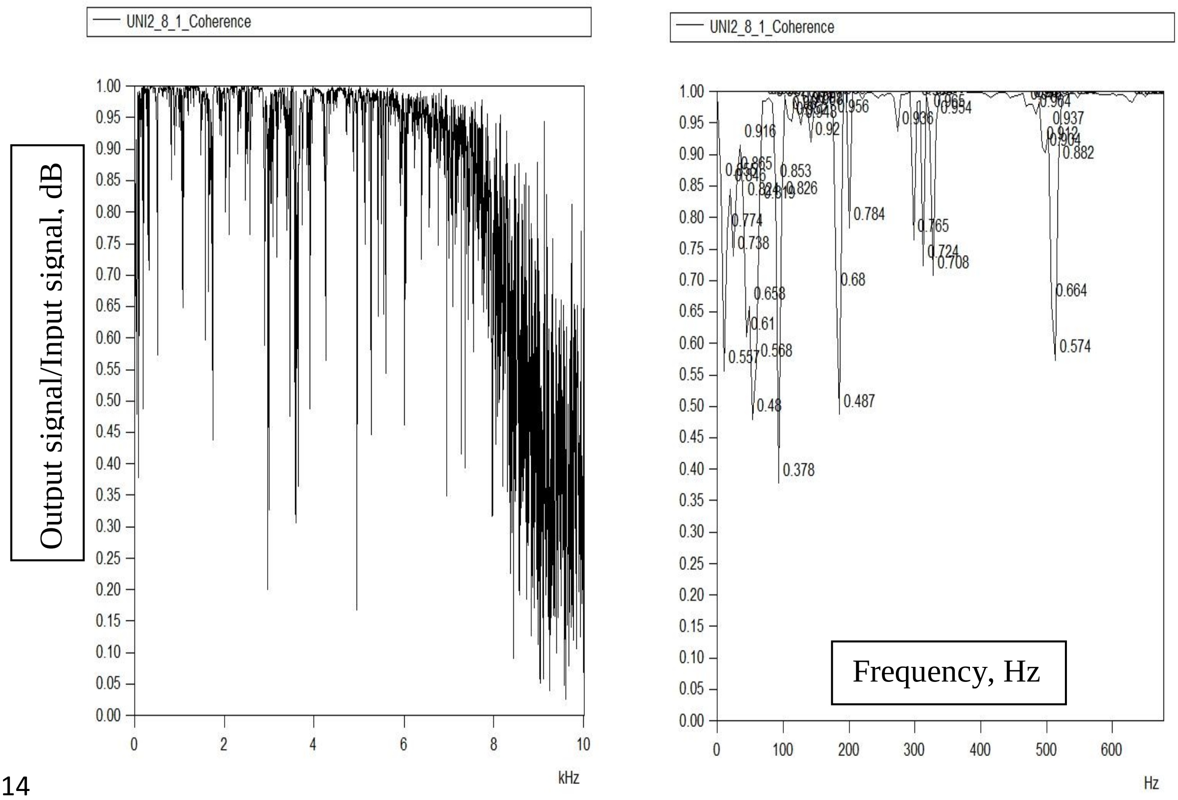

Figure 6.11: Coherence graph and enlarged image of channel 1 based on reference 3.

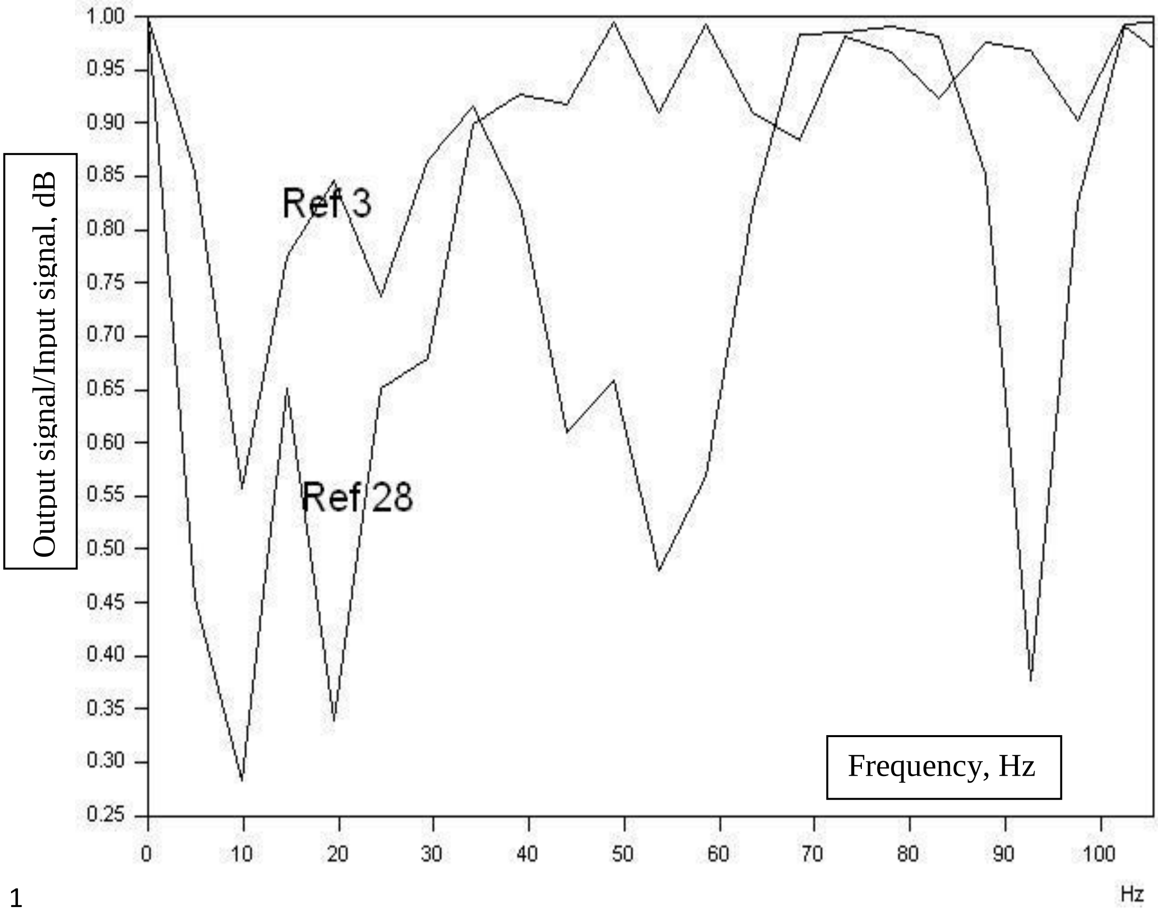

Figure 6.12: Coherence graph of channel 1 and 2 based on references 3 and 28.

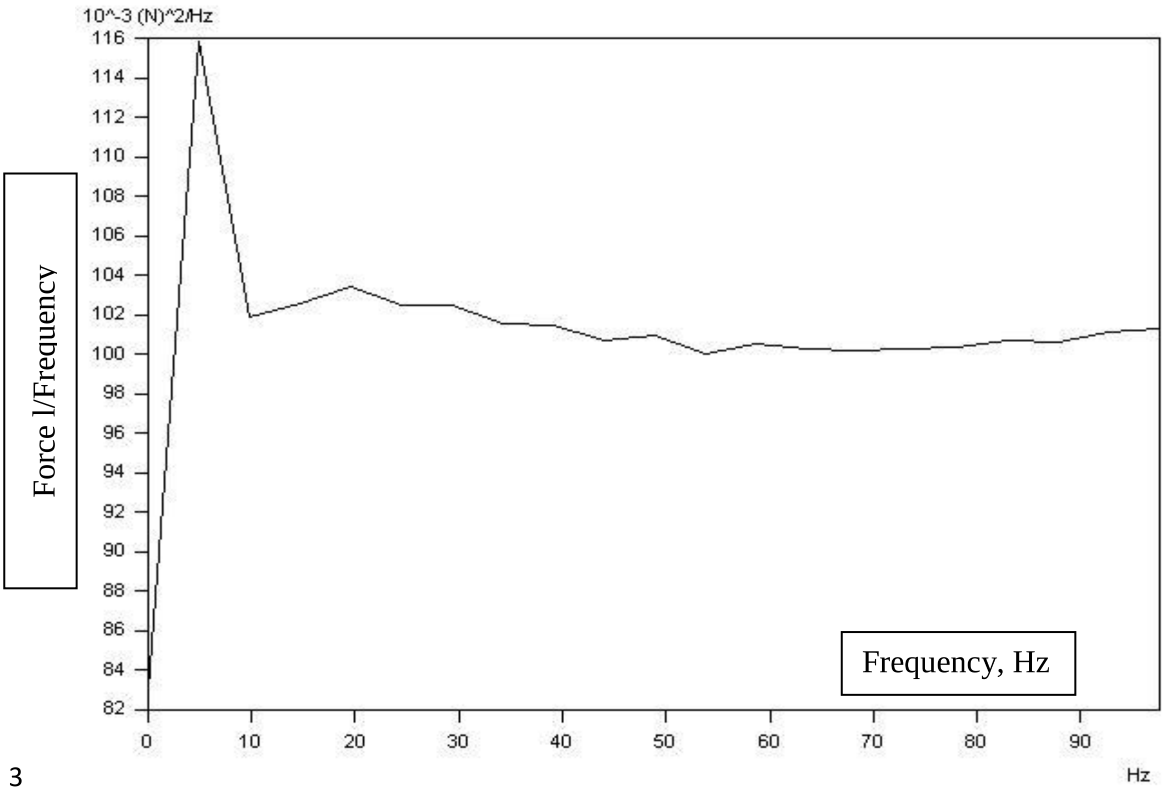

Figure 6.13: Excitation graph of channel 1 based on reference 3.

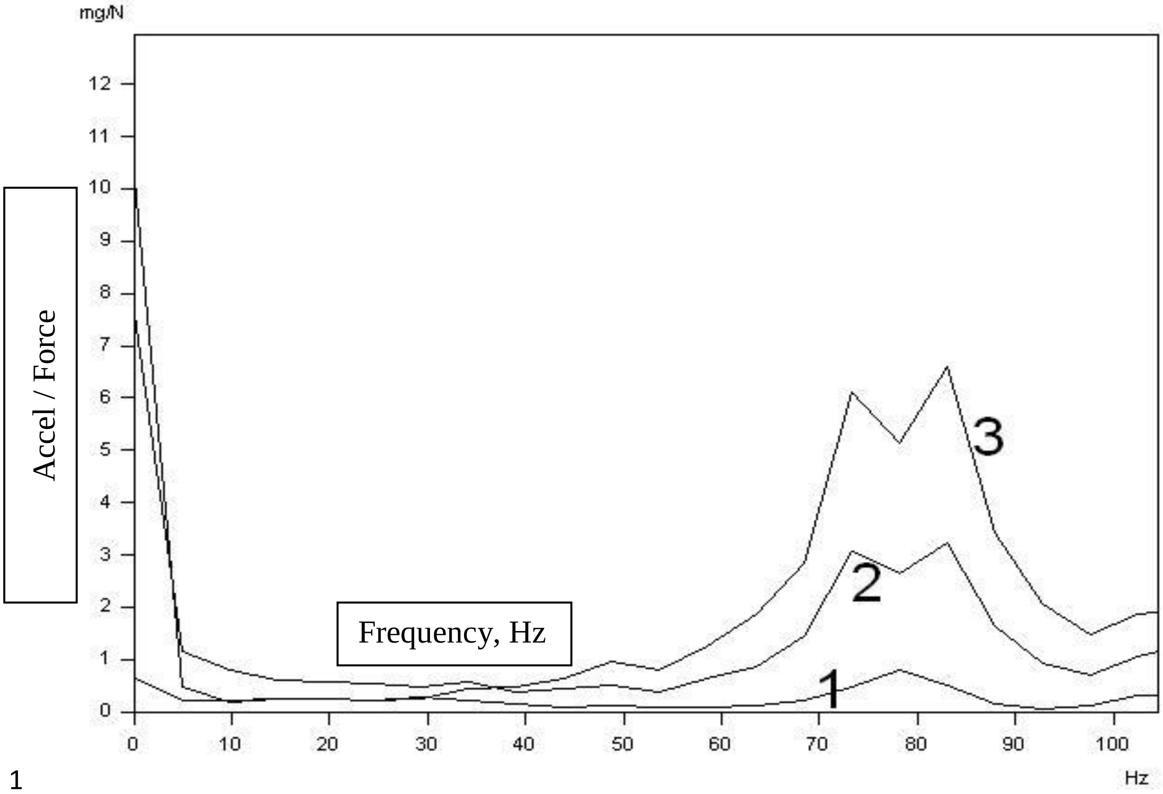

Figure 6.14: Transfer function plot for nodes 1 to 3 based on references 3.

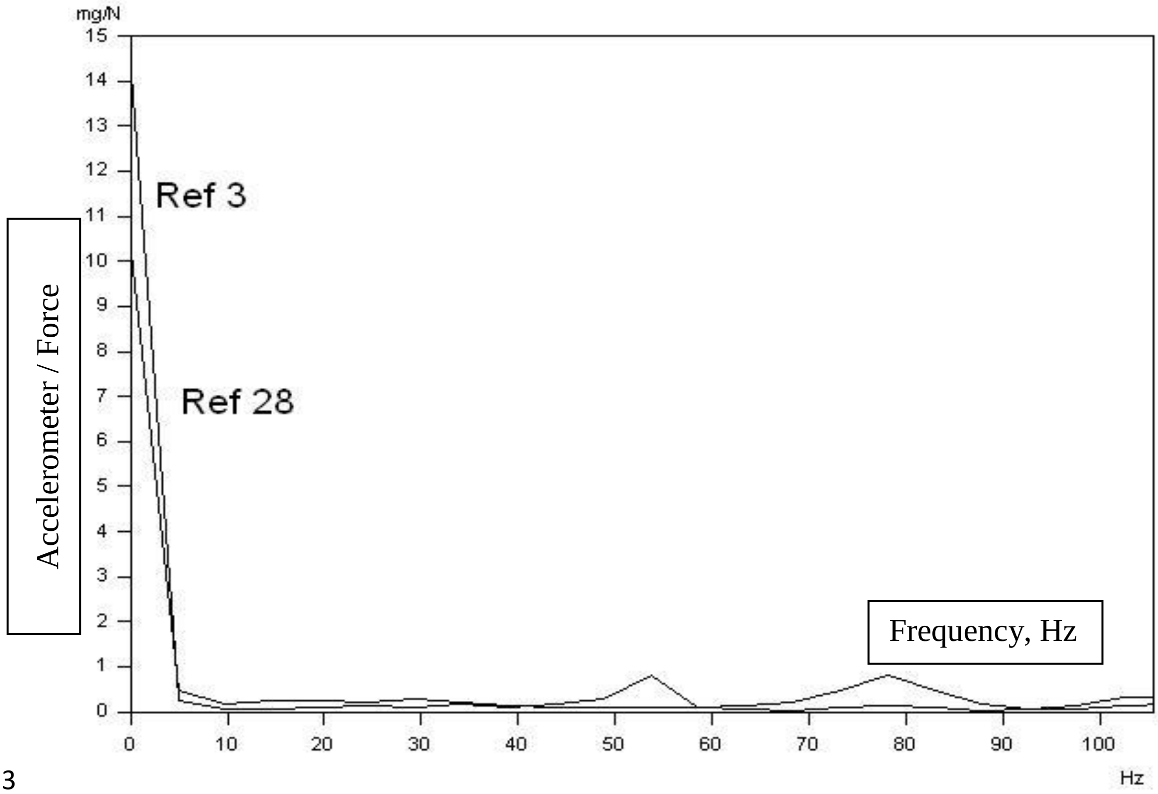

Figure 6.15: Transfer function graph for node 1 based on references 3 and 28.

Figure 6.16 shows the 3D cursor colour map for nodes 1 to 8. The 3D cursor colour map consists of three curve windows. The left curve window presents a colour map which shows the relationship of time signal _x and time signal_y. In this colour map it is demonstrated that the frequency decreases slightly from 75 million seconds later. The third curve window shows that the signal climbed rapidly between 0 and 6 from -6 to -3 mg and fell again after 10 seconds.

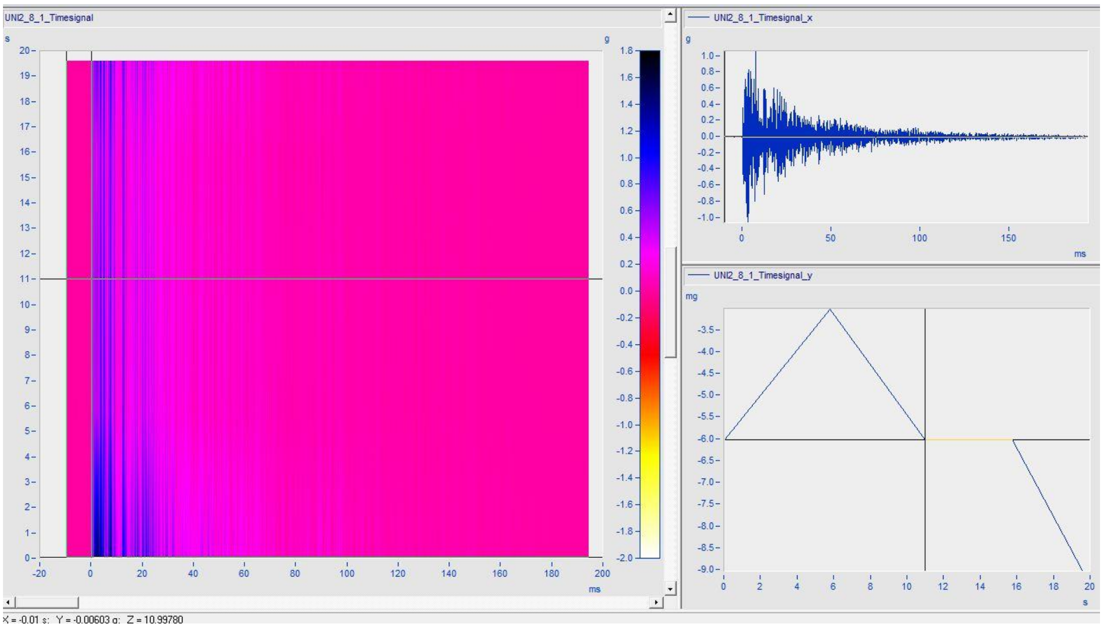

Figure 6.16: Display of the 3D cursor colour map for nodes 1–8 corresponding to reference 3.

As mentioned above, magnitudes can be displayed in dB units. The magnitude is displayed as follows

Magnitude (dB) =20 Log 10(Magnitude). 6.5

For power (MS) quantities such as auto-spectra and cross-spectra, the magnitude is displayed as

Magnitude (dB) = 10 Log 10(Magnitude). 6.6

The highest changes signals for nodes 1 to 8 in transfer function are between -80 dB and 5 dB. The time signal graph and excitation force graph for nodes 9 to 16 based on reference 3 are shown in Figure 6.17 and it can be seen that the amplitude of force dropped sharply between 0 and 4 kHz from 270e-3 (N^2/Hz) to 0 units. The time signal bar plot of nodes 9 to 16 for the period of 150 milliseconds is also shown in Figure 6.18, which shows that the amplitude of the signal for node 10 is highest between 9 and 16 nodes.

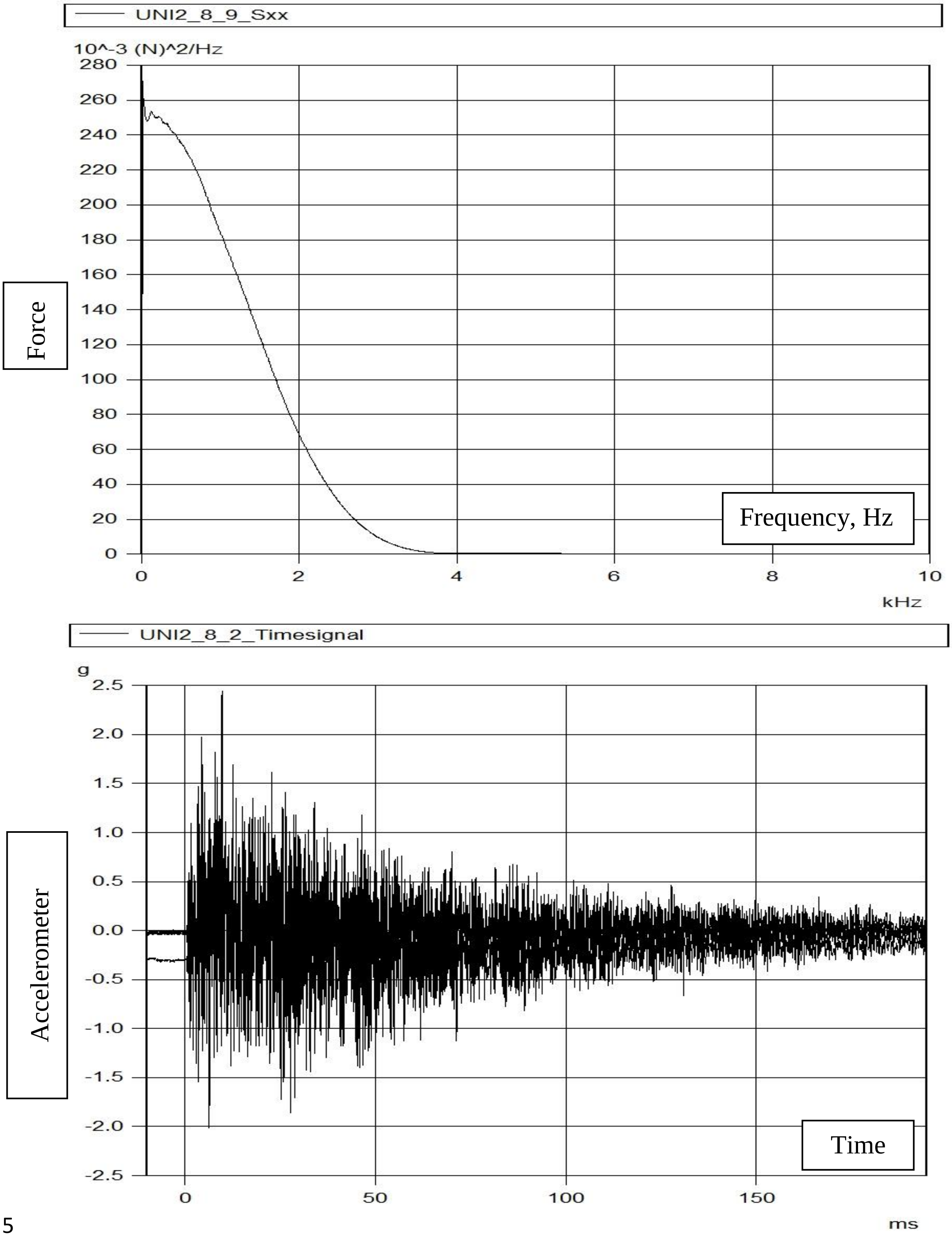

Figure 6.17: Time signal graph of channel 3 based on references 3.

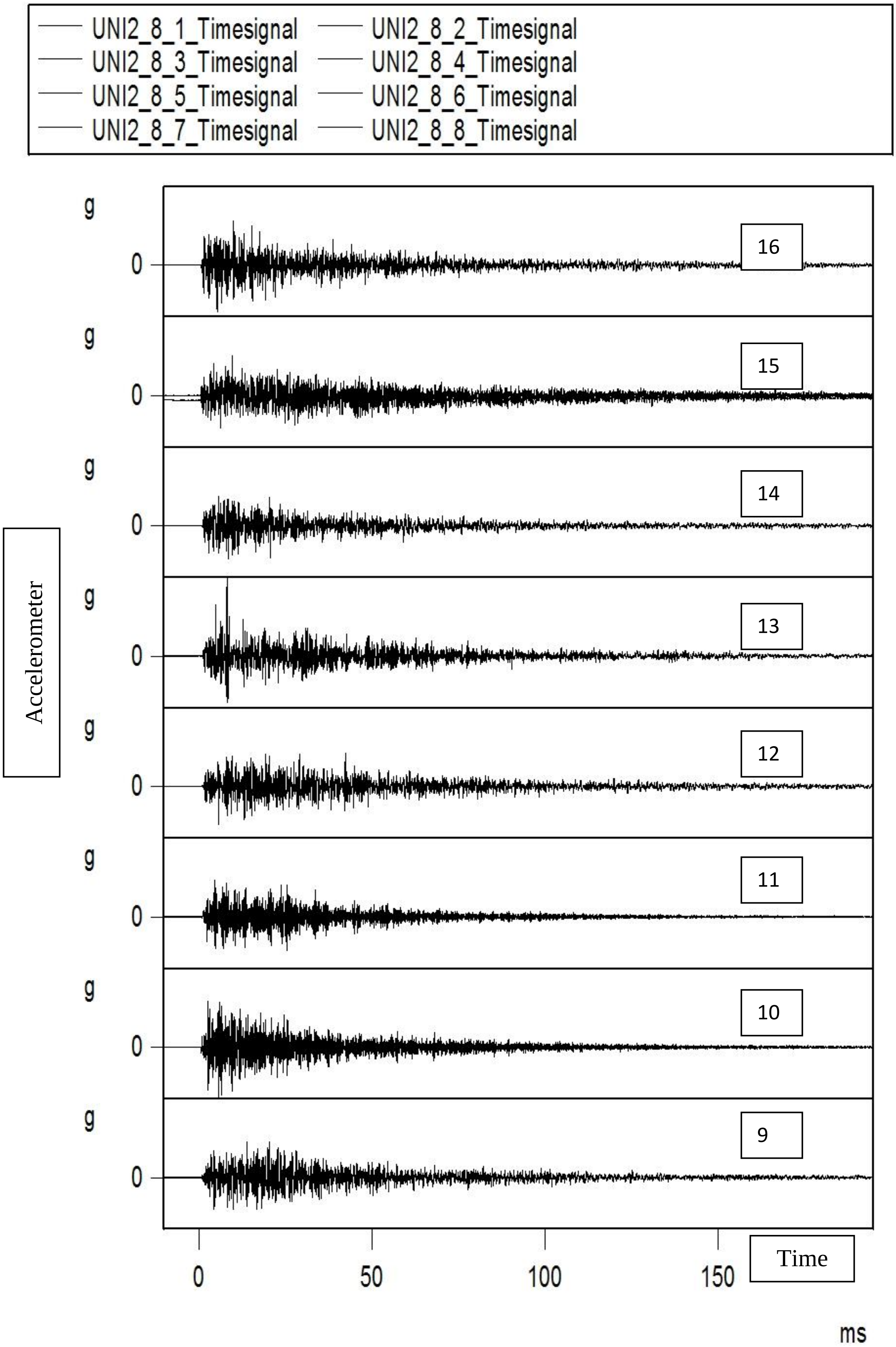

Figure 6.18: Time signal between nodes 9 and 16 corresponding references 3.

The excitation force graph for nodes 17 to 24 based on references 3 is shown in Figure 6.19. The graph leapt rapidly between 3.5 kHz and 4.1 kHz from 0.95 e-3 (N^2/Hz) to -0.2e–3(N^2/Hz). From this point onwards, the graph increased gradually from -0.2e–3(N^2/Hz) to 4.2 kHz and is projected to reach -045e-3(N^2/Hz) in 4.6 kHz. The water fall plot of the time signal graph is shown in Figure 6.20. This graph helps to make a visual comparison of the signal between nodes 25 and 32. The acquired data is presented in more detail in Appendix F.

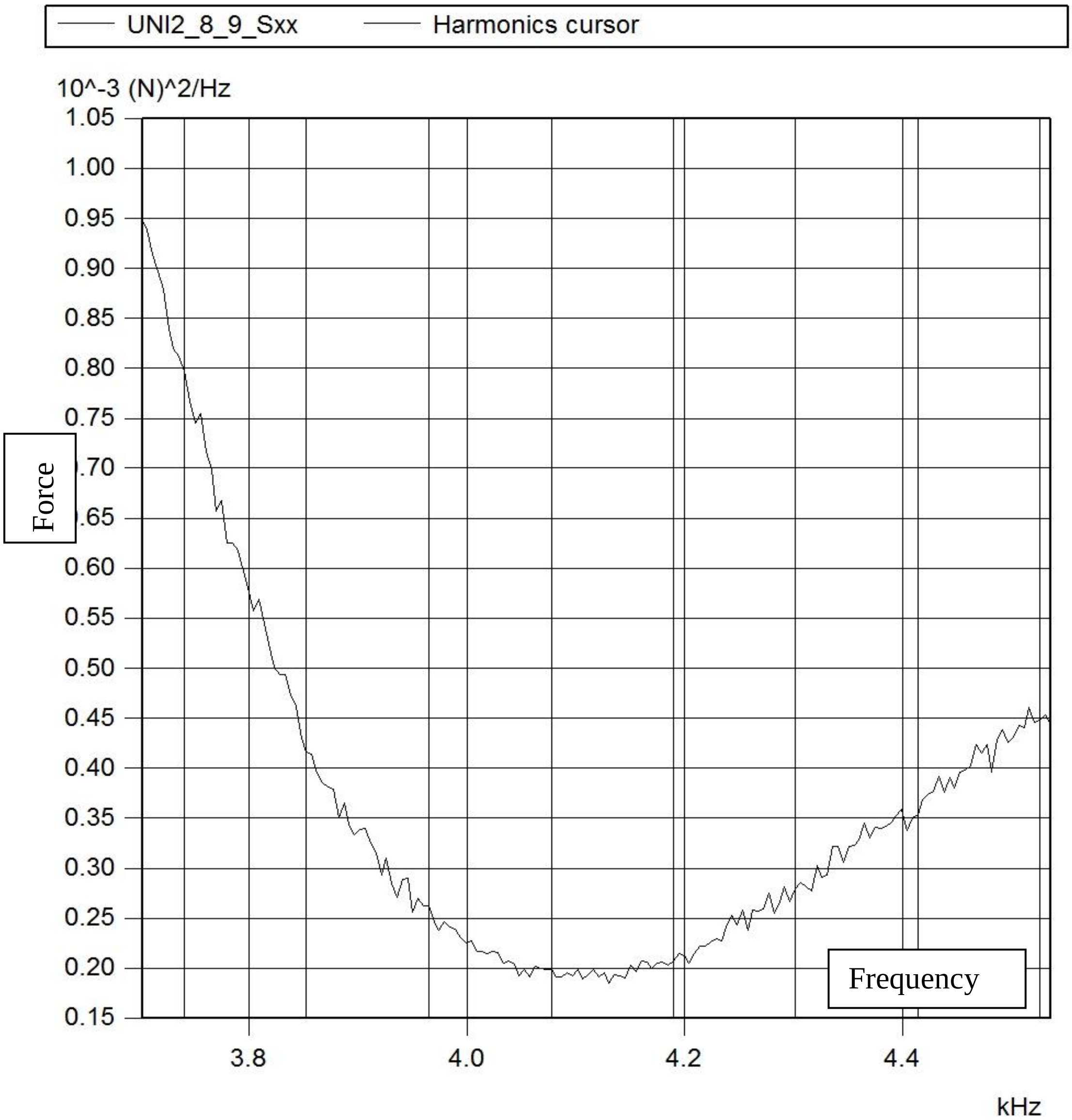

Figure 6.19: Harmonic cursor of excitation force for channel 5 based on reference 3.

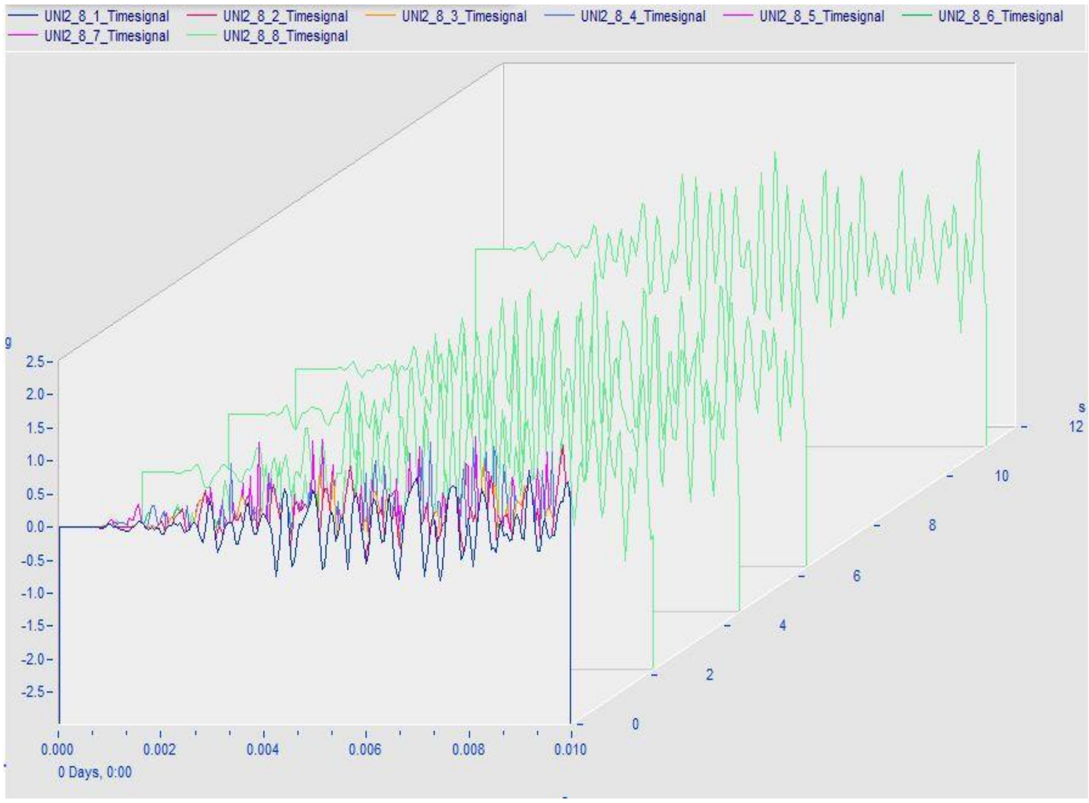

Figure 6.20: The waterfall plot of time signal for nodes 25- 32 based on reference 3.

6.5.8 Modal parameter estimation

Modal analysis is the study of the dynamic properties of structures under vibration excitation. In the ME'scope the program, the modal parameters are estimated by curve fitting a set of experimentally derived measurements using an analytical form of a Frequency Response Function (FRF). Modal parameters can be estimated from a set of experimental derived FRFs or from Fourier Spectra (FFTs), auto-power spectra, cross-power spectra, and ODSs The FRFs that are derived from operating data and are properly windowed. In this project, single reference methods are used versus multiple reference methods. A single reference set of FRFs is measured using a single fixed exciter location, or a single fixed response transducer location. In order to scrutinize the frequency response function application of a new technique is needed. In the present work, the newest method for optimization of the modal parameter is used. Optimization and Scrutinization of modal parameter

6.5.8.1 Phase plot

Gain is a measure of the ability of a circuit to increase the amplitude of a signal from the input to the output. It is usually defined as the mean ratio of the signal output of a system to the signal input of the same system. It may also be defined on a logarithmic scale (LaMar, Xin, & Qi, 2006). The phase Bode plot is obtained by plotting the phase angle of the transfer function given by

$$\Phi = - \tan^{-1} (w/w_c) \qquad 6.7$$

where ω and ω_c are the input and cutoff angular frequencies, respectively. For input frequencies much lower than the corner, the ratio w/w_0 is small and the phase angle is close to zero. As the ratio increases, the absolute value of the phase increases and becomes -45 degrees when $w = w_c$. As the ratio increases for input frequencies much greater than the corner frequency, the phase angle asymptotically approaches -90 degrees. The frequency scale for the phase plot is logarithmic. It should be mentioned that the phase starts at 0^o at low frequencies and the phase goes to -90^o at high frequencies.

6.5.8.2 Bode plot

A Bode plot is a graph of the transfer function of a linear, time-invariant system versus frequency. A Bode plot shows the system's frequency response. It is usually a combination of a Bode magnitude plot, expressing the magnitude of the frequency response gain, and a Bode phase plot, expressing the frequency response phase shift. Bode plots are really log-log plots, so they collapse a wide range of frequencies (on the horizontal axis) and a wide range of gains (on the vertical axis) into a viewable whole. Bode plot content consists of magnitude plotted (dbs), phase plotted (degrees), and frequency plotted (on a logarithmic scale). The Bode plot program used in this study is mentioned in Appendix D.

6.5.8.3 Nichols plot and Nyquist plot

A Nichols plot is a plot used in signal processing in which the logarithm of the magnitude is plotted against the phase of a frequency response on orthogonal axes. This plot combines the two types of Bode plot, magnitude and phase, on a single graph, with frequency as a parameter along the curve. A Nyquist plot is used to ascertain the stability of a system and is a way of showing the frequency responses of linear systems. A Nyquist plot describes the gain and phase of a frequency response in polar coordinates by plotting the imaginary part of the complex frequency response versus the real part. Using polar coordinates, a Nyquist plot shows the phase as the angle automatic control and signal processing in order to assess the stability of a system with feedback. This plot also combines the two types of Bode plot, magnitude and phase, on a single graph. The important points to note in relation to a Nyquist plot are as follows:

- The low frequency portion of the plot is near +1.
- The high frequency portion of the plot is near the origin in the plane.
- The high frequency of the plot approaches the origin at an angle of -90^{o}.

The Nyquist plot is made by computing the transfer function. The transfer function would be a ratio of polynomials and may be expressed in terms of zero and pole factors in the numerator and denominator. The Nyquist open loop polar plot indicates the degree of stability, the adjustments required to achieve stability, and provides stability information for systems containing time delays. The Nyquist plot is obtained by simply plotting a locus of imaginary (G (j ω)) versus Real (G (j ω)) at the full range, as shown in Figure 6.21.

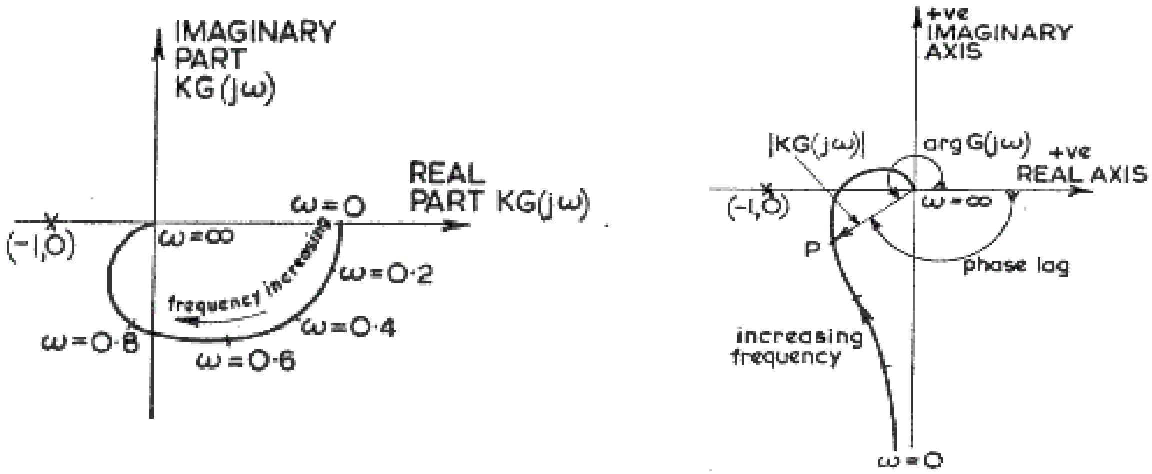

Figure 6.21: The Nyquist plot fundamentals.

6.5.8.4 Nyquist stability criterion

The Nyquist stability criterion provides a simple test for stability of a closed-loop control system by examining the open-loop system's Nyquist plot. The stability of the closed-loop control system can be determined directly by computing the poles of the closed-loop transfer function. In contrast, the Nyquist stability criterion allows stability to be determined without computing the closed-loop poles. Two relative stability indicators, namely the gain margin and the phase margin, can be determined from the suitable Nyquist plots. The phase margin is the angle where the phase is less than 180^0 when the gain is unity. The values are generally identified by the use of Bode plots. The Nyquist stability criterion program used in this study is mentioned in Appendix A.

6.5.8.5 CoQuad method

The CoQuad method is implemented by detecting a resonance peak in the Real (Coincident) part or the Imaginary (Quadrature) part in a set of frequency. Modal damping is not estimated with this method.

Each of the 63 FRFs in the saved file was measured between a pair of DOFs (points & directions) on a real plate structure. Each FRF was measured by impacting the structure with a hammer at a different point, all in the vertical direction. The vibration response of the plate was measured with an accelerometer fixed at point 3 in the Z direction. Since the accelerometer was fixed at DOF 1Z throughout the test, 1Z is called the Reference DOF. The set of 63 FRF measurements was made by impacting at two points in the vertical or Z direction. Since each point had a different DOF, these DOFs are called Roving DOFs. This type of modal test is very common and is called a roving impact test. In this project, also perform modal and ODS Tests to identify and correct vibration on structures. An ODS FRF is a complex valued function of frequency that has magnitude and phase. An ODS FRF is calculated for each roving response on a structure. Its magnitude is the auto spectrum of the roving response. Its phase is the difference between the phases of the roving response and a (fixed) reference response. This phase difference is the same as the phase of the cross-spectrum between the roving and reference responses.

Amplitude frequency for node 1 based on the Bode diagram for reference 3 is shown in Figure 6.22. As previously mentioned, the Bode plot is formed from a magnitude and phase diagram. The transfer function graph of node 1 is converted to a linear graph related to time by the Bode technique. In this plot, in the magnitude part, the amplitude of signal appears to level off and remain constant at about 5.5e-4 at 1.2e3 Hz and between this point and 2.3e-3

Hz is a sprawling of the signal occurs. In contrast, the magnitude part of Figure 6.23 shows that in the case of node 1 based on the Bode diagram for reference 28 the graph dropped slowly to reach 5.5e-3 units between 0 Hz and 2.4e3 Hz. From this point onward, the graph has many peaks until it reaches 1e4 Hz. Figure 6.22 and Figure 6.23 mainly demonstrate the ratio of input frequency over cutoff angular frequencies in the phase diagrams. The figures show the ratio of phase in frequency response when using reference 28 is close to zero in comparison to when reference 3 is used, and this means that the response is weak and is insufficient to use for mode shape. The comparison of two Bode diagram shows that the magnitude of frequency at reference 28 is less than at reference 3 for exciting the structure. Hence, it does seem that the output signals at reference 28 are too close to local frequency, which is the opposite of the case for output signals used at reference 3. The signal in Figure 6.23 is made up of parts which are different from each other and are heterogeneous.

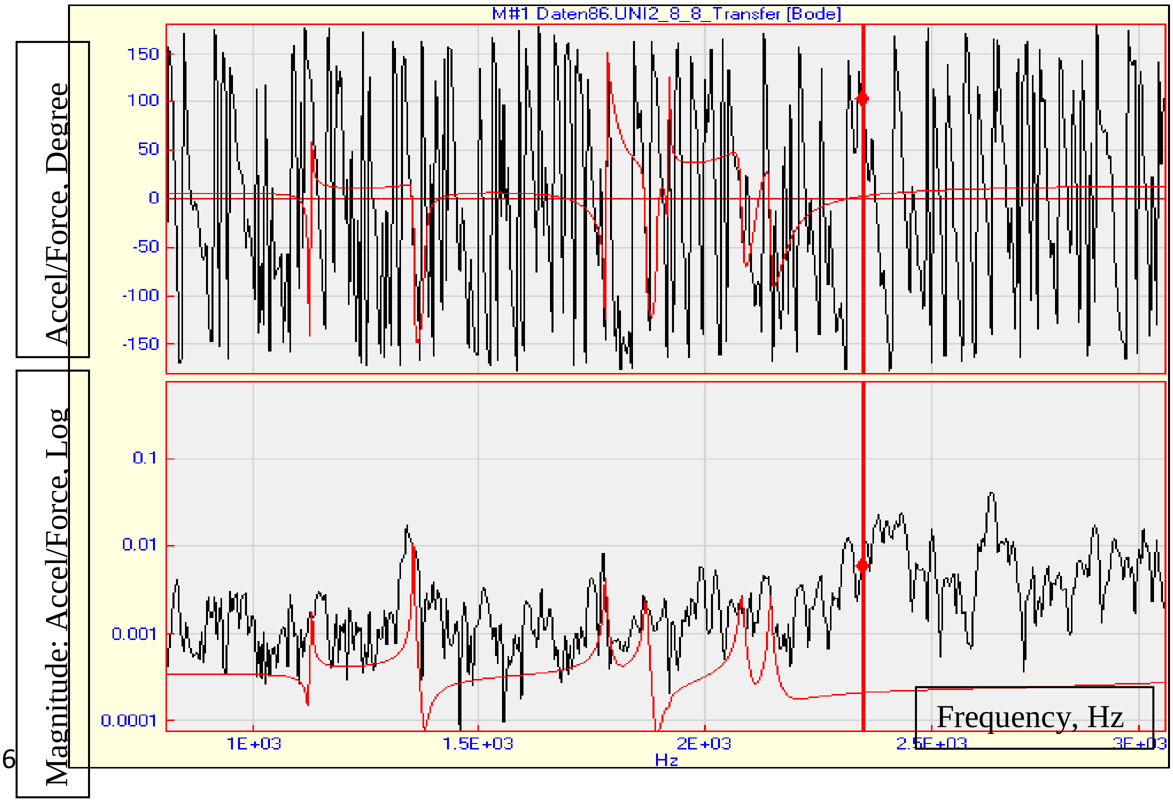

Figure 6.22: Bode diagram of an FRF for node 1 based on reference 3.

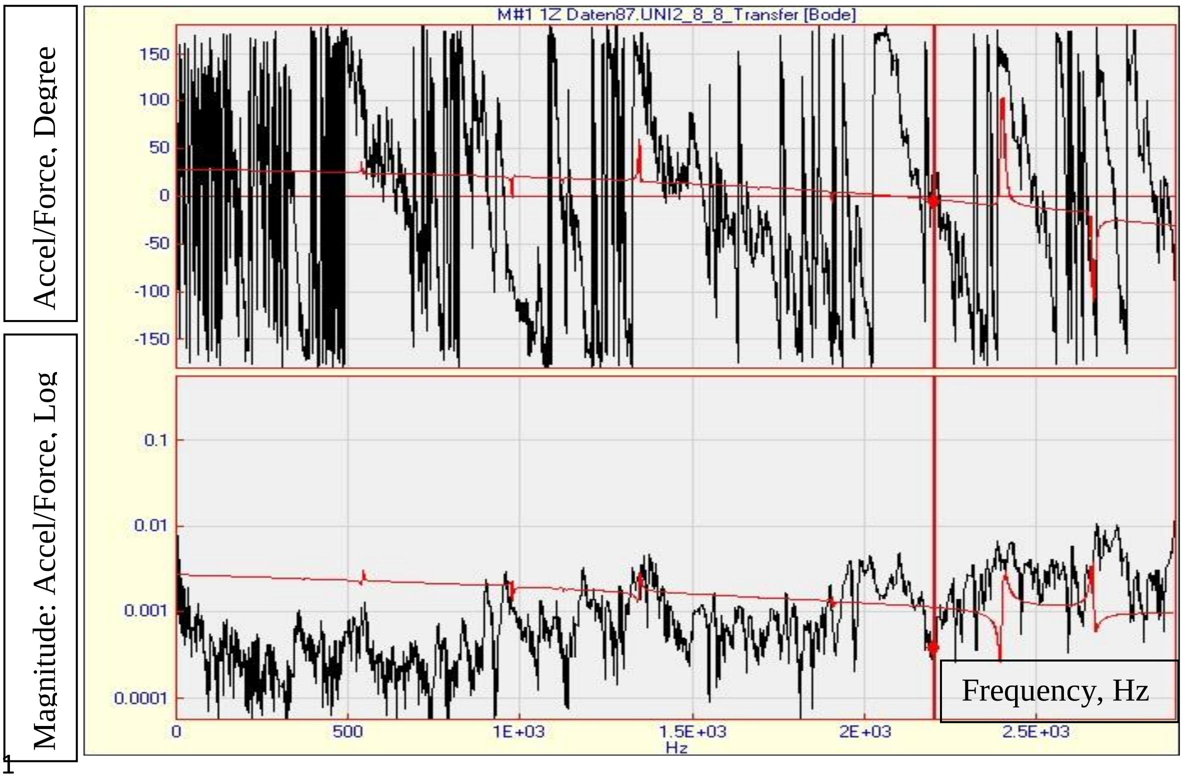

Figure 6.23: Bode diagram of an FRF for node 1 based on reference 28.

Figure 6.24 and Figure 6.25 show the CoQuad diagrams for node 1 based on references 3 and 28, respectively. The plot implements a resonance peak in the Coincident part or the Quadrature part in a set of received signals. The signals in the two plots show that the plot based on reference 3 has the lowest resonance to reference 28. The imaginary part of the data acquisition from reference 3 shows that the output signal has a reasonable wave and is well-suited in relation to reference 28. The Nyquist plots for node 1 based on references 3 and 28 are given in Figures 6.26 and 6.27, respectively. The frequency asymptote is at -270o, which suggests that it is for a system with three more poles than zeroes. The FFT is an algorithm that calculates the Digital Fourier Spectrum (DFT) of a time-domain signal. The Nyquist technique is key equations that govern the use of the FFT. A Nyquist plot displays the Real part on the horizontal axis and the Imaginary part on the vertical axis. Since, it is clearly evident that the frequency of the Nyquist plot in Figure 6.27 shows a scattered signal and that future distance relates to the frequency of the Nyquist diagram in Figure 6.27. These sprawling frequencies on reference 28 indicate that the stability of a system is inadequate and that ratio amplitude frequency between output and input signal is unsuitable. All plots used for node 1 absolutely confirm that the signal received from reference 3 is more appropriate than that received from reference 28.

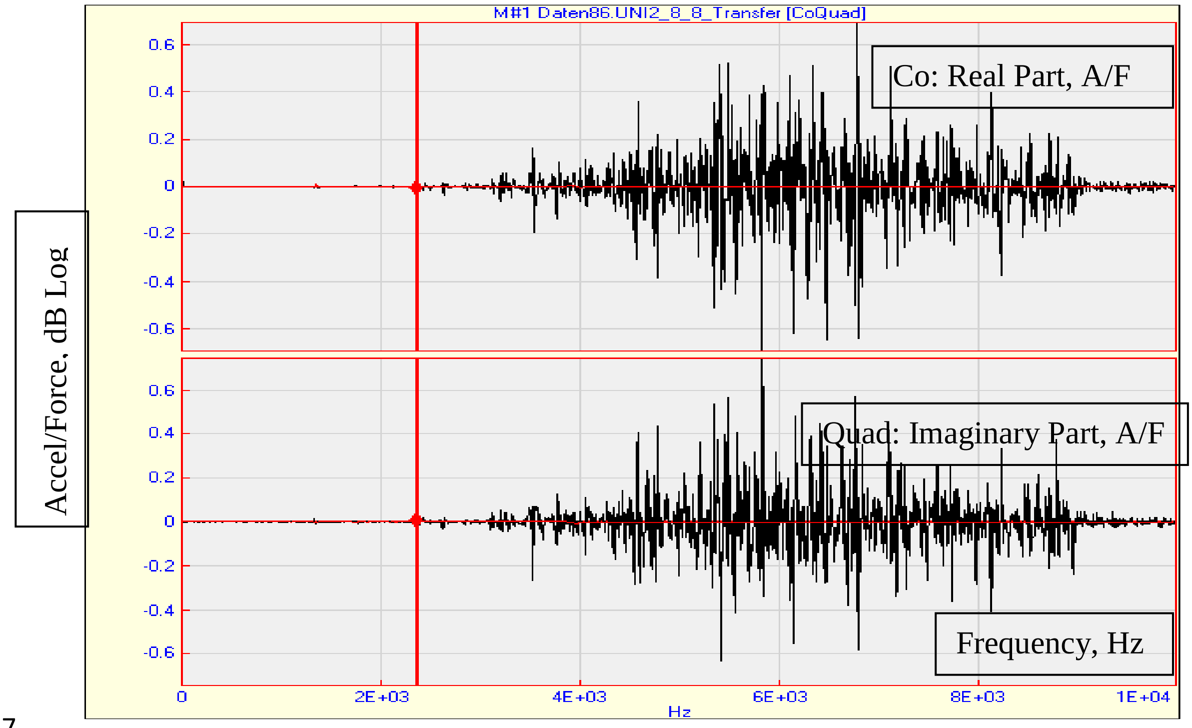

Figure 6.24: CoQuad plot of an FRF for node 1 based on reference 3.

The phase diagrams for node 3 corresponding to references 3 and 28 are also shown in Figure 6.27 and Figure 6.28, respectively. Phase values are usually plotted in degrees. In Figure 6.27, the phase degree appears to level off from 0 and remains almost constant until 800 Hz and the ratio w/w0 is so small that the phase angle is close to zero. However, in contrast to reference 3, in the case of reference 28, the phase degree decreased dramatically from 160 degrees to 105 degrees between 0 Hz at 2e3 Hz. Thus the phase degree shows a low frequency in input signal. These figures demonstrate that the lag phase when using the exciter on reference 3 is lower than when using the exciter on reference 28. Therefore, the output signal at reference 3 is well-suited for utilization in the analysis of the structure.

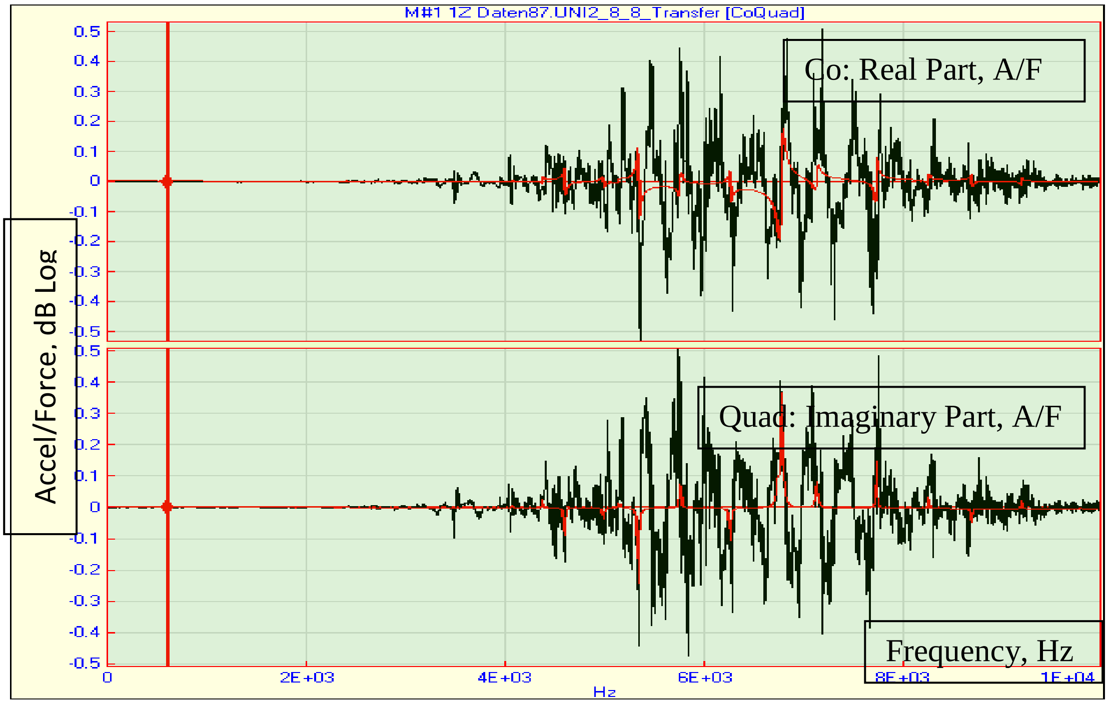

Figure 6.25: CoQuad plot of an FRF for node 1 based on reference 28.

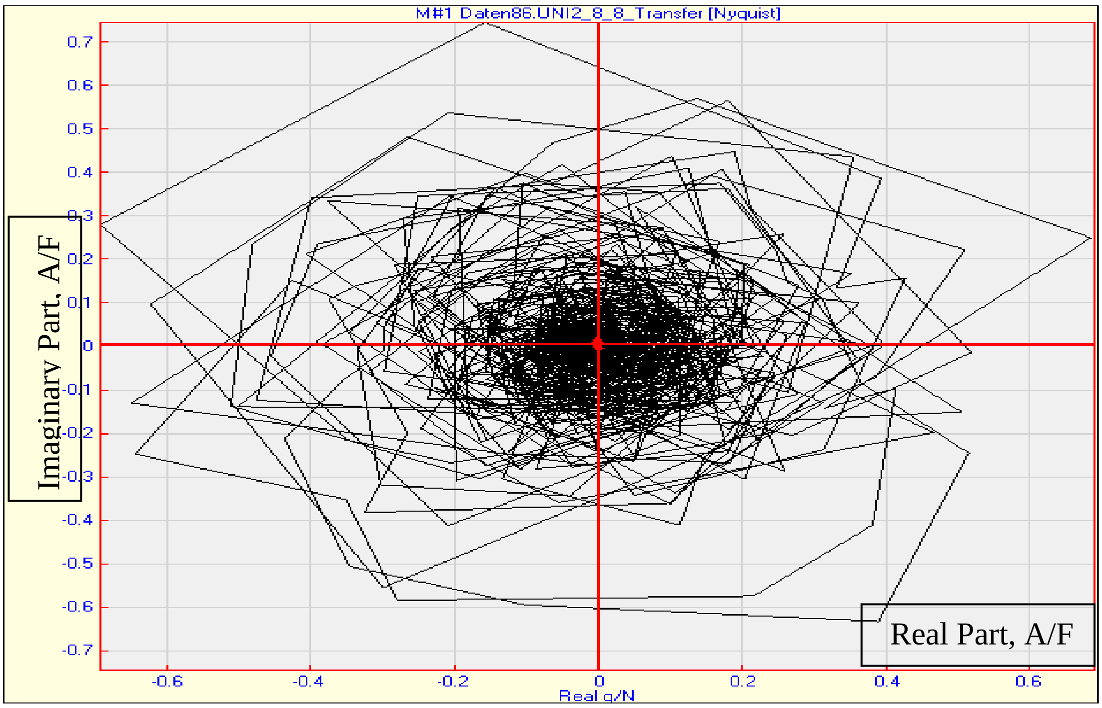

Figure 6.26: Nyquist Plot of an FRF for node 1 based on reference 3.

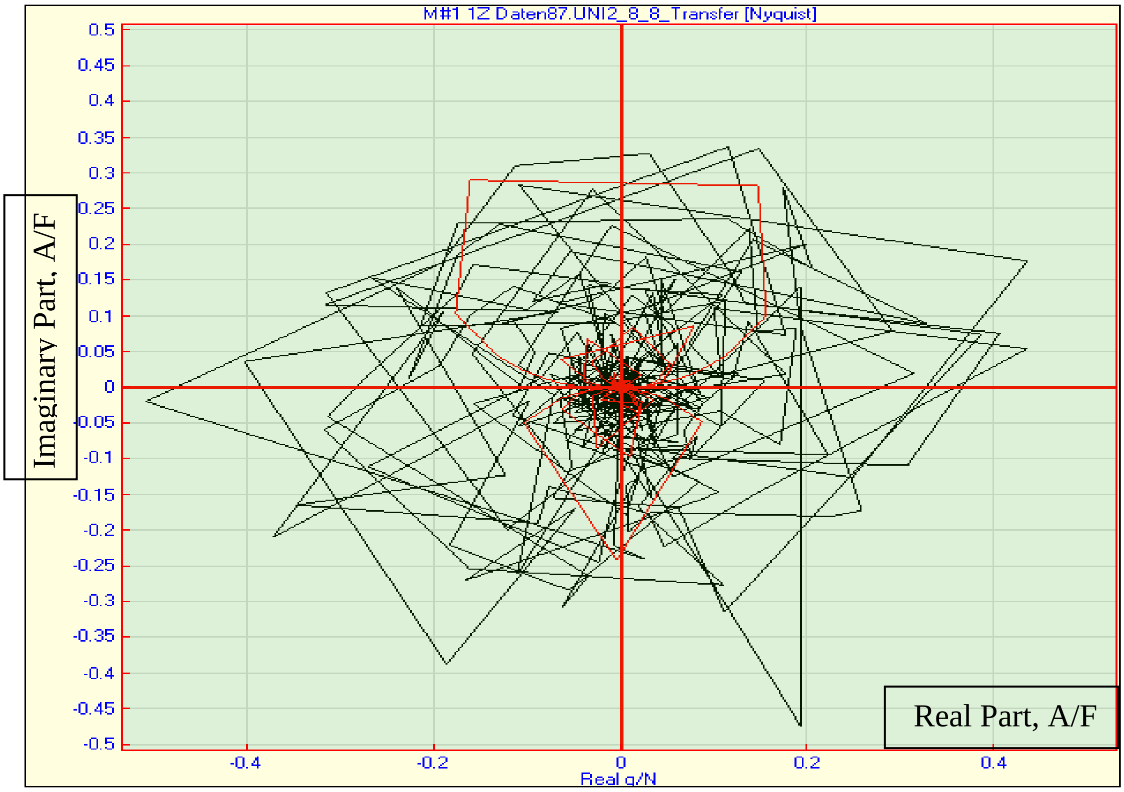

Figure 6.27: Nyquist diagram of an FRF for node 1 based on reference 28.

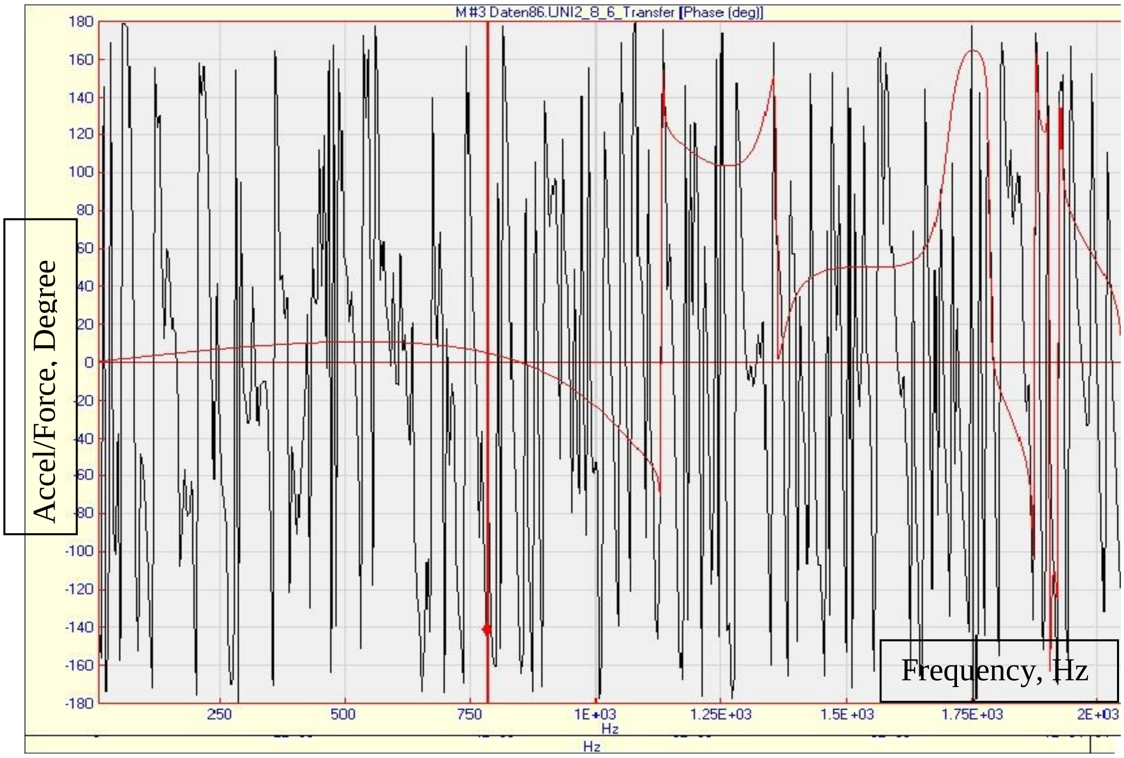

Figure 6.28: Phase diagram of an FRF for node 3 based on reference 3.

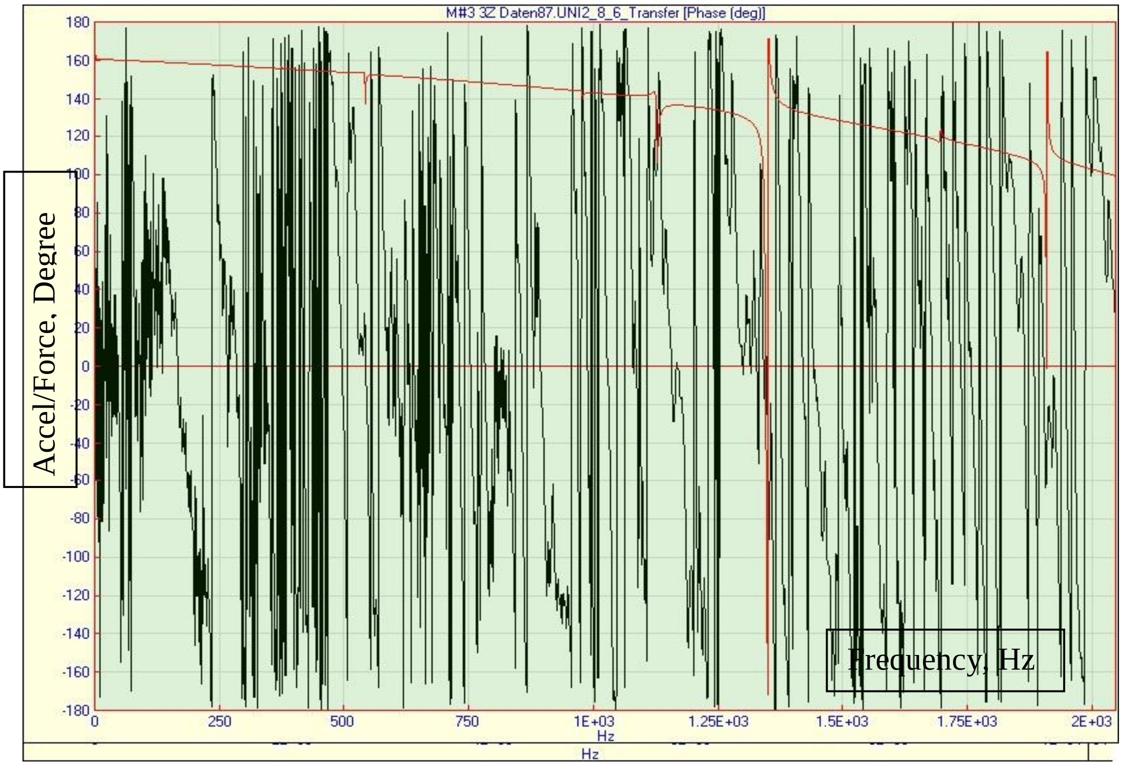

Figure 6.29: Phase diagram of an FRF for node 3 based on reference 28.

6.5.9 Mode shape

A mode of vibration is characterized by a modal frequency and a mode shape, and is numbered according to the number of half waves in the vibration. A mode shape is a specific pattern of vibration executed by a mechanical system at a specific frequency. This process involves identifying the eigenvalues and eigenvectors of the equations of motion. These parameters also define the modes of vibration of the structure. The purpose of modal testing is to artificially excite a structure so that the frequencies, damping and mode shapes of its predominant modes of vibration can be identified. The different mode shapes will be associated with different frequencies. The experimental technique of modal analysis discovers the mode shapes and the frequencies.

6.5.10 Procedure of modal analysis with ME'scope

Modal damping and mode shape for each mode is identified in the bandwidth of the frequencies measurements. Experimental modal parameters are estimated by analytical FRF parametric model data. Each mode has a modal frequency and damping estimate, and a different residue estimate for each measurement. Each residue is a different component of the mode shape. The outcome of curve fitting is a set of modal parameters (frequency, damping, and residues) for each mode that is identified in the frequency range of the measurements. Curve fitting is based on the fact that an FRF for any vibrating structure can be represented in terms of modal parameters. The parametric model is used to estimate experimental modal parameters by curve fitting a set of measurements. The denominators all contain the same frequency and damping. Frequency and damping can be estimated by curve fitting a single measurement or any number of measurements taken from the same structure. When each measurement is curve fit for frequency and damping, this is called local curve fitting. When two or more FRFs are curve fit together, this is called global curve fitting. Each mode should only have one estimate of frequency and damping. However, local curve fitting may be necessary when the experimental data has variations in the resonance peak frequencies due to mass loading, temperature changes, or other effects that can cause the mode frequencies to change during the course of a modal test. In general, modal residues are complex numbers. The modal residues are made up by magnitude and phase in the modal parameters. Since the denominator of the FRF has units of Hertz, or (radians/second), residues must have the following units:

$$\text{Residue units} = (\text{FRF units}) \times (\text{radians / second}) \qquad 6.8$$

The undamped natural frequency (Ω_0) and percent critical damping (ζ_0 = cosine (β_0)) are polar coordinates of the pole location. The damped natural frequency (ω0) and damping coefficient (σ_0) are rectangular coordinates of the pole location. The modal frequency and damping plot is shown in Figure 6.30.

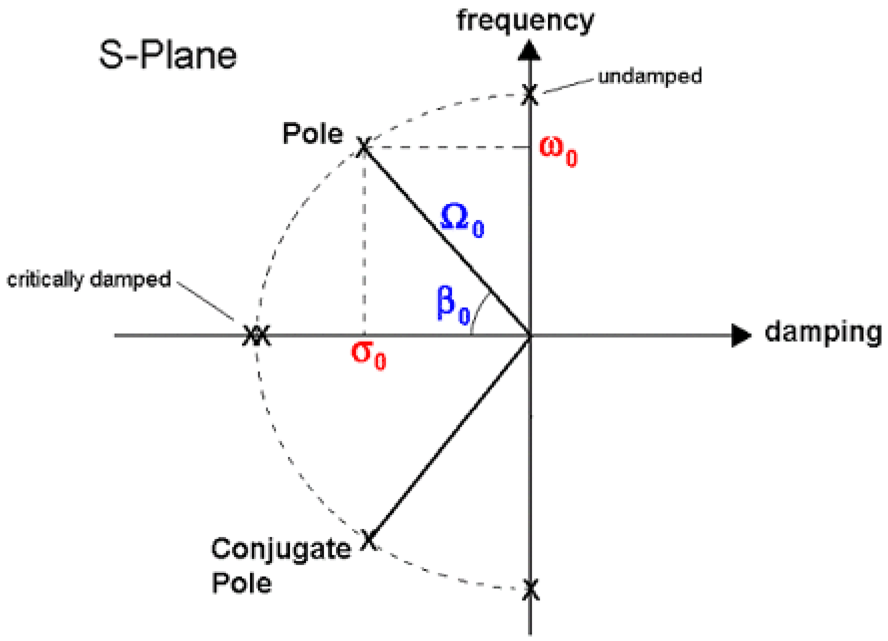

Figure 6.30: The modal frequency and damping plot.

The CoQuad and peak curve fitting methods are used for single mode methods. The orthogonal polynomial curve fitting method is used for multiple mode method. The polynomial method is a method that simultaneously estimates the modal parameters of two or more modes. The polynomial method is a frequency domain curve fitting method that utilizes the complex (real and imaginary) units. Local curve fitting should be used when the FRF data has slight variations in the resonance peak frequencies from one measurement to another, due to changes in mass loading (moving the sensors) during acquisition of the FRFs. When global fitting is chosen, all FRFs are curve fit together and a global modal frequency and damping estimate is saved for each mode. Each mode should have only one estimate of frequency and damping. Global curve fitting yields better estimates if the structure contains local modes. The residue for each mode is listed as a complex number (magnitude and phase). The magnitude units are the units of the trace multiplied by radians per second. Phases are in degrees. The effective mass, damping and stiffness are calculated with the following respective formulas:

Effective Mass = 1 / (Frequency x Residue real + Damping x Residue Imaginary) 6.9

Effective Damping= 2 x Damping x Effective Mass 6.10

Effective Stiffness= (Frequency2 + Damping2) x Effective Mass 6.11

Where: Residue real = Real part of the residue.

Residue Imaginary= Imaginary part of the residue.

In the present study, a mathematical step is needed to represent the FRF matrix in terms of mode shapes instead of residues. Notice that a mode shape is unique in shape, but not in value. Many structures exhibit resonant vibration in a localized region of the structure. In other words, energy becomes ‘trapped’ between stiff boundaries in a local region, and cannot readily escape, causing a standing wave of vibration, or local mode shape. Global modes have mode shapes that are mostly nonzero, except at node points. Local modes have mode shapes that are nonzero in a local region of the structure, and zero elsewhere. The first step of modal parameter estimation is to determine how many modes are represented by resonance peaks in the frequency band of a set of measurements.

The investigation of mode shape in this experimental work demonstrates that the mode shapes from reference 28 are similar to the local mode and are not sufficient for use in the analysis. Mode shapes in the experimental work based on node 28 are shown in Figure 6.35 and Figure 6.36. In contrast, the mode shapes based on reference 3 are global and show the accurate behaviour of the structure. In this project, for sufficient acquisition of data, all mode frequency responses are investigated by complex exponential and Z polynomial methods. The resulting multiple sets of frequency and damping estimates are referred to as a stability diagram. A stability diagram is useful when resonance peaks cannot be counted on the modeindicator curves. When a modal frequency and damping estimate does not change substantially from one curve fitting mode size to the next, this is an indication that the pole estimates are stable, and they are therefore the correct modal parameters for each mode in question.

6.5.11 Complexes Exponential

This method is a time-domain method that estimates poles from a set of FRFs by curve fitting their corresponding set of IRFs by using a least squared error method. Prior to curve fitting, each FRF is transformed to its equivalent IRF by applying the inverse FFT to the FRF data.

6.5.12 Z Polynomial

This method is an extension of the orthogonal polynomial method and uses the Z transform to obtain poles from larger curve fitting model sizes than the orthogonal polynomial method. Like the orthogonal polynomial method, this method works better with small cursor bands of data at a time. The predicted nonlinear response corresponding to the 5th mode of vibration using one vibrator is compared with the same mode shapes calculated by an eigenvalue in the finite element analysis and in the experimental work, as shown in Figures 6.31 to 6.36. For more accuracy and efficiency, all mode shapes are normalized by complexes exponential. The numbers of nodes are assigned in Figure 6.31.

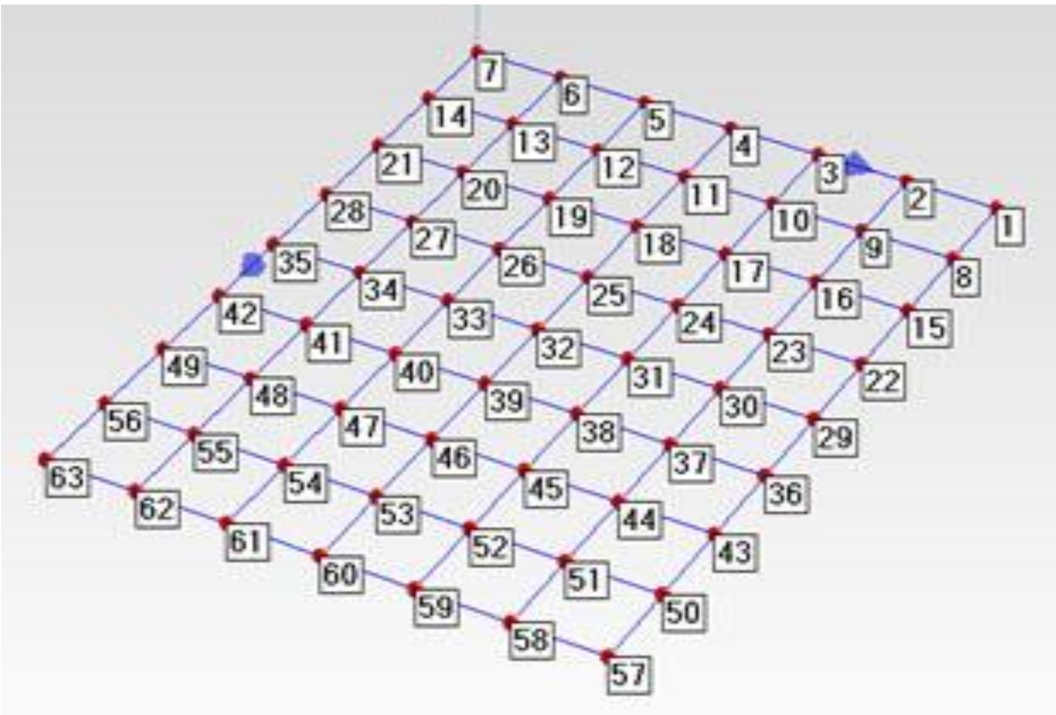

Figure 6.31: The general view of the steel construction under study.

<table>
<tr>
<td>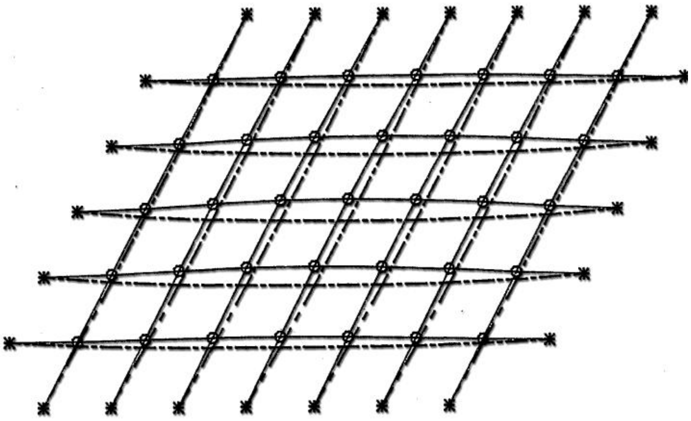</td>
<td>Theoretical Analysis

Mode shape: 1

Frequency: 2.97 Hz

Damping ratio: 0.09%</td>
</tr>
<tr>
<td>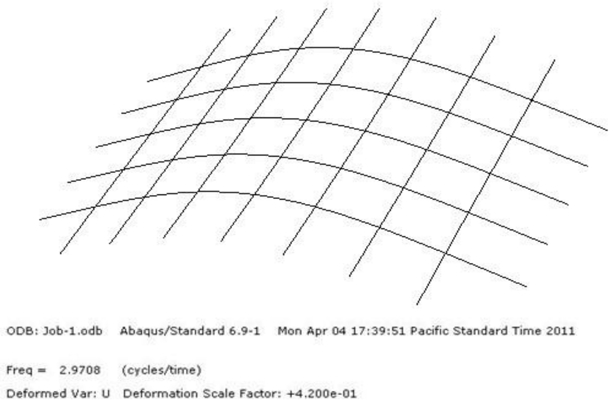
</td>
<td>Finite Element Modelling

Mode shape: 1

Frequency: 2.96 Hz

Damping ratio: 0.05%</td>
</tr>
<tr>
<td>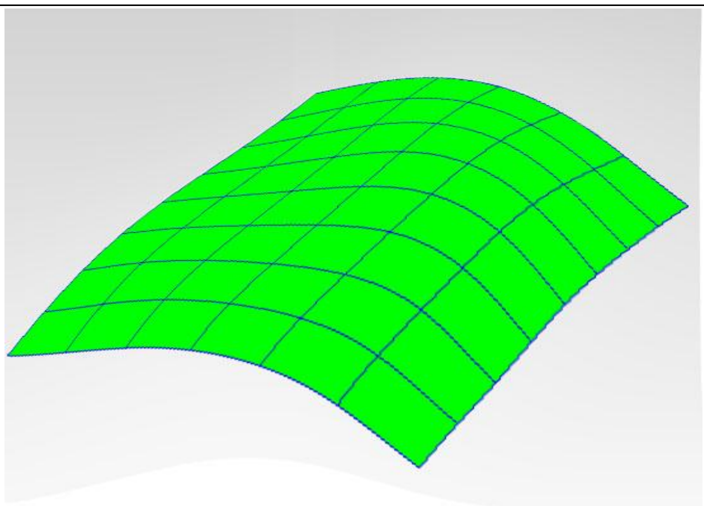</td>
<td>Experimental Work

Mode shape: 1

Frequency: 2.95 Hz

Damping ratio: 0.1%</td>
</tr>
</table>

Figure 6.32: Mode shape 1 of the structure.

<table>
<tr><td>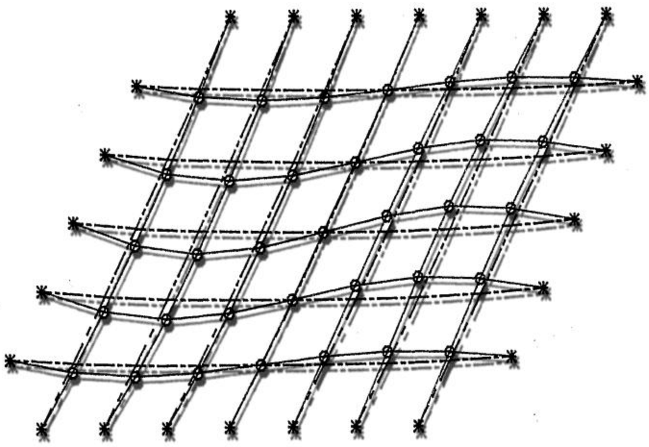</td><td>Theoretical Analysis
Mode shape: 2
Frequency: 6.46 Hz
Damping ratio: 0.01%</td></tr>
<tr><td>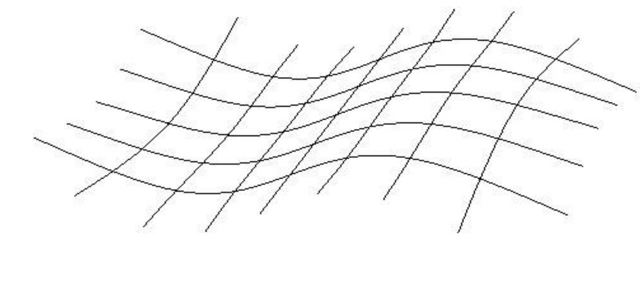
</td><td>Finite Element
Modelling
Mode shape: 2
Frequency: 6.42 Hz
Damping ratio: 0.05%</td></tr>
<tr><td>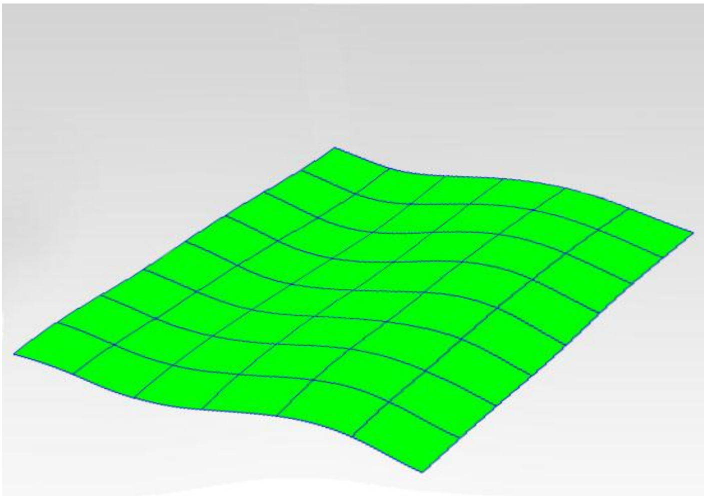</td><td>Experimental Work
Mode shape: 2
Frequency: 6.41 Hz
Damping ratio: 0.01%</td></tr>
</table>

Figure 6.33: Mode shape 2 of the structure.

<table>
<tr><td>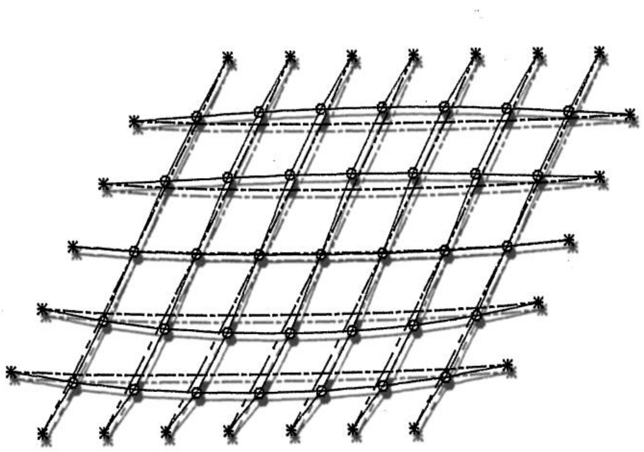</td><td>Theoretical Analysis
Mode shape: 3
Frequency: 8.01 Hz
Damping ratio: 0.01%</td></tr>
<tr><td>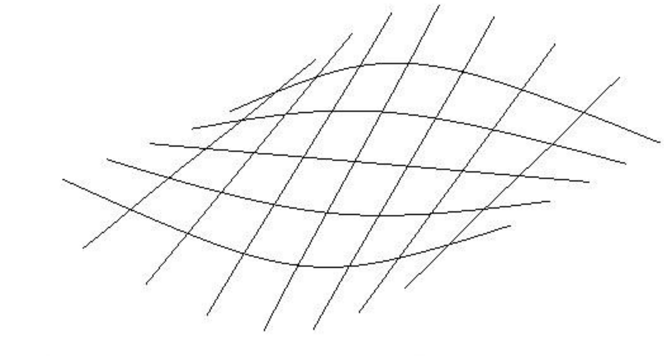
</td><td>Finite Element Modelling
Mode shape: 3
Frequency: 7.96 Hz
Damping ratio: 0.05%</td></tr>
<tr><td>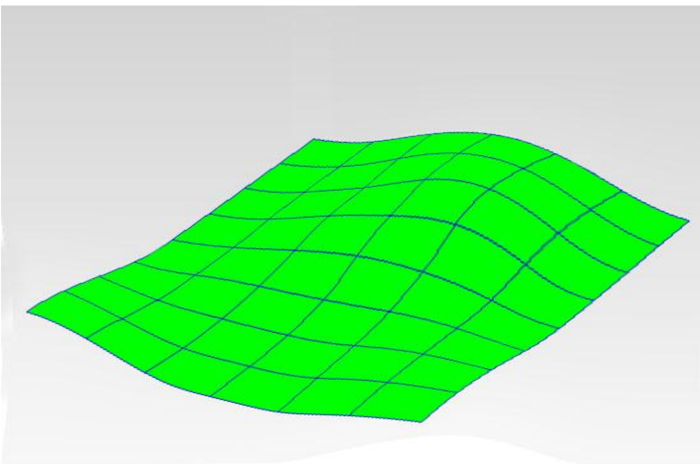</td><td>Experimental Work
Mode shape: 3
Frequency: 7.90 Hz
Damping ratio: 0.01%</td></tr>
</table>

Figure 6.34: Mode shape 3 of the structure.

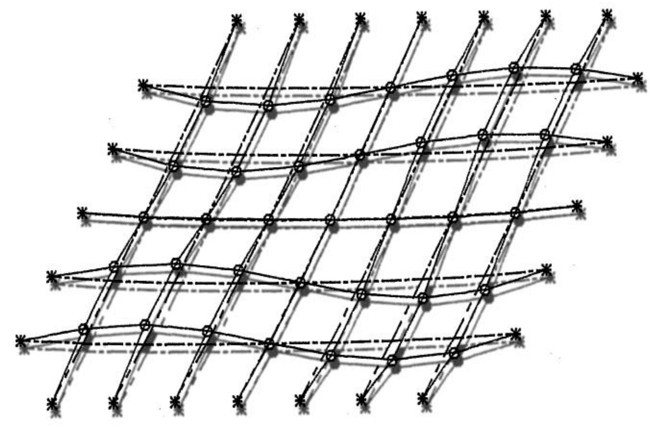	Theoretical Analysis Mode shape: 4 Frequency: 9.12 Hz Damping ratio: 0.01%
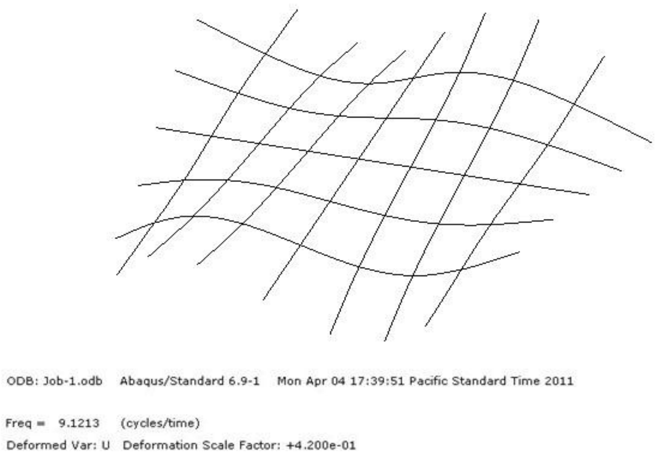	Finite Element Modelling Mode shape: 4 Frequency: 9.11 Hz Damping ratio: 0.05%
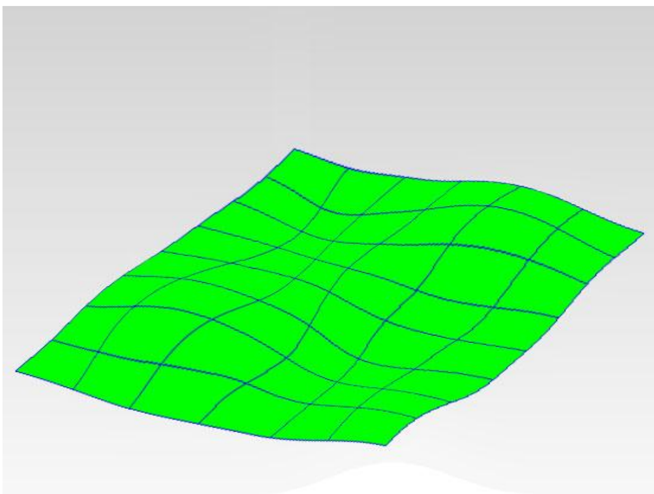	Experimental Work Mode shape: 4 Frequency: 9.10 Hz Damping ratio: 0.01%

Figure 6.35: Mode shape 4 of the structure.

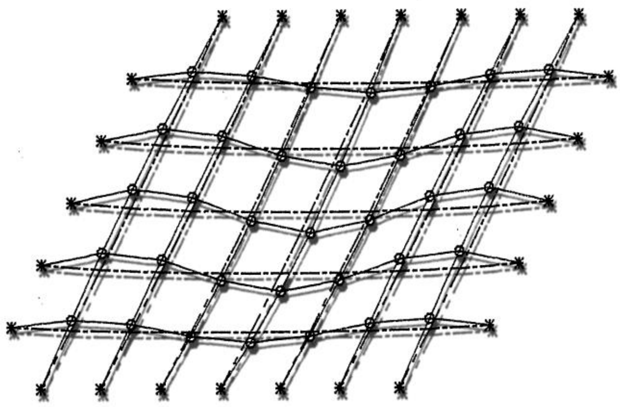	Theoretical Analysis Mode shape: 5 Frequency: 14.24 Hz Damping ratio: 0.05%
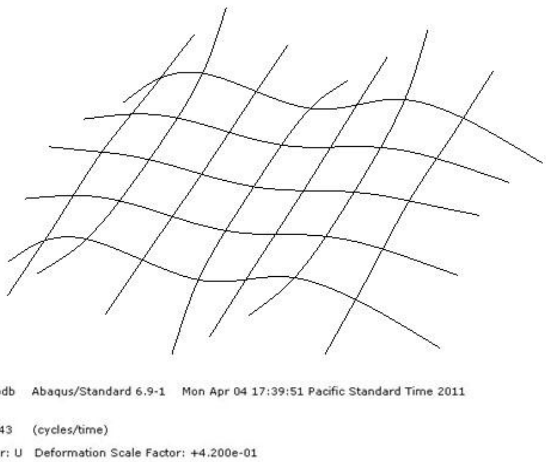	Finite Element Modelling Mode shape: 5 Frequency: 14.13 Hz Damping ratio: 0.05%
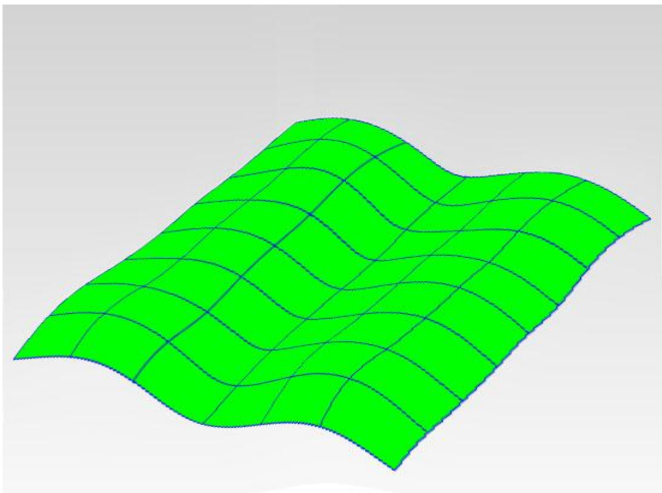	Experimental Work Mode shape: 5 Frequency: 14.55 Hz Damping ratio: 0.005%

Figure 6.36: Mode shape 5 of the structure.

The damping ratio for modes decreases with increase mode number and they are not similar to each others. Because damping ratio is function of frequency. And damping ratio values come out from different formulation in either of finite element, theoretical and experimental. Hence, values of damping ratio could not same to each other's when frequencies are not same values. Frequencies value decrease in period of time. As shown by the above figures, all the theoretical and experimental mode shapes are close to each other and verify the proposed theory. For better accuracy, all mode shapes should be normalized. A complexity plot displays the magnitudes and phases of all shape components in a single plot. A mode shape is called a 'normal' mode shape if all of its shape components have phases of 0 or 180 degrees. In other words, all of the shape components lie along a straight line defined by 0 or 180 degrees in a complexity plot. If no damping is included in a FEA model, all of its FEA mode shapes will be normal mode shapes. In the present work, all mode shapes are normalized according to the above mentioned complexity plot. For example, the complexity plot for mode shape 1 based on reference 3 is shown in Figure 6.37. In Figure 6.37, the red shape components denote a 0 degree phase and the blue shape components denote a 180 degree phase.

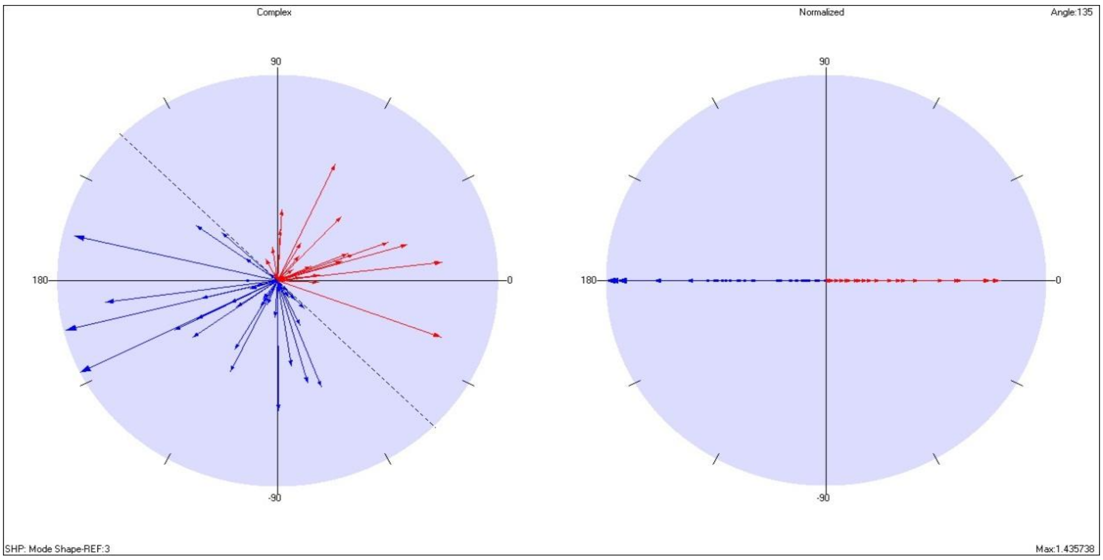

Figure 6.37: Complexity plot of mode shape 1.

The right-hand side of Figure 6.37 shows the normalization of mode shape components. Experimental mode shapes are often complex because real structures have damping in them. The components of a complex shape do not necessarily lie along a straight line in a complexity plot. Shape normalization helps simplify the animated display of complex shapes. The dashed line on a complexity plot is called the normalization line. When a complex shape is normalized, the magnitudes of all of its components are retained, but the phases are changed to either 0 or 180 degrees. For each position of the vibrator, the net is excited with a frequency corresponding to the mode on pre-tensioned cables. Each cable was tensioned at 11500 N. The comparisons between the theoretical and experimental natural frequencies are presented in Table.6.5.

Table 6.5: Theoretical and experimental natural frequencies.

PRETENSION LOAD (N) = 11500	NATURAL FREQUENCIES (Hz)					
	Reference 3			Reference 28		
	ω_T THEORETICAL	ω_E EXPERIMENTAL	$\frac{\omega_E - \omega_T}{\omega_E}$ %	ω_T THEORETICAL	ω_E EXPERIMENTAL	$\frac{\omega_E - \omega_T}{\omega_E}$ %
Mode 1	2.9708	2.9531	0.60	2.9708	2.1231	28.53
Mode 2	6.4601	6.4142	0.71	6.4601	5.9142	8.45
Mode 3	8.0102	7.8945	1.44	8.0102	6.7945	15.18
Mode 4	9.1213	9.1023	0.21	9.1213	8.1023	11.17
Mode 5	14.243	14.553	2.18	14.243	12.965	8.97
Mode 6	17.347	17.235	0.65	17.347	15.255	12.06
Mode 7	23.762	23.151	2.57	23.762	17.713	25.46

The net had to be excited five times for each setup to reach a suitable response for each of the nodes. For each frequency, the modal damping was found by calculating the logarithmic decrement from the decay function. It should be mentioned that the logarithmic decrement method is utilized to calculate damping in the time domain. In the present work, the free vibration displacement amplitude history of a system for an impulse is calculated and recorded. The logarithmic decrement is the natural logarithmic value of the ratio of two adjacent peak values of displacement in free decay vibration. The logarithmic decrement, δ, is utilized to find the damping ratio of an under damped system in the time domain. Since cable nets are nonlinear structures because of their stiffness, their natural frequencies vary with the amplitude of vibration. The reported tests of other researchers indicate that the frequencies are approximately independent of the amplitudes of response achieved (Kirsch et al., 2007). Some initial tests were carried out to mention that the natural frequency is independent of amplitude. From a particular time until now the maximum response and hence the maximum change of stiffness was achieved in the first mode. This was deemed sufficient only to study the variations of the natural frequencies with the amplitude of response in this mode. In general, specific damping over a range is detected by mode or frequency and damping value is calculated by direct modal or composite modal methods such as the Rayleigh method. Table 6.6 gives the finite element results and theoretical frequencies of the net for the five modes. The effect of damping value is calculated by a composite modal method between mode 1 and mode 5 and load variation with time is detected as instantaneous. The result presented shows that the natural frequencies decrease only slightly with the increase in the amplitude. This means that the natural frequency is constant and independent of the amount of the force's value.

Table 6.6: Theoretical and finite element result of natural frequencies for the first five modes.

	NATURAL FREQUENCY (Hz)					
LOAD	0 (N)			500 (N)		
MODE NUMBER	THEORETICAL ω_T	FINITE ELEMENT ω_{FE}	$\frac{\omega_{FE}-\omega_T}{\omega_{FE}}\%$	THEORETICAL ω_T	FINITE ELEMENT ω_{FE}	$\frac{\omega_{FE}-\omega_T}{\omega_{FE}}\%$
1	2.9708	2.9621	0.31	2.9708	2.8696	2.91
2	6.4601	6.4235	0.56	6.4601	6.3568	0.90
3	8.0102	7.9584	0.64	8.0102	7.7895	1.35
4	9.1213	9.1101	0.12	9.1213	8.9653	1.53
5	14.243	14.131	0.78	14.243	14.2556	2.09
LOAD	1000 (N)			2000 (N)		
MODE NUMBER	THEORETICAL ω_T	FINITE ELEMENT ω_{FE}	$\frac{\omega_{FE}-\omega_T}{\omega_{FE}}\%$	THEORETICAL ω_T	FINITE ELEMENT ω_{FE}	$\frac{\omega_{FE}-\omega_T}{\omega_{FE}}\%$
1	2.9708	2.9365	0.57	2.9708	2.9865	1.12
2	6.4601	6.2356	2.86	6.4601	6.3365	1.23
3	8.0102	7.6981	2.55	8.0102	7.5362	4.75
4	9.1213	9.236	1.45	9.1213	8.8652	2.67
5	14.243	14.6322	0.54	14.243	14.1425	2.90

The logarithmic decrements δ against amplitudes of vibration are shown in Figure 6.38. The logarithmic decrement is calculated from the natural logarithm of the ratio of the amplitudes of any two oscillations. Its formulation is:

$$\text{Delta}\ (\nabla) = \frac{1}{n} \operatorname{Ln} \left(A_{i+n} / A_i \right) \qquad 6.9$$

where $\boldsymbol{A_i}$ = amplitude of the i_{th} oscillation.

$\boldsymbol{A_{(i+n)}}$ = amplitude of the oscillation n vibrations after the i_{th} oscillation.

By calculating the values of δ at various points along the decay curve it was found that the logarithmic decrements varied with the amplitude and reduced with increasing amplitude. During the calculation, the logarithmic decrement appears to approach a constant value as the amplitude increases.

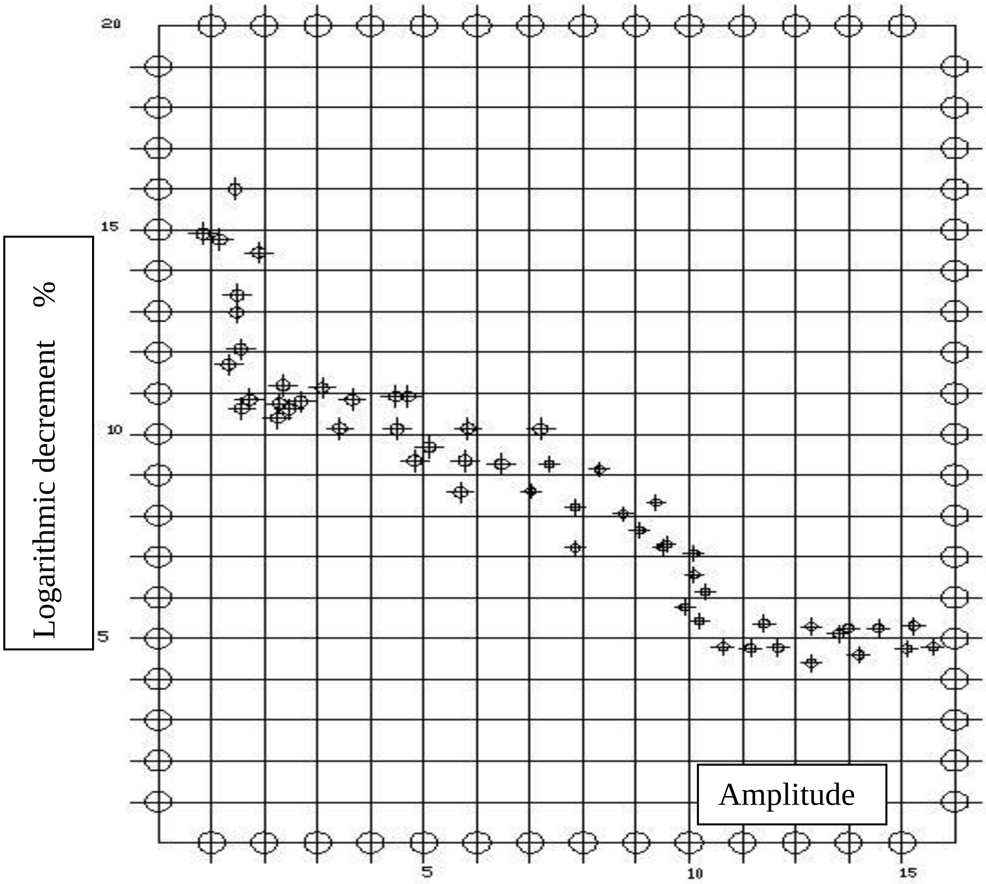

Figure 6.38: The logarithmic decrements against amplitudes of vibration.

6.6 Parametric study on dynamic response

6.6.1 Comparison of the response predicted between the Fletcher-Reeves and the Newton-Raphson methods and linear dynamic response

The proposed method for the nonlinear dynamic response analysis of pre-tensioned structures is based upon the minimization process carried out by the Fletcher-Reeves and the Newton-Raphson algorithms. A comparative study of the two algorithms can help in choosing one of the two algorithms for the analysis of a given structure.

In order to extend the analysis to a larger problem, the following numerical modelling is carried out on the 7*5 net. The logarithmic damping was assumed to be the same in all modes and equal to 10%. In this section, the calculated nonlinear response is compared with those predicted by the linear Newton-Raphson and mode superposition method. In each case analysed, the dynamic load is applied as the excitation force of the structure. The response in each case is calculated for a period of 15 seconds. Table 6.7 gives the amplitude of the steady state vibration in the 7th mode for joints 4, 11, 18, 25, 32, 39, 46, 53, and 60 for dynamic analysis while the dynamic load is on node 32. These results show the extent of the differences between the linear and nonlinear calculated response. In numerical dynamic analysis, the dynamic load applied as the excitation force of the form is P (t) = P_0 sin (w_n* t), where w_n is the n_{th} natural angular frequency. The dynamic load plot based on mode shape 1 is shown in Figure 6.40. The details of dynamic load are written as

Static load = 200 N per joint, Pre-tension = 11500 N per link

P=50 sin 2.97*t at joint 32 w_1=2.97 mode shape 1 based on node 32

Figure 6.39 shows a full time history. The full time history is the response of a structure over time during and after the application of a load.

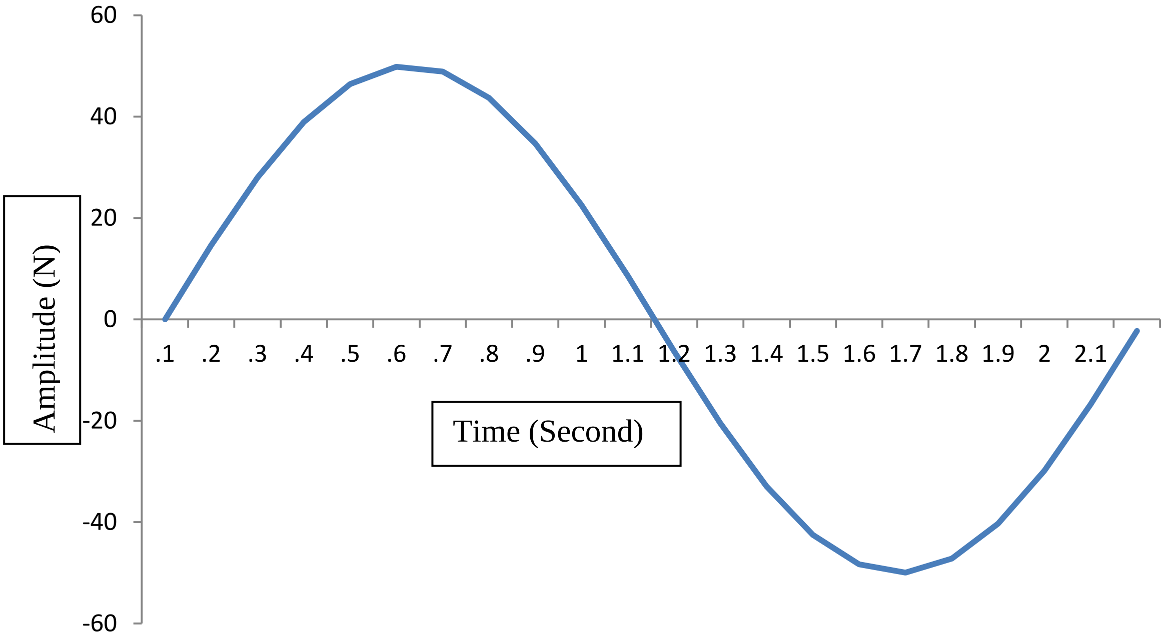

Figure 6.39: The dynamic load plot based on mode shape 1.

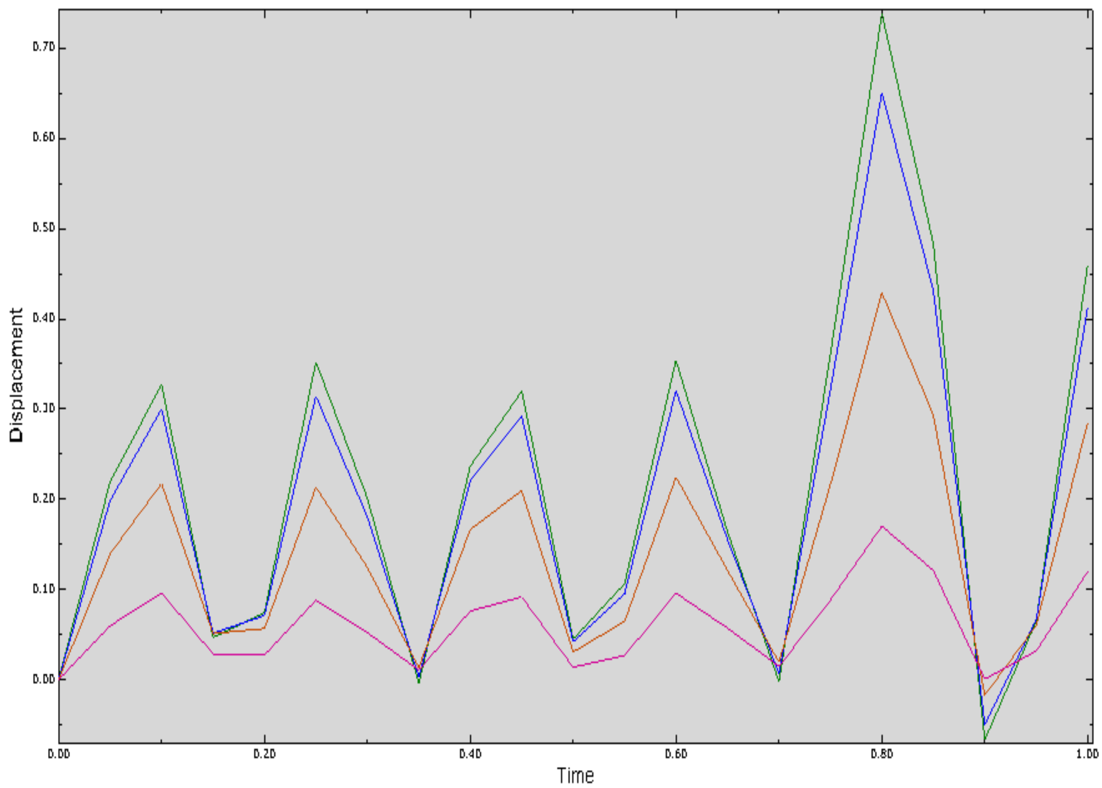

Figure 6.40: The time history of dynamic load based on mode shape 1.

The full time history of a structure's response is achieved by solving the structure's equation of motion. The best time step is detected based on the time history. The best time step is recognized based on which increment time step creates the most deflection in the structure. The maximum deflection is used to compare the theoretical and finite element results.

From Table 6.7 it can be seen that the differences between the linear and the nonlinear calculated responses are significant and that the differences increase with the increase in nonlinearity.

Table 6.7: The amplitude (mm) of joints 4, 11, 18, 25, 32, 39, 46, 53, 60 at steady state vibration and pre-tension of 11500 N/link

Joint	Exciting force on node 32, Dynamic load= 50*Sin(2.97*t)		
	Superposition (Linear)	Newton-Raphson (Nonlinear)	Fletcher-Reeves (Nonlinear)
4	0	0	.2
11	12.7	8.25	8.02
18	27.6	19.8	19.3
25	45.1	28.6	28.4
32	51	34.1	32.3
39	45.1	28.6	28.4
46	27.6	19.8	19.3
53	12.7	8.25	8.02
60	0	0	.2

Table 6.8 show that the differences are very small when only one exciting force is applied, but when two exciting forces are applied, the differences reach a large value. The amplitude (mm) of joints 4, 11, 18, 25, 32, 39, 46, 53, and 60 are given in Table 6.8.

In this case, when tension load had reduced to 5500 N, the nonlinearity of the structure increased. The amplitude of response of joint 32 calculated by the linear method was 1.6 times greater than that calculated by the nonlinear method. It can also be noted that when the linear method calculated the upwards and downwards movements of joints 4, 11, 18, 25, 32, 39, 46, 53, and 60 the measures are all equal, whereas the use of the nonlinear method of analysis shows that the upwards movements are greater than the downwards movements. The difference is approximately 5.6% of the upward movement. This is to be expected because the rate of change of stiffness is greatest when moving downwards from the static equilibrium position. The investigation also showed that the shapes of modes obtained by exciting the net do not differ from those obtained by an eigenvalue analysis.

The comparison between responses of linear and nonlinear modes for nodes 4, 11, 18, 25, 32, 39, 46, 53, and 60 is shown in Figure 6.41 when subjected to an exciting force. The amplitudes in Figure 6.41 show that the linear response is more than the nonlinear predicted response. The nodes detected are major nodes in the structure in that they have maximum deflection in the behaviour of structure by a high degree of freedom. Figure 6.42 shows that when the response is calculated nonlinearly the maximum amplitudes occur during the transient period of vibration, whereas in the linearly calculated response the amplitudes reach their maximum value when the net vibrates in steady state. The sufficiency of the Fletcher-Reeves method to calculate response and analyse structures according to their high nonlinearity behaviour is clearly shown in Figure 6.42.

Table 6.8: The amplitude (mm) of joints 4, 11, 18, 25, 32, 39, 46, 53, 60 at steady state vibration and pre-tension of 11500, 5500 N/link

Pre-tension 11500 N/link.				
Joint	Exciting force on Node 25		Exciting force on Node 25,39	
	Superposition (Linear)	Fletcher – Reeves (Nonlinear)	Superposition (Linear)	Fletcher – Reeves (Nonlinear)
4	0	0	0	0
11	8.76	7.97	7.35	5.07
18	19.5	18.7	18.7	12.1
25	31.7	29.9	27.7	17.9
32	29.7	28.3	32.1	20.1
39	29.1	27	25.9	17.9
46	19.6	18.7	17.5	12.1
53	7.26	7.21	7.41	5.07
60	0	0	0	0
Pre-tension 5500 N/link.				
4	0	0	0	0
11	10.7	9.35	10	7.42
18	23.6	22.5	24.4	16.3
25	40.5	36.9	33	22.0
32	37.6	33.8	34.2	23.6
39	33.4	30.8	33	22.0
46	25.5	22.4	24.4	16.3
53	9.62	8.3	9.7	7.42
60	0	0	0	0

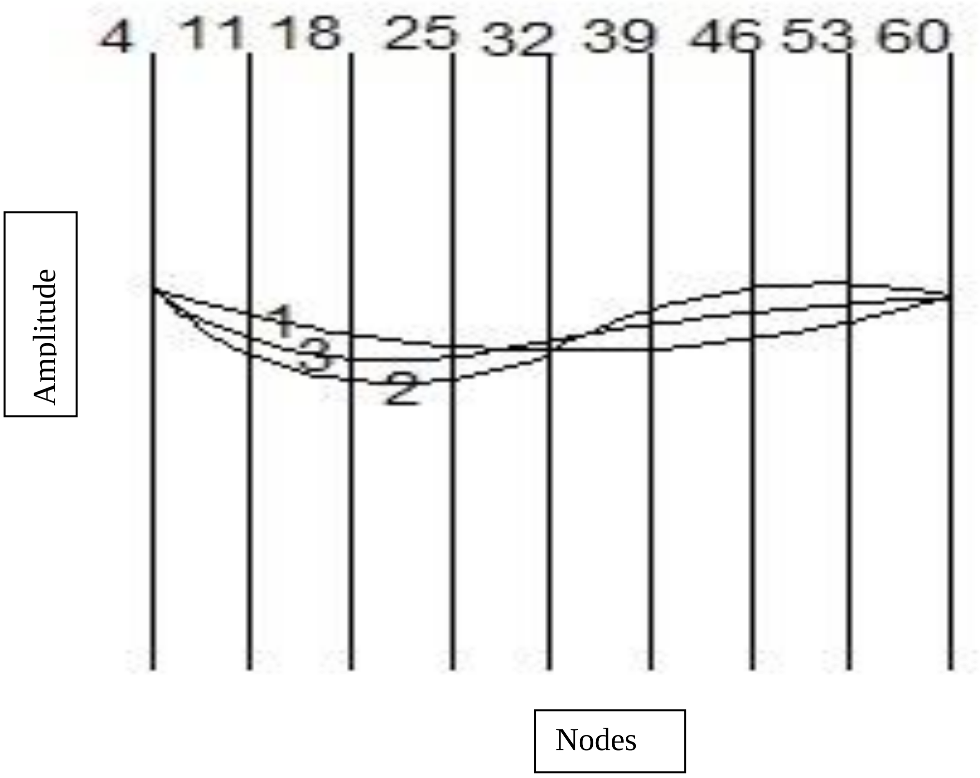

Figure 6.41: The linear and nonlinear dynamic response of joints 11, 25, 32, 39, 46, 53, and 60.

1) The net at static equilibriums 2) Linear responses 3) Nonlinear responses

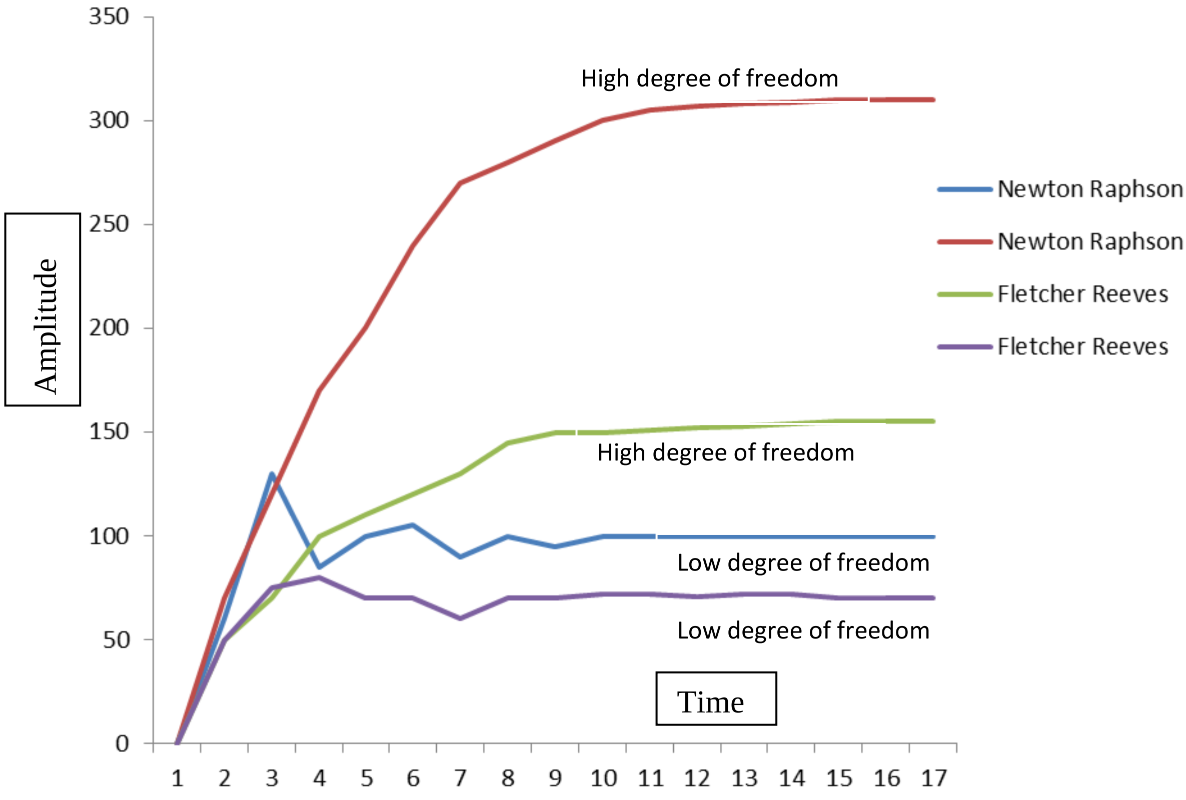

Figure 6.42: Build up of the amplitude of joint 32 from t=0 to steady state vibration.

Figure 6.42 shows that the differences between the Fletcher-Reeves and Newton-Raphson methods are negligible in linear structures, whereas the differences between the Fletcher-Reeves and Newton-Raphson methods are evident in nonlinear structures. The Fletcher-Reeves method shows that this method is well sufficient in structures which have large degree of freedom such as 3D space structures. In fact, the response predicted by the nonlinear analysis showed that the maximum amplitude of joint 32 occurred from one to three time steps later. From experience of practical testing, this is expected for cases where dynamic load is used.

6.6.2 The effect of the magnitude of modal damping on dynamic response

The main aim of this section is to present the results of the study of the variations in the dynamic response of the 7*5 nets due to changes in the damping ratios used to construct the damping matrix given by composite damping. Combined damping is able to give variations in damping in different modes and enables the study of the effect of those variations on the dynamic response. The 7*5 flat is analysed for various combinations of damping ratios. The assumed values of the damping ratios used in the analysis of damping are given in Table 6.9.

Table 6.9: Assumed values of percentage of logarithmic decrement for damping.

Damping case	Mode 1	
	LD %	DR
1	8	0.0127
2	6	0.0095

LD: Logarithmic decrement

DR: Damping ratio

The dynamic response is calculated for two different combinations of damping ratios by both the Fletcher-Reeves and the Newton-Raphson algorithms. The maximum amplitude of joint 18, 25, and 32 is calculated with assumed damping is given in Table 6.10.

Table 6.10: The maximum amplitude of joint 18, 25, and 32 for composite damping calculated by Newton Raphson and Fletcher- Reeves method.

Case	Method	Node 18	Node 25	Node 32
1	Fletcher-Reeves	19.3	28.1	32.4
2		19.5	28.2	33.7
1	Newton-Raphson	21.7	30.3	35.8
2		21.9	30.8	36.1

From these results it can be observed that for any type of excitation of the structure, the effects of damping on the structural response depend on the level of damping and the time and duration of measurement. The initial response for reasonably chosen values of damping in the lower modes is only marginally affected by changes of damping in the higher modes. The values of the result indicate that the amplitude calculated does not vary by more than 1% from that of the largest amplitude. Table 6.11 below shows that the amplitudes of response calculated by the two algorithms vary only marginally in the cases examined and not by more than 6.64%. The comparison of the computing time of the two algorithms is more complicated than when comparing the calculated amplitude of response. There are basically two ways of comparing the computing time.

Table 6.11: The maximum amplitude (mm) of the joint subjected by the Fletcher-Reeves and Newton-Raphson algorithms.

Model	7*5
Joint	32
Fletcher-Reeves (FR)	33.7
Newton –Raphson (NR)	36.1
(NR-FR)/NR %	6.64

In the case of this particular structure, it is appropriate to compare the computing time for the calculation of the response during a given period. Moreover, in general, when considering a structure with n degrees of freedom, it is more helpful to compare the time consumed to complete each iteration. The complexity of comparing the computing time for each algorithm becomes more evident when it is considered that the number of iterations required per time step to achieve the same degree of convergency differs for each algorithm. The number of iterations also varies from structure to structure and with different types of loading and for different convergency criteria. The size of time increment will also vary for different structures.

In general, three factors affect the computing time:

a) The length of the response time;

b) The size of the time increment;

c) The number of iterations per time step.

In order to make a comparison between the computing time of Fletcher-Reeves and Newton-Raphson methods, the 7x5 flat net for a period of five seconds and 350 iterations is selected. The computing time is recorded for each method. The logarithmic decrement in all modes of the 7x5 net was taken as 10%. Table 6.12 gives the computing times for the 7*5 net during a five-second response and after 350 iterations as well as the time consumed for the eigenvalue solutions and calculations of the damping matrices.

Table 6.12: The computational time (seconds) for the mathematical models.

Mathematical Model		7*5
Degree of freedom		105
Second Response	Fletcher-Reeves	967.3
	Newton- Raphson	2345.50
350 Iteration	Fletcher-Reeves	84.31
	Newton- Raphson	1057.21
Eigen solution and damping		104.71

In the present work, the same criterion of convergency is given. The results show that the Fletcher-Reeves are more suitable. The resulting relationship between degrees of freedom and computing time for 350 iterations for the Fletcher-Reeves and the Newton-Raphson algorithms are shown in Figure 6.43. This figure shows that the computing time against the degree of freedom for the Newton-Raphson method increases sharply, but in Fletcher-Reeves method computing time increases slightly. It does seem that the result derived from the Fletcher-Reeves method is sufficient and reasonable for high nonlinearity structures. Hence, the Newton-Raphson method, which is commonly used for systems with high degree of freedom, cannot achieve an accurate result. Moreover, it should be noted that the computer storage required by the Newton-Raphson method is considerably more than that required by the Fletcher-Reeves method, because in the Newton-Raphson algorithm the dynamic stiffness matrix K^*, as mentioned in chapter 4, has to be stored in addition to the damping matrix which is required by both algorithms.

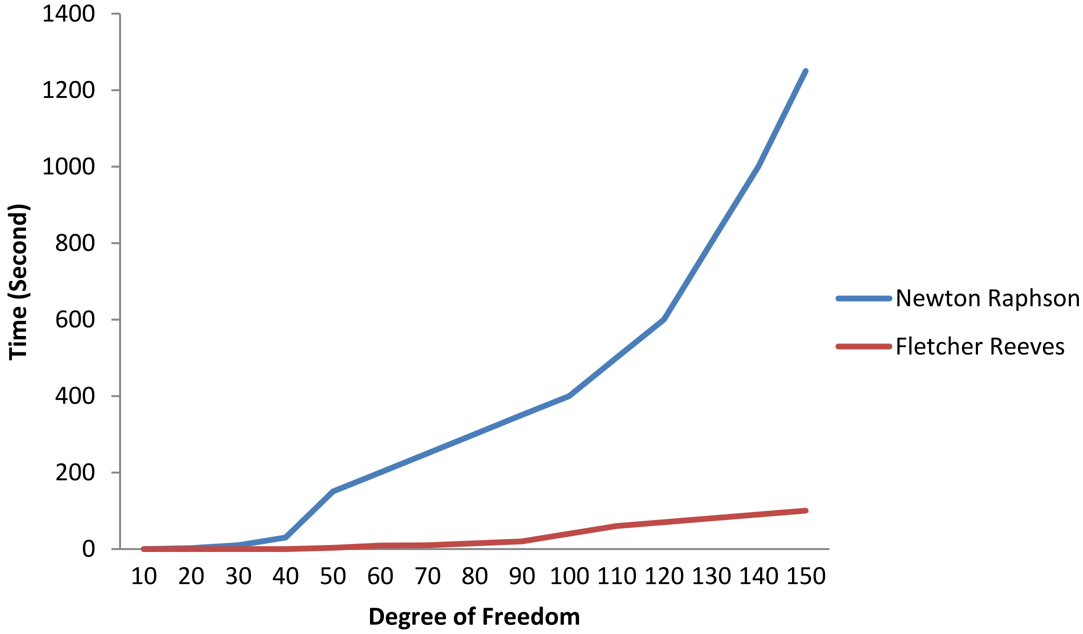

Figure 6.43: Visual relationship between degrees of freedom and computing time.

From the comparisons given in previous Figures and Tables it can be concluded that the Fletcher-Reeves algorithm is the more efficient of the two algorithms in terms of computing time and storage because both algorithms give almost identical responses.

6.6.3 The size of the time step, stability and accuracy

The size of the time step used for the dynamic response analysis of the flat net is in all cases equal to half the smallest periodic time of the net concerned. This size of time step proved to be adequate since the dynamic analyses were simple. For more complicated dynamic analyses, the time step may have to be smaller to take into account all the frequency components of the dynamic loading. Experiments conducted with various sizes of time increments showed that, for the type of dynamic analyses employed, either of the time increments was small enough to ensure stability and accuracy was not increased by reducing the time step further. Indeed, a reduction in the time step only increased computing time. On the other hand, increasing the period of the time steps leads to more iteration per time step because the starting point at the beginning of each time step is further removed from the position where the total potential dynamic work is a minimum. Hence, increase and reduction in the time step are not valid reasons for the stability and accuracy of the structure results.

6.6.4 The comparison of the natural frequencies on case study for cables

The Comparison of the natural frequency between the proposed method and the finite element is based upon the minimization process carried out by the Fletcher-Reeves and the Newton-Raphson algorithms. A comparative study can help to verify proposed method for the analysis structure. In order to the structural analysis, the numerical modelling is carried out on the pretention cables. The cable is modelled as three-dimensional tensioned beam elements. It includes the nonlinearities due to low strain large deformation and pre-tension. A hybrid beam element is used to model the cable. It is hybrid because it employs a mixed formulation involving six displacements and axial tension as nodal degrees of freedom. The logarithmic damping was assumed to be the same in all modes and equal to 10%. The grid line of the beam model with node numbers is shown in Figure 1. Nodes are assigned at a certain density throughout the material depending on the anticipated stress levels of a particular area. The specification of beam is given in Table 6.13. In the present study, the modelling space is 3D and wire is used for the shape of model. This type of model is deformable and planar. Mass density according laboratory testing is 7860 kg/m^3 and Young's Modulus is 2.1e11 N/m^2. The selected property type is isotropic elastic. The analysis has different steps. The model is considered as symmetric and linear. Total number of nodes and line elements are 62 and 55, respectively.

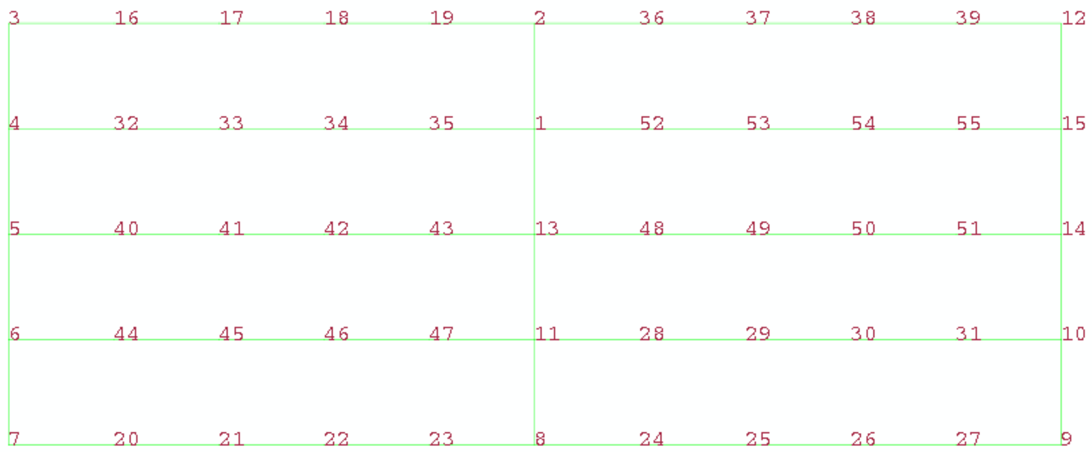

Figure 6.44: Visual of elements mesh.

Table 6.13: The specifications beam steel.

Description	Details
Overall dimensions	10000x5000 mm
Young's Modulus	2.1 e11 N/ mm^2
Diameter	10 mm^2
Breaking Load (kN)	280
Proof Load (kN)	240

6.6.5 Linear perturbation on finite element analysis

The finite element analysis method is a numerical technique used to find approximate solutions of partial differential equations. This mesh is programmed to contain the material and structural properties which define how the structure will react to certain loading conditions. In this case, procedure of finite element is given Table 6.14. In the present study, the modelling space is 3D and wire is used for the shape of model. This type of model is deformable and planar. Mass density is 7860 kg/m^3 and Young's modulus is 1.926e11 N/m^2. The selected property type is isotropic elastic. The analysis has different steps. The model is considered as symmetric and linear. A general static test is selected to analyse the model.

Table 6.14: Details of procedure of finite element analysis.

Modelling space	3D
Shape	Solid, Deformable
Type	Deformable
Mass Density	7860 kg/m^3
Poisson's Ratio	0.3
Type of Elasticity	Isotropic
Young's Modulus	1.926e11 N/m^2
Step 1	Initial Static, Linear
Step 2	Perturbation, Method: direct Matrix
Step 3	Symmetric, Static, Linear perturbation
Step 4	Direct Matrix: symmetric, Frequency

Some initial tests were carried out to mention that the natural frequency is independent of amplitude. Table 6.15 gives the finite element results and theoretical frequencies of the net for the four modes. The result presented shows that natural frequencies come out from theoretical and finite element are in good agreement. All mode shapes 1-3 of the structure are shown in Figures 6.45.6.46, and 6.46.

Table 6.15: Theoretical and experimental natural frequencies.

PRETENSION LOAD (N) = 0	NATURAL FREQUENCIES (Hz)		
	ω_T Proposed method Theoretical	ω_{FE} Finite Element	$\frac{\omega_{FE}-\omega_T}{\omega_{FE}}\%$
Mode 1	4.18	4.03	3.50
Mode 2	5.52	5.40	2.23
Mode 3	12.65	12.29	2.92

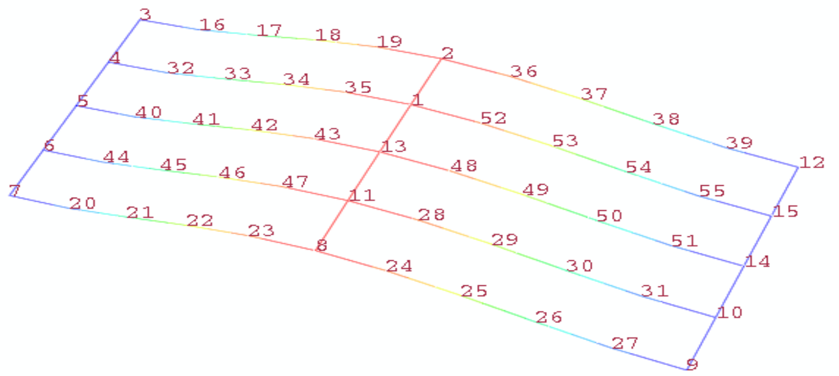

Finite Element Modelling

Mode shape: 1

Frequency: 2.597Hz

Damping ratio: 0.1%

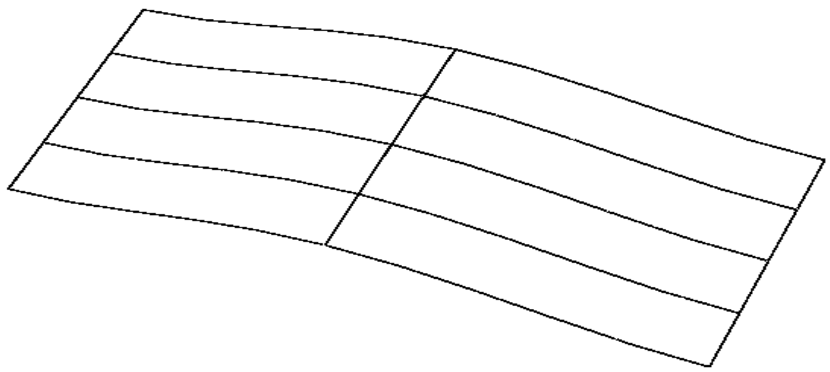

Theoretical Analysis

Mode shape: 2

Frequency: 6.46 Hz

Damping ratio: 0.1%

Figure 6.45: Mode shape 1 of the structure.

<table>
<tr><td>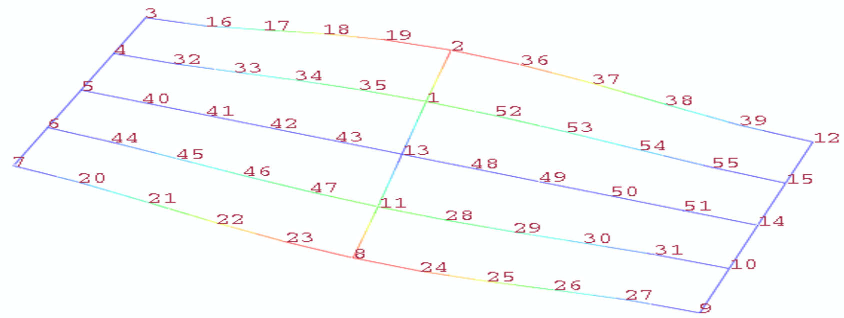</td><td>Finite Element Modelling

Mode shape: 2

Frequency: 3.819Hz

Damping ratio: 0.1%</td></tr>
<tr><td>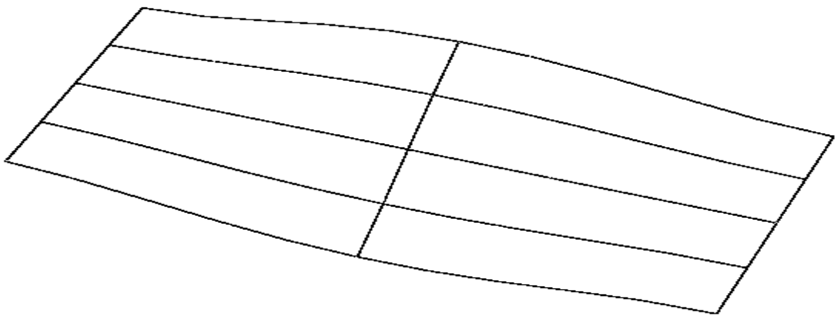</td><td>Theoretical Analysis

Mode shape: 2

Frequency: 6.46 Hz

Damping ratio: 0.1%</td></tr>
</table>

Figure 6.46: Mode shape 2 of the structure.

<table>
<tr><td>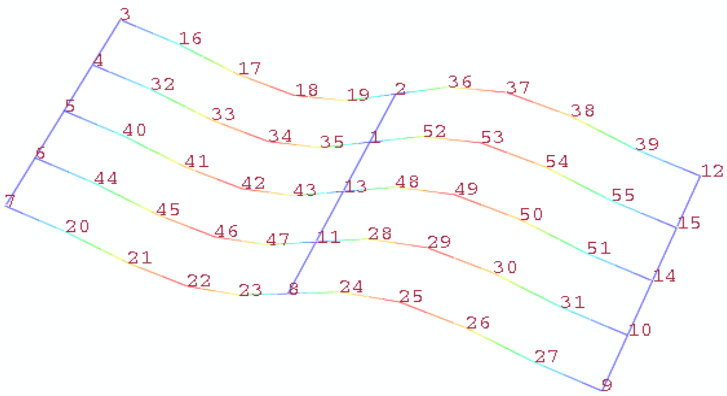</td><td>Finite Element Modelling

Mode shape: 3

Frequency: 4.915Hz

Damping ratio: 0.1%</td></tr>
<tr><td>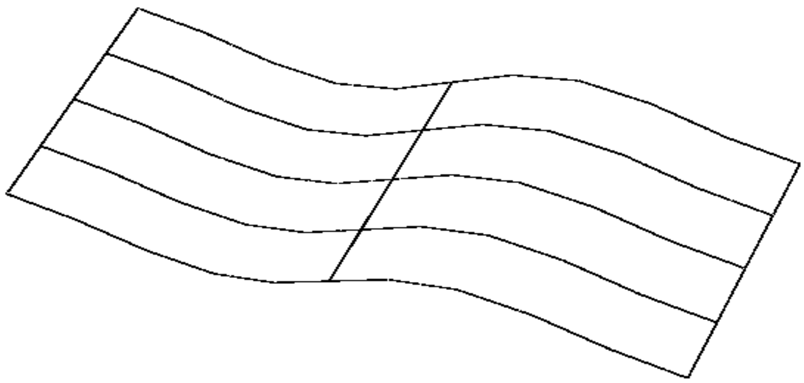</td><td>Theoretical Analysis

Mode shape: 2

Frequency: 6.46 Hz

Damping ratio: 0.1%</td></tr>
</table>

Figure 6.47: Mode shape 3 of the structure.

As shown by the above figures, all the theoretical and finite element mode shapes are close to each other and verify the proposed theory.

6.7 Conclusions

The differences between the calculated deflections and measured static deflections in this field are mainly due to the inherent differences between the experimental and mathematical models. In this study, the predicted natural frequencies for different modes are within 2% of the measured frequencies. The differences are thought primarily to be due to the differences between the theoretical and experimental static deflections. These differences are reflected in the degree of stiffness of the experimental and mathematical models at the starting point of the vibrations, and are also due to the fact that the theoretical frequencies were calculated for an undamped system by using an eigenvalue analysis, whereas the experimental model included damping and nonlinearity. As expected, the use of only one vibrator limited the number of modes which could be excited at resonance and hence limited the measurement of logarithmic decrements to the first few modes. Thus, in the calculation of the damping matrix only the first few logarithmic decrements are used. The comparison of the experimental and theoretically predicted values of the dynamic response showed that the response calculated by the proposed nonlinear method gives reasonably accurate results.

Finally, it be concluded that, the Fletcher-Reeves algorithm is the more efficient in terms of computing time and storage practically in high nonlinear structures.

CHAPTER 7: CONCLUSIONS

CONCLUSIONS AND RECOMMENDATIONS FOR FUTURE WORK

7.1 General summary and remarks

The main objective of this work is to develop a solution scheme for the nonlinear analysis of 3D space structures that are subjected to various types of dynamic loading and to verify the theory by numerical and experimental work. From the research conducted and the results obtained, it can generally be concluded that the proposed theory can successfully be used for the nonlinear dynamic response analysis of 3D structures with fixed boundaries. The results of the static test also demonstrate that the boundary by notice to assess the degree of elastic deformation of the frame is rigid. The comparison of the experimental and theoretically predicted values of the dynamic response showed that the proposed nonlinear method gives reasonably accurate results for dynamic response.

The comparison of the predicted nonlinear responses with those calculated by a linear method showed that for stiffening structures the linear analysis gives too large amplitude and results in mode shapes which differ from those obtained by the nonlinear analysis. This finding emphasizes the importance conducting the nonlinear analysis. The comparison of the two minimization techniques showed that the Fletcher-Reeves method is more efficient in terms of using less computing time and less storage. This is particularly the case for problems with a large number of degrees of freedom. The percentage differences between the theoretical and experimental results did not in any case exceed 10%, and this is considered to be acceptable.

Experimental mode shapes are often complex because real structures have damping within them. Shape normalization helps simplify the animated display of complex shapes. When a complex shape is normalized, the magnitudes of all of its components are retained but the phases are changed to either 0 or 180 degrees. In this research, all mode shapes are normalized for more accurate results.

With more sophisticated equipment, it would have been possible to measure the variation in the logarithmic decrements with amplitude as well as the damping in higher modes. However, since the damping in the first few modes could be measured, a damping matrix based on assumed values for the damping in the higher modes was used. The result showed that the assumptions made are reasonable for the first few seconds of response. However, for longer periods of vibration, the correlation between the experimental and theoretical results is not as good as those for shorter periods.

Finally, it should be noted that the damping matrix for the proposed theory is calculated separately and its calculation does not affect the formulation of the theory. In general, the damping matrix used gives reasonable results as long as the damping ratios in the dominant modes are assigned realistic values. The proposed method was found to be stable for time steps equal to or less than half the smallest time period of the system.

7.2 Conclusion

The main points arising from this research are summarized below:

1. The values of the calculated and measured static deflections were similar to each other. Result of this test showed that the degree of error

for any elastic deformation of the frame is almost zero. The result verifies that the frame is symmetric.

2. The result of static test with different patterns and intensities of static loading were showed that the deflection calculated by the proposed nonlinear method gives reasonably accurate results and differences with experimental result is less than 4.7 %. The results of static tests also indicate that the boundary of the frame is rigid and symmetric.

3. The predicted natural frequencies for different modes are within 2% of the measured frequencies. The differences are thought primarily to be due to the differences between the theoretical and experimental static deflections. This is a reflection of the difference in the stiffness of the experimental and mathematical models at the starting point of the vibrations. These differences may also be due to the fact that the theoretical frequencies were calculated for an undamped system using an eigenvalue analysis, whereas the experimental model included damping and nonlinearity.

4. For highly nonlinear structures such as cable structures in space structures, the effect of assuming that stiffness remains constant during each time step can lead to a considerable degree of inaccuracy even when the time steps are small. The proposed method, which is based upon the minimization of the total dynamic work in order to achieve

dynamic equilibrium at the end of each time step, considers the effect of variations in stiffness in each time step.

5. By calculating the values of δ at various time steps along the decay curve it was found that the logarithmic decrements varied with amplitude and that they decreased with increasing amplitude. During the calculation, it appeared that the logarithmic decrement approached a constant value as the amplitude increased.

6. The comparison of the experimental and theoretically predicted values of the dynamic response showed that the proposed nonlinear method gives reasonably accurate results for dynamic response, especially when one takes into account the differences between the theoretical and experimental static deflections and frequencies, and also that the logarithmic decrements in the higher modes were given assumed values.

7. The differences the between linear and nonlinear calculated responses are significant and these differences increase with the increase in nonlinearity. In the case of the nonlinearly calculated response, the maximum amplitudes occur during the transient period of vibration and not in the steady state condition. In contrast, in the linearly calculated response, the amplitudes reach their maximum value when the net vibrates in the steady state condition.

8. The amplitude of response calculated by the linear method is greater than that calculated by the nonlinear method. It should also be noted that when the upwards and downwards movements of a joint are calculated, the values resulting from the linear analysis are all equal, whereas the use of the nonlinear method of analysis showed that the values of the upwards movements are greater than the downwards movements. This is to be expected since the rate of change of stiffness is greatest when moving downward from the static equilibrium position.

9. The variations in the dynamic response due to changes in the damping ratios as a result of different combinations of damping ratios showed that, regardless of the type of method used to excite the structure, the responses of the structure are very similar and independent of the amount of damping across all modes. The results indicated that for any given combination of damping values, the amplitude calculated does not exceed the largest amplitude by more than 3%.

10. The comparison of the computing showed that, in the case of the Newton-Raphson algorithm, the computing time against the degree of freedom increases sharply, but in the case of the Fletcher-Reeves algorithm, computing time increases slightly, thus it would appear that result of the Fletcher-Reeves method is sufficient and reasonable.

11. The computer storage required by the Newton-Raphson method is considerably greater than that required by the Fletcher-Reeves method because, as mentioned chapter 4, in the Newton-Raphson algorithm the

dynamic stiffness matrix, K^*, has to be stored in addition to the damping matrix which is required by both algorithms.

12. The sizes of the time step used for the dynamic response analysis are in all cases equal to half the smallest periodic time of the net concerned. The experiment was conducted with various sizes of time increments. The result showed that for the type of dynamic analysis, when the time increment is small enough to ensure stability, the increase in accuracy is independent of the reduction the time step and it only leads to an increase in the computing time.

Finally, all statements above conclude that proposed method is more sufficient to use in account of high nonlinear structure such as space structure.

7.3 Recommendations for future work

7.3.1 Convergency and scaling

There was no specific problem with regard to convergence of the analysis. The number of iterations per time step was acceptable. It is possible that for structures with large degrees of freedom the rate of convergence might decrease and the number of iterations might increase to an unacceptable level. This may be overcome by the introduction of scaling and, if necessary, extrapolation.The scaling technique was applied to the static deformation theory. This technique introduces scaling mainly to increase the rate of convergency of convergency of ill-conditioned problems. The same technique could be used in the proposed nonlinear dynamic response theory to extend the theory's application in respect of flexible boundaries.

In general, the position of the minimum of the step-by-step time integration method appears to not be far from the starting point. Thus convergency with the required accuracy can be achieved after only a few iterations. In cases when either the load increment is too large or the time step is too long, the starting point for the next time step might be improved by extrapolating the displacements and internal forces in order to reduce the number of iterations.

Since the proposed theory basically seeks the equilibrium of dynamic forces at time (t+Δt) by minimization of the total potential dynamic work, any appropriate minimization technique could be employed to perform this task. The Fletcher-Reeves method of minimization that was chosen in this research was determined to be the most suitable among the available methods. The development of new techniques for the minimization of the function of several variables may improve the proposed theory in terms of reducing computing time and storage requirements. Apart from the calculation of the damping matrix, the theory does not require the solution of eignvalues if other ways can be found to select the time step.

7.3.2 Extension of the dynamic theory to include flexible members

Fleury (2006) and Buchholdt (1982) extended the theory for the analysis of cable structures based upon the minimization of the total potential energy to include cable roofs with flexible boundaries. These researchers have identified the contributions of the flexible elements to the energy and gradient vector in terms of the individual member stiffness matrices. In doing so, it was found that the problems become numerically ill-conditioned when using the Fletcher-

Reeves method. In this research study, this was overcome by the introduction of a diagonal scaling matrix.

The theory for the nonlinear dynamic response analysis of 3D space structures with flexible boundary members has yet to be programmed and tested for stability and convergency. However, if the performance of the aforesaid static theory can be taken as a guide for speculation about the performance of its dynamic counterpart, it is likely that a scaling technique will be needed to reduce the number of iterations per time step even if the starting point for each time step in a dynamic analysis is usually closer to the minimum position than in a static analysis.

The energy formulation of the flexible members requires investigation, particularly in relation to the way in which the mass of those members are taken into account. The use of lumped mass matrices requires the use of condensed member stiffness matrices. This could lead to considerable errors in the calculation of the strain energy of flexible members; in which case, consistent mass matrices which can take into account the mass distribution of the members need to be used.

7.3.3 Damping

The use of the two orthogonal damping matrices discussed in previous chapters has some limitations. Firstly, they are costly to construct of them because the functions of the natural frequencies and combination damping require calculation of the eigenvectors.

Secondly, both matrices require knowledge of damping ratios in different modes. However, for most structures, only the damping ratios in the first few modes are known with any level of accuracy, thus the damping ratios in the higher modes need to be assumed. For Rayleigh damping, knowledge of the damping model for at least two modes is required, thus this form of damping cannot assign damping ratio values to the higher modes with any accuracy. Moreover, the use of the above type of damping matrices adds considerably to storage as well as to the computational effort of the nonlinear dynamic analysis. The above formulations of the damping become even more questionable when the dynamic forces due to wind and ground movements are considered. The damping can be estimated approximately; however, the formulation of damping matrices as functions of damping ratios cannot take into account aerodynamic damping due to lift and drag forces. Such forces are functions of the wind velocity on structure. Buchhold (1982) has suggested the use of equivalent damping forces which are proportional to the forces in the members but in phase with the rate of change of strains with respect to time. This method, if it can be experimentally verified, would result in a considerable reduction in the computational load.

7.3.4 Inclusion of various types of dynamic loading

The formulation of the theory in its present form can be used to calculate the response of cable structures subjected to dynamic forces which are independent of the movement of the structure and can be described by a function of time, f (t), or as a series of load increments related to each time interval. Examples of such dynamic loads are simple harmonic loading, blast loading and suddenly applied or released loads.

In the case of dynamic response due to the movements of the supports as a result of an earthquake, the strain energy and the energy dissipation due to damping are functions of the relative displacements and velocities of the ground, whilst the inertia forces are functions of the absolute acceleration at any point. The theory in its present form cannot be used to predict the response of the structures caused by wind since the aerodynamic forces due to drag and vortex shedding are functions of the relative velocity of wind to that of the structure.

REFERENCES

Ademoyero, O. O., Bartholomew-Biggs, M. C., Davies, A. J., & Parkhurst, S. C. (2004). Conjugate gradient algorithms andthe Galerkin boundary element method. *Computers & Mathematics with Applications, 48*(3-4), 399-410.

Argyris, J. H., Balmer, H., Doltsinis, J. S., Dunne, P. C., Haase, M., Kleiber, M.(1979). Finite element method the natural approach. *Computer Methods in Applied Mechanics and Engineering, 17-18*(Part 1), 1-106.

Aschheim, M., Tjhin, T., Comartin, C., Hamburger, R., & Inel, M. (2007). The scaled nonlinear dynamic procedure. *Engineering Structures, 29*(7), 1422-1441.

Avitabile, P., & O'Callaghan, J. (2009). Efficient techniques for forced response involving linear modal components interconnected by discrete nonlinear connection elements. *Mechanical Systems and Signal Processing, 23*(1), 45-67.

Babaie-Kafaki, S., Ghanbari, R., & Mahdavi-Amiri, N. (2001). Two new conjugate gradient methods based on modified secant equations. *Journal of Computational and Applied Mathematics, 234*(5), 1374-1386.

Bernard, P., & Fleury, G. (2002). Stochastic Newmark scheme. *Probabilistic Engineering Mechanics, 17*(1), 45-61.

Bradford, M. A., & Yazdi, N. A. (1999). A Newmark-based method for the stability of columns. *Computers & Structures, 71*(6), 689-700.

Buchholdt, H. A., & Moossavinejad, S. (1982). Nonlinear dynamic response analysis using conjugate gradients. *Engineering Structures, 4*(1), 44-52.

Carayannis, G., Manolakis, D., & Kalouptsidis, N. (1986). A unified view of parametric processing algorithms for prewindowed signals. *Signal Processing, 10*(4), 335-368.

Celebi, M. E., Celiker, F., & Kingravi, H. A. (2009). On Euclidean norm approximations. *Pattern Recognition, 44*(2), 278-283.

Daston, L. J. (1979). D'Alembert's critique of probability theory. *Historia Mathematica, 6*(3), 259-279.

Doltsinis, I., & Kang, Z. (2004). Robust design of structures using optimization methods. *Computer Methods in Applied Mechanics and Engineering, 193*(23-26), 2221-2237.

El-Beltagy, M. A., & Keane, A. J. (1999). A comparison of various optimization algorithms on a multilevel problem. *Engineering Applications of Artificial Intelligence, 12*(5), 639-654.

Farshi, B., & Alinia-Ziazi, A. (2010). Sizing optimization of truss structures by method of centers and force formulation. *International Journal of Solids and Structures, 47*(18-19), 2508-2524.

Fletcher, R. (1972). Methods for the solution of optimization problems. *Computer Physics Communications, 3*(3), 159-172.

Fleury, G. (2006). Convergence of schemes for stochastic differential equations. *Probabilistic Engineering Mechanics, 21*(1), 35 -43.

Gloec er, D. H., Macfarlane, M. H., & Pieper, S. C. (1976). The use of first and second derivatives in optical model parameter searches. *Computer Physics Communications, 11*(3), 299-312.

Gopalakrishna, H. S., & Greimann, L. F. (1988). Newton-raphson procedure for the sensitivity analysis of nonlinear structural behaviour. *Computers & Structures, 30*(6), 1263-1273.

Guo, Y. Q., & Chen, W. Q. (2007). Dynamic analysis of space structures with multiple tuned mass dampers. *Engineering Structures, 29*(12), 3390-3403.

Ha, T. X. D. (2005). Lagrange multipliers for set-valued optimization problems associated with coderivatives. *Journal of Mathematical Analysis and Applications, 311*(2), 647-663.

Harrison, H. R., & Nettleton, T. (1997). Hamilton's Principle. In *Advanced Engineering Dynamics* (pp. 46-54). London: Butterworth-Heinemann.

Hughes, T. J. R., Hilber, H. M., & Taylor, R. L. (1976). A reduction scheme for problems of structural dynamics. *International Journal of Solids and Structures, 12*(11), 749-767.

Huang, C., & Chang, Q. (2002). Stability analysis of numerical methods for systems of functional-differential and functional equations. *Computers & Mathematics with Applications*, *44*(5-6), 717-729.

Kaveh, A., & Koohestani, K. (2008). Graph products for configuration processing of space structures. *Computers & Structures*, *86*(11-12), 1219-1231.

Kirsch, U., & Bogomolni, M. (2007). Nonlinear and dynamic structural analysis using combined approximations. *Computers & Structures, 85*(10), 566-578.

Kilic, B., & Madenci, E.(2009) An adaptive dynamic relaxation method for quasi-static simulations using the peridynamic theory. *Theoretical and Applied Fracture Mechanics*, *53*(3), 194-204.

Kukreti, A. R. (1989). Dynamic response analysis of nonlinear structural systems subject to component changes. *Computers & Structures*, *32*(1), 201-212.

Jong,I (2005). Teaching Students Work and Virtual Work Method in Statics:A Guiding Strategy with Illustrative Examples . Proceedings of the 2005 American Society for Engineering Education Annual Conference & Exposition. American Society for Engineering Education. Retrieved 2007-09-24.

LaMar, M. D., Xin, J., & Qi, Y. (2006). Signal processing of acoustic signals in the time domain with an active nonlinear nonlocal cochlear model. *Signal Processing, 86*(2), 360-374.

Li, C., & Yuan, Y. (2008). Explicit/implicit domain decomposition method with modified upwind differences for convection-diffusion equations. *Computers & Mathematics with Applications, 55*(11), 2565-2573.

López-Mellado, E. (2002). Analysis of discrete event systems by simulation of timed Petri net models. *Mathematics and Computers in Simulation, 61*(1), 53-59.

Nazmy, A. S., & Abdel-Ghaffar, A. M. (1990). Three-dimensional nonlinear static analysis of cable-stayed bridges. *Computers & Structures*, *34*(2), 257-271.

Noels, L., Stainier, L., & Ponthot, J. P. (2004). Combined implicit/explicit time-integration algorithms for the numerical simulation of sheet metal forming. *Journal of Computational and Applied Mathematics, 168*(1-2), 331-339.

Park, K., C.(1975).An Improved stiffening stable method for direct integration of nonlinear structural dynamic equations. *Journal of Applied Mechanics*, *42*, 464-470.

Qi, L., Sun, D., & Zhou, G. (2002). A primal-dual algorithm for minimizing a sum of Euclidean norms. *Journal of Computational and Applied Mathematics, 138*(1), 127-150.

Raman, N. V., Surya Kumar, G. V., & Sreedhara Rao, V. V. (1988). Large displacement analysis of guyed towers. *Computers & Structures*, *28*(1), 93-104.

Rio, G., Soive, A., & Grolleau, V. (2005). Comparative study of numerical explicit time integration algorithms. *Advances in Engineering Software, 36*(4), 252-265.

Roy, D., & Dash, M. K. (2002). A stochastic Newmark method for engineering dynamical systems. *Journal of Sound and Vibration, 249*(1), 83-100.

Sorenson, H. W. (1969). Comparison of some conjugate direction procedures for function minimization. *Journal of the Franklin Institute*, *288*(6), 421-441.

Stefanou, G. D., & Nejad, S. E. M. (1995). A general method for the analysis of cable assemblies with fixed and flexible elastic boundaries. *Computers & Structures, 55*(5), 897-905.

Stefanou, G. D., Moossavi, E., Bishop, S., & Koliopoulos, P. (1992). Dynamic analysis approach of nonlinear structures by minimizing the total potential dynamic work. *Computers & Structures, 44*(6), 1197-1203.

Such, M., Jimenez-Octavio, J. R., Carnicero, A., & Lopez-Garcia, O. (2009). An approach based on the catenary equation to deal with static analysis of three dimensional cable structures. *Engineering Structures*, *31*(9), 2162-2170.

Synge, J-I., Conway.A.W.(2000). The mathematical papers of Sir *William Rowan Hamilton. Royal irish academy. Cambridge university press. Vol(4)*

Telles, J. C. F., & Carrer, J. A. M. (1994). Static and transient dynamic nonlinear stress analysis by the boundary element method with implicit techniques. *Engineering Analysis with Boundary Elements, 14*(1), 65-74.

Thai, H.-T., & Kim, S.-E. (1977). Nonlinear static and dynamic analysis of cable structures. *Finite Elements in Analysis and Design, 47*(3), 237-246.

Torby, B. (1984). Energy Methods. *Advanced Dynamics for Engineers*. HRW Series in Mechanical Engineering. United States of America: CBS College Publishing. ISBN 0-03-063366-4.

Trench, W. F. (1961). A General Class of Discrete Time-Invariant Filters. *Journal of the Society for Industrial and Applied Mathematics, 9*, 405-421.

Trujillo, D. M. (1977). An unconditionally stable, explicit algorithm for finite-element heat conduction analysis. *Nuclear Engineering and Design, 41*(2), 175-180.

Twigg, C., & Hasler, P. (2009). Configurable analog signal processing. *Digital Signal Processing, 19*(6), 904-922.

Udwadia, F. E., & Kalaba, R. E. (2002). On the foundations of analytical dynamics. *International Journal of Nonlinear Mechanics, 37*(6), 1079-1090.

Vujanovic, B. (1978). Conservation laws of dynamical systems via d'alembert's principle. *International Journal of Nonlinear Mechanics, 13*(3), 185-197.

Wang, c.y., & Lian, S.j. (2006). Global convergence properties of the two new dependent Fletcher-Reeves conjugate gradient methods. *Applied Mathematics and Computation, 181*(2), 920-931.

Wang, P.-H., Lin, H.-T., & Tang, T.-Y. (2002). Study on nonlinear analysis of a highly redundant cable-stayed bridge. *Computers & Structures, 80*(2), 165-182.

Wilson, J. F., & Callis, E. G. (2004). The dynamics of loosely jointed structures. *International Journal of Nonlinear Mechanics, 39*(3), 503-514.

Yang, X., & Stepanenko, Y. (1994). A stability criterion for a class of discrete nonlinear systems with random parameters. *Systems & Control Letters, 22*(3), 187-194.

Yuan, G., Lu, X., & Wei, Z. (2009). A conjugate gradient method with descent direction for unconstrained optimization. *Journal of Computational and Applied Mathematics*, *233*(2), 519-530.

Zienkiewicz, O. C., Taylor, R. L., & Zhu, J. Z. (2005). 4 - Inelastic and non-linear materials. In *The Finite Element Method Set (Sixth Edition)* (pp. 62-126). Oxford: Butterworth-Heinemann.

APENDIX A

Nyquist plot of frequency response

```
nyquist
nyquist(sys)
nyquist(sys,w)
nyquist(sys1,sys2,...,sysN)
nyquist(sys1,sys2,...,sysN,w)
```

Description

Nyquist creates a Nyquist plot of the frequency response of a dynamic system. Nyquist plots are used to analyse system properties including gain margin, phase margin, and stability. Nyquist (explicitly specifies the frequency range or frequency points to be used for the plot. To focus on a particular frequency interval, set w = {Wmin,Wmax}.

$$\text{Nyquist}\ (\ \text{sys1},\ \text{sys2},\ldots,\ \text{sys}_n,\ w)$$

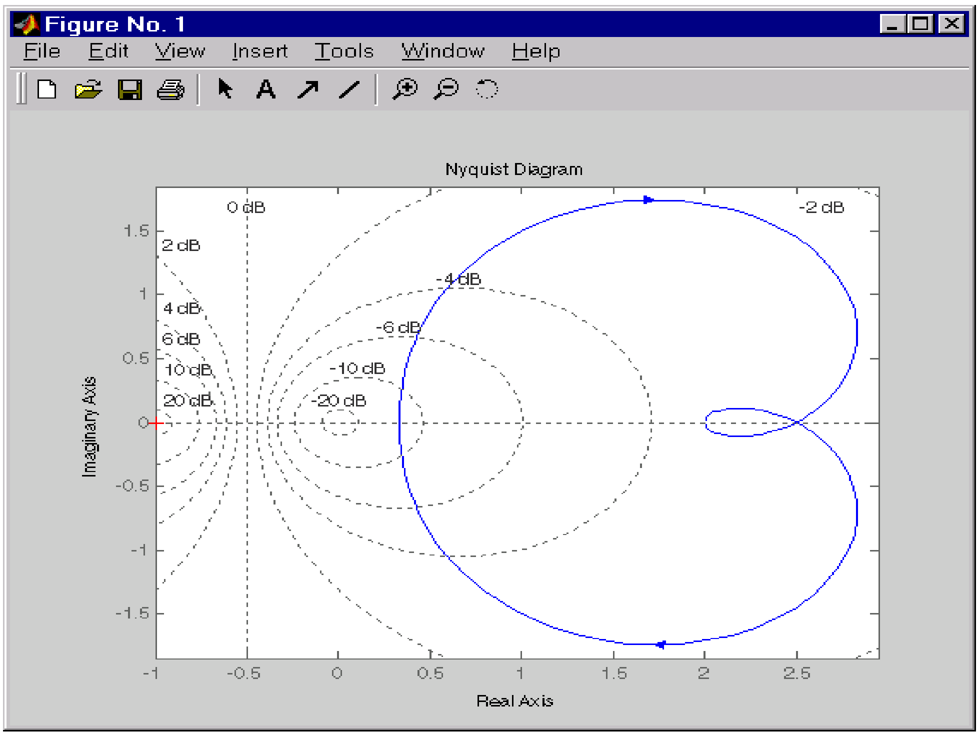

Figure 1: Interface of output plot from programme.

APPENDIX B

Visual Basic language

The present programme is a complete graphical development environment. This programme develops useful Microsoft Windows applications which have the ability to use OLE (Object Linking and Embedding) objects such as an Access data sheet. The current programme also has the ability to develop programs that can be used as linear analysis software. The user interface which collects user input and displays formatted output in a more appealing and useful form input data on each of interface sheets.

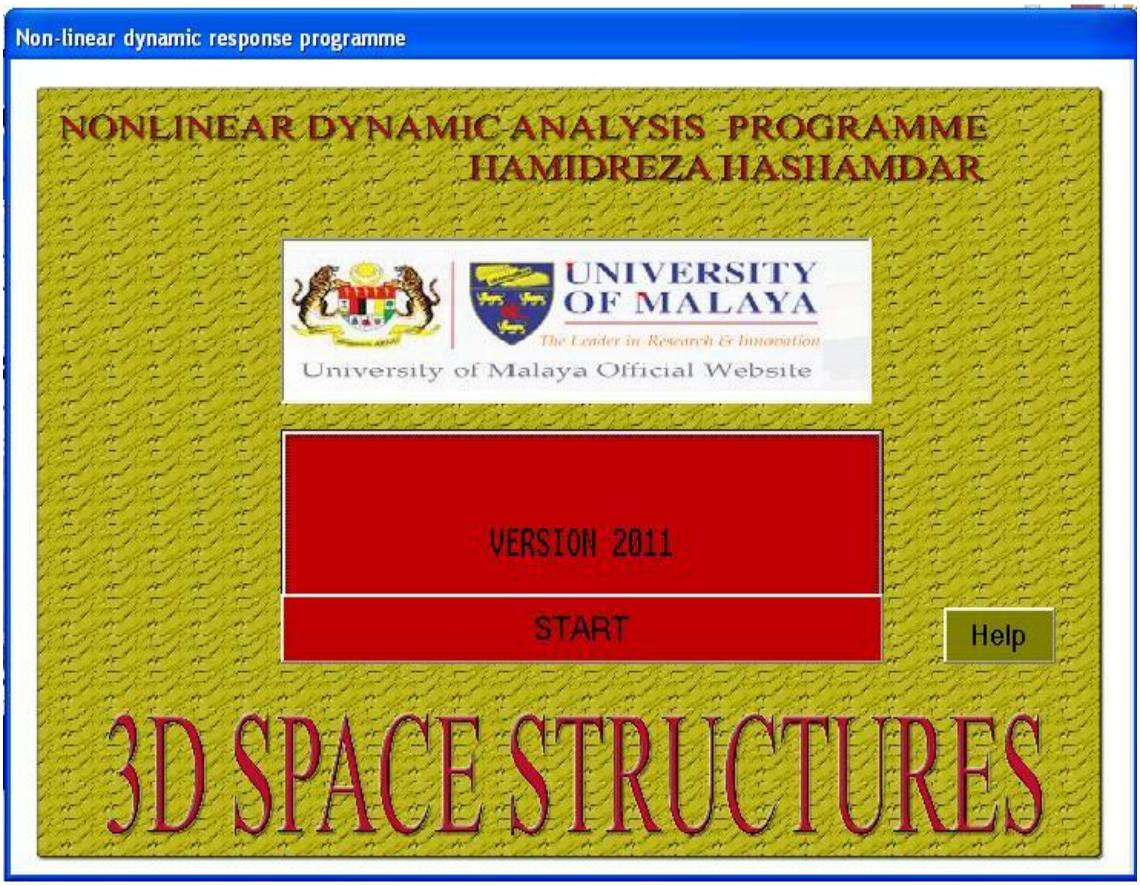

Figure.1: Main interface sheet of nonlinear response programme.

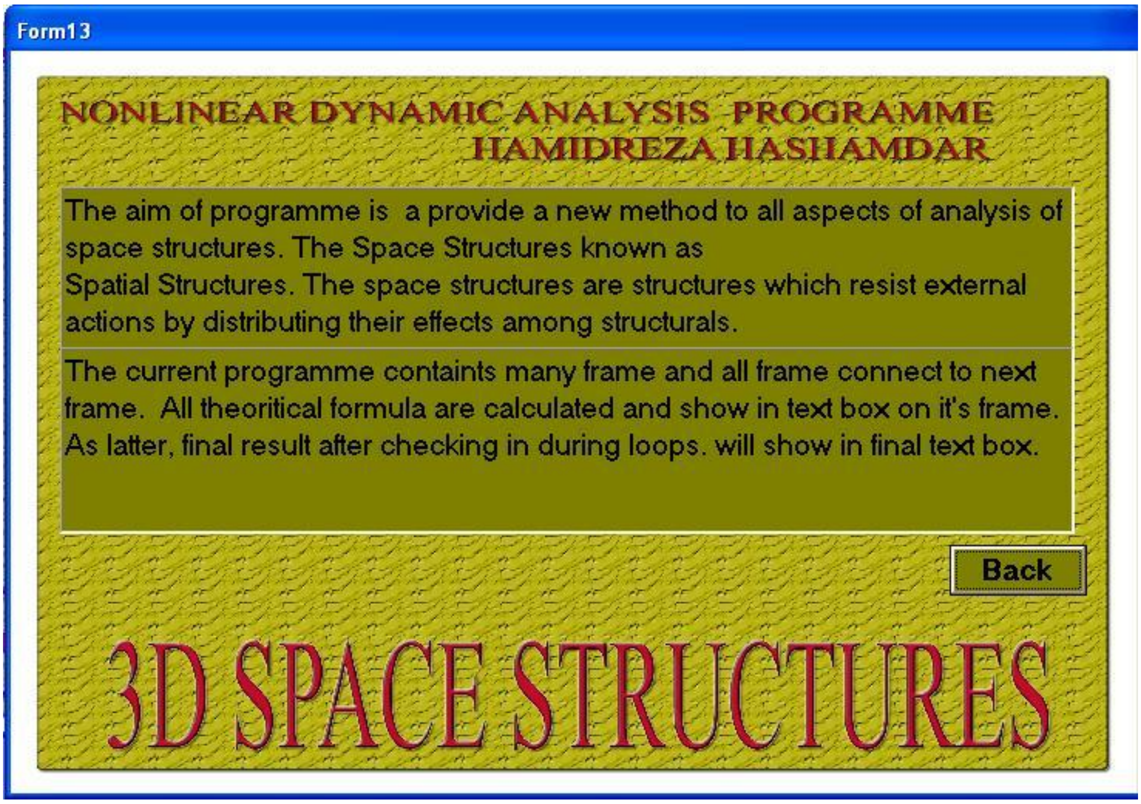

Figure.2: Help interface sheet of nonlinear response programme.

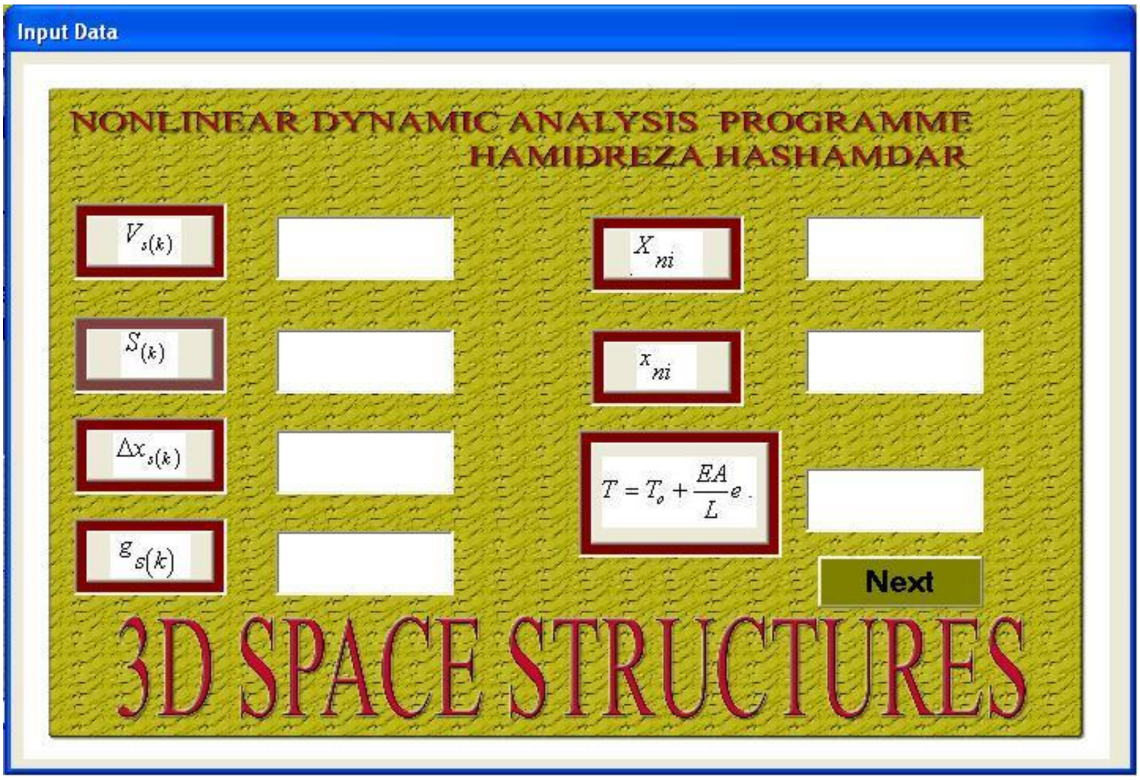

Figure.3: Data interface sheet of nonlinear response programme.

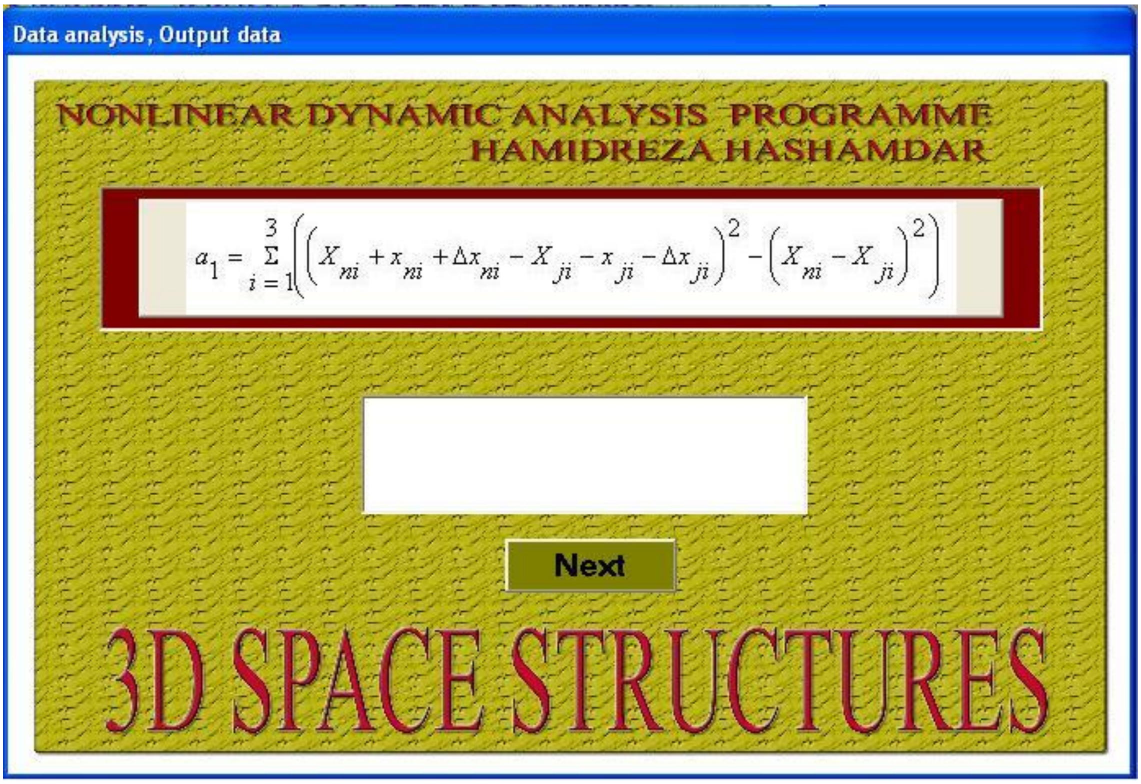

Figure.4: Data interface analysis sheet of nonlinear response programme.

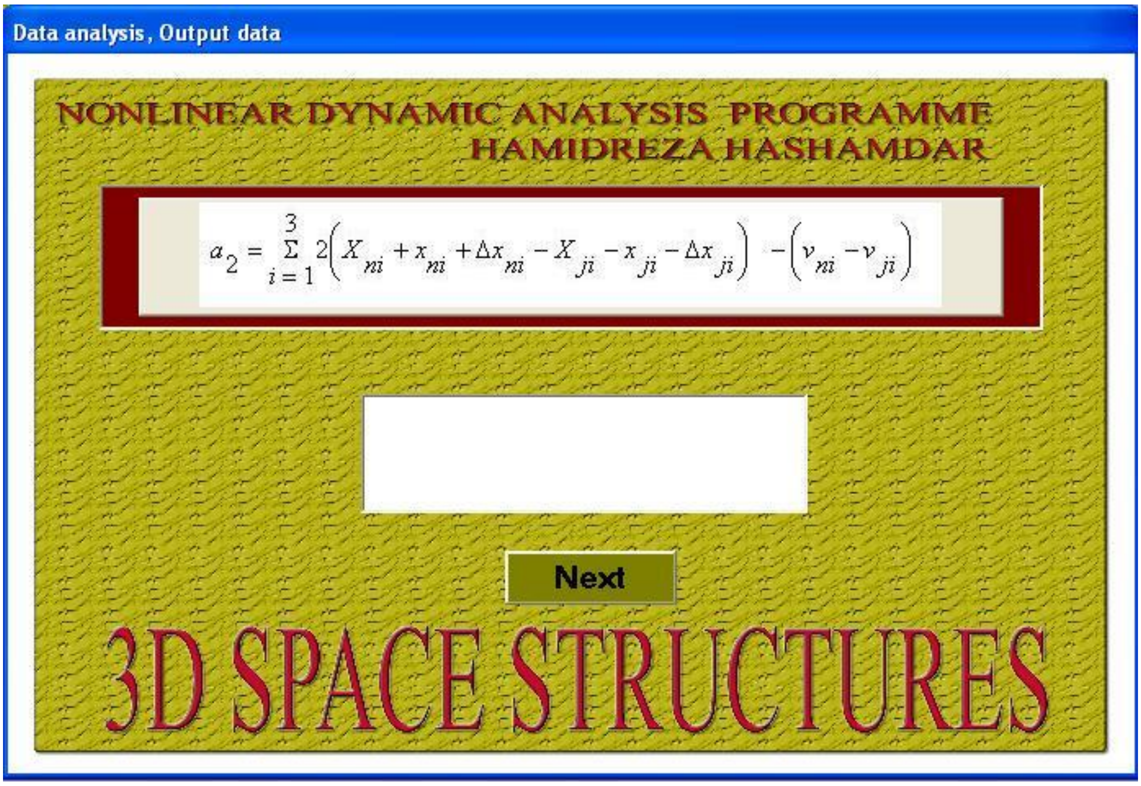

Figure.5: Data analysis interface sheet of nonlinear response programme.

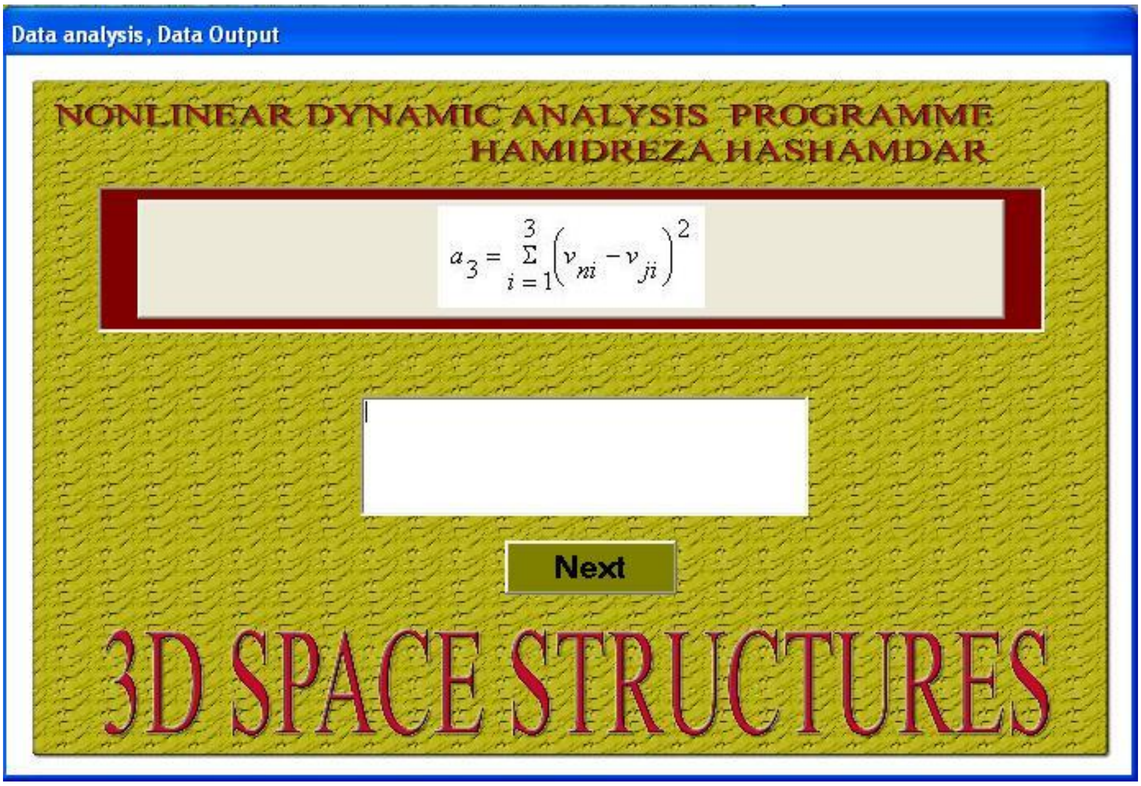

Figure.6: Data analysis interface sheet of nonlinear response programme.

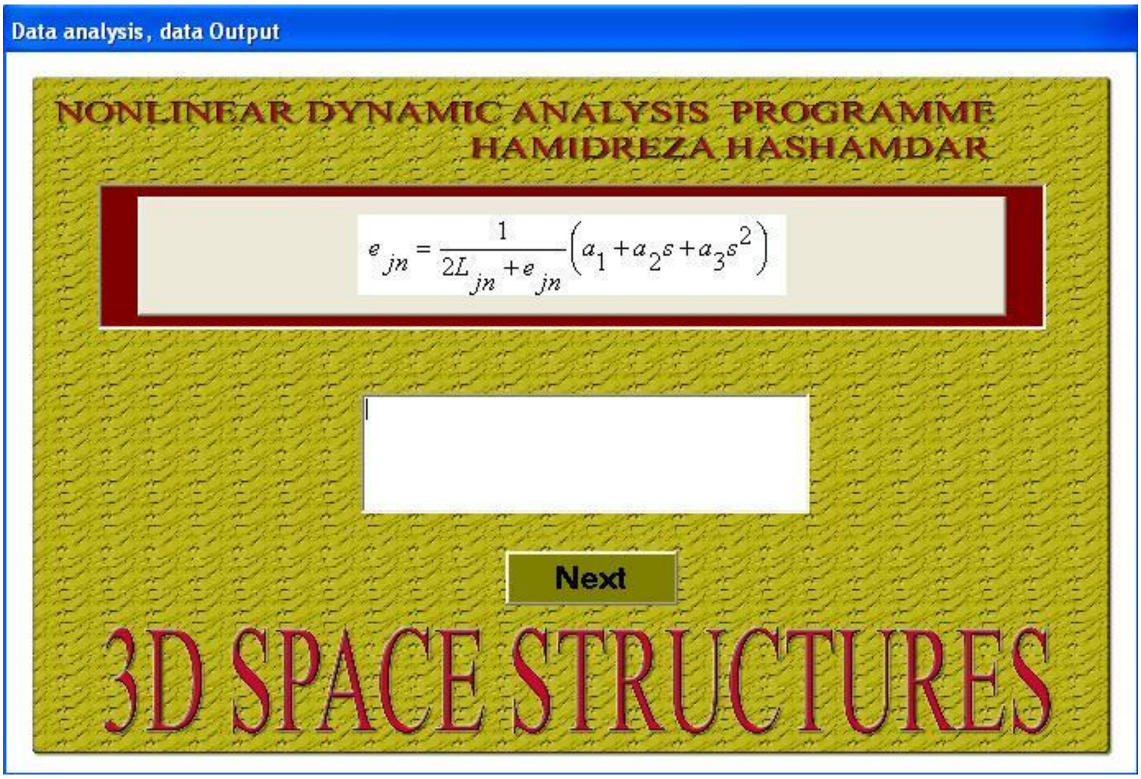

Figure.7: Data analysis interface sheet of nonlinear response programme.

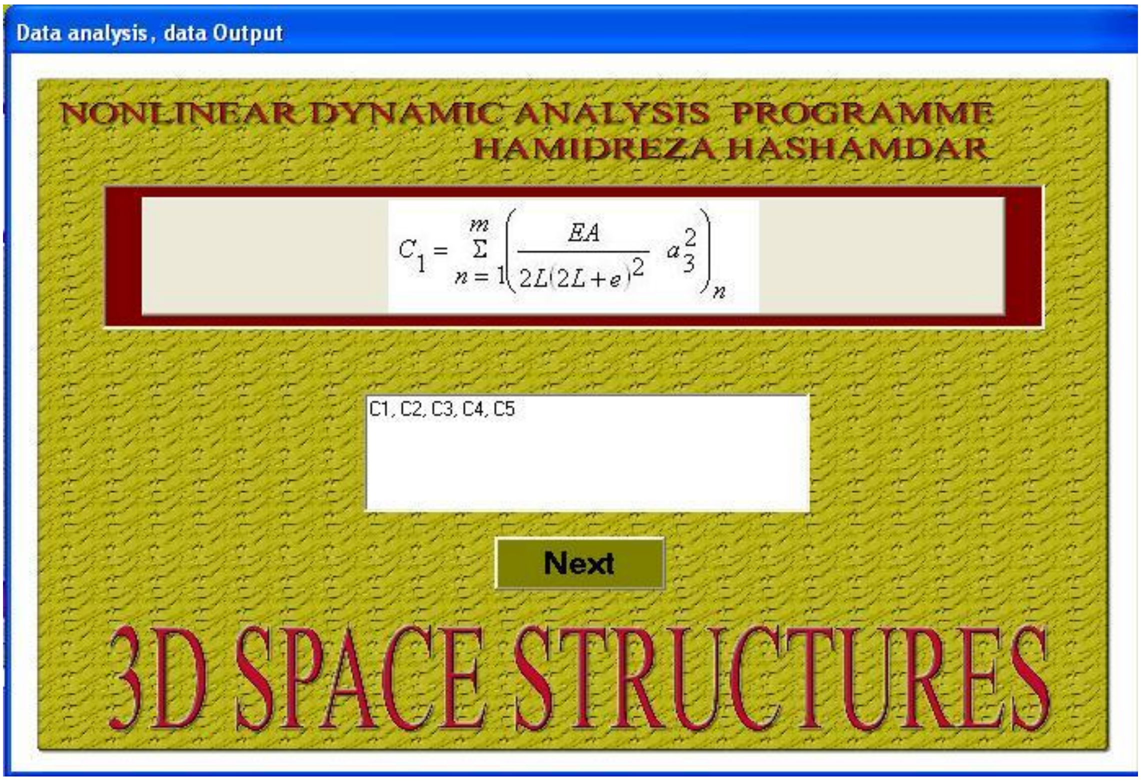

Figure.8: Data analysis interface sheet of nonlinear response programme.

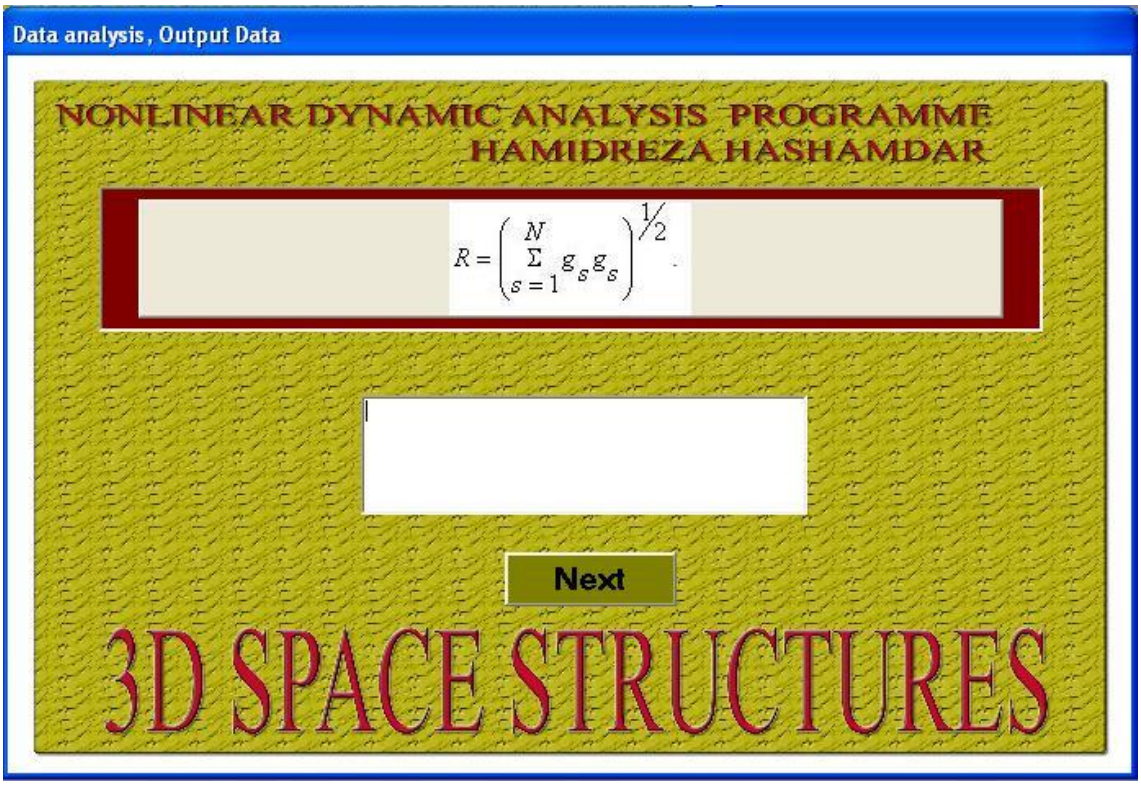

Figure.9: Data analysis interface sheet of nonlinear response programme.

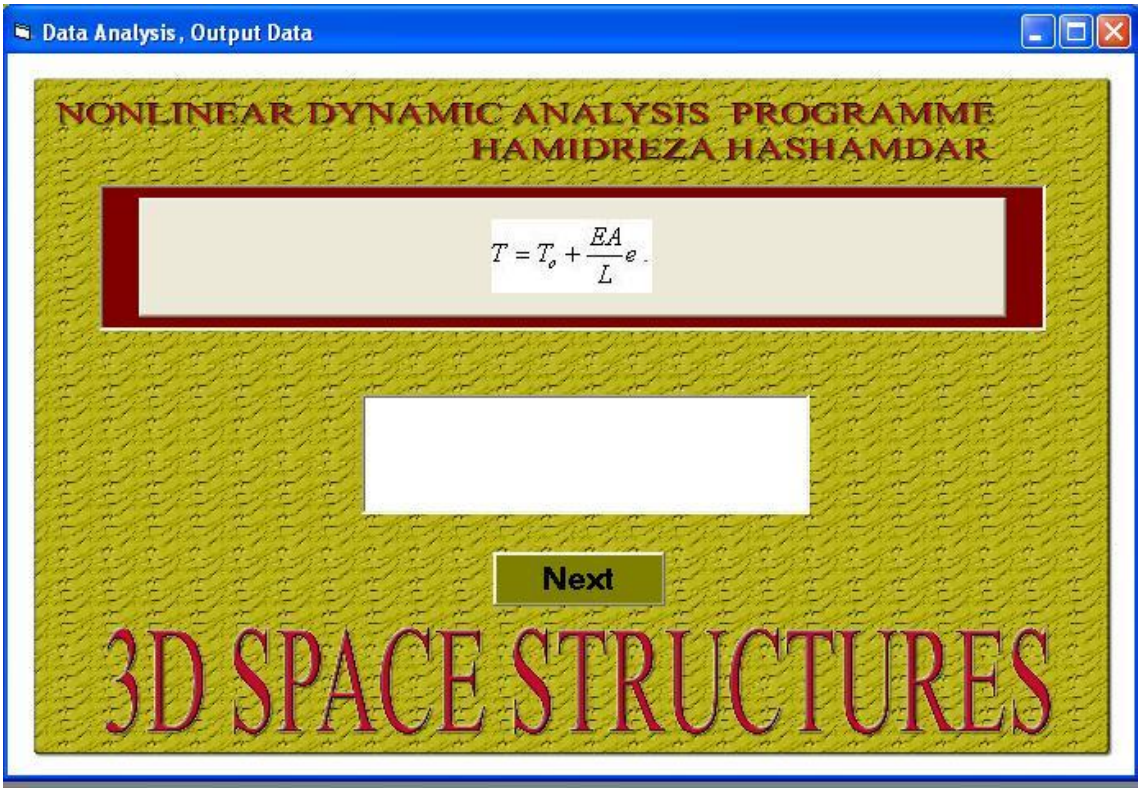

Figure.10: Data analysis interface sheet of nonlinear response programme.

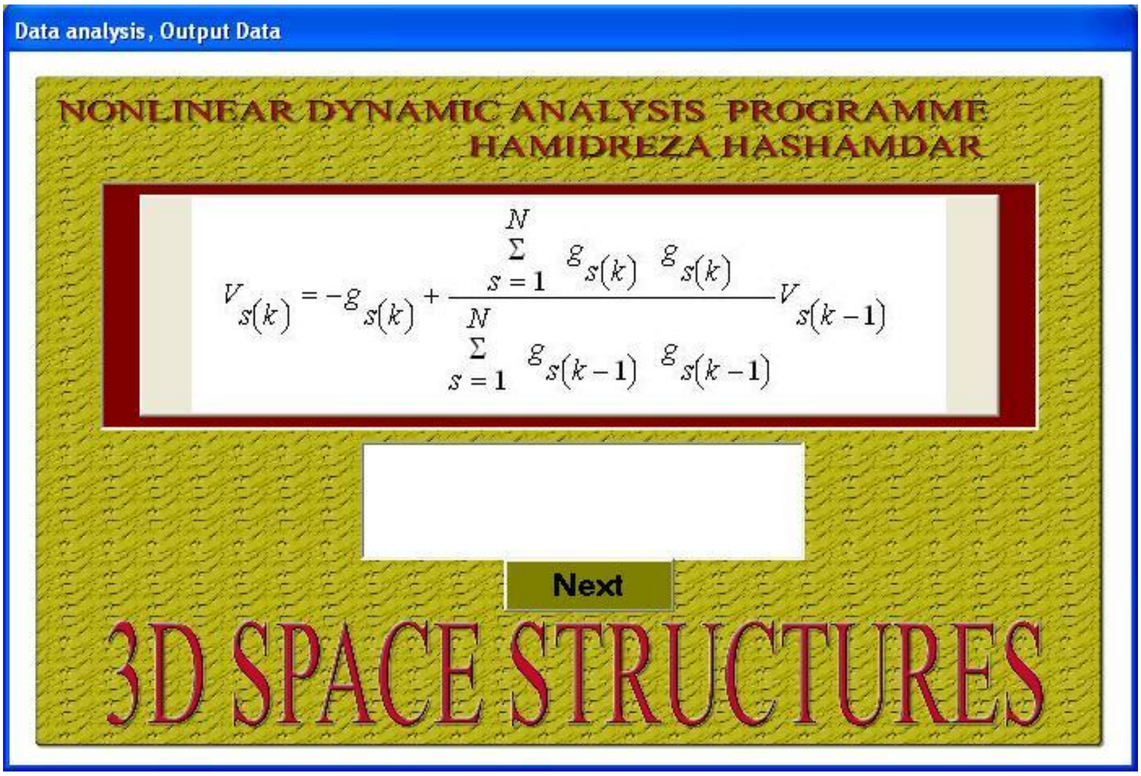

Figure.11: Data analysis interface sheet of nonlinear response programme.

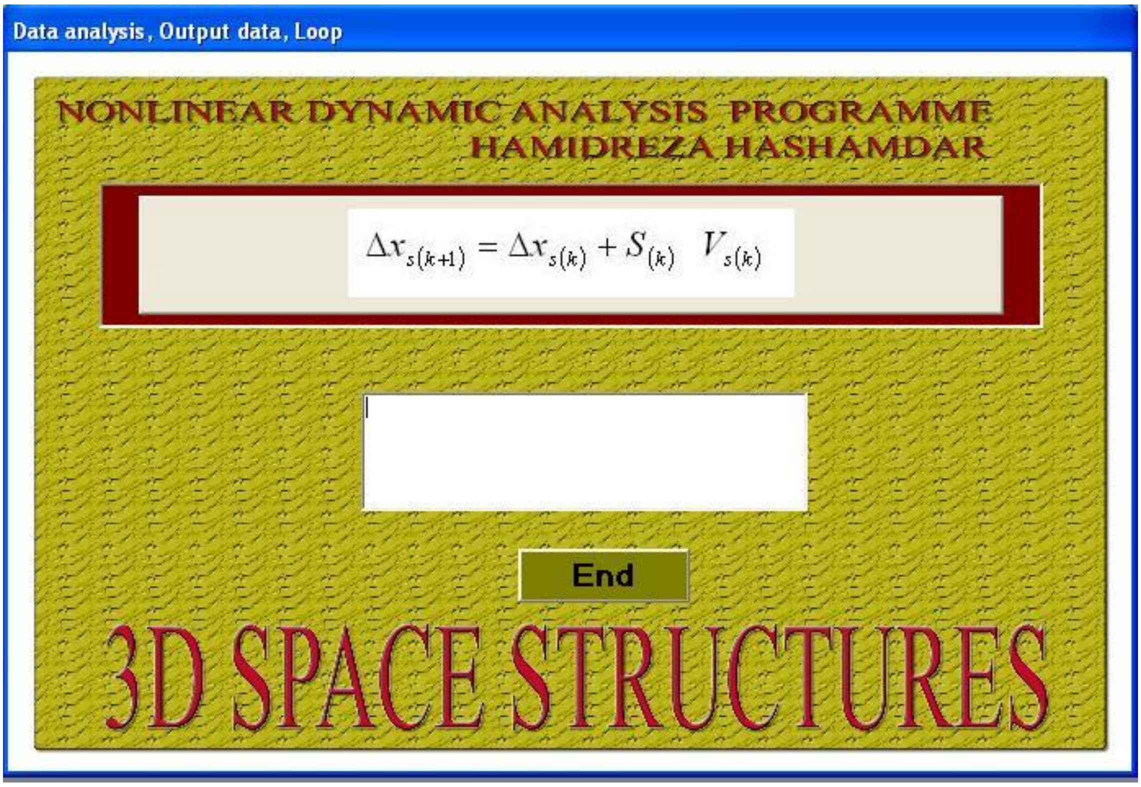

Figure.12: Data analysis interface sheet of nonlinear response programme.

The last interface sheet shows final result, and the codec programme follows the developed algorithm in chapter 4. The programme show all result in process of analysis data sequent. The user can monitoring acquisition data and debug a programme. The programme has a capacity to receive data from Microsoft Excel and Microsoft access as data link directly. The stability and accurate calculated data is investigated based on increment time step and condition of them is given in Figure.9. Definition of variable in programme is specified by dynamic variable for increasing execute of programme. The programme can be used such as macro in Excel developer tab in ribbon check box.

APPENDIX C

A Coherence and Cross Spectral Estimation Program

```
 MAIN PROGRAM:  A COHERENCE AND CROSS SPECTRAL ESTIMATION
           AUTHORS:       HAMIDREZA HASHAMDAR

 INPUT:          NNN IS THE NUMBER OF DATA POINTS PER
SEGMENT
                  4 < NNN < 1025
                ISR IS THE SAMPLING RATE
                NDSJP IS THE NUMBER OF DISJOINT SEGMENTS
                SFX IS THE SCALE FACTOR FOR THE INPUT DATA
STORED IN
                   THE XX ARRAY
                SFY IS THE SCALE FACTOR FOR THE INPUT DATA
STORED IN
                   THE YY ARRAY
 SPECIFICATION AND TYPE STATEMENTS
      DIMENSION XX(1024), YY(1024)
       DIMENSION GXX(513), GYY(513), GXYRE(513), GXYIM(513)
        DIMENSION WEGHT(513), PHI(513)
         DIMENSION LINE(50)
          EQUIVALENCE (WEGHT(1),PHI(1))

SET UP MACHINE CONSTANTS
      IOIN1 = I1MACH(1)
       IPRTR = I1MACH(2)
        SMALL = R1MACH(1)

READ INPUT CONTROL PARAMETERS FROM COMPUTER DATA CARD
      READ (IOIN1,9999) NNN, ISR, NDSJP, SFX, SFY
 NNN IS THE NUMBER OF DATA POINTS PER SEGMENT
  ISR IS THE SAMPLING RATE
   NDSJP IS THE NUMBER OF DISJOINT SEGMENTS
    SFX AND SFY ARE SCALE FACTORS FOR THE INPUT DATA
     9999  FORMAT (3I5, 2F10.5)
       NFFTS = NDSJP

PRINT INPUT CONTROL PARAMETERS
      WRITE (IPRTR,9998) NNN, ISR, NDSJP, SFX, SFY
       9998  FORMAT (/1X, 5HNNN =, I6, 5X, 5HISR =, I7, 5X,
7HNDSJP =, I7,
     *    5X//1X, 5HSFX =, E15.8, 8X, 5HSFY =, E15.8/)

 CALCULATE CONSTANTS
      TPI = 8.0*ATAN(1.0)
       DEG = 360.0/TPI
        IF (NNN.GT.0 .AND. NNN.LE.1024) GO TO 10
         WRITE (IPRTR,9997)
          9997  FORMAT (10X, 9HNNN ERROR)
           STOP
```

```
   10  CONTINUE
       VARX = 0.0
        VARY = 0.0
         DT = 1.0/FLOAT(ISR)
          SF = SQRT(ABS(SFX*SFY))

  PRINT OUT USER INFORMATION

       TIME = FLOAT(NDSJP*NNN)*DT
         WRITE (IPRTR,9996) NDSJP, TIME
          9996  FORMAT (10X, 3HTHE, I4, 25H DISJOINT PIECES
COMPRISE, F8.2,
     *     16H SECONDS OF DATA)

  COMPUTE NEW COMPOSITE NUMBER NNN

       CALL HICMP(NNN, NPFFT)
        IF (NPFFT.GT.1024) STOP
         WRITE (IPRTR,9995) NPFFT
          9995  FORMAT (10X, 21HNUMBER OF POINT FFT =, I5/)

  CALCULATE CONSTANTS

       NNNP1 = NNN + 1
        NNND2 = NNN/2
         NND21 = NNND2 + 1
          NP2 = NPFFT + 2
           ND2 = NPFFT/2
            ND2P1 = ND2 + 1
             DF = 1.0/(DT*FLOAT(NPFFT))
              FNYQ = FLOAT(ISR)/2.0
       CONST = 0.25*DT/FLOAT(NNN)
            FLOW = 0.0
              FHIGH = FNYQ
                ISTRT = IFIX(FLOW/DF) + 1
                  ISTOP = IFIX(FHIGH/DF) + 1

  COMPUTE AND SAVE WEIGHTING FUNCTION

       TEMP = TPI/FLOAT(NNN+1)
        SCL = SQRT(2.0/3.0)
         DO 20 I=1,NNND2
          WEGHT(I) = SCL*(1.0-COS(TEMP*FLOAT(I)))
   20  CONTINUE

  STORE ZEROS IN THE SUMMING ARRAYS

       CALL ZERO(GXX, ND2P1)
        CALL ZERO(GYY, ND2P1)
         CALL ZERO(GXYRE, ND2P1)
          CALL ZERO(GXYIM, ND2P1)
```

```
 COMPUTE AND SUM NPFFT ESTIMATES
      DO 80 KOUNT=1,NFFTS
        CALL ZERO(XX, NPFFT)
         CALL ZERO(YY, NPFFT)

 LOAD XX AND YY ARRAYS WITH NNN DATA POINTS

        CALL LOAD(XX, YY, NNN, KOUNT, ISR)

         PRINT OF FIRST 50 INPUT VALUES

        IF (KOUNT.NE.1) GO TO 40
         WRITE (IPRTR,9994)
9994      FORMAT (1H1, 9X, 41HPRINTOUT OF FIRST 50 VALUES
OF INPUT DATA///
     *       )
        LPMAX = MIN0(NPFFT,50)
         DO 30 I=1,LPMAX
          WRITE (IPRTR,9993) I, XX(I), YY(I)
9993       FORMAT (1X, I5, 1X, 2F15.8, 6X)
  30     CONTINUE
          WRITE (IPRTR,9992)
9992       FORMAT (/1H1)
  40        CONTINUE

 REMOVE THE LINEAR TREND AND COMPUTE THE VARIANCE
 IF IS3 = 0 DO NOT REMOVE DC COMPONENT OR SLOPE
C = 1 REMOVE THE DC COMPONENT
C > 1 REMOVE THE DC COMPONENT AND SLOPE

        IS3 = 0
        CALL LREMV(XX, NNN, IS3, DX, SX)
         CALL LREMV(YY, NNN, IS3, DY, SY)
          VARXI = 0.0
           VARYI = 0.0
        DO 50 I=1,NNN
          VARXI = VARXI + XX(I)*XX(I)
           VARYI = VARYI + YY(I)*YY(I)
  50    CONTINUE
        VARXI = VARXI/FLOAT(NNN-1)
         VARYI = VARYI/FLOAT(NNN-1)
          WRITE (IPRTR,9991) KOUNT, DX, DY, SX, SY, VARXI,
VARYI, IS3
9991    FORMAT (1X, I3, 4H DX=, E12.5, 4H DY=, E12.5, 4H
SX=, E12.5,
     *      4H SY=, E12.5/4H VX=, E12.5, 4H VY=, E12.5, I5)
        VARX = VARX + VARXI
         VARY = VARY + VARYI

 WEIGHT THE INPUT DATA WITH COSINE WINDOW

        DO 60 I=1,NNND2
          ITMP = NNNP1 - I
```

Gjhjhdfk;gu

Dfghdf

```
      DIMENSION POWER(1), LINE(1)
      DATA ISTAR /1H*/

 FIND PEAK AND MINIMUM DB VALUES OF ARRAY POWER BETWEEN
FLOW AND FHIGH

      ISTRT = IFIX(FLOW/DF) + 1
       ISTOP = IFIX(FHIGH/DF) + 1
      FMIN = 10000.0
       PEAK = -10000.0
      DO 10 K=ISTRT,ISTOP
        PEAK = AMAX1(PEAK,POWER(K))
         FMIN = AMIN1(FMIN,POWER(K))
   10 CONTINUE
      WRITE (IPRTR,9999) FMIN, PEAK
9999  FORMAT (///5X, 6HFMIN =, F7.2, 3H DB, 4X, 6HPEAK =,
F7.2, 3H DB//
     *    1X, 5HINDEX, 4X, 4HFREQ, 5X, 2HDB/)

 PLOT SPECTRUM ON PRINTER

      DO 20 K=1,50
        LINE(K) = ISTAR
   20 CONTINUE

      FBEG = FLOAT(IFIX(FLOW/DF))*DF
      DO 30 K=ISTRT,ISTOP
        FREQ = FBEG + DF*FLOAT(K-ISTRT)
         INDEX = IFIX(POWER(K)-FMIN)/2
        IF (INDEX.LT.1) INDEX = 1
         IF (INDEX.GT.50) INDEX = 50
        WRITE (IPRTR,9998) K, FREQ, POWER(K),
(LINE(I),I=1,INDEX)
9998    FORMAT (I6, F8.3, F7.2, 1X, 50A1)
   30 CONTINUE

      RETURN
      END
SUBROUTINE:  ZERO
 THIS SUBROUTINE STORES ZEROES IN A FLOATING POINT ARRAY
      SUBROUTINE ZERO(ARRAY, NUMBR)
 INPUT:  ARRAY = AN ARRAY OF FLOATING POINT VALUES TO BE
                 ZERO FILLED
         NUMBR = NUMBER OF ARRAY VALUES

      DIMENSION ARRAY(1)

      DO 10 K=1,NUMBR
        ARRAY(K) = 0.0
```

```
   10 CONTINUE

      RETURN
      END
```

APPENDIX D

Bode plot of frequency response (Magnitude, Phase)

```
bode(sys)
bode(sys1,...,sysN)
bode(sys1,PlotStyle1,...,sysN,PlotStyleN)
bode(...,w)
[mag,phase] = bode(sys,w)
[mag,phase,wout] = bode(sys)
```

Description

Bode (sys) creates a Bode plot of the response of the dynamic system `sys`. The plot displays the magnitude (in dB) and phase (in degrees) of the system response as a function of frequency. bode (...,W) plots system responses at frequencies determined by w.

- If w is a cell array {wmin,wmax}, bode(sys,w) plots the system response at frequency values in the range {wmin,wmax}.
- If w is a vector of frequencies, bode(sys,w) plots the system response at each of the frequencies specified in w.

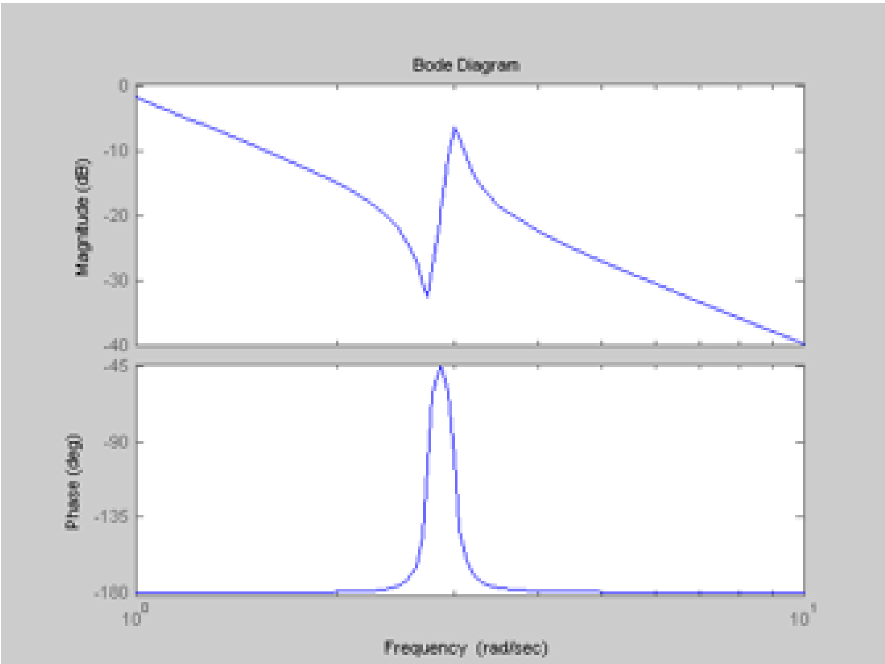

Figure 1: Interface plot of output programme.